UC Santa Barbara
UC Santa Barbara Electronic Theses and Dissertations

Title

Dynamic Allostatic Modulation During Appraisal, Cognitive Challenge, and Across the Menstrual Cycle

Permalink

Author

Babenko, Viktoriya

Publication Date

2023

Peer reviewed|Thesis/dissertation

UNIVERSITY OF CALIFORNIA

Santa Barbara

Dynamic Allostatic Modulation During Appraisal, Cognitive Challenge, and Across the

Menstrual Cycle

A dissertation submitted in partial satisfaction of the

requirements for the degree Doctor of Philosophy

in Psychological and Brain Sciences

by

Viktoriya Babenko

Committee in charge:

Professor Scott T. Grafton, Chair

Professor Michael S. Gazzaniga

Professor Barry Giesbrecht

Professor Emily G. Jacobs

March 2023

This dissertation of Viktoriya Babenko is approved.

_____

Michael Gazzaniga

_____

Barry Giesbrecht

_____

Emily Jacobs

_____

Scott T. Grafton, Committee Chair

January 2023

Dynamic Allostatic Modulation During Appraisal, Cognitive Challenge, and Across the

Menstrual Cycle

ACKNOWLEDGEMENTS

I want to express my deep gratitude and appreciation for the long list of individuals that made this work possible. Firstly, I'd like to thank my advisor, Dr. Scott T. Grafton, for his mentorship throughout my graduate career, as well as for always supporting me in my various research interests. I would also like to thank my committee members: Dr. Michael S. Gazzaniga, Dr. Barry Giesbrecht, and Dr. Emily G. Jacobs. I am truly honored to have had your support and guidance over these years. You have helped me in solidifying the details of my research projects, as well as challenging me to take a step back to understand the broader implications of my research questions. Most importantly, you have all filled my heart with gratitude for being a part of such an inspiring academic community.

I have been a part of the Psychological & Brain Sciences (PBS) community at the University of California, Santa Barbara from when I first started as an undergraduate student, about twelve years ago. I have lived nearly half of my life in this UCSB community, and everyone from the faculty, to the administrative staff, postdoctoral researchers, graduate and undergraduate students, have helped shape me into the person that I am today. Particularly within the PBS staff, I'd like to thank Chris McFerron (and his dog Tucker), for being a ray of sunshine for me and all of my colleagues, on days (or months) when it felt like all we could see were storms. You have always ensured that I felt seen and valued, and I truly believe you are the heart of the PBS community.

I would like to next thank the long list of collaborators that I have worked with over the years. Thank you to Alan Macy for your guidance in the use of psychophysiology equipment and for instilling in me an excitement towards the extent of its capabilities.

Additionally, thank you to my basement crew for your collaborations and friendship: Elizabeth Rizor, Evan Layher, Courtney Durdle, Tom Bullock, Mario Mendoza, Tyler Santander, Jessica Simonson, Caitlin Gregory, Alexander Stuber, Liann Jimmons, and Jamie Raymer. It takes a truly special group of people to make coming to work underground an enjoyable experience that I actually looked forward to. Next, I'd like to thank everyone who helped me with completing Experiment 5 of this dissertation, including my participants. It was a truly special experience to lead a research project in which the participants felt like a part of our team. Thank you to Emily Jacobs for your contagious passion in broadening the scope of the scientific literature towards understanding the effects of hormones on the brain and body. Thank you to Elizabeth Rizor, Caitlin Taylor, and Tyler Santander, for your expertise towards preprocessing and analyzing the brain data. Shuying Yu and Laura Pritschet, thank you for being so willing to share your wisdom of working with the endocrine data. I'd like to *especially* thank my team who for a year, woke up almost every morning (including weekends) to my texts informing them of our schedule for the day based around our participants' menstrual cycles, ovulation results and availability on the day-of. Renee Beverly-Aylwin, Elizabeth Rizor, Alexandra Stump, and Mario Mendoza: each of you have been imperative to the completion of this experiment, and there are not enough words in my vocabulary to thank you for your support and patience throughout this project. It is not easy to live our lives on a calendar based around 30 individuals' menstrual cycles, but after my 8+ years in this lab, my most valued memories are the support and teamwork that I felt from you all throughout this project.

Thank you to all of my past and current lab mates that I have had the pleasure to work alongside with: Neil Dundon, Elizabeth Rizor, Jaron Colas, Matthew Cieslak, Allison Shapiro, Michelle Marneweck, Deborah Barany, Dara Yang, Gold Okafor, James Elliott, Taraz Lee,

and Lukas Volz. Matt, thank you for your mentorship with the psychophysiology data and for your patience while training me on how to communicate with computers with a number of coding languages. Allison, thank you for the much-needed support and advice that you have provided me throughout these years. Neil…it would likely be frowned upon for me to take up three pages of my acknowledgements with the long list of times that you have helped me throughout my graduate career, so I will try to keep it simple. Thank you for being a constant source of both technical and emotional support. You have truly created a collaborative and supportive research environment within our lab, and I am especially grateful for that. *Importantly*, thank you for introducing our lab to the wondrous world of bears. I'd also like to thank the research assistants that taught me how to be a mentor, for all of your assistance with our studies, and for helping with the endless accumulation of psychophysiology data analysis: Alexandra Stump, Renee Beverly-Aylwin, Cepideh Razavi, Shefali Verma, Macey Turbo, Luna Herschenfeld-Catalan, Margaret Hayes, Hannah Erro, and Zoe Rathbun.

Elizabeth Rizor, thank you for being the best fellow-graduate-student-labmate that I could have ever dreamed of. From the day that we video-chatted about your interest in the lab, I knew we would get along well. Although, I didn't know that I would be lucky enough to have you become a life-long best friend. It takes a special bond to work together in a basement underground, and to then continue to want to spend a majority of our time together. I am beyond grateful to have received your support both as a coworker and as a friend while working on this dissertation. Thank you for helping me grow into the person that I am today, and for opening my eyes to a new degree of trust and friendship. I have also been lucky enough to have made a number of other lifelong friendships within the department. Notably, Anudhi Munasinghe, Evan Layher, Jack Strelich, and Courtney Durdle – your friendship and support

means everything to me. And to Jessica Cooper – as you know, I am immediately brought to tears when I consider how grateful I am to have you in my life. I believe that you have played an essential role in the reason that I have these authentic relationships. You have taught me how to attend to myself and to the people around me to a degree that I didn't know was possible. Importantly, you have instilled in me the importance of opening my heart to those that I love, to being gentle with myself, and to balancing both the joys and tribulations that are a part of life.

Importantly, I need to thank my dog, Data. (Yes, he is named after Star Trek. Yes, I am that much of a nerd). Particularly, thank you for your love, for making me smile even on the toughest days, and for halting the panic attack that I was beginning to have the last week of writing this dissertation. And lastly, to my family – my grandparents (Galina Kaminskaya and Leonid Kaminskiy) and my parents (Yelena Kaminsky and Vadim Vysotskiy). You are the foundation that has brought me to who and where I am in life today. You made the difficult and brave decision to emigrate from Ukraine to America when I was three years old. You gave up all that you knew, and that gave me everything that I have today. You have taught me persistence, drive, and resilience. Most importantly, you taught me how it feels to be endlessly loved and supported. You have always believed in me, and have never allowed me to doubt myself and my abilities. You never pressured me to be the straight-A student or the star gymnast – you always taught me that it was more important to have a balanced life. Thank you for raising me to be the gymnast child that was dancing to my own beat in a group-choreographed competition (true story).

To my grandparents: Galina Kaminskaya and Leonid Kaminskiy

Thank you for your endless love and support, and for always believing in me

VITA OF VIKTORIYA BABENKO
JANUARY 2023

EDUCATION

Bachelor of Science in Biopsychology, University of California, Santa Barbara, June 2014

Doctor of Philosophy in Psychological and Brain Sciences, University of California, Santa Barbara, January 2023

PROFESSIONAL EMPLOYMENT

2019 – 2022: Psychophysiology Fellowship, Department of Psychological and Brain Sciences, University of California, Santa Barbara

2016 – 2018, 2020, 2021: Teaching Assistant, Department of Psychological and Brain Sciences, University of California, Santa Barbara

2014 – 2016: Junior Specialist, Department of Psychological and Brain Sciences, University of California, Santa Barbara

PUBLICATIONS

Bullock, T., MacLean, M. H., Santander, T., Boone, A. P., **Babenko, V.**, Dundon, N. M., Stuber, A., Jimmons, L., Raymer, J., Okafor, G. N., Miller M. B., Giesbrecht, B., & Grafton, S. T. (2023). Habituation of the stress response multiplex to repeated cold pressor exposure. *Frontiers in Physiology*, 2542. https://doi.org/10.3389/fphys.2022.752900

Dundon, N. M., Shapiro, A. D., **Babenko, V.**, Okafor, G. N., & Grafton, S. T. (2021). Ventromedial prefrontal cortex activity and sympathetic allostasis during value-based ambivalence. *Frontiers in Behavioral Neuroscience*, *15*, 24. https://doi.org/10.3389/fnbeh.2021.615796

Dundon, N. M., Garrett, N., **Babenko, V.**, Cieslak, M., Daw, N. D., & Grafton, S. T. (2020). Sympathetic involvement in time-constrained sequential foraging. *Cognitive, Affective, & Behavioral Neuroscience*, *20*(4), 730-745. https://doi.org/10.3758/s13415-020-00799-0

Cieslak, M., Ryan, W. S., **Babenko, V.**, Erro, H., Rathbun, Z. M., Meiring, W., Kelsey, R. M., Blascovich, J., & Grafton, S. T. (2018). Quantifying rapid changes in cardiovascular state with a moving ensemble average. *Psychophysiology,* *55*(4), e13018. https://doi.org/10.1111/psyp.13018

ABSTRACT

Dynamic Allostatic Modulation During Appraisal, Cognitive Challenge, and Across the

Menstrual Cycle

by

Viktoriya Babenko

Unlike males, naturally menstruating females undergo a distinct hormonal monthly cycle, in which hypothalamic-pituitary-gonadal (HPG) sex hormones undergo drastic concentration changes across a single menstrual cycle. Furthermore, major regions of the brain are packed with receptors for both HPG and stress hormones. For these reasons, both HPG and stress hormones have numerous direct as well as indirect effects on the brain and body. The present research seeks to enhance the measurement of stress by developing definitive sympathetic drive measurement techniques to then record dynamic fluctuations of allostatic processes in relation to performance feedback and quantitative concentrations of HPG hormones within menstruating females.

Current methods of measuring allostatic dynamics include the electrocardiogram (ECG) and impedance cardiography (ICG), which are typically combined to estimate actions of cardiac sympathetic nervous system (SNS); an indicator of stress responses mediated by the autonomic nervous system (ANS). Current methods of ICG are time intensive in subject preparation and analysis, and the measurements are vulnerable to non-reproducible subject-

specific electrode configuration. With the present research, we present alternative state-of-the-art methods for tracking actions of the SNS. In Experiments 1 – 3, we present evidence of an electro-resonator, an accelerometer, and a trans-radial electrical bioimpedance velocimetry device (TREV) appropriately tracking SNS responses to physical stress tasks known to induce disruptions of allostatic processes. We further determine that the TREV device (Experiment 3) has the capacity to replace the need for ICG and ECG in estimating ANS activity, proving to be a reliable and capable method that is robust, time efficient, and readily accessible to researchers.

In Experiment 4, we demonstrate the ability of false and predetermined performance appraisals to modulate dynamic allostatic responses, regardless of the individuals' actual performance. Specifically, we find that the SNS acts as a perturbation-tracking system, in which compounding negative performance appraisal following a trend of positive feedback actuates a sympathetic drive. Conversely, we find that states of challenge and threat function at a grander, state-tracking level, in which any negative performance appraisal elicits a physiological response categorized as a "threat", while only excessively outstanding performance feedback elicits a "challenge" response. Previous research has observed individual differences in challenge and threat states. However, the present findings demonstrate dynamic trial-by-trial changes within an individual, altering between states of challenge and threat.

In Experiment 5, we examine the relationships between the concentrations of fluctuating cyclic HPG hormones at unique phases of the menstrual cycle and the modulation of behavior, allostasis, brain function, and brain morphology within individuals. We find that

progesterone and follicle-stimulating-hormone (FSH) are related to a slower response time on hard arithmetic problems, while progesterone alone is related to a decrease in allostatic efficiency (i.e. SNS recovery) following feedback from hard trials. Furthermore, we find that estradiol is associated with an increased SNS response to both the onset of arithmetic problems and to the accompanying feedback that follows. In the brain, estradiol is found to be positively associated with the volume of the CA2/3 hippocampal subregion, yet negatively associated with resting-state functional coherence across the whole brain. Furthermore, both estradiol and luteinizing hormone (LH) are positively linked to white matter integrity across the brain. Ultimately, we believe that allostatic processes and the role of HPG hormones are at the core for understanding stress and well-being. We hope that the present combination of studies will provide better methods for tracking health within individuals, from moment-to-moment dynamics, to monthly cycles, and throughout the lifespan.

TABLE OF CONTENTS

Chapter 1

Dynamic Allostatic Modulation During Appraisal, Cognitive Challenge, and Across the Menstrual Cycle

1.1   Introduction

Mechanisms of the central and autonomic nervous system (ANS) are fine-tuned to assist the human body in quickly and efficiently responding to the constant needs of, not only our physical environment around us, but also to the delicate intricacies of social interactions, and even further to the constantly fluctuating state of our very own bodies. The present research aims to examine the degree to which these dynamic mechanisms are influenced by both exogenous and endogenous factors. We use the term "exogenous" to define elements that are external to our immediate biological functions, such as social pressure and performance feedback, while we define "endogenous" factors as internal, biological mechanisms that are fundamental to human existence, such as the fluctuating hormonal state of the female menstrual cycle. For instance, both hypothalamic-pituitary-gonadal (HPG) sex hormones and hypothalamic-pituitary-adrenal (HPA) stress hormones have numerous direct as well as indirect effects on the brain and the body, from structural and functional plasticity of the brain to actions on the mitochondria and brain metabolism, affecting daily mood, decision making, and bodily functions (Mahmoodzadeh & Dworatzek, 2019; McEwen, 2006, 2018). While the effects of these mechanisms are well documented and supported in animal models, there remains a gap in the literature in credibly understanding the intricate and directional effect that these two mechanisms have on each other, and consequently, on the human body and behavior (Handa et al., 1994; Kawata, 1995).

Firstly, in Chapters 2 – 5, we aim to enhance the psychophysiological methods used to interpret the stress response by zoning in on the dynamic moment-to-moment behavior of the ANS. In Chapter 6, we examine the effects of exogenous factors on the ANS by asking whether fine-tuned dynamic regulations can be manipulated by predetermined, false performance feedback, regardless of the behavior that is being judged. Furthermore, in Chapter 7, we examine the degree to which these ANS processes are influenced by "endogenous" factors, as we investigate the interactions between the regulation of the ANS and cyclic endogenous fluctuations of HPG sex hormones occurring in menstruating females across their menstrual cycles. Given the supremely intertwined relationships between HPG hormones, HPA axis regulation, and neural circuitry, we further our investigations to determine how these naturally-occurring changes in HPG hormone concentrations may present dynamic cognitive effects, extending into brain morphology and functional activity.

1.2   The Stress Response and Autonomic Nervous System (ANS)

Stress is traditionally thought of as a variety of mechanisms engaged by the body in response to external and internal threats to homeostasis, which is a state of balanced equilibrium (Chrousos, 2009). At homeostasis, the two branches of the ANS, the parasympathetic and sympathetic nervous system (SNS), are constantly running in balance with each other (McCorry, 2007). The parasympathetic system is known as the constant "brake" on the system, responsible for "rest and digest" functions such as dialing down blood pressure (BP), constricting our lungs, and increasing blood flow toward systems that govern long-term functions within the body, such as reproductive organs and the digestive system. As stressors occur, the parasympathetic system will mitigate its control of the "brake", and the SNS, often referred to as the "fight or flight" system, increases its functioning. The SNS is

responsible for preparing our bodies for action by influencing heart contractility, dilating our pupils, activating our adrenals to produce catecholamines (such as epinephrine; i.e. adrenaline), and directing blood flow towards the lungs and muscles to assist in overcoming a demanding situation.

The stress response consists of a highly coordinated interaction between the ANS and the neuroendocrine system (McEwen, 2006; McEwen & Sapolsky, 1995). Some of the most significant mediators of stress are stress hormones, such as SNS-modulated catecholamines (including dopamine, norepinephrine and epinephrine), and HPA axis-modulated glucocorticoids (GCs; such as cortisol), which are released from the adrenal gland. Catecholamines act rapidly, often producing effects on the mind and body only seconds after secretion, whereas GCs primarily function on timescales of minutes to even hours, often enacting longer-lasting effects on the brain and body. In scientific research, the stress response is often measured at acute time-scales by quantifying the SNS drive, or at longer time-scales by quantifying saliva or blood GC concentrations.

The stress mechanisms discussed here began as an old evolutionary response to promote survival – to surge when face to face with a predator. Yet, stress has a U-shaped "dose-response" relationship when it comes to keeping the brain and body functioning properly (McEwen, 2018; McEwen & Sapolsky, 1995). While small doses of stress are manageable and can even be beneficial by aiding in the development of coping mechanisms for the future, chronic doses of stress can cause wear and tear, acting as a slow drip of poison; the longer the stress response acts, the more it can damage the body and become "toxic stress." Sapolsky's "glucocorticoid-cascade hypothesis" states that chronic exposure to elevated levels of GCs are associated with wear and tear on the hippocampus, leading to impairments in memory, mood,

and spatial ability. Furthermore, it can lead to an inability to shut off the production of GCs, giving rise to a "vicious cycle" (Sapolsky et al., 1986).

For instance, previous research has identified long-term caregivers, such as mothers of chronically ill children, as one of the most chronically stressed groups of people (Cohn et al., 2020; Lovell & Wetherell, 2011). Investigations of caregiver well-being have determined that chronic stress erodes telomeres (regions of repetitive nucleotide sequences at the end of each chromosome), which are designed to protect the chromosome from deterioration (Epel et al., 2004). In turn, the deterioration and shortening of these telomeres contribute to the aging process and have been connected to an increased risk for developing illness, accelerated cell-aging, and higher rates of inflammation (Blackburn & Epel, 2017; Calado & Young, 2009; Zhang et al., 2016). Stress and telomeres have a negative dose-response relationship: as one's dose of stress increases and remains chronically high, telomeres shorten accordingly.

However, being under long-term stress does not necessarily mean one must escape their difficult situation to avoid telomere erosion. In one study, caregiving mothers underwent a classic stress-inducing task involving social-evaluative pressure (O'Donovan et al., 2012). Some caregivers, despite working the same number of hours and facing similar demands as other caregivers, reported experiencing less stress and had longer telomeres, demonstrating no significant differences from the control mothers (non-caregiving mothers of healthy children). This difference was attributed to the categorization of their stress response as either a "challenge" or "threat" response, with seemingly resilient caregivers demonstrating a "challenge" stress appraisal. Conversely, those participants who exhibited a "threat appraisal" were found to have shorter telomeres and reported experiencing greater levels of stress. Researchers have determined that the appraisal of one's situation (i.e. as either a "challenge"

or a "threat") has direct implications on one's health (Blascovich, 2008b). In Chapter 6, we take a deeper dive into the physiological differences between these responses of challenge and threat, and we describe a study in which we examined the dynamic allostatic activity of both the SNS and states of challenge and threat within single individuals in response to performance feedback.

Much is still unknown about the complex and delicate relationship between "beneficial" and "toxic" stress and what bodily and neural processes lead to one or the other. Fundamentally, "stress" is too broad of a term to tackle this question, as it is used in many different scenarios to explain a broad variety of situations and processes. For the purpose of the present research, it is simpler and more direct to refer to "stress" in the context of allostasis. Allostasis is defined as the body's actions it takes to adjust to its environmental challenges and to then return to homeostasis once the challenge has passed. When a "stressful" event occurs, our body's mediators of allostasis (our ANS and central nervous system) must fluctuate accordingly and eventually bring the body back to homeostasis (McEwen, 2006). In an ideal situation, our body would increase catecholamine production and SNS drive when faced with a challenge and then quickly return to homeostasis by attenuating those systems when the challenge has passed. To simplify this concept, we will refer to this ideal response of the nervous system as "high allostatic efficiency".

"Allostatic efficiency" can have many implications on a person's neural, physiological, and metabolic health. For instance, when the allostatic response is excessive or extended beyond when the challenge has subsided, it can become pathologic on multiple timescales. At an acute scale, a single major physical or emotional stressor can lead to over-activation of the SNS, causing a weakening of the heart muscles. This condition, defined as Takotsubo

cardiomyopathy, also known as "broken heart syndrome", is known to primarily affect females, and can be fatal in extreme circumstances (Amin et al., 2020; Indorato et al., 2015). On a longer timescale, these mediators can lead to "allostatic load" and in extreme cases "allostatic overload" at chronically "toxic" stress levels. This type of chronic stress reactivity can cause damage to the immune system and lead to prolonged changes in structural neural architecture, neural function, and prolonged dysfunctions of cardiovascular reactivity (Eskandari & Sternberg, 2002; Golkar, et al., 2014; McEwen, 2006; Steptoe & Kivimäki, 2012; Veer, et al., 2011). For instance, excessive stress may lead to pathophysiologies such as gastrointestinal disorders, hypertension, cardiovascular disease, poor metabolism, or even the inhibition of reproduction (Grundy et al., 2006; Whirledge & Cidlowski, 2010).

Furthermore, stress activates the HPA axis neural circuitry, which is essential in maintaining homeostasis between the body and current situational demands, triggering corticotropin-releasing hormone (CRH) from the hypothalamus, adrenocorticotropic hormone (ACTH) from the pituitary, and GCs from the adrenals. Allostatic processes of the ANS are largely intertwined in limbic regions and HPA circuitry, which are integral to emotional and cognitive regulation. These regions, specifically the hypothalamus, hippocampus, PFC and amygdala, are profoundly reciprocally interconnected both structurally and functionally to a point where a change in one of these structures can impact the function of the others (McEwen, 2022; Mulkey & du Plessis, 2019; Thayer & Brosschot, 2005). Furthermore, they exhibit high densities of both GC receptors and estrogen and progesterone (HPG sex hormone) receptors (Donahue et al., 2000; Österlund & Hurd, 2001). There are three major endogenous estrogens, of which the most active and the most commonly discussed in the scientific literature is 17β-estradiol (E2; from here on referred to as "estradiol" for simplicity). These HPG hormones,

such as progesterone (P4), testosterone, and estradiol, have been shown to exhibit changes in synaptic transmission, structure, and functional connectivity, and play integral roles in mediating mood states and cognitive processes (Beltz & Moser, 2019; Jacobs et al., 2015; Toffoletto et al., 2014). Unlike males, naturally menstruating females not only operate on a 24-hour biological (circadian) rhythm, but undergo a distinct hormonal monthly cycle, in which HPG hormones such as estradiol and progesterone undergo drastic concentration changes across a single menstrual cycle. For instance, during ovulation, there can be a 12-fold increase in concentrations of estradiol as compared to menses, and a nearly 800-fold increase in progesterone concentrations during the premenstrual luteal phase (Figure 1; Taylor et al., 2020). For this reason, behavior, allostasis, cognition, and brain structure are likely to be modulated by the dominant HPG hormones present in a female's body at different phases of their menstrual cycle.
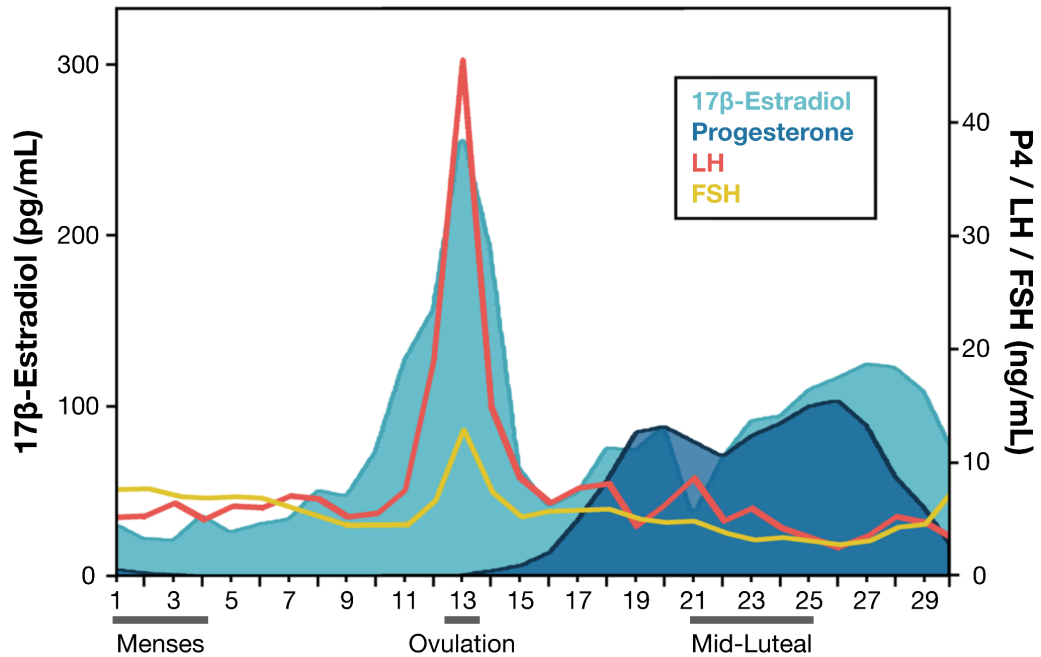
Figure 1 A single female's daily sex hormone concentrations across one menstrual cycle. At menses, estradiol (E2), progesterone (P4), luteinizing hormone (LH) and follicle stimulating hormone (FSH) are all low. During ovulation, E2, LH, and FSH are at peak concentrations. During mid-luteal, E2 is high, and P4 is at peak concentrations. Figure adapted with author's permission from "Functional reorganization of brain networks across the human menstrual cycle," by Pritschet et al., 2019. Copyright 2019.

1.3   The Human Menstrual Cycle: Hypothalamic-pituitary-gonadal (HPG) Hormones

The human menstrual cycle consists of three main stages: the follicular phase, ovulatory phase, and luteal phase, and typically ranges in length from $21 - 35$ days, on average (Bull et al., 2019; Lenton, Landgren & Sexton, 1984; Lenton, Landgren, Sexton, et al., 1984). The follicular phase begins with the onset of menses and is initiated by the release of follicle-stimulating hormone (FSH) from the hypothalamus and pituitary glands, which in turn stimulates the production of estradiol (Baird, 1987). FSH acts by stimulating the growth of follicles along the lining of the ovaries, where a mature egg resides until ovulation. The follicular phase proceeds with a mid-level rise and peak of estradiol during pre-ovulation, followed by a peak in luteinizing hormone (LH). When LH reaches its peak (the "LH-surge"), it prompts the start of ovulation, during which the mature egg is released from the follicle on

8

the ovary surface and it travels down the fallopian tube into the uterus where it can be fertilized (Shupnik, 2003). Following ovulation, the luteal phase begins as progesterone levels rise and LH, FSH, and estradiol levels begin to decrease. While estradiol levels remain heightened, progesterone levels peak and surpass estradiol, stimulating the thickening of the uterus, which is essential for giving a fertilized egg a location for implantation and development. If fertilization does not occur, progesterone and estradiol levels will drop, the thickening uterine lining will shed, and menstruation (i.e. menses) will occur, thus completing a full loop of the menstrual cycle (Reed and Carr, 2015).

1.4   Stress and HPG Hormones: Animal Models

Research in animal models has provided evidence that HPG hormones have significant effects on stress. One subset of findings links estradiol to the exacerbating effects of stress, such as an increase in the release of stress-induced GCs (Shansky & Lipps, 2013). For instance, across the rodent's estrous cycle (i.e. their menstrual cycle), female rats in their proestrus phase (during a time of high estradiol secretion) presented higher baseline GC levels than both female rats within their diestrus phase (low-estradiol) and male rats. Another study linked stress susceptibility and a decline in working memory performance to female rats high in estradiol, and additionally found that ovariectomized rats (with removed circulating estradiol and progesterone), were more susceptible to stress after they underwent estradiol replacement therapy (Shansky et al., 2004). From this finding, it is feasible that females with high estradiol levels may be primed for an amplified GC surge following exposure to lower levels of stress, which may exacerbate working memory impairments.

In contrast, other animal models suggest neuroprotective capabilities of estradiol during times of recurrent stress. One such study explored the benefits of aromatase, an enzyme

precursor for the biosynthesis of estradiol, in response to acute stress in female rats (Wei et al., 2014). Following the administration of aromatase, female rats demonstrated stress resilience compared to male rats. Furthermore, female rats presented higher levels of aromatase in the prefrontal cortex (PFC) compared to male rats, likely associated with a greater quantity of estrogen receptors within the PFC. Additionally, the blockage of aromatase in female rats demonstrated significantly higher stress-induced glutamatergic deficits and memory impairments. Further evidence in animal models suggests an attenuated allostatic response during times of high progesterone, which is likely linked to its sedative and anxiolytic effects (Landgren et al., 1987; Zhu et al., 2004). Additionally, across genders, progesterone therapy has been found to dampen psychological and physiological responses to stress and anxiety in both humans (Childs et al., 2010; Del Rio et al., 1998) and mice (Frye et al., 2006).

1.5   Stress, HPG Hormones, and the ANS: Human Models

In humans, several studies have shown sexual dimorphism in the incidence of neuropsychiatric disorders regarding PTSD (Kessler et al.,1995), depression (Kessler et al., 1993), and other affective disorders (Rapaport et al., 1995), as well as differences in therapeutic responses (Kornstein et al., 2000; Simon et al., 2006). Moreover, sexual dimorphic differences have been observed in the structure and function of brain regions regarding emotional processing, such as the hippocampus and the amygdala (Goldstein et al., 2001). Within females, evidence supports psychoneuroendocrine changes across the menstrual cycle, regulation of the excretion of adrenaline and noradrenaline, and variability in mood (Collins et al., 1985). Specifically, it is likely that estradiol plays a role in regulating the HPA, likely by attenuating BOLD activation in neural stress circuitry (Albert et al., 2015; Jacobs et al., 2015) perhaps via cortical-subcortical control within the HPA (Goldstein et al., 2005), or by

GC receptor mediation by estrogen-receptor activation. Previous findings suggest that estradiol may have attenuating effects on autonomic activity, potentially via increasing oxytocin (Taylor et al., 2000).

The presence of estrogen receptors (ERs) in the heart, vascular smooth muscle, and autonomic brainstem centers (Perrot-Applanat, 1996) and hormone-mediated changes in adrenergic receptor density (Wilkinson & Herdon, 1982) suggest a likely involvement of sex hormones in the regulation of the cardiovascular system. For instance, some evidence reports longer repolarization of the heart with estradiol, and shorter repolarization with progesterone, leading to slower heart rate with estradiol and the opposite with progesterone (Salem et al., 2016). Furthermore, the effects that these hormones have may be further influenced by the ratio level between the two hormones, with some evidence from postmenopausal females supporting estradiol's role in decreasing blood pressure and cortisol responses to stress, and other evidence showing that the combination of progestin (an artificial progesterone) may blunt those effects (Lindhelm et al., 1994).

Not only has it proven challenging to separate the effects of estradiol and progesterone on stress, but there also remains a gap in the literature regarding the effect that HPG hormones may have on allostatic dynamics across the menstrual cycle. There has, however, been evidence supporting a relationship between menstrual cycle phase and singular time-scale measures of autonomics, such as baseline, mid-task blocks, or post-task recovery. For instance, some studies have found heightened skin conductance (an estimate of the ANS) and decreased allostatic efficiency (measured by prolonged muscle sympathetic nerve activity (MSNA) following a stress task) during the luteal phase as compared to the early follicular phase, suggesting that progesterone increases allostatic response and prolongs its recovery after stress,

11

hindering allostatic efficiency (Carter & Lawrence, 2007; Guasti et al., 1999). Furthermore, another study found increased resting baseline levels of MSNA during the mid-luteal phase when compared to the early follicular phase (Minson et al., 2000). Additionally, another study periodically measured HRV data throughout a stress task and at recovery and found that a loose estimate of SNS activity (low frequency HRV) was significantly higher in the luteal phase than in the follicular, in which parasympathetic activity (measured by high frequency HRV) was predominant (Sato & Miyake, 2004).

These results together suggest that hormonal concentrations during the luteal phase not only contribute to an increase in autonomic engagement and a decrease in allostatic efficiency following stress, but also to an increase in baseline levels of autonomic drive. However, while the luteal phase contains peak-concentrations of progesterone, a confound in interpreting these results is that it is also accompanied by high concentrations of estradiol, and thus it is possible for either estradiol or the combination of progesterone with estradiol to be the cause. Therefore, these results support either high levels of progesterone or estradiol (or a ratio of both) relating to increased allostatic drive and decreased allostatic efficiency following stress, but fall short in distinguishing between the two. In Chapter 7, we present a study in which we retrieved blood plasma levels of HPG hormones across three well-differentiated times of the menstrual cycle to directly quantify hormone concentrations in relation to robust dynamic allostatic processes and help discern between the potential effects of estradiol and progesterone.

Chapter 2

Psychophysiological Methods Review

2.1   Introduction

Research quantifying autonomic nervous system activity (ANS) and cardiac mobilization is becoming increasingly important and prevalent - not only in medical domains, but also in psychological and brain sciences (Cybulski et al., 2012; Thayer et al., 2010). These measures provide insight into motivational states, stress reactivity, reward sensitivity, task engagement, and decision making (Kuipers et al., 2017; Richter et al., 2008; Richter & Gendolla, 2007, 2009). There are various methods in use to measure the psychophysiological response of the ANS such as skeletomuscular activation, hormonal fluctuations, systolic blood pressure dynamics, and assays of the immune response (Blascovich & Mendes, 2010). One common noninvasive method to obtain measures of cardiovascular reactivity is the utilization of electrocardiography (ECG) to estimate heart rate variability (HRV). High frequency HRV is associated with parasympathetic tone. While low frequency HRV is claimed to be an indicator of a sympathetic tone, recent work establishes that it is an unreliable index due to influences by both sympathetic and parasympathetic activity (Berntson et al., 1997; Reyes del Paso et al., 2013; Valenza et al., 2018). As an alternative to HRV, combining ECG with impedance cardiography (ICG) allows for the extraction of temporal indices of cardiac function sensitive to autonomic tone such as pre-ejection period (PEP) and left-ventricular ejection time (LVET).

PEP (Figure 2.1) is the sum of the electromechanical delay and isovolumic contraction time (contraction of the ventricle prior to the opening of the aortic valve) (Kelsey et al., 2004; Tomaka et al., 1997; Wright & Kirby, 2001). PEP in particular has been shown to be a reliable indicator of sympathetic nervous system (SNS) activity, resulting in an inverse relationship where a decrease in PEP represents an increase in sympathetic activity. PEP is sensitive to the predictive effects of task manipulations (Kelsey et al., 2000, 2004), decision making (Dundon et al., 2020, 2021), and individual differences in a variety of tasks (Kelsey, 1991; Kelsey et al., 2001). LVET is defined by the time interval between the opening and closing of the aortic valve, representing the interval during which the left ventricle ejects blood into the aorta (Figure 2.1). LVET demonstrates a trend of decreasing duration with increased sympathetic tone. However, it also provides insight into the preload effects on the heart (Uijtdehaage & Thayer, 2000). As intrathoracic pressure is changed during baroreflex, the preload effects will vary with LVET (Hassan & Turner, 1983). This mechanism is influenced by the Frank-Starling effect (Spodick, 1979). Thus, unlike PEP, it is not considered to be a measure that represents isolated SNS activity. When continuous blood pressure (CBP) is available, it is also possible to combine LVET with models of the chest to estimate cardiac output (CO) and total peripheral vascular resistance (TPR) (Kelsey et al., 2004; Kreibig et al., 2013; Matthews et al., 2003; Seery, 2013; Wright et al., 1986). These model based measures have been used broadly to study baseline levels of health (Kelsey, 2004) and to test the biopsychosocial model of challenge and threat to distinguish between varying states of motivation (Blascovich, 2008a; Tomaka et al., 1997).

14
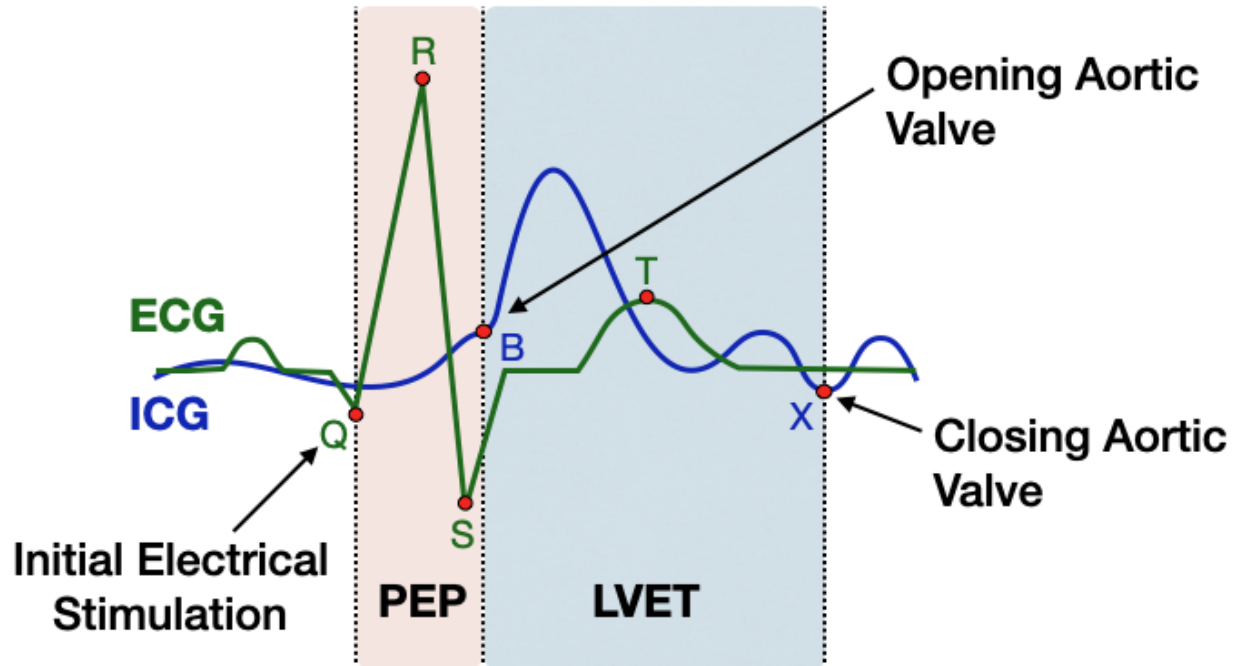
Figure 2.1 Pre-ejection period (PEP) and left ventricular ejection time (LVET) measures extracted from impedance cardiography (ICG) and electrocardiogram (ECG) waveforms. The characteristic ICG waveform (in blue) is displayed overlapping the ECG waveform (in green), with the ICG B-point representative of the opening of the aortic valve and the X-point representative of the closing of the aortic valve. The time interval between the ECG Q-point and the ICG B-point represents PEP, the sum of electromechanical delay and isovolumic contraction of the ventricle. The time interval between the ICG B- and X-point represents LVET.

2.2 Advanced Impedance Cardiography and Electrocardiogram Methodology

The following procedure and materials were followed for the ICG data collection in Chapter 4, the ICG and ECG data collection in Chapter 3, and the ICG, ECG, and CBP data collection in Chapter 6. These psychophysiology techniques vary amongst different research labs. In collaboration with Biopac Systems, Inc., the following methodology and protocol is one that our lab has perfected over the years. We believe that our methodology produces the most reliable signal, with the least signal-to-noise interference.

2.2.1 General psychophysiology procedure

Upon arrival, a researcher described the general procedure of these studies. Participants then completed consent forms and a screening form to ensure no history of cardiovascular or related diseases. Each consecutive session (where it applies) began with the participant initialing and dating each consent and screening form. Participants were taken into a private room, in which a trained female researcher placed ICG and/or ECG electrodes on their neck and torso (Figure 2.2). They were then taken to the experiment room and connected to the appropriate hardware (described in Section 2.2.3) by carbon fiber leads. During psychophysiology setup, the researcher reviewed the importance of minimizing all unnecessary movements and vocal sounds throughout the course of the study in order to avoid disruptions in the psychophysiology data. Once the setup (described in Section 2.2.2) was complete, each session began with a non-recorded resting period of varying time per study for the participant to become adjusted to the environment. Following this resting period, an ICG, ECG, and/or CBP baseline recording was collected, shortly followed by the experimental task.
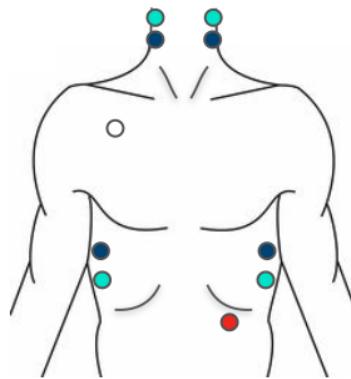
Figure 2.2 Impedance cardiography (ICG) and electrocardiogram (ECG) setup uses a total of 10 electrodes. Eight ICG electrodes are shown in blue: two on each side of the neck and two on each side of the torso. ICG electrodes in cyan are current-injecting electrodes, while electrodes in dark blue are voltage sensing. These are paired with two total ECG electrodes: one placed underneath the right collar bone (in white), and one placed underneath the left rib cage (shown in red).

2.2.2   Psychophysiology protocol

Psychophysiological data was collected through noninvasive approaches to measure ICG, ECG, and/or CBP. Researchers found that cleaning and exfoliating each area of the skin where electrodes would be placed was helpful for minimizing signal noise. Prior to placement of each electrode, an approximate 1-inch area of the skin was disinfected and exfoliated gently with an abrasive pad, followed by the application of Nu-Prep gel (ELPREP, Biopac Systems Inc.), a skin exfoliant. Once the area was fanned dry, a small dab of electrode gel (GEL100, Biopac, Inc.) was placed on each of the 10 strong adhesive disposable foam electrodes (EL500, Biopac, Inc.) before they were placed on the body. For psychophysiology experiments with ICG and ECG inside a magnetic resonance imaging (MRI) scanner, MRI-safe carbon fiber electrodes were used (EL509, Biopac, Inc.). For ICG (Figure 2.2, in blue and cyan), a total of eight electrodes were placed on the torso and neck: two on each side of the neck, and two on each side of the torso as suggested by Bernstein (1986). Electrodes on the upper neck and lower torso (Figure 2.2, in cyan) were each injecting a 4 mA alternating current into the thoracic cavity at 50 kHz, while the inner electrodes (Figure 2.2, in blue) were voltage sensing. In combination, these electrodes provide basal trans-thoracic impedance (Z0) data and the first derivative (dZ/dt) of the pulsatile changes in transthoracic impedance. Inter-electrode distances between each pair of inner electrodes (Figure 2.2, in cyan) were measured and recorded for analytic purposes. For studies where a total of two electrodes were used for ECG (Figure 2.2, in red), one was placed just under the right collarbone, and one under the left rib cage. ICG electrodes provided the necessary grounding. For CBP, participants' index and middle fingers of their left hand were placed in the accompanying finger cuffs, and a blood pressure cuff was placed around their upper arms just above their brachial artery to provide occasional measures

of systemic blood pressure. The finger cuffs provided continuous blood pressure data, which was directly integrated into the Acqknowledge software.

2.2.3 ICG, ECG, and CBP equipment

ICG and ECG non-invasive psychophysiological recording equipment were used for continuous real-time data acquisition. All physiology equipment and software was from Biopac Systems, Inc. (Goleta, CA). Signals were integrated using the MP160 and collected at a 2 kHz sampling rate. ICG data were collected using a NICO100C amplifier, ECG data were collected using an ECG100C amplifier, and CBP data were collected using the CNAP monitor 500 and connected to a DA100C amplifier through a TCI105 transducer. The DA100C amplifier settings were adjusted to a gain of 1000 and a low pass filter of 10 Hz – 300 Hz. The ECG100C amplifier settings were adjusted to filter the incoming signal at 0.05 Hz – 35 Hz and NICO100C amplifier settings were adjusted to filter at DC (no filter) – 10 Hz. For experiments inside the MRI, the ECG100C-MRI and NICO100C-MRI amplifiers were used for ECG and ICG, respectively. All signals were displayed and stored on a laptop running AcqKnowledge software version 5.0.2.

2.3 Psychophysiology preprocessing: the Moving Ensemble Analysis Pipeline (MEAP)

We worked in collaboration with Dr. Matthew Cieslak to implement a custom open-source software tool, written in Python, for accelerating the analysis of dynamic sympathetic changes (Cieslak, 2018). Previous literature has struggled to reliably define the location of the B-point (estimation of the opening of the aortic valve), a highly valuable point for the interpretation of the sympathetic nervous system. This has added to the lack of use of

impedance cardiography across laboratories that aim to study autonomic responses. MEAP presents a simple combination of user-friendly labeling of this point along with a machine classifier to assist in reliably marking this point. Additionally, MEAP introduces the use of a moving-ensemble averaging window rather than ensemble averaging. This allows for capturing rapidly fluctuating cardiovascular dynamics that might be smoothed out by the classic ensemble averaging method.

Psychophysiology data for all of the following research experiments were preprocessed using MEAP. Data for studies in Chapters 3, 4, and six were moving ensemble-averaged along a 15 second window, allowing for continuous estimations of the physiological measures of interest as demonstrated by Cieslak et al. (2018). Trained researchers manually checked each classification and edited out any artifacts.

Enhancing the Collection and Preprocessing of Dynamic Allostatic Responses

Chapters 3 – 5

Current methods for recording ECG and ICG are generally time intensive for researchers. In terms of apparatus preparation, the combined recording requires a total of 10 electrodes, placed on the neck, chest, and abdomen of the participant (Figure 2.2). This procedure routinely requires ~20 minutes and there can be significant variability in electrode placement by different researchers. There is also the issue of data processing. Current preprocessing techniques of the resulting time series have improved significantly with automated pipelines (Cieslak et al., 2018; described in Section 2.3). Nevertheless, even with these software tools it can be difficult to localize precisely the opening of the aortic valve (the B-point) within the ICG signal. These software tools require the researchers to build a classifier based off of 20 or more hand labeled B-points drawn from the full time series of data. For combined ICG-MRI experiments, the location of B-points is even more challenging and time consuming due to MRI-induced noise; 100 or more points must be manually labeled for classifiers to model an extended time series of data (Cieslak et al., 2018). Clearly, any technique that requires hand-labeling of the B-point, even if for just a subset of heartbeats, runs the risk of researcher bias. To address these challenges in subject preparation and data preprocessing, the following three experiments were conducted in collaboration with Biopac Systems Inc. to create and test new devices for measuring the dynamic moment-to-moment behavior of the ANS.

Chapter 3

Experiment 1: A Wearable Heart Monitor For Measuring Changes Of The Autonomic Nervous System Using an Electro-Resonator

3.1   Introduction

In the following experiment, a wearable heart monitor that directly records the opening and closing of the aortic valve was created in collaboration with Biopac Systems, Inc. to bypass the limitations of ICG in estimating ANS activity. An electro-resonator (a single round electrode with a frequency of 2.4 GHz) transmits electrical energy directly into the human body. In turn, the heart's mechanical motion influences the signal received by the resonator during each heartbeat, producing a continuous waveform that estimates the opening and closing of the aortic valve. During a single heartbeat, when paired with ECG, the time between the Q-point of the ECG and the first pulse from the resonator waveform (the opening of the aortic valve) provides us with a measure of the pre-ejection period (PEP; Figure 2.1). Accordingly, the time between the two pulses from the resonator (the opening and closing of the aortic valve) provide a measure of left-ventricular ejection time (LVET; Figure 2.1). PEP and LVET are discussed in further detail in Section 2.1.

In Part One of the study, researchers determined the ideal placement of the resonator that produced the most reliable signal. Afterwards, in Part 2, researchers tested whether the resonator was capable of comparably capturing PEP and LVET measures when paired with ECG as compared to ICG. Participants were fitted with the resonator, ICG, and ECG as they completed classical physiological stressors known to trigger a complex cascade of autonomic reflexes: the cold pressor task (CPT; Bullock et al., 2023; Kasagi et al., 1995; Kelsey et al.,

2007) and Valsalva maneuver (VM; Blackburn et al., 1973; Ermishkin et al., 2007; Gorlin et al., 1957; Levin, 1966; Novak, 2011). These stressors are typically accompanied by an initial parasympathetic bradycardia and increase in peripheral autonomic tone, followed by increased cardiac contractility that is based on sympathetic-related drive. The resulting measures of PEP and LVET obtained from each method (the resonator and ICG, respectively), paired with ECG, were confirmed to be comparable.

3.2   Methods

3.2.1   Participants

Ten healthy undergraduate and graduate students (4 females, average age 23 years +/- 4.5) at the University of California, Santa Barbara were recruited by word of mouth to participate in these two experiments, for which they were compensated US $10/hour. All participants provided informed consent in accordance with the Institutional Review Board/Human Subjects Committee, University of California, Santa Barbara. They passed a screening protocol for physiological recording experiments to exclude anyone with a cardiovascular abnormality. Six participants partook in Part One of the study to determine the placement of the resonator. In Part Two of the study, six of the participants were fitted with psychophysiological sensors, and completed both a cold pressor task and the Valsalva maneuver.

3.2.2   General procedure

In Part One of the study, the most reliable placement of the resonator was determined following one minute of data collection from each of the five classic auscultation points demonstrated in Figure 3.1a (Hanifin, 2010; Spiers, 2011). These five auscultation points are commonly used regions on the chest to listen to the heart with a stethoscope: (1) aortic, (2)

pulmonic, (3) Erb's point, (4) tricuspid, and (5) mitral. In Part Two of the study, researchers tested the resonator's reliability in estimating activity of the ANS by having participants complete both a 30 second VM and a one minute bilateral foot CPT. Each experimental condition began with a 1-minute baseline recording of ICG, ECG, and resonator time series as the participants were in a seated posture with their hands resting on their thighs, breathing regularly. At the researcher's signal, the participant engaged in one of the two stressors in a randomized order across subjects. Following each task, participants began a two minute recovery phase to allow sympathetic activity to return to baseline.
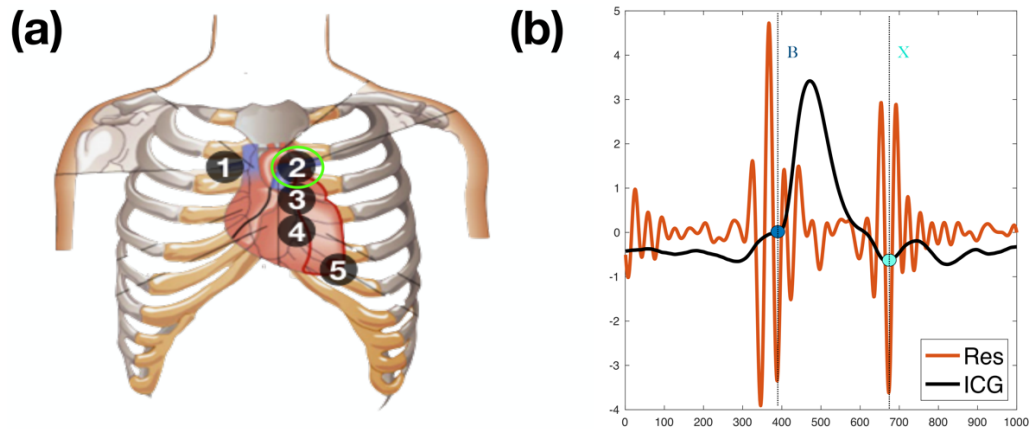
Figure 3.1 **(a)** The five classic heart auscultation points: (1) aortic, (2) pulmonic, (3) Erb's point, (4) tricuspid, and (5) mitral. In Part One, one minute of physiological data was collected from each of these auscultation points, at rest. Results showed auscultation point 2 (the pulmonic; circled in green) to be the most reliable. **(b)** The electro-resonator signal in red is shown overlaid on the impedance cardiography (ICG) signal in black. In dark blue, the B-point of ICG (representing the opening of the aortic valve) is lined up with the trough of the initial strong resonator pulse. In cyan, the X-point of ICG (the closing of the aortic valve) is lined up with the trough of the second resonator pulse.

3.2.3 Experiment protocol

For Part One of the study, six participants were recruited to determine the most reliable placement of the resonator over the heart. For each participant, the resonator surface was disinfected with an alcohol wipe and adhered to the skin with body tape at each auscultation point listed in Figure 3.1a. The participant was seated at rest and asked to limit any movement

while the researcher recorded one minute of data from each of the five auscultation points. Researchers compared the resulting data and determined that the second auscultation point produced the most robust waveform representing the closing and opening of the aortic valve (Figure 3.1b).

For Part Two of the study, researchers recruited six participants to undergo a one minute bilateral foot CPT and 30 second VM. Three of the participants from Part One of the study also partook in this second portion. Each participant's session was completed independently from the others. For each participant, ICG and ECG electrodes were placed on their neck, chest and torso following the procedure listed in Section 2.2. The resonator was disinfected with an alcohol wipe and adhered to the second auscultation point with body tape (Figure 3.2). In order to prevent the weight of the circuit board from interfering with the signal from the resonator, the circuit board was placed in a sling that hung around the participant's torso. The sling had a hole at the base, allowing the wire from the circuit board to pass through.
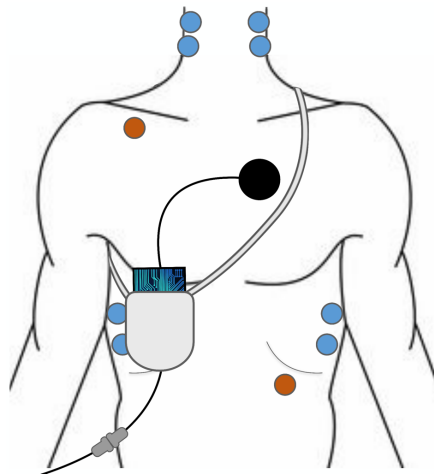
Figure 3.2   The electro-resonator (demonstrated by a single black round electrode connected to a circuit board) was placed on the pulmonic auscultation point on the chest, with the wire pointed to the left. The resonator's circuit board was placed inside a sling that wrapped around the neck and under the right arm. Eight electrodes used for the impedance cardiography (ICG) are shown in blue on either side of the neck and torso. Two electrodes used for the electrocardiogram (ECG) are shown in red under the right collarbone and left rib cage.

For each cold pressor task, the participant was seated barefoot in a chair with a large metal bucket placed in front of their feet. The bucket was filled with ice water at a temperature that varied between 33 °F – 36 °F. The participant sat at rest with both feet on a towel until a researcher signaled for them to submerge both of their feet in the ice bucket. The participant then swiftly moved their feet into the bucket, with their feet resting at the base and the water covering several inches above their ankles. They were instructed to make every effort to refrain from altering their position and to remain in their same relaxed and seated position with little to no movement apart from breathing. After one minute, the researcher instructed the participant to swiftly remove their feet from the bucket and place them back at their initial position on the towel and rest for another two minutes for the recovery period. Following this trial, each participant was given the opportunity to dry their feet with the towel and rest before the next task began, or before the experiment was concluded.

Prior to the VM task, researchers gave participants instructions on how to perform the VM: the participant was instructed to create pressure in their abdomen by holding their breath and simultaneously trying to breathe out. Participants were instructed to do their best to remain in the same resting posture during the VM and to refrain from any additional movements. Each VM task began with the participant seated in a chair in a standard resting posture with their hands resting on their thighs. After a one minute baseline period, a researcher instructed them to begin the VM. After 30 seconds, the researcher informed them that they may stop the VM and return to regular breathing for a two minute recovery phase.

3.2.4 Psychophysiology materials

All ICG and ECG materials and equipment were identical to those listed in section 2.2. The electro-resonator consisted of a single round electrode (2.5 cm diameter) connected to a

circuit board, which was then connected by a split cable to two DA100C amplifiers (Biopac Systems, Inc.). Both amplifiers were set to a gain of 1000, filtering the incoming signal with a low pass filter from 0.05 Hz – 300 Hz.

3.2.5 Resonator signal filtering and preprocessing

An initial infinite impulse response (IIR) bandpass filter of 10 Hz – 50 Hz was applied to the raw resonator signal. Then, an additional comb band stop filter fixed at 60 Hz was applied. Finally, an IIR bandpass filter was applied, fixed at 30 Hz. All of these filters were applied to the raw resonator signal in real-time. For preprocessing of the data, resonator detection algorithms were implemented into MEAP (described in Section 2.3) for preprocessing. The resonator waveform was imported as "doppler". At the "Label Waveform Points" step, the opening of the aortic valve in the doppler waveform ("DB") was set at the trough following the first major peak in the first pulse (Figure 3.3a). The closing of the aortic valve ("DX") was set at the trough following the first peak in the second pulse (Figure 3.3b). "DB" and "DX" align with the B- and X-points of the ICG waveform (Figure 3.4).

26
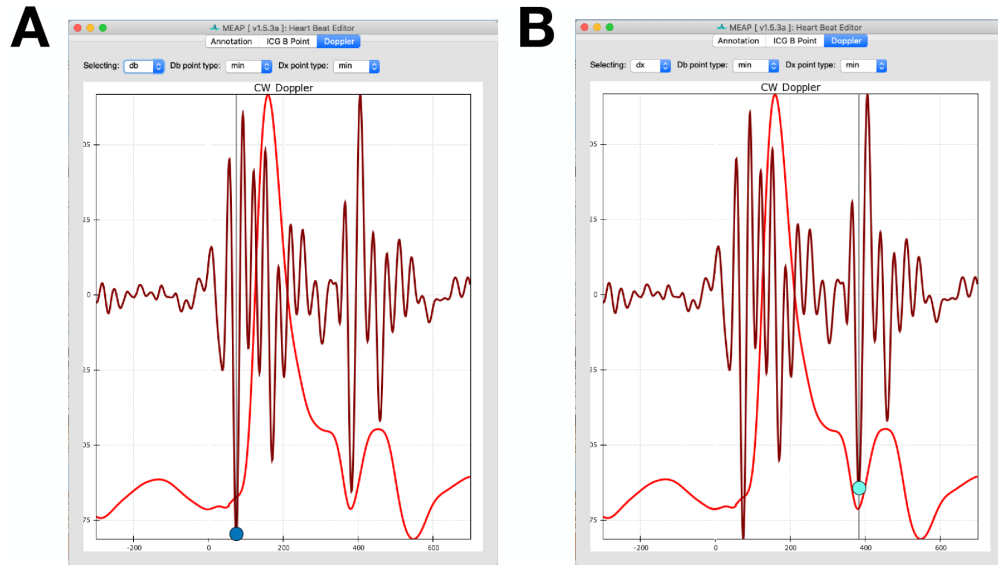
Figure 3.3 Preprocessing of the electro-resonator was implemented into the open-source Moving Ensemble Averaging Pipeline (MEAP) software **(a)** The opening of the aortic valve (labeled "DB") is marked at the trough of the first spike of the first pulse (in dark blue). **(b)** The closing of the aortic valve (labeled "DX") is marked at the trough of the first peak of the second pulse (in cyan).
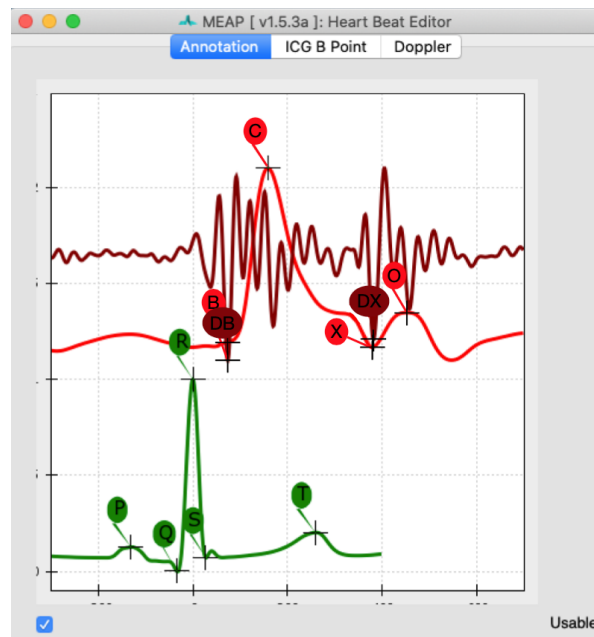
Figure 3.4 Impedance cardiography (ICG), resonator, and electrocardiogram (ECG) waveforms. The ICG waveform is in red, containing the opening of the aortic valve (the B-point), labeled "B", and the closing of the aortic valve (the X-point), labeled "X". The resonator waveform is in brown, with the opening of the aortic valve labeled "DB" and the closing of the aortic valve labeled "DX". The ECG waveform is in green, with each point of the complex labeled.

3.3 Results

In Part 1, both the directionality and physical placement of the electro-resonator greatly affected the signal-to-noise ratio. The pulmonic auscultation point (point 2), with the wire pointing directly to the left, was verified to be the most robust placement and directionality of the resonator across all six of the participants in Part One (Figure 3.2). In Part 2, beat-to-beat changes in PEP and LVET could be seen with the physical stressors across all participants when combining the ECG and resonator waveforms (Figure 3.5). It is readily visible that the resulting continuous PEP and LVET waveforms composed using the resonator are comparable to those from the ICG.
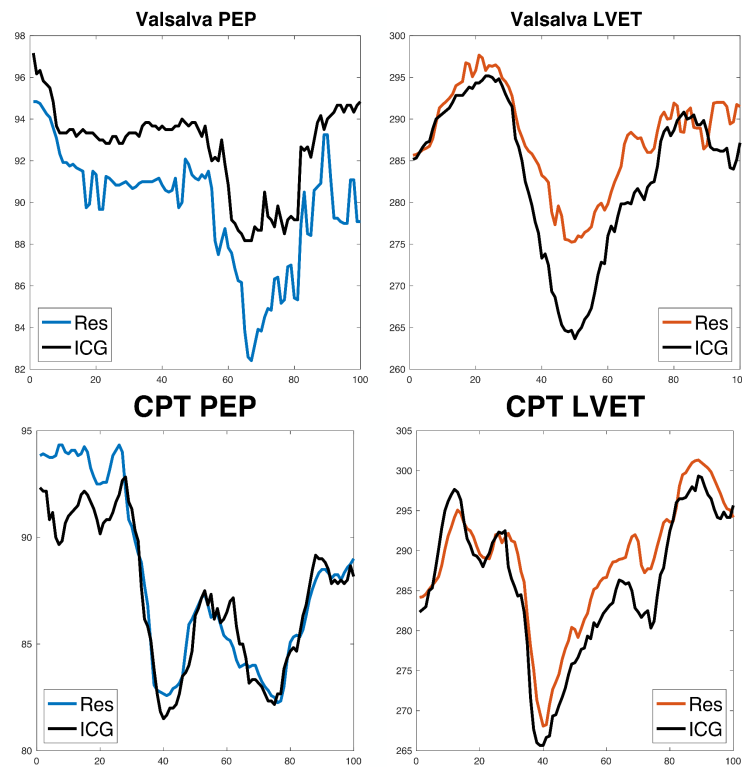
Figure 3.5 On the right, continuous data of pre-ejection period (PEP) for Valsalva and cold pressor task (CPT) are displayed with the electro-resonator signals in blue. On the left, continuous left ventricular ejection time (LVET) data for Valsalva and CPT are displayed, with the electro-resonator signals in red. All impedance cardiography (ICG) signals are represented in black. Beat-to-beat changes are seen comparably across both resonator and ICG signals following the classic stressors.

3.4   Discussion

With these findings, we introduced an innovative and additional method for acquiring high-temporal resolution recordings of cardiac contractility as a means for tracking changes of ANS activity, along with the accompanying software for preprocessing the data. The electro-resonator provided a faster and simpler application method for tracking the opening and closing of the aortic valve compared to the classic ICG application. In combination with a 3-lead ECG, the resonator provided estimates of dynamic beat-to-beat ANS activity (PEP and LVET) in response to two classic physical stressors. Limitations to the resonator included hyper-sensitivity to signal-to-noise ratio, likely caused by a combination of movement from the participant and sensitivity to the positioning of the device. Another limitation was the challenge in preprocessing the resonator data, as it was difficult to consistently identify which spike in the resonator signals to mark as the opening and closing of the aortic valves without the use of the ICG waveform for assistance. Moving forward, we created a second wearable heart monitor, with the goal that it may be more robust to signal artifacts and generate signals that are easier to preprocess (Experiment 2, Chapter 4).

Chapter 4

Experiment 2: An Accelerometer Based Heart Monitor to Measure Changes of the Autonomic Nervous System

4.1   Introduction

After running into detrimental problems with using an electro-resonator to measure the mechanical motion of the heart, researchers worked with Biopac Systems Inc. to create a simple wearable and wireless heart monitor that includes a 3-lead ECG, but replaces the eight electrodes needed for ICG with a single-lead accelerometer (ACC) (Figure 4.1b). The ACC is placed flat in the suprasternal notch of the neck. Here, it senses motion orthogonal to the skin surface associated with the abrupt onset and offset of blood flow in the region of the aortic arch and great vessels. The resulting ACC waveform is composed of two smooth waves identifying key physiological events for quantifying both PEP and LVET, where the first peak represents the opening of the aortic valve, and the second peak represents its closing.

In this Chapter, we find that the ACC device can cut down on the time necessary for subject preparation and provide wave forms that simplify the subsequent data analysis while improving reliability. We also compare ACC based measures of PEP and LVET with measures from conventional ICG, and demonstrate equivalence between the two apparatuses, both in terms of event-related moment-to-moment fluctuations, and also in their estimation of the latency of key events resulting from a well-known and strong physiological perturbation – the Valsalva maneuver. The Valsalva maneuver is a classic physiological stressor known to trigger

a complex cascade of autonomic reflexes, as described in Section 3.1 (Blackburn et al., 1973; Ermishkin et al., 2007; Gorlin et al., 1957; Levin, 1966; Novak, 2011).

4.2   Methods

4.2.1   Participants

Twenty healthy young adults (12 females, average age 23.6 years, +/- 3.6) were recruited to participate in this 1.5 hour study, for which they were compensated US $10/hour. All participants partook in a stressor condition where they performed the Valsalva maneuver. Nineteen participants performed a 2-minute seated baseline session (one participant was unable to perform the seated baseline due to timing constraints). Following the first eight participants, researchers were given the opportunity to add a third session, in which the remaining 12 participants partook in a 2-minute supine baseline session. All participants provided informed consent in accordance with the Institutional Review Board/Human Subjects Committee, University of California, Santa Barbara. They passed a screening protocol for physiological recording experiments to exclude anyone with a cardiovascular abnormality.

4.2.2   General procedure

Upon arrival, a researcher described the general procedure of the study. Participants then completed consent forms and the screening form of cardiovascular related disease. Participants were taken into a private room where they changed into a surgical scrub top. A trained female researcher placed eight ICG electrodes and three ECG electrodes on each participant. The electrodes used, the skin preparation procedure, and the ICG electrode placement, was identical to that described in Section 2.2.2. A total of three electrodes were

used for ECG (Figure 4.1b, in white, black and red), one placed just under the right collarbone, one under the left collar bone, and one on the upper left arm.

Participants were then taken to the experiment room and the ICG leads were connected to the respective hardware by carbon fiber leads. The ACC sensor was wiped down with an alcohol pad and allowed to dry between each participant. It was placed as flat on the suprasternal notch of the neck as possible with the wire oriented vertically and secured with 2 – 3 pieces of body tape (Figure 4.1a). Placement of all leads/sensors was standardized across participants and tasks. The ACC and ECG leads were permanently attached to an integrated wireless transducer that was placed in the pocket of the scrub shirt. During cardiovascular setup, the researcher reviewed the importance of minimizing any and all movements of the seated posture throughout the course of the study in order to reduce noise in the cardiovascular readings. Researchers estimated the time required to prepare each subject for the ACC method, from the start of skin exfoliation until the placement of the third ECG electrode. They added an estimate of the remainder of the time taken to apply the ICG electrodes, up until the recording of the inter-electrode ICG measurement, with the ACC time to produce an overall ICG preparation estimate. A minute was added to the ACC estimate to account for it being secured to the neck.
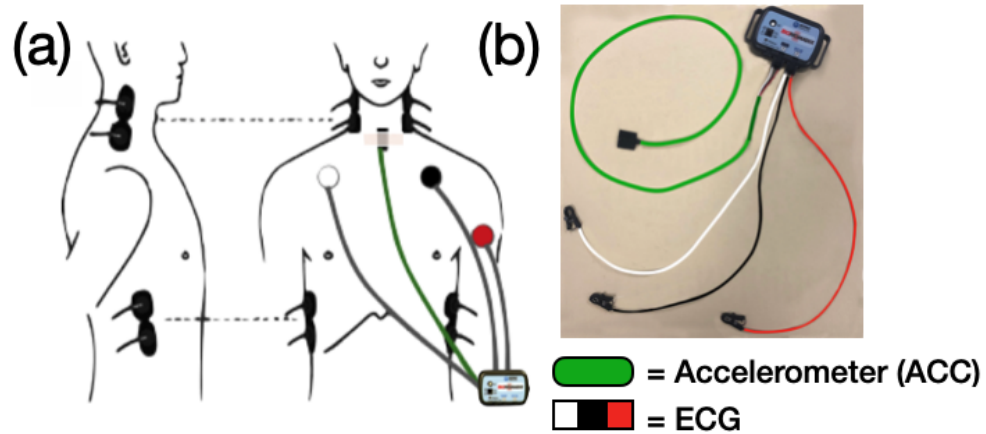
Figure 4.1 Impedance cardiography (ICG) and electrocardiogram (ECG) setup and the accelerometer device (ACC) **(a)** Experiment setup of the eight ICG electrodes (in black on either side of the neck and ribs), three ECG electrodes (white lead placed under right collarbone, black lead under the left collarbone, and red lead on the left tricep), and the ACC sensor (black rectangle secured in place with body tape at the suprasternal notch). ECG and ACC sensors are all connected to the BioNomadix wireless transducer. **(b)** A Biopac Systems Inc. BioNomadix wireless transducer with three leads for ECG (represented by white, black, and red) and a single accelerometer (in green).

4.2.3 Experiment protocol

To test the ACC's reliability, a validation study was completed with a 15 second Valsalva maneuver. Each experimental condition began with a 2-minute baseline recording of ICG, ECG and ACC time series as the participants were in a seated posture with their hands resting on their thighs, breathing regularly. For each Valsalva trial, the participant was seated in a chair in a standard resting posture with their hands resting on their thighs. After a one minute baseline, a researcher instructed them to begin the Valsalva maneuver. The instructions for this maneuver were standardized between participants to "bear down" on their abdominal muscles as if they were lifting something very heavy, creating a large amount of pressure in their gut region, and to hold this maneuver until the researcher told them to release. Prior to this, each participant was instructed to do their best to remain in the same posture and to refrain as much as possible from any additional movement. After 15 seconds, the researcher informed

the participant that they may release the Valsalva and return to regular breathing for a 2-minute recovery phase to allow autonomic activity to return to baseline. We had the opportunity to run 12 of the participants in an additional 2-minute condition in a supine position, lying flat on a gurney with their arms at their sides in the same experiment room.

4.2.4   Psychophysiology materials

Non-invasive physiological recording equipment was used for continuous real-time data acquisition throughout the study. All physiology equipment and software was from Biopac Systems, Inc. (Goleta, CA). Signals were integrated using the MP160 and collected at 2 kHz sampling rate. The ACC and ECG data were collected using a modified BN-RSPEC BioNomadix Transmitter to create a new "Cardio-Seismic" wireless transmitter unit. This unit employed a detachable +/- 2 G accelerometer containing very low noise (20uG/sqrt(Hz)). The respiration input channel was modified to accommodate the accelerometer, while the ECG channel was left as is. ACC raw data was filtered from 0.1 Hz – 100 Hz. The ECG channel was filtered in real time from 1 Hz – 35 Hz (the default bandwidth setting for that amplifier). However, additional filters were added using AcqKnowledge later in the processing chain (detailed in Section 4.2.5). ICG was collected using a NICO100C amplifier, with settings adjusted to filter at DC (no filter) – 10 Hz. All of these settings were kept constant across the sessions and therefore any delay contributions would be stable. All signals were displayed and stored on a laptop running AcqKnowledge software version 5.0.2.

4.2.5   ACC signal filtering

An initial finite impulse response (FIR) bandpass filter of 20 – 30 Hz was applied to the ACC signal. The signal was then converted to its absolute value, after which an additional

low pass filter of 15 Hz was applied. Finally, mean-value smoothing was applied at a smoothing factor of 221 samples. All these filters were applied post-collection and pre-processing. Following these filters, researchers were able to convert the original ACC signal into two smooth waves, with the first wave's peak indicating the opening of the aortic valve, and the second wave's peak indicating the closing (Figure 4.2a). Collectively, these measures are capable of potentially replacing the entire ICG setup, as the main points necessary to measure the SNS and other ANS perturbations are the mechanistic movement of the aortic valves (Figure 4.2b).
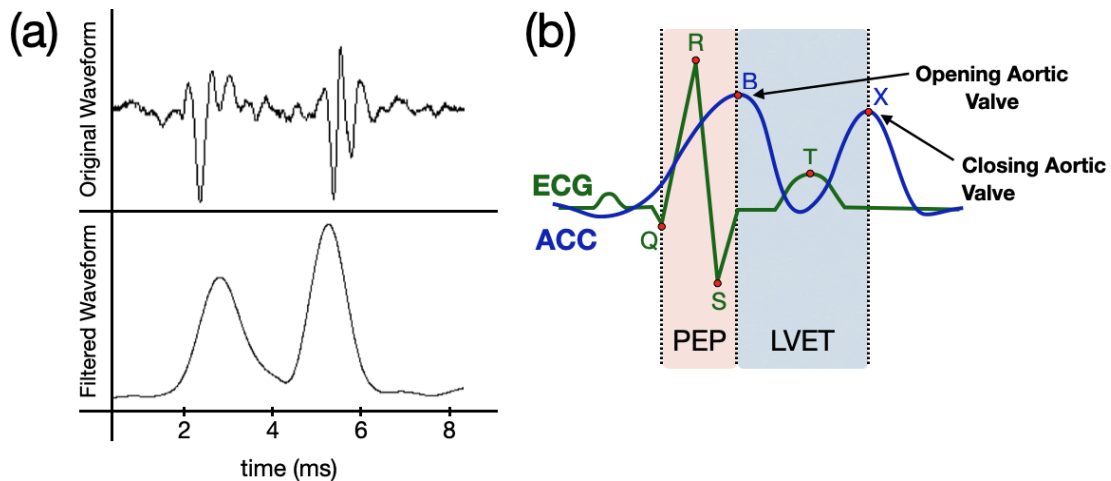
Figure 4.2 Extracting pre-ejection period (PEP) and left ventricular ejection time (LVET) using characteristic electrocardiogram (ECG) and filtered accelerometer (ACC) waveforms. **(a)** Original ACC waveform of a single heartbeat representing movement in the z-direction of the mechanistic pulse wave moving through the trachea, displayed above the filtered waveform. The first peak of the filtered waveform is analyzed as the opening of the aortic valve (the B-point). The 2nd peak is analyzed as the closing (the X-point). **(b)** The filtered ACC waveform (in blue) is displayed overlapping the ECG waveform (in green). The peak of the first waveform of the ACC is labeled as the B-point (opening of the aortic valve), while the peak of the second waveform is labeled as the X-point (closing of the aortic valve). The time interval between the Q-point of the ECG waveform and B-point peak of the ACC is measured as PEP. The time interval between the b- and x-peak of the ACC is measured as LVET.

4.2.6　Psychophysiology preprocessing

Analysis of the ICG time series, including preprocessing and B-point and X-point labeling using the open-source Moving Ensemble Analysis Pipeline (MEAP) has been described in detail previously (Cieslak et al., 2018). The MEAP software was modified to also import the filtered ACC time series where automated B- and X-point labels were applied to the two peaks of the ACC signal. Trained researchers manually checked each classification and edited out any artifacts in the ICG and ACC time series. The automation of ACC time point classifications required little to no outlier edits, while the same time point estimations for ICG required significant outlier detection and hand labeling. For this study, the ICG and ACC data were each combined with the ECG times series and processed with a moving ensemble-average along a 15 second window, allowing for continuous estimations of two physiological measures of interest: PEP and LVET. Researchers estimated the time required to perform manual checking of standard ICG and ACC time series. For ACC, this time was estimated from the start of opening the file in MEAP, up until the completion of the correction of any obvious outliers following the initial computation of moving ensembles. Following this step, the researcher created an ICG B-point classifier based on 25 hand-labeled B-points, applied this classifier to the data, and repeated the correction for outliers. This remaining time was added to the previous ACC estimate to create an ICG analysis estimate. To control for reliability across researchers scoring the data, the same researcher analyzed within-participant trials.

4.2.7 Statistical analyses

To compare the ICG and ACC derived physiology time series we conducted four analyses. The first analysis estimated the overall similarities between moment to moment fluctuations recorded by both sensors. We computed a summarized delta time series for each measure: change in average activity across successive five second windows. For both PEP and LVET, and in each of the seated, supine and Valsalva conditions, we tested the similarities between the ICG and ACC delta time series across subjects. To this end, we used a linear mixed effects (random intercept) model that tested for agreement between moment-to-moment changes in our physiological indices (PEP, LVET) recorded with ICG and ACC. Given the relatively small size of this exploratory sample, we also included a hierarchical Bayesian analogue of the linear mixed effects model (hierarchical regression), to directly capture the uncertainty of our estimated model parameters in a manner that accounts for between subject variability.

In the second analysis we assessed whether both sensors would estimate similar latency of event-related peak physiological change during our Valsalva stressor condition. For this, we used a hierarchical Bayesian changepoint model; the model predicts the likelihood that the summarized delta time series have two means. From these two distributions a switchpoint can be identified. In theory, one side of the peak should be predominantly unidirectional and a mean of one sign, while the return to baseline should be unidirectional in the opposite direction. The switchpoint therefore estimates the critical point when there is a maximal change between distributions, without assuming signal valence. If the ACC is similar to ICG then this switchpoint should be at the same time.

In the third and fourth analyses, we examined the internal consistency (i.e., within session reliability) and criterion validity (i.e., cross-instrument), separately for each subject, and for PEP and LVET values expressing the percentage change in the Valsalva condition, relative to the baseline condition at each data point. To align baseline and Valsalva conditions for meaningful percentage-change estimation, all sessions were cropped to the first 120 seconds worth of data and linearly resampled to provide one estimate of physiology (PEP or LVET) at each second.

All linear mixed effects models were fitted using the lmerTest (Kuznetsova et al., 2017) package in R (version 4.2.1, R Core Team, 2020). Bayesian hierarchical regression, changepoint , internal consistency and criterion validity analyses were run using PyMC3 (Salvatier et al., 2016) libraries in Python 3. All other data preprocessing was carried out in MATLAB version 2020a.

4.3   Results

We found that the ACC method cut down on human labor estimates from about 20 minutes for application/preparation and one hour for analysis per one hour of data collected, to about five minutes of application and 20 minutes of analysis per hour of data. To compare the results between the performance of the ACC and ICG, we examined the time courses of two temporal features (PEP and LVET), using our two different methods (the ACC and ICG). The following analyses were used to determine the validity of the ACC compared to the classic ICG method for both PEP and LVET measures. Mean and standard deviation for both ACC and ICG-derived PEP and LVET are summarized in Figures 4.3 and 4.4.

1. *Linear mixed effects (random intercept) model.* We tested the similarities between the ICG and ACC delta time series across participants. For instance, as ICG's PEP values change, does the ACC's PEP change with it? We fitted separate models for PEP and LVET, in each case modeling the signals measured by ICG as a function of the signals measured from ACC. The model fitted a single parameter ACC and a separate intercept for each subject (random intercept model).

2. *Hierarchical Bayesian delta regression.* The concern with the random intercepts model (which only fits a single ACC beta to account for all subjects) is that significant effects may be driven by a single outlier participant. To mitigate the effects of individual participants, we ran a Bayesian regression as a group-based analysis. This analysis method estimates the parameters (mu and sigma) of a hierarchical Gaussian distribution, from which each subject's ACC beta is drawn. Significance at the group level is determined by the posterior distribution of the hierarchical distribution's mu parameter exceeding 0, using a 94% highest density interval (HDI). In other words, allowing for individual differences, the mean of the distribution that characterizes betas across all subjects is confidently above or below 0.

3. *Hierarchical Bayesian changepoint in delta time course.* While the previous two analyses were performed for all three trials (seated baseline, supine, and Valsalva), this changepoint analysis was only performed on the Valsalva condition. For these Valsalva trials, we assume that the physiologic measure (either PEP or LVET) will undergo a significant change at some time point after the initiation of the maneuver. Thus, we assume deltas in the time series of each measure can be best categorized by two distributions, one distribution for a change in one direction (e.g., with a positive mean

delta if measure increases) and another, with an opposite signed mean when the measure returns to baseline. We also estimate the changepoint, i.e., the point in time that most likely reflects when the observed deltas transition from being best summarized by one distribution to the other. In other words, this model determines when the critical point of an event-related change in deltas occurs in both LVET and PEP (peak max or peak min) in response to the Valsalva maneuver, without a priori assumptions on the direction of change. This analysis was performed only on the Valsalva trials.

4. *Internal Consistency.* We measured the consistency of each subject's data recorded across discrete moments in time. For each of the eight measurements - two conditions (BL,V), two sensors (ACC, ICG) and two physiology measures (PEP, LVET) - we computed a second-by-second estimate of the standard deviation (SD) of the distribution for that measurement across subjects. We fitted these SD values using a Bayesian model. By computing a posterior for each SD, we could compare the SD at every timepoint, with the SD for each other time point for a given measurement. The results confirm very strong internal consistency for all measurements. Within each of the eight measurements, we saw no strong evidence that the SD across subjects at any timepoint was credibly different to those at all other timepoints (See Supplementary Materials for an exhaustive pairwise departure analysis). We conclude that both ICG and ACC record consistent measures of both PEP and LVET across subjects at discrete moments in time, in both the baseline and Valsalva condition (Figures 4.5b and 4.6b).

5. *Criterion Validity.* We assessed criterion validity between departures from the baseline condition driven by the Valsalva condition. For both PEP and LVET, we computed the

40

percentage difference between each timepoint of the Valsalva condition and the corresponding timepoint in the baseline condition (% Δ V-BL), for both ACC and ICG for each subject. We then used a Bayesian model to estimate the mean of the distribution of subjects' (% Δ V-BL) at each second in time for both ICG and ACC. Sampling each timepoint's posterior for mean (% Δ V-BL – ICG) and mean (% Δ V-BL – ACC), we computed a distribution of Pearson coefficients that quantified the relation between ICG Valsalva-baseline departure and ACC Valsalva-baseline departure across 120 seconds of data. For both PEP and LVET, this n = 10,000 simulation produced a distribution of all positive coefficients, confirming a strong association between measurements derived by the ACC and ICG, using a procedure that accounted for the random effects at each timepoint due to individual difference (Figures 4.5a and 4.6a).

subject	Baseline - PEP				Baseline - LVET			
	mu_icg	sd_icg	mu_acc	sd_acc	mu_icg	sd_icg	mu_acc	sd_acc
1	107	2.59	123	5.22	305	6.29	317	6.99
2	88	1.53	130	1.49	281	3.14	222	3.85
3	85	3.26	151	2.49	317	4.41	279	5.35
4	68	2.42	120	9.07	266	6.04	256	7
5	62	2.19	97	2.51	254	4.76	243	2.7
6	81	1.09	171	2.16	269	1.74	217	5.25
7	86	3.54	108	5.01	332	5.85	306	8.55
8	80	2.29	135	6.64	241	2.24	215	5.57
9	77	2.53	118	2.46	287	2.26	287	4.41
10	73	1.12	108	1.76	313	3.44	275	3.96
11	88	2.59	121	7.17	283	3.57	259	7.1
12	76	2.15	113	7.96	308	2.46	295	4.89
13	81	2.46	75	6.09	277	6.06	301	5.34
15	95	1.65	142	3.7	307	4.39	275	5.33
16	50	5.42	240	3.41	276	8.87	279	9.24
17	72	2.66	102	4.36	325	3.37	298	4.9
18	82	2.3	116	9.25	316	13.65	310	11.32
19	96	3.46	122	3.6	284	3.45	251	3.64
20	81	2	144	5.11	282	3.95	267	6.43
mu	80.42	2.5	128.21	4.71	290.68	4.73	271.2	5.9
sd	12.71	0.98	34.41	2.44	24.8	2.79	31.18	2.12

Figure 4.3   Summary data for pre-ejection period (PEP) and left ventricular ejection time (LVET) for the baseline condition. Mean (mu) and standard deviations (sd) for both the accelerometer (ACC) and impedance cardiography (ICG)-derived PEP and LVET (across the entire session). Participant 14 did not have a baseline condition.

subject	Valsalva - PEP				Valsalva - LVET			
	mu_icg	sd_icg	mu_acc	sd_acc	mu_icg	sd_icg	mu_acc	sd_acc
1	108	4.4	137	9.6	300	9.14	304	10.35
2	78	5.06	124	6.88	271	7.77	218	7.66
3	84	5.15	151	10.31	315	17.46	282	12
4	72	4.92	129	12.26	267	9.98	244	5.09
5	52	6.91	92	7.66	257	17.14	244	11.84
6	79	6.29	173	15.16	266	15.62	211	16.03
7	87	6.96	119	12.16	329	23.58	289	19.95
8	75	7.93	128	14.86	243	6.27	219	12.57
9	75	3.96	118	6.89	286	9.77	291	10.44
10	70	2.47	108	6.67	313	7.89	279	8.61
11	77	10.37	115	16.54	291	9.28	272	11.58
12	76	2.91	118	7.25	307	8.86	294	10.17
13	78	2.53	77	9.28	271	3.98	294	9.25
14	70	3.22	131	5.37	264	8.74	252	7.19
15	91	12.76	148	8.01	315	11.46	269	10.4
16	52	10.54	242	14.1	284	25.88	283	31.48
17	73	9.65	115	8.46	318	15.86	280	16.25
18	79	4.08	116	7.4	309	16.42	302	13.46
19	103	3.38	124	4.75	268	8.6	239	6.65
20	78	7.45	138	13.13	300	11.98	280	14.44
mu	77.85	6.05	130.15	9.84	288.7	12.28	267.3	12.27
sd	13.33	2.98	33.36	3.52	24.3	5.7	29.03	5.77

Figure 4.4   Summary data for pre-ejection period (PEP) and left ventricular ejection time (LVET) for the Valsalva condition. Mean (mu) and standard deviations (sd) for both the accelerometer (ACC) and impedance cardiography (ICG)-derived PEP and LVET (across the entire session).
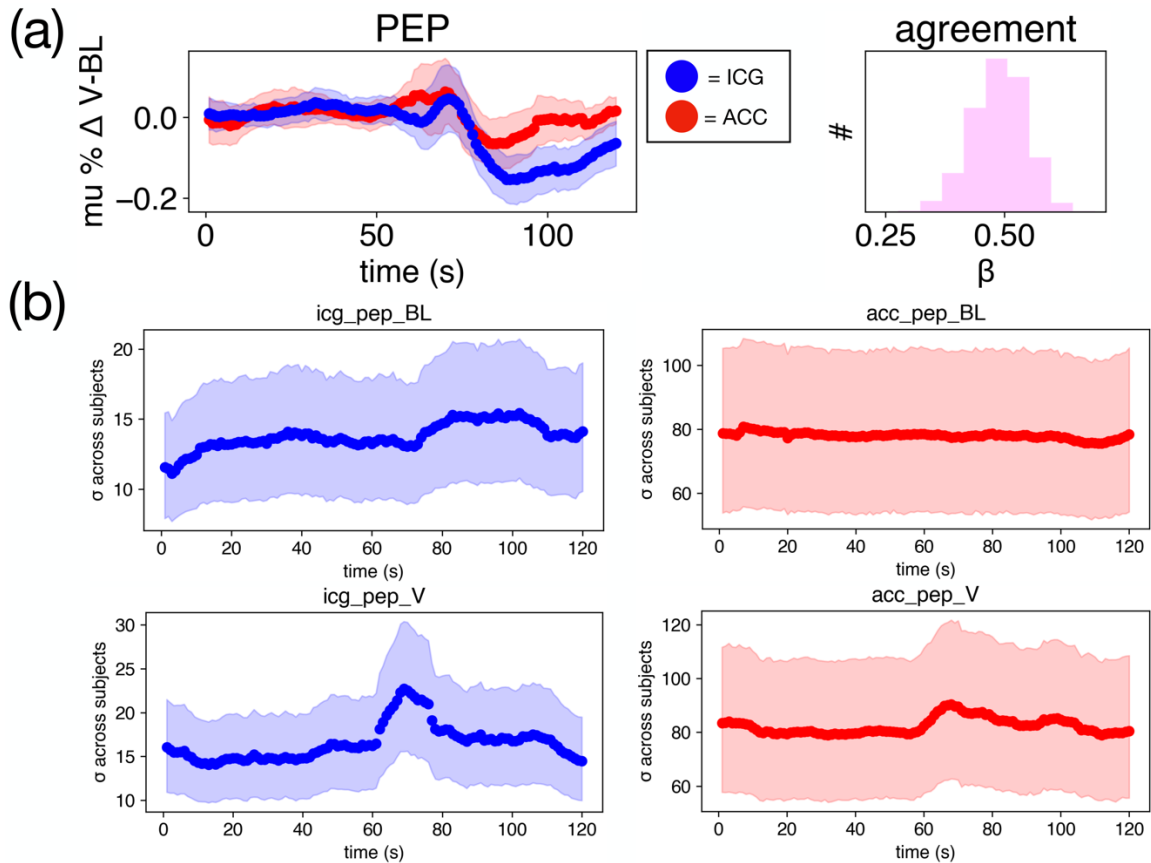
Figure 4.5 Pre-ejection period (PEP) PEP internal consistency and criterion validity. **(a)** Criterion validity between departures from the baseline condition driven by the Valsalva condition (% Δ V-BL). For impedance cardiography (ICG; blue) and accelerometer (ACC; red) we estimated the mean (% Δ V-BL – dots) across subjects at each data point, with the shaded region reflecting the HDI of each mean estimate. Agreement histogram on the right represents the distribution of Pearson correlation coefficients from n = 10,000 draws from the (% Δ V-BL – ACC) and (% Δ V-BL – ICG) posteriors at each data point. **(b)** Dots show the mean of the posterior estimating the standard deviation across subjects at each data point, while the shaded region depicts the HDI, i.e., the credible range of variability across subjects at each moment in time.
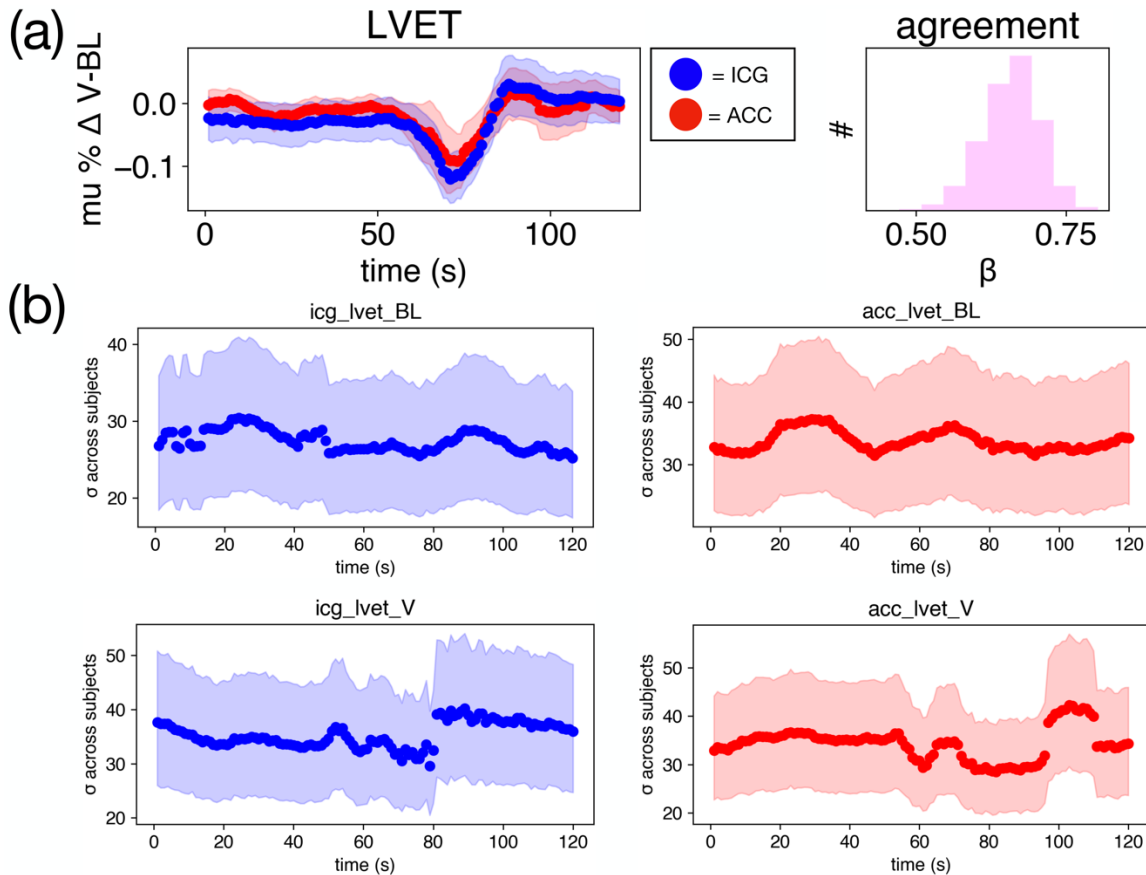
Figure 4.6 Left ventricular ejection time (LVET) internal consistency and criterion validity. **(a)** Criterion validity between departures from the baseline condition driven by the Valsalva condition (% Δ V-BL). For impedance cardiography (ICG; blue) and the accelerometer (ACC; red) we estimated the mean (% Δ V-BL – dots) across subjects at each data point, with the shaded region reflecting the HDI of each mean estimate. Agreement histogram on the right represents the distribution of Pearson correlation coefficients from n = 10,000 draws from the (% Δ V-BL – ACC) and (% Δ V-BL – ICG) posteriors at each data point. **(b)** Dots show the mean of the posterior estimating the standard deviation across subjects at each data point, while the shaded region depicts the highest density interval (HDI), i.e., the credible range of variability across subjects at each moment in time.

4.3.1 Pre-ejection period (PEP)

Overall, PEP measures collected using the ACC closely followed PEP measures from ICG. Results of the linear mixed effects model for 19 participants in a seated 2-minute baseline confirmed a positive relationship between the delta of the ACC's PEP with the ICG's PEP (β = 0.216, SE = 0.059, p < 0.001). In the Bayesian delta regression of the same baseline period,

45

the mean of the hierarchical posterior distribution of subjects' beta values was 0.102 with a

94% HDI of -0.012, 0.218], indicating a marginally positive relationship between ACC and

ICG recorded PEP perturbations (Figure 4.7).

Figure 4.7   Pre-ejection period (PEP) 2-minute seated baseline hierarchical Bayesian delta regression model. **(a)** Summarized delta time series for each of the accelerometer's (ACC) and impedance cardiography's (ICG) pre-ejection period (PEP), each time point reflects the change (delta) in average activity across successive five second windows. Light gray lines represent data from individuals, while dashed black lines represent the central tendency. **(b)** A Bayesian estimate of the mean of a Gaussian distribution from which each subject's beta parameter (modeling ICG as a function of ACC) is drawn. The blue line denotes the 94% highest density interval (HDI). Most of the HDI above 0 reflects a marginally positive relationship between the deltas estimated with ICG and ACC.

Results of the linear mixed effects model for 12 participants in a supine 2-minute

baseline confirmed a positive relationship between the delta of the ACC's PEP with the ICG's

PEP ($\beta = 0.216$, SE = 0.059, $p < 0.001$). In the Bayesian delta regression of the same baseline

period, the mean of the hierarchical posterior distribution of subjects' beta values was 0.079

with a 94% HDI of [-0.016, 0.182], indicating a marginally positive relationship between the

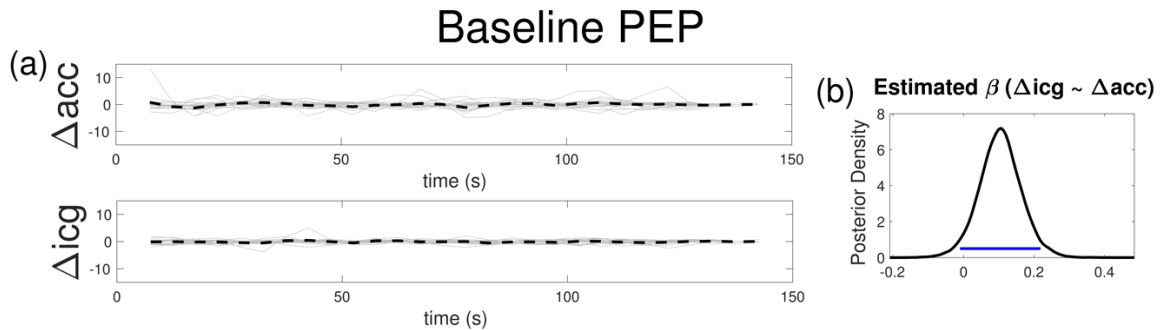ACC and ICG recorded PEP perturbations (Figure 4.8).

Figure 4.8   Pre-ejection period (PEP) 2-minute supine hierarchical Bayesian delta regression model. **(a)** Summarized delta time series for each of the accelerometer's (ACC) and impedance cardiography's (ICG) pre-ejection period (PEP), each time point reflects the change (delta) in average activity across successive five second windows. Light gray lines represent data from individuals, while dashed black lines represent the central tendency. **(b)** A Bayesian estimate of the mean of a Gaussian distribution from which each subject's beta parameter (modeling ICG as a function of ACC) is drawn. The blue line denotes the 94% highest density interval (HDI). Most of the HDI above 0 reflects a positive relationship between the deltas estimated with ICG and ACC.

Results of the linear mixed effects model for 20 subjects performing Valsalva confirmed a positive relationship between the delta of the accelerometer's PEP with the ICG's PEP ($\beta = 0.688$, SE = 0.097 p < 0.001). Additionally, in the Bayesian delta regression during the Valsalva, the mean of the hierarchical posterior distribution was 0.168 with a 94% HDI of [0.076, 0.259], indicating a positive relationship between ACC and ICG recorded perturbations (Figure 4.9a). The Bayesian changepoint model estimated that peak ICG-recorded PEP change occurred at 82.79 seconds (posterior mean; note that the Valsalva onset was at 60 seconds), while the peak of ACC-recorded PEP change occurred at 80.75 seconds (posterior mean). In both cases, the changepoints characterizing these peaks marked the point in time where the delta of PEP went from a negative to a positive slope (Figure 4.9c), consistent with the expected increase in sympathetic drive following the Valsalva. Of note, the ICG's changepoint 94% HDI [73.4, 92.3] fell 100% within the ACC's changepoint 94% HDI [69.15, 92.35]. We therefore observe overall strong agreement between PEP measures recorded from the ACC and ICG in

all trials (baseline, supine, and Valsalva), with the strongest positive relationship occurring in the Valsalva condition.

Valsalva PEP

Figure 4.9 Valsalva pre-ejection period (PEP) hierarchical Bayesian models. The blue line denotes the 94% highest density interval (HDI). Most of the HDI above 0 reflects a positive result. **(a)** A Bayesian estimate of the mean of a Gaussian distribution from which each subject's beta parameter (modeling ICG as a function of ACC) is drawn. **(b)** Summarized delta time series for each of the accelerometer's (ACC) and impedance cardiography's (ICG) pre-ejection period (PEP), each time point reflects the change (delta) in average activity across successive five second windows. Light gray lines represent data from individuals, while dashed black lines represent the central tendency. **(c)** A Bayesian model that estimated the latency of peak event-related change driven by the Valsalva, separately for the ACC and ICG recorded PEP. The latency of this peak is the modeled changepoint between two distinct distributions of delta values (in this case mostly negative distribution and a mostly positive distribution).

4.3.2 Left ventricular ejection time (LVET)

Results of the linear mixed effects model for 19 participants during baseline recording confirmed a positive relationship between the delta of the ACC's LVET with the ICG's LVET ($\beta = 0.885$, SE $= 0.118$, $p < 0.001$). In the Bayesian delta regression of the LVET recorded during baseline, the mean of the hierarchical posterior distribution of subjects' beta values was

0.349 with a 94% HDI of [0.213, 0.499], supporting a positive relationship between ACC and

ICG recorded LVET perturbations during a seated baseline (Figure 4.10).
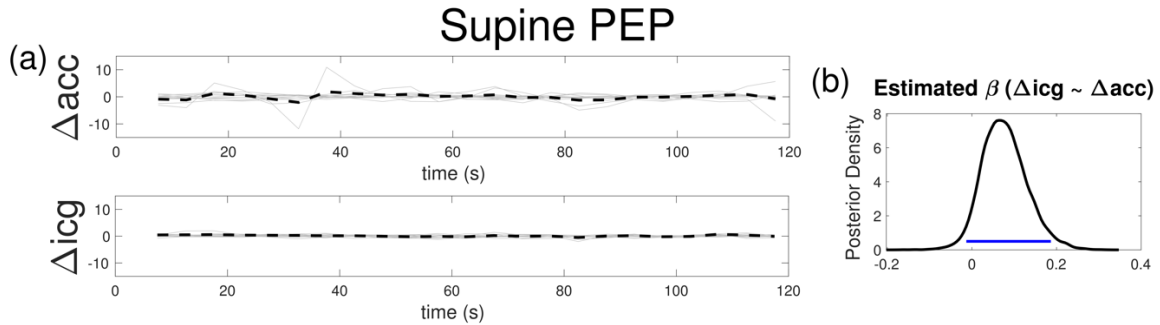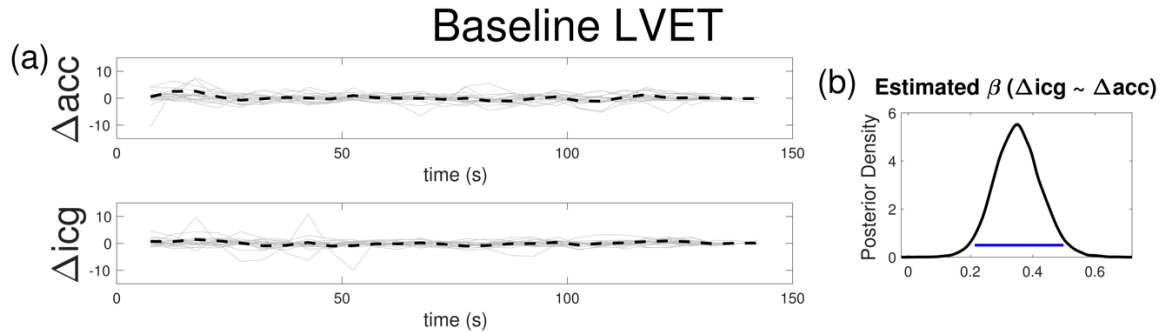

Figure 4.10   Left ventricular ejection time (LVET) 2-minute baseline hierarchical Bayesian delta regression model. **(a)** Summarized delta time series for each of the accelerometer's (ACC) and impedance cardiography's (ICG) LVET, each time point reflects the change (delta) in average activity across successive five second windows. Light gray lines represent data from individuals, while dashed black lines represent the central tendency. **(b)** A Bayesian estimate of the mean of a Gaussian distribution from which each subject's beta parameter (modeling ICG as a function of ACC) is drawn. The blue line denotes the 94% highest density interval (HDI). Most of the HDI above 0 reflects a positive relationship between the deltas estimated with ICG and ACC.

Results of the linear mixed effects model for 12 participants during supine recording

showed no relationship between the delta of the ACC's LVET with the ICG's LVET ($\beta = -0.014$, SE $= 0.1$, p > 0.1). In the Bayesian delta regression of LVET recorded during the supine

condition, the mean of the hierarchical posterior distribution of subjects' beta values was 0.178

with a 94% HDI of [-0.021, 0.401], indicating a marginally positive relationship between the

ACC and ICG recorded LVET perturbations while lying in a supine position (Figure 4.11).
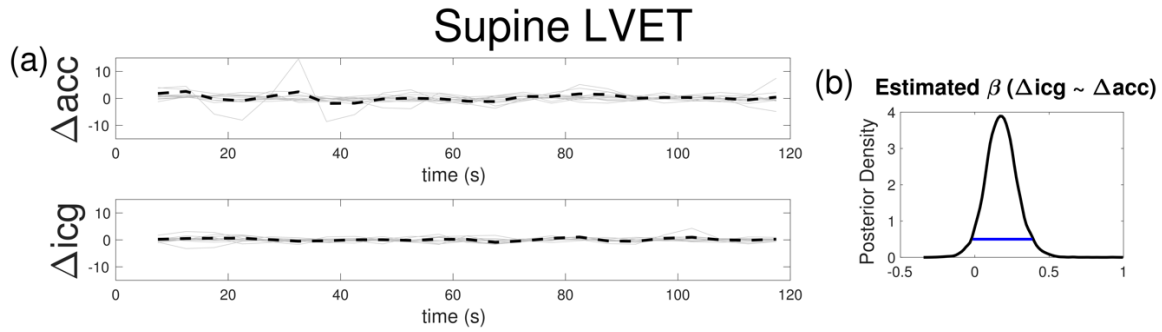
Figure 4.11 Left ventricular ejection time (LVET) 2-minute supine hierarchical Bayesian delta regression model. **(a)** Summarized delta time series for each of the accelerometer's (ACC) and impedance cardiography's (ICG) LVET, each time point reflects the change (delta) in average activity across successive five second windows. Light gray lines represent data from individuals, while dashed black lines represent the central tendency. **(b)** A Bayesian estimate of the mean of a Gaussian distribution from which each subject's beta parameter (modeling ICG as a function of ACC) is drawn. The blue line denotes the 94% highest density interval (HDI). Most of the HDI above 0 reflects a positive relationship between the deltas estimated with ICG and ACC.

Results of the linear mixed effects model for 20 subjects performing Valsalva confirmed a positive relationship between the delta of the ACC's LVET with the ICG's LVET ($\beta = 3.581$, SE = 0.208, $p < 0.001$). In the Bayesian delta regression of LVET during Valsalva, the mean of the hierarchical posterior distribution of subjects' beta values was 0.459 with a 94% HDI of [0.289, 0.631], supporting this positive relationship between ACC and ICG recorded LVET perturbations during a Valsalva (Figure 4.12a). The Bayesian changepoint model estimated that peak ICG-recorded LVET change occurred at 79.1 seconds (posterior mean; note that the Valsalva onset was at 60 seconds), while the peak of ACC-recorded LVET change occurred at 78.6 seconds (posterior mean). In both cases the changepoints characterizing these peaks marked the point in time where the delta of LVET went from a positive to a negative slope (Figure 4.12c), consistent with the expected increase in autonomic drive following the Valsalva. Of note, the 94% HDI of the ACC's changepoint [69.1, 87.95] fell 94.15% within the HDI of the ICG's changepoint [70.25, 91.55]. We therefore observe

strong agreement between LVET measures recorded from the ACC and ICG in both baseline

and Valsalva trials, with the strongest positive relationship occurring in the Valsalva condition.

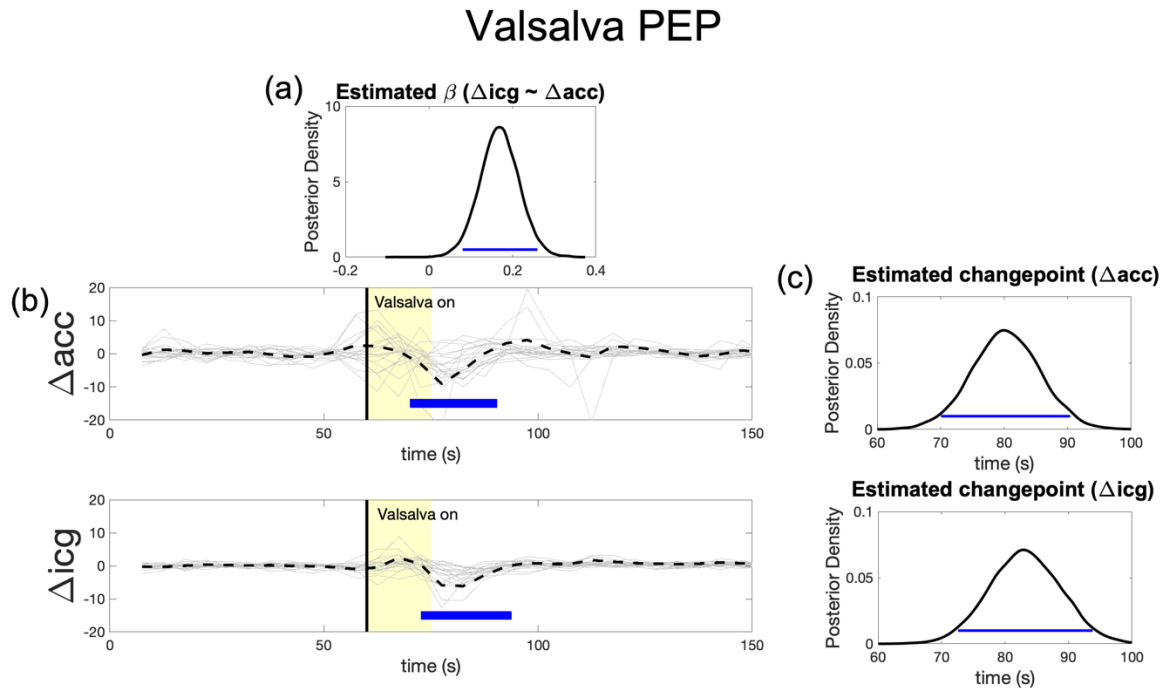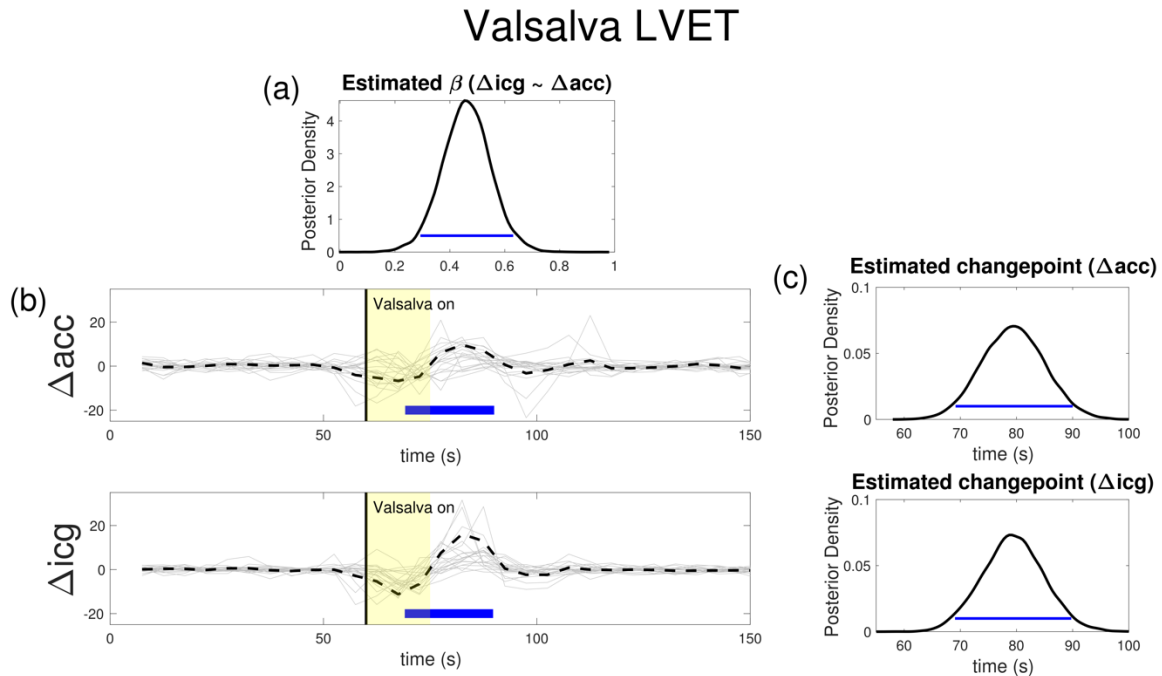## Valsalva LVET

Figure 4.12   Valsalva left ventricular ejection time (LVET) hierarchical Bayesian models. The blue line denotes the 94% highest density interval (HDI). Most of the HDI above 0 reflects a positive result. **(a)** A Bayesian estimate of the mean of a Gaussian distribution from which each subject's beta parameter (modeling ICG as a function of ACC) is drawn. **(b)** Summarized delta time series for each of the accelerometer's (ACC) and impedance cardiography's (ICG) LVET, each time point reflects the change (delta) in average activity across successive five second windows. Light gray lines represent data from individuals,while dashed black lines represent the central tendency. **(c)** A Bayesian model that estimated the latency of peak event-related change driven by the Valsalva, separately for the ACC and ICG recorded LVET. The latency of this peak is the modeled changepoint between two distinct distributions of delta values (in this case mostly negative distribution and a mostly positive distribution).

4.4   Discussion

The main goal of the present study was to investigate whether a single contact

accelerometer device could sufficiently measure dynamic changes of the sympathetic nervous

system (PEP) and preload effects on the heart (LVET) as compared to the eight electrode ICG.

Overall, the results indicate a positive relationship between the ACC and ICG's values of PEP

and LVET. This study demonstrates that the simpler ACC could act as a complementary method of quantifying event-related changes in both PEP and LVET.

Notably, the exact moment of opening and closing of the aortic valve within the raw ACC waveform was not readily decipherable prior to the application of appropriate signal filters (Figure 4.2). While two separate pulses are clearly visible (the first for the opening of the aortic valve, and the second for the closing), it is not as apparent which peak/trough to choose when analyzing the data. To solve this, we applied the filters described in the methods (detailed in Section 4.2.5) post-collection to create two distinct and smooth peaks to place the representative points in analysis. These filters were consistent and reliable across all participants and trials. Following this filtering, the automated analysis pipeline, MEAP, was able to consistently label the opening and closing of the valves with little to no outliers. While these filters are likely to introduce a bit of delay, we found this to be acceptable considering that the delay would be a fixed offset within participants. The delay effect should be considered when these filters are applied to data in experiments that are not solely concerned with relative changes of autonomic activity within individuals. If other researchers consider running these filters in real-time, they should be mindful of an added delay, particularly from the FIR filter. If researchers are concerned about the alterations that an FIR filter might make to the PEP and LVET values, alternative filtering methods of choice can be readily applied.

While PEP measured by ICG during the baseline could be predicted from the ACC with a linear mixed effect model ($p < 0.001$), the complementary Bayesian model resulted in only marginal significance. This suggests that a subset of participants might be driving the results in the linear mixed effects model. It is important to recognize that in the baseline resting condition the natural variation of PEP is very low. Furthermore there may be sources of noise

52

that are different in the two measures. This suggests that the ACC measure might not be suitable for measuring minor fluctuations of baseline PEP within a given subject. Alternatively, the difference between ACC and ICG measures of PEP at rest may also diminish with a larger sample size. To help account for the limited sample size, Bayesian models provided the addition of a more informative prior for studies that try to replicate or build upon our effect. Future studies will need to test the robustness of our observed effects with a larger sample size.

In this study, we tested whether the ACC device is capable of acting as a reliable complement to the ICG's measure of the mechanistic movement of the aortic valve. While calculating PEP required indices from two apparatuses (ICG and ECG), LVET is quantified as the time period between the opening and closing of the aortic valve (requiring only ICG). LVET therefore provides a more reliable comparison between ACC and ICG. Importantly, our results indicate a strong positive relationship between the ACC and ICG's LVET measures for both baseline and Valsalva trials, suggesting that this device may be used to measure both minor and major fluctuations in preload effects on the heart.

It should be noted that the ACC and ICG signals arise from different mechanisms, resulting in differing lengths of PEP and LVET per method, as observed in Figure 4.3 and Figure 4.4. While the ICG signal is an impedance measure of electrical activity driven by change in the orientation of red blood cells with blood flow velocity, the ACC is a mechanical effect of a pressure wave that the heart is generating. Light travels faster than sound, therefore the electrical signal from ICG is faster than the mechanical signal resulting from the ACC. This bias remains constant across both baseline and Valsalva conditions, suggesting that these differences are resulting from slightly different physiological measures. Because of this difference, researchers should put this under consideration when comparing raw PEP and

LVET values resulting from ACC to the more typical ICG raw PEP and LVET. We recommend the use of the accelerometer for measuring a relative change in PEP and LVET over time in response to physiologic event changes, such as in detecting changes of sympathetic drive and ANS stress response.

An alternative approach to derive measures of aortic movement is with a phonocardiogram. In comparison to a phonocardiogram, which measures sound waves related to valve closure or blood flow, the ACC isolates the acceleration of underlying tissue along three spatial axes (X, Y, Z) simultaneously. By choosing the appropriate axes, cardiac valve opening and closure activity can be reliably identified. An advantage of using acceleration is that it has a flat frequency response at low frequencies whereas a phonocardiogram does not. The ACC is more sensitive at detecting low frequency components associated with valve closure. Furthermore, phonocardiograms come in many different masses, sizes and frequency responses, and their "in-band" frequency response depends greatly on the coupling (attachment) strategies from the phonocardiogram to the skin's surface. Meanwhile, the ACC technology can be configured to be highly repeatable over a range of ACC chips, assuming the chips have similar acceleration ranges and signal-to-noise ratios (Durand & Pibarot, 1995).

The wireless nature of the ACC device discussed in the present study provides the potential to be used to measure ANS changes in ambulatory tasks, such as with the use of a virtual reality system. For ambulatory or other active performance tasks, an ECG configuration with the red ECG at a more stable body location (e.g. rib cage) as opposed to the triceps, may produce results that are more resilient to movement artifacts. The use of other ECG placements are to the discretion of the investigator, as this ACC method should be stable across any reliable

ECG configuration. Future experimentation is required to determine the reliability of this application in this manner.

Chapter 5

Experiment 3: Trans-radial Electrical Bioimpedance Velocimetry for Detecting Cardiac Contractility

5.1   Introduction

In Experiments 1 and 2, we discovered that a wearable electro-resonator (Experiment 1), and a single accelerometer (Experiment 2), were each able to detect cardiac contractility in response to reliable physiological perturbations. However, these devices also had their constraints, such as difficulties in preprocessing, and limitations in their abilities. Here, we present the trans-radial electrical bioimpedance velocimetry device (TREV), a recently-developed state-of-the-art device that is capable of non-invasively estimating cardiac contractility from the radial and ulnar arteries of the human forearm (Macy and Bernstein, 2020). In this experiment, we demonstrate TREV's ability to capture expected event-related SNS data in response to a maximum-grip task, known to elicit allostatic activity (Richter, 2015; Richter, Gendolla & Wright, 2016; Stanek & Richter, 2016, 2021).

TREV is capable of continuously measuring the impedance of blood flow through the arm by estimating the drop in resistance that results from intraluminal red blood cells aligning in response to a pressure wave transmitted through the arteries in association with the opening and closing of the aortic valve (Bernstein et al., 2015). This raw impedance waveform provides an estimate of the velocity of this pressure wave, from which the derivative provides the acceleration. A subsequent derivative of the acceleration waveform provides the strength with which the acceleration is generated, otherwise known as "jerk", or contractility: a direct and

unobscured index of the sympathetic drive. Similarly to the combination of impedance cardiography (ICG) and electrocardiogram (ECG), the TREV device is not only capable of estimating SNS activity, but also provides estimates of the left ventricular ejection time (LVET) and stroke volume (SV). In addition, TREV requires only four strip electrodes placed on the arm, as compared to the ten electrodes that ICG and ECG require placed throughout the neck and torso. We believe the TREV device is capable of replacing the use of ICG and ECG in estimating dynamic ANS activity, and provides a simpler and quicker application process with easily analyzable data output.

5.2   Methods

5.2.1   Participants

Thirty one healthy young adults (19 females, average age 23.4 years, +/- 7.9) were recruited to participate in this study, for which they were compensated US $10/hour, plus a potential additional $10 bonus, depending on their task performance (described in Section 5.2.2). One participant was excluded from data analysis due to excessively noisy data, leaving a final sample of n = 30. All participants provided informed consent in accordance with the Institutional Review Board/Human Subjects Committee, University of California, Santa Barbara. They passed a screening protocol for physiological recording experiments to exclude anyone with a cardiovascular abnormality. All participants were fitted with psychophysiology recording electrodes and took part in a grip task, and each session lasted about 45 minutes.

5.2.2 General Procedure

Upon arrival, the participant completed a consent form and screening form of cardiovascular related disease. The participant was then taken to the experiment room and seated in front of a table with the experiment computer. Researchers then trained the participant on how to properly hold and squeeze the grip bulb, with the tubing facing down, and squeezing with their whole hand, rather than with only their fingers. The researcher then "calibrated" the participant's maximum grip threshold, by asking the participant to grip the bulb as hard as possible with each hand, recording each value. Afterwards, the researcher described the general procedure of the study, and participants were fitted with the TREV device, ECG, and a respiration belt, which were all connected to the respective hardware via carbon fiber leads (Figure 5.1; as described in Sections 5.2.4 and 5.2.5). A three minute baseline recording was collected while the participant was at rest. Afterwards, the participant completed two blocks of a maximum-force grip task, consisting of three trials each, and gripping with a different hand per each block. Initial grip hand order was randomized to produce an even split across participants. To incentivize participants to grip with their maximum strength throughout the task, we imposed a bonus system, in which participants were informed that if they reached a threshold of $\pm$ 0.04 Kgf/m2 of their hand-specific max-thresholds on all six of the grips, they would win a \$10 bonus. The researcher disclosed this rule to participants after recording the max thresholds and did not inform participants if they had achieved the bonus until after all testing was completed.
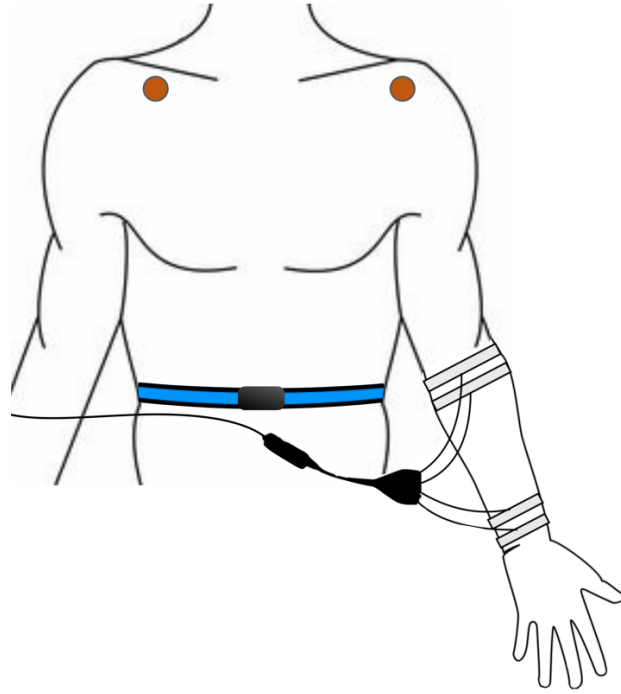
Figure 5.1   Psychophysiology setup, with the trans-radial electrical bioimpedance velocimetry device (TREV; represented by three strip electrodes) placed either on the left or right forearm. TREV was always placed on the opposite arm from the gripping hand. Electrocardiogram (ECG) electrodes (in red) were placed below the right collar bone and where the left deltoid meets the chest. Respiration belt (in blue) was secured around the waist via a hook and loop strap.

5.2.3   Experiment Protocol

The participant was seated in front of a table, so that both their arms (the one containing TREV electrodes, and the opposite arm holding the grip bulb) were positioned with their elbows and forearms resting comfortably and relaxed on the table. They were instructed to loosely hold the grip bulb in their hand, with their arm completely relaxed, until a "GO" cue on the screen informed them to squeeze for two seconds. Prior to the start of each block, psychophysiology recordings and the experiment task were started, and the researcher would leave the room. During the task, a 2-minute countdown timer would count down until the "GO" cue appeared (Figure 5.2). At the cue, participants squeezed the grip bulb as hard as they possibly could for two seconds, until the next 2-minute count-down immediately began. The

third grip of each block resulted in a final 2-minute count-down, after which the task would instruct the participant to ring a bell positioned on the table to inform the researcher that they had completed the block. After completing the first block, the researcher transferred the TREV electrodes to the opposite arm, and the next block would begin.

120	GRIP	120	GRIP	120	GRIP	120	RING BELL
rest 1 (120 s)	grip 1 (2 s)	rest 2 (120 s)	grip 2 (2 s)	rest 3 (120 s)	grip 3 (2 s)	rest 4 (2 s)	final screen

120   240   360

time (s)
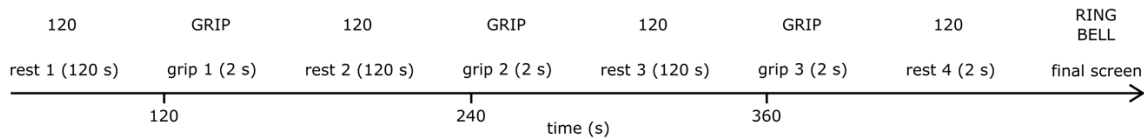
Figure 5.2   An outline of the grip task, per each block (i.e. per each block). Following an initial two min rest period, participants completed a total of three grips with either their left or right hand, with a two min rest break following each grip. Afterwards, researchers switched the same trans-radial electrical bioimpedance velocimetry device (TREV) electrodes to their opposite forearm and the same protocol was completed with the other hand.

5.2.4   Psychophysiology Protocol

Prior to beginning the behavioral task, the participant was fitted with the TREV device and a respiration belt to collect measures of SNS, heart rate and respiration rate. Prior to the placement of electrodes, the participant was asked to wash their left forearm, from their elbow to their hand, with soap and water, and then to thoroughly dry it with paper towels. Afterwards, four TREV strip electrodes were placed on the participant's forearm, such that two of the electrodes were positioned ventrally on the distal part of the forearm, just above where the wrist meets the hand, and the other two were positioned on the proximal part of the forearm, just below where the elbow meets the forearm (Figure 5.1). The pairs of electrodes were spaced apart by approximately one cm, and the two outer-most electrodes (closest to the upper arm and hand), were current-injecting electrodes, while the two inner electrodes were voltage sensing. Additionally, two ECG electrodes were placed on the participant's chest, one under the left collar bone, and one where the left deltoid meets the chest (Figure 5.1). Lastly, a

60

respiration belt was secured around the waist with a hook and loop strap to measure respiration rate. During psychophysiology setup, the researcher reviewed the importance of minimizing any and all muscle activity or movement from their arm containing the TREV electrodes throughout the course of the study.

5.2.5   Psychophysiology materials

The trans-radial bioimpedance velocimetry (TREV) device was composed of four carbon fiber bioimpedance strip electrodes (16.5 cm in length) with carbon fiber leads (EL526, Biopac Systems Inc.), connected to a NICO100D smart amplifier (Biopac Systems Inc.). ECG electrodes (EL509, Biopac, Inc.) were connected to the ECG100D smart amplifier (Biopac Systems Inc.). Both NICO100D and ECG100D were connected to the AMD100D amplifier input module (Biopac Systems Inc.). A TSD221-MRI respiration belt (Biopac Systems Inc.) was connected to a DA100C amplifier (Biopac Systems Inc.) through a TSD160A differential pressure transducer. The DA100C amplifier settings were adjusted to a gain of 1000, filtering the incoming signal with a low pass filter of 10 Hz – 300 Hz, and a 0.05 Hz high pass filter. The respiration belt was secured around the waist with a hook and loop strap. Force exerted in the Grip Task was recorded using a SS56L (Biopac, Inc.) precision transducer grip bulb. All continuous signals were integrated using an MP160 (Biopac, Inc.), collected at 1 kHz sampling rate, and displayed and stored on a laptop running AcqKnowledge software version 5.0.2 (Biopac, Inc.).

5.2.6   Psychophysiology signal filtering and preprocessing

In real-time, a number of filters were applied to the raw data by the AcqKnowledge software. An online lowpass filter fixed at 15 Hz ($Q = 0.707$) was applied to the raw impedance

waveform (velocity; Z0), and an infinite impulse response (IIR) bandpass filter of 0.5 Hz – 20 Hz (Q = 0.707) was applied to the raw acceleration signal (dz/dt), after which another 40 Hz (Q = 0.6) lowpass filter was applied to the filtered acceleration signal. Following data collection, the contractility ("jerk") waveform was computed within the AcqKnowledge software by taking the derivative of the final acceleration waveform, using a frequency cutoff of 20 Hz, and fixed at 201 coefficients. This contractility waveform (the 3rd derivative of the raw TREV impedance waveform), provided a continuous estimation of SNS activation (Bernstein et al., 2015). Within this waveform, the amplitudes of the contractility epochs represent the degree/strength of SNS activation, while the distances between epochs provides a continuous estimate of heart rate (Figure 5.3).

For preprocessing, contractility, ECG, and respiration timeseries were imported into MEAP software (described in Section 2.3). First, MEAP automatically labeled the R-peaks of the ECG timeseries, which provided estimates of heart rate at each beat. Next, R-peak time indices were used to extract epochs spanning 700 ms around each heartbeat from the raw contractility timeseries. Next, MEAP outputs were transferred to MATLAB, where the maximum amplitude of each contractility epoch was computed as an estimation of each heartbeat's contractility (providing a continuous beatwise contractility timeseries). Then, separately for each subject, and for each block, an additional regression procedure was conducted to remove the additional confounding effects of heart-rate and respiration from the beatwise contractility timeseries (Dundon et al., 2020).
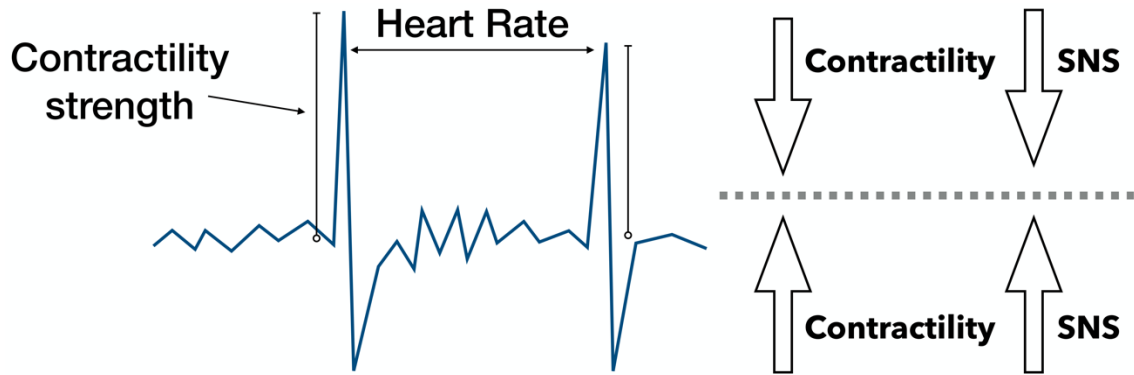
Figure 5.3   An example of two contractility ("jerk") epochs. The amplitude of each epoch represents the "contractility strength", which in turn represents sympathetic nervous system (SNS) activation at that moment-in-time. The greater the amplitude, the greater the SNS response, and vice versa. The contractility timeseries as a whole provides a continuous estimation of SNS activity. Additionally, the distance between epochs provides continuous estimates of heart rate.

In a multiple regression model, we regressed the vector beatwise contractility as a function of an intercept and three regressors. The first regressor was the phase of respiration at each heartbeat, the second was the amplitude of respiration at each heartbeat, and the third was the heart rate at each heartbeat. Next, we used the value from the raw timeseries closest to the time of each R-peak to down-sample each regressor into beatwise estimates. We then removed the three regressors and added the new estimated intercept to the residuals from this model as the "residualized" contractility timeseries. Given both between-subject and within- subject variation in heart rate, we next applied temporal resampling of each block's residualized timeseries to allow for meaningful comparisons across participants. For this, we used a 1-dimensional linear interpolation across-time to recreate residualized timeseries, sampled at equal time intervals. Specifically, we took 479 estimates, spaced exactly one second apart, from two seconds post-block-onset, to 480 seconds post-block-onset. Finally, we took each interpolated contractility estimate expressed as a t-statistic relative to the timeseries' remaining 478 values, to normalize the interpolated contractility timeseries as a t-statistic. The resulting

t-statistic-normalized timeseries provided us with our final "contractility" timeseries. Finally, a grand-averaged contractility timeseries across participants was estimated, separately for each block (Figure 5.5).

5.3   Results

Our findings demonstrate that the TREV device is sensitive to dynamic underlying physiological processes. As expected, beat-to-beat fluctuations in contractility were easily detected at the expected times in-respect to maximum grip force. For instance, in the example shown in Figure 5.4, contractility estimates derived from the TREV device remain low prior to grip-onset, and are visibly elevated following that grip. Specifically, a pre-grip low-amplitude heartbeat is extracted, representing an expected low contractility (low SNS activity), followed by an example of a high-amplitude heartbeat after the grip, representing an expected SNS activation. Furthermore, a grand-averaged contractility timeseries depicts a clear dynamic beat-to-beat increase and decrease in contractility (i.e. SNS recovery), following each grip (Figure 5.5).
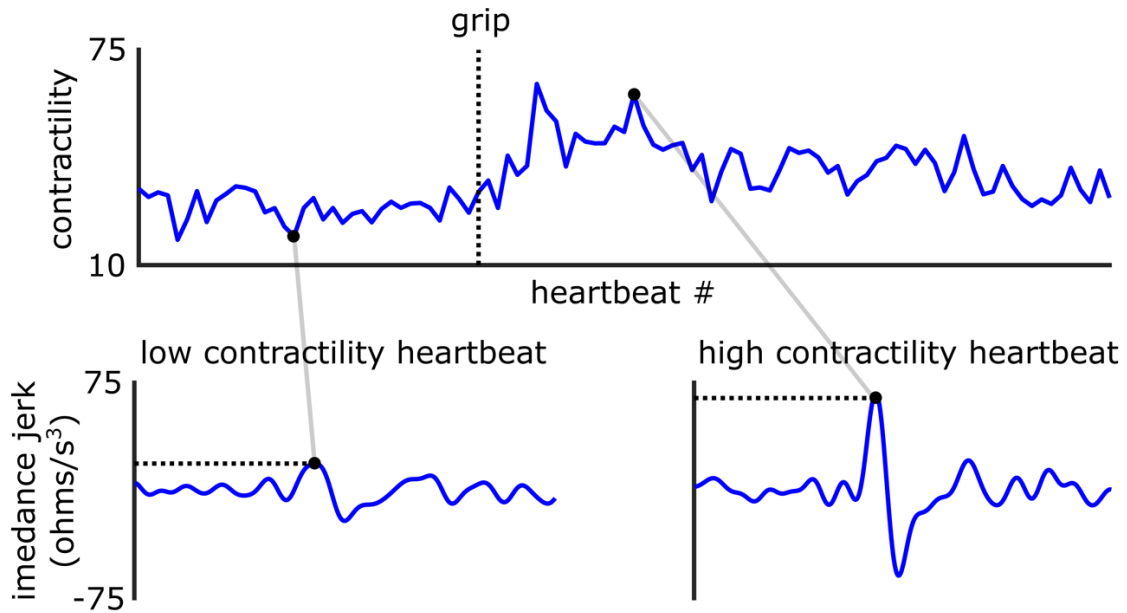
Figure 5.4 An example of a participant's contractility timeseries following a right handed grip. Within the overall timeseries, two example epochs are depicted: one at low contractility (prior to the grip), and one at high contractility (following the grip). The low contractility epoch has a blunted tip (representing low SNS drive), while the high contractility epoch has a sharp high-amplitude peak (representing high SNS drive). Each epoch spans 700 ms relative to the electrocardiogram (ECG) R-peak, and depicts the third derivative of impedance (the "jerk"; i.e. contractility).
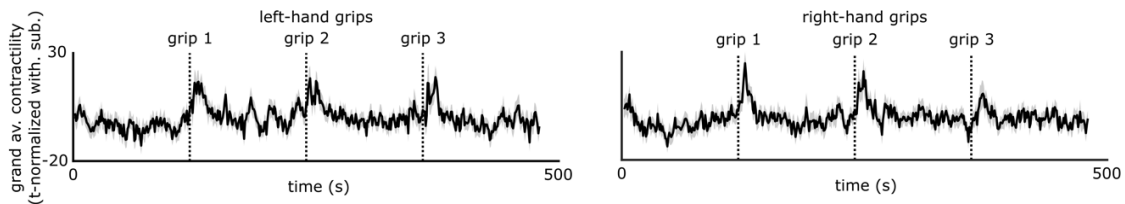
Figure 5.5 Grand-averaged beatwise contractility timeseries from the trans-radial electrical bioimpedance velocimetry device (TREV), representative of continuous contractility values averaged across participants, for left and right hand grips. The shaded areas depict the standard error of the mean across subjects at each timepoint.

5.4 Discussion

The present experiment demonstrated that the trans-radial electrical bioimpedance velocimetry (TREV) device could reliably measure dynamic fluctuations of the sympathetic nervous system (SNS; via "contractility") in response to a task that is known to elicit allostatic reactivity. These results suggest that the TREV device could act as a complementary, or even

alternative, method of quantifying event-related changes in SNS activity, as compared to the use of impedance cardiography (ICG) and electrocardiogram (ECG). The TREV device has a simple and fast application process, and provides easily analyzable output data, making it accessible to more researchers, as compared to the time-extensive ICG procedure and complex analysis.

Additionally, the SNS response is subject to a predictive "top-down" cognitive control, making it especially interesting to examine simultaneously with functional magnetic resonance imaging (fMRI) activity (Critchley, 2005; Shoemaker et al., 2012). The combination of ICG with fMRI has recently been introduced and is gaining increased interest (Cieslak et al., 2015; Dundon et al., 2021). Given that the composition of the TREV electrodes is already MRI-compatible, they are readily accessible for simultaneous use during MRI experiments. Early experimentation in our lab has seen promising results obtaining contractility signals via the TREV device from within the MRI, when this device is paired with a NICO100C-MRI amplifier (Biopac, Inc.), and is used in place of the ICG set up, as described by Cieslak et al. (2005). We encourage further research to be conducted to compare TREV output data in response to psychological and other physical test conditions that are known to elicit SNS effects, both inside and outside of the MRI. In conclusion, with this experiment, we witness a clear and reliable dynamic contractility response in coordination with a reliable physiological perturbation. As a result, we believe that the TREV device introduces a simple procedure, with easily analyzable output, and contains the potential to be used at a greater capacity than current ICG methods, while providing comparable psychophysiological estimates.

Exogenous and Endogenous Influences on Dynamic Allostatic Regulation, Cognition, and Brain Structure and Function

Chapters 6 & 7

The following two chapters were conducted to examine the degree to which dynamic allostatic processes are influenced by both exogenous and endogenous factors. In Chapter 6, we ask whether these fine-tuned allostatic regulations can be dynamically manipulated by the exogenous factor of social-pressure and performance appraisal, even when the appraisal is false, pre-determined, and incongruent to the judged behavior itself. Furthermore, in Chapter 7, we examine the degree to which these allostatic processes are influenced by cyclic endogenous fluctuations of hypothalamic-pituitary-gonadal (HPG) sex hormones in females across their menstrual cycle. Furthermore, we extend this question to ask whether these fluctuating concentrations of HPG hormones are associated with cognitive abilities, or with the structure and function of the brain. In particular, we examine changes in behavior, medial temporal lobe (MTL) volume, cerebral white matter integrity, and functional resting state connectivity, across the menstrual cycle.

Chapter 6

Experiment 4: Dynamic Autonomic Nervous System Response Following Performance Feedback

6.1   Introduction

The biopsychosocial model (BPSM) of challenge and threat postulates that when an individual is engaged in a self-relevant goal, various psychological processes will correspond to specific physiological responses that can be characterized as either a "challenge" or a "threat" (Blascovich, 2008a; Seery, 2013). Task engagement is dependent upon the relevancy of the task to the individual and can be determined by factors such as monetary incentive, social pressure, or fear of comparison among peers (i.e. social pressure) (Matthews et al., 2002; Matthews et al., 2010). Once an individual is engaged in the task and pursuing a self-relevant goal, the extent of the experiences of challenge and threat depend on the individual's assessment of their personal resources and situational demands. Personal resources may include but are not limited to ability, skills, or knowledge. On the other hand, demand refers to situations such as potential danger, required effort, or uncertainty and fear of the unknown. A state of challenge occurs when personal resources meet or exceed situational demands, leading to an increase in oxygenated blood flow to the brain and heart. With this, the body enters a heightened state of awareness (Blascovich, 2008a). The converse is the threat state, in which personal resources do not meet situational demands. This leads to the restriction of blood flow to major organs including the brain and heart, the withdrawal of vagus nerve activity, an overall increase in blood pressure, and the release of cortisol from the adrenal glands (Gaab et al., 2005; Schlotz et al., 2011). The challenge response is associated with

increased performance on tasks and tends to be associated with highly successful people, while the threat response is associated with anxiety, shame, anticipatory worry, poor decision making, avoidance behaviors, and decreased performance outcome (Blascovich & Mendes, 2010; Hase et al., 2019; Kassam, et al., 2009; Kreibig, 2010; Peters & Jamieson, 2016). However, both challenge and threat responses are adaptive. For instance, it's not difficult to imagine that evolutionarily, people who wielded a threat response to stressful situations (e.g. those high in anticipatory worry) may have aided in the survival of their tribe by alerting others of danger. Nonetheless, the threat response is linked to HPA activation which triggers the release of cortisol, a hormone that can linger in the body even after the stressor ceases to exist. When this state of threat is repeatedly prolonged for extended periods of time, it can mimic the negative effects of chronic stress. As discussed in Chapter 1, although stress is an adaptive response to dynamic situations, chronic stress can incite a variety of physiological problems such as impaired growth, cardiovascular symptoms, and autoimmune disorders, as well as behavioral and psychological disorders (Chrousos, 2009; Eskandari & Sternberg, 2002; Kemeny, 2003).

6.1.1   Physiological markers

The BPSM is determined by physiological responses of total peripheral resistance (TPR), which controls arterial constriction and dilation and is estimated from cardiac output (CO) and continuous blood pressure (CBP) (Seery, 2013). Both challenge and threat states generally cause an increase in ventricular constriction (measured by decreased PEP), and HR, while TPR and CO show distinctive directions of activation depending on the individual's state assessment. In the context of describing the physiological reactions as an evolutionarily adaptive response, the body prepares for physical trauma as an individual enters a threatened

state. In response, TPR increases and CO decreases such that blood flow is constricted and the likelihood of quickly bleeding out decreases, not unlike a hose being squeezed to allow less water to flow out of it. Conversely, in a challenged state, TPR decreases, CO increases, and increased blood flow is directed towards the muscles and brain, mobilizing the body towards either fighting or escaping the situation at hand. To summarize, states of threat are correlated with increased TPR and decreased CO, while states of challenge are correlated with decreased TPR and increased CO. For the purposes of this study, the primary physiological markers that were appraised were PEP to estimate responses of the sympathetic nervous system, and TPR to distinguish between states of challenge and threat.

While HRV has been the most common method of studying the sympathetic stress response thus far, such a single-measure index is limited as a peripheral measure that is vulnerable to a variety of psychological and physiological states (Cacioppo & Tassinary, 1990). Alternatively, the use of a combination of multiple measures (ICG, ECG and CBP) hones in on the subtle changes that occur in vasomotor fluctuations produced by the SNS, mainly observed by PEP (Figure 2.1). PEP is related to the ventricular contractility of the heart muscle before blood is ejected and is a dynamic estimate of sympathetic drive (Kelsey et al., 2004; Tomaka et al., 1997; Wright & Kirby, 2001). Further information on PEP and the SNS is provided in Chapter 2.

6.1.2   Allostatic responses to performance feedback

The present study aimed to determine whether the SNS, along with states of challenge and threat, could be dynamically manipulated within single individuals on a trial-by-trial scale through the use of performance feedback. Social pressure can have detrimental effects on performance outcome, sometimes leading to choking under pressure (Cappuccio et al., 2019;

Yu, 2015). Interestingly, there is evidence that those that are most highly suited to perform well (individuals with high working memory capacity) tend to have a higher susceptibility to choking under pressure than those with less working memory capacity (Beilock & Carr, 2005).

One way in which social pressure can present itself is in performance feedback. For instance, androgens, such as dehydroepiandrosterone (DHEA), testosterone, and cortisone, are responsive to threat, sensitive to social status and opportunities, and have been shown to modulate with verbal performance feedback (Phan et al., 2017). In fact, even fake performance feedback on a cognitive task, regardless of performance, can manipulate an individual's emotional state (Besser et al., 2004; Frings et al., 2014; Venables & Fairclough, 2009). Even in those who perform well on a cognitive task, negative feedback can lead to rumination, irrational task importance, and performance dissatisfaction.

6.1.3 Stress appraisal

There are many theories that postulate whether there are strong individual differences in response to stress with either a challenge or threat reaction (Schlotz et al., 2011). Further research is expanding into the theory that individuals may have a propensity to respond with a specific BPS state, and that the state outcome not only depends on the stressor they experience, but also on the context in which the stressor appears (Moore et al., 2019; Moore et al., 2013). This theory is supported by the BPSM, which states that the evaluations, or appraisals, of personal resources and situational demands depend on both internal and external factors (Blascovich et al., 2009; Seery, 2011). External factors, such as gain-framing and loss-framing conditions, can potentially affect states of challenge and threat (Frings et al., 2014; Seery et al., 2009). Gain-framing conditions (e.g. focusing on monetary gain based on performance) are

associated with the challenge response, while loss-framing conditions (e.g. avoiding monetary loss) are associated with the threat response.

Furthermore, Schachter and Singer's two-factor theory of emotion postulates that individuals perceive an emotional event based on the cognitive interpretation of internal physiological cues (Mattarella-Micke, 2011). Therefore, given a stressful situation such as a math problem, whether someone chokes or thrives might depend on their interpretation of their physiological state (Maloney & Beilock, 2012). For instance, someone with high math anxiety may have a heightened physiological response (higher cortisol, greater SNS activation, elevated HR), and interpret their physiological state as fear, which may lead them to perform poorly. Conversely, someone with low math anxiety may interpret the same heightened physiological arousal as a state of challenge/excitement and thus perform better (Hase et al., 2019).

Moreover, challenge and threat states exist on a spectrum, rather than two distinct states. A simple change in an individual's perception of their internal resources (i.e. their own physiological state), can have significant effects on their cardiovascular activity, mindset and behavior. During a stressful task, individuals re-appraising their physiological arousal as "functional and adaptive" or "exciting" have demonstrated increased states of challenge (decreased TPR), an increased perception of available resources, a decrease in threat-related attentional bias, and increased performance outcome (Brooks, 2014; Jamieson et al., 2012). However, evidence as to whether an experiment paradigm is able to dynamically oscillate individuals' states of challenge and threat has yet to be introduced.

6.2   Methods

6.2.1   Participants

Twenty five young, healthy adult undergraduates (14 females, average age 20.2 years, +/- 1.7) at the University of California, Santa Barbara were recruited by word of mouth to participate in this two hour study, for which they were compensated US $10/hour in addition to a $5 bonus. All participants provided informed consent in accordance with the Institutional Review Board/Human Subjects Committee, University of California, Santa Barbara. They passed a screening protocol for physiological recording experiments to exclude anyone with a cardiovascular abnormality. All participants completed questionnaire assessments, were fitted with materials to record psychophysiological measures, and partook in a modular arithmetic task, after which they completed more assessments and were debriefed by a semi-structured interview process on their perception of the study as well as the modes of deception used.

6.2.2   Experiment Paradigm

Prior to beginning the task, participants completed a variety of assessments for future analyses, including state questionnaires, menstrual cycle and birth control history, as well as assessments of math anxiety, challenge and threat personality characteristics, and current stress levels. Participants then underwent a combination of classic stressors: Gauss's modular arithmetic (Beilock, 2008; Bogomolny, 1996) and social evaluative threat (Dedovic et al., 2005; Dickerson & Kemeny, 2004; Pruessner et al., 1999). This combination of math tasks with social evaluative threat have been continuously and reliably used in many experiments investigating stress and its functions at a relatively fast time scale to look at beat-by-beat responses, including in the commonly used Trier Social Stress Task (TSST) (Kirschbaum et al., 1993; Pruessner et al., 1999). The aim of the present study was to oscillate responses of the

SNS and states of challenge and threat within single individuals as a function of performance feedback. Every participant received the same predetermined feedback, regardless of their performance, to account for individual differences in math performance or anxiety. Following the task, participants re-took assessments of challenge and threat personality characteristics and stress.

6.2.2.a Modular Arithmetic (MA)

In MA, the participant is given an equation such as: $10 \equiv 2 \pmod 4$. In this example, they have to answer whether or not 4 is wholly divisible by the difference of 10 - 2. Here, the answer would be true; the difference of 10 - 2, 8, is wholly divisible by 4. Whereas, in a problem such as $54 \equiv 17 \pmod 9$, the answer would be false, as the difference between 54 - 17, 37, is not wholly divisible by the mod number 9. MA is a useful tool for studying the stress response while controlling for task familiarity and learning effects due to its unique equation format, with which none of the present participants had any past experience.

6.2.2.b Experiment Task

Following task instructions, participants were given 16 practice trials. To induce social evaluative pressure, participants were falsely misinformed of the following: (1) their "speed/performance ability" has been estimated based on their performance on practice trials, (2) that performance on the task trials will be compared with an estimate of their "speed ability", and (3) that a time penalty will be applied for incorrect responses. Details on how these aspects are accomplished are purposely not described to allow for conceptual gaps in the experiment format, in an attempt to prevent participants from recognizing that the feedback they are receiving is fake. Participants were informed that their feedback on their performance will be shown by a feedback bar (Figure 6.1). The closer they perform to their estimated

"maximum ability", the closer a blue cursor would be to the right of the bar. Conversely, the worse they perform, the closer the cursor would be to the left of the bar. Furthermore, a monetary and social pressure paradigm was established as participants were encouraged to perform in the top 25% of their "speed ability" (to the right of a designated red zone) by instructions stating that if they finished on average in the red zone, the researchers would not be able to use their data and the participant would not receive an additional $5 bonus (bringing their total bonus to $0) (Figure 6.2). However, if they performed exceptionally well and finished in the green area on the right, they would receive an additional $5 bonus (bringing their total bonus to $10). In reality, all the participants received the same feedback and a total $5 bonus, regardless of their task performance. Performance feedback was predetermined to follow a sinusoidal wave with some added jitter within the gray region of the feedback bar nearing between both red and green zones (Figure 6.3). Participants received a total of 96 trials, with a feedback screen given every three trials, for a total sum of 32 feedback bars. Furthermore, as an added complexity to prevent participants from realizing the feedback manipulation, participants were reminded of the time penalty given for wrong responses when the false feedback would offset significantly with participants' real performance (Figure 6.4).

Figure 6.1 **(a)** The feedback bar participants see **(b)** Participants are told that the closer they perform to their estimated maximum ability, the closer a blue cursor will be to the right of the bar **(c)** Participants are told that the closer they perform to their estimated minimum ability, the closer the cursor will appear to the left of the bar.
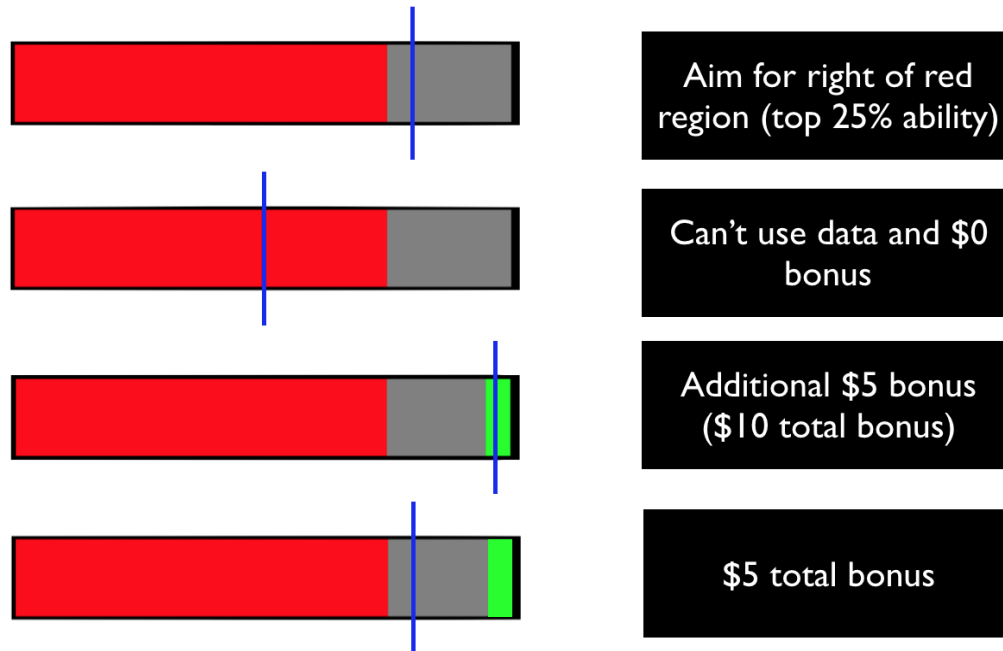
Figure 6.2   The instructions given to participants describing how their average performance feedback will relate to the monetary reward they receive.
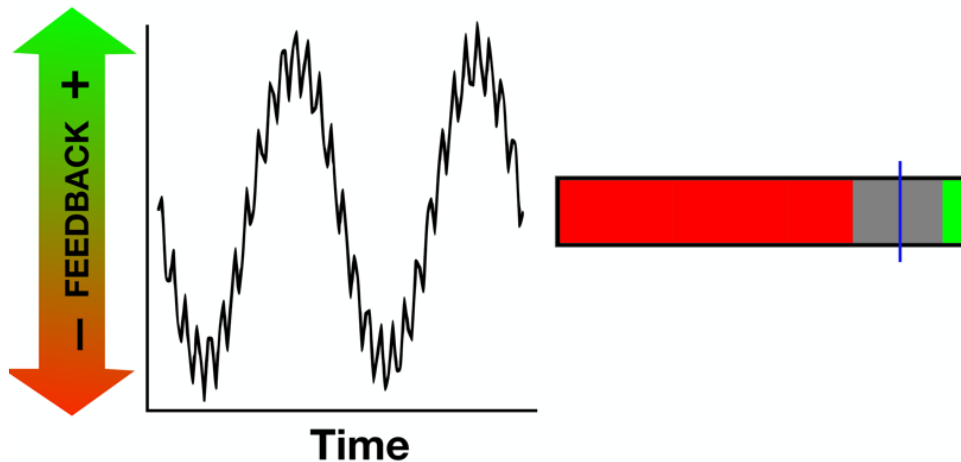
Figure 6.3   Sinusoidal wave with added jitter to demonstrate how predetermined false feedback was delivered. Higher up from the center of the wave (middle of the y axis) represents increasing positive feedback, moving the blue cursor from the center of the gray zone closer to the green. As feedback moves down from the center of the wave, it represents increasingly negative feedback with the blue cursor moving closer to the red zone.
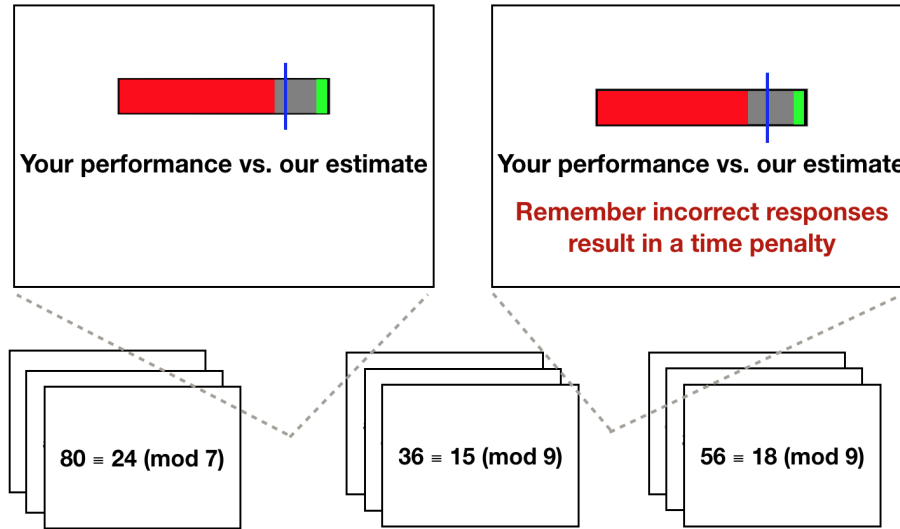
Figure 6.4 An example of the feedback provided to participants once every three trials.

6.2.2.c Psychophysiological Measures

Psychophysiological equipment, materials, protocol, preprocessing, and analysis were identical to those outlined for ICG, ECG, and CBP in Chapter 2. Once the psychophysiology setup was complete, each session began with about a five minute resting period for the participant to become adjusted to the environment while researchers described the task instructions. Following this resting period, a three minute ICG, ECG, and CBP baseline recording was collected. Experiment triggers were collected via Digital I/O using a LabJack U3-LV (LabJack, Inc.) connected to a UIM100C amplifier (Biopac Systems Inc.).

6.3 Results

For analytic purposes, the data was divided into separate macro- and micro-states. Assuming a center zeroing of the sinusoidal feedback wave, the macro-states were divided into high macro-states (the positive portions above the centerline), and low macro-states (the negative portions below the centerline). A measure of "feedback change" was determined within the macro-states by either declining (moving closer to the red portion of the feedback bar), or as improving (moving closer to the green portion of the feedback bar) (Figure 6.5).

Macro-states were then further divided into extreme and mid micro-states (Figure 6.6). The extreme micro-states were set to the extreme outer ends of the feedback received, whereas the mid micro-states were closer to the neutral center of the feedback.
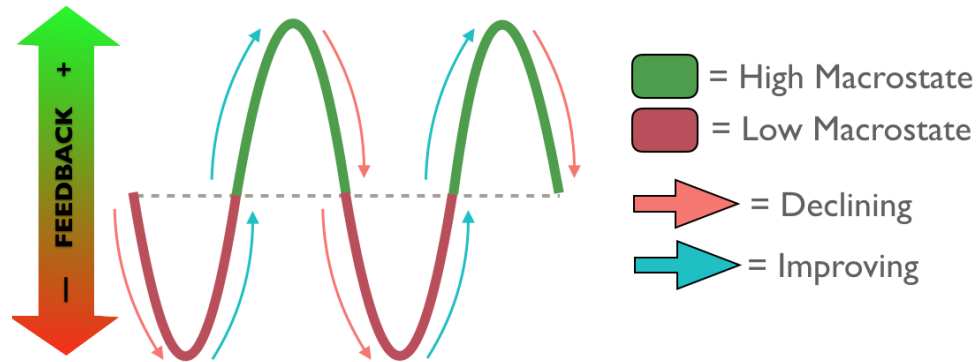
Figure 6.5   Macro-states are shown in green and red, with high macro-states above the centerline of the sinusoidal wave and low macro-states below the centerline. Feedback change is shown as declining feedback (in pink) moving closer to the red left end of the feedback bar, or improving feedback (in blue) moving closer to the right green end of the feedback bar.
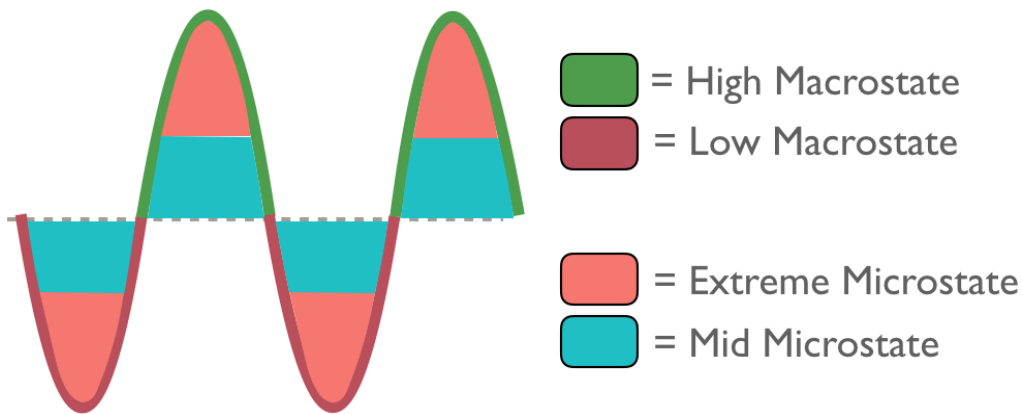
Figure 6.6   Macro- and micro-states. The macro-states (outlined in green and red), were divided further into extreme (pink) and mid (blue) micro-states.

All linear mixed effects models were fitted using the lmerTest (Kuznetsova et al., 2017) package in R (version 4.2.1, R Core Team, 2020). TPR values were normalized and scaled on an individual basis due to other extraneous factors affecting TPR between individuals, since TPR is a ratio estimate. We fitted four separate models for high vs. low macro-states of sympathetic drive (set to the inverse of PEP) and TPR, in each case modeling these values

during the extreme vs. mid feedback micro-states, their feedback change (represented by pink and blue arrows in Figure 6.5), as well as their interactions.

There was a significant negative main effect of sympathetic drive in the high macro-state following perturbations in feedback (beta = -0.69, t = -2.92, p = 0.005), such that when feedback was in the positive range, receiving negative feedback caused greater sympathetic drive (low PEP) (Figure 6.7). While no significance was found as a function of feedback change within TPR values, there was a significant negative main effect of TPR in the extreme feedback micro-state within the high macro-state (beta = -0.12, t = -2.22, p = 0.031), such that TPR values were significantly low (reflecting a challenge state) in the extreme high micro-state (when feedback is extremely positive) (Figure 6.8).

An independent samples t-test determined that TPR was significantly greater during the low macro-state feedback (M = 0.13, SD = 0.35) than during that of the high macro-state (M = -0.07, SD = 0.36), t(98) = 2.72, p = 0.004, d = 0.54. Additionally, TPR levels in the low macro-state of feedback were significantly different from zero as confirmed by a 1-sample t-test, t(49) = 2.57, p = 0.01, d = 0.63. Thus, on average throughout the overall experiment, all negative feedback was associated with high TPR values, reflective of a state of threat (Figure 6.8). Task performance was estimated from a combination of accuracy and response time. No significant effects were observed with task performance across all conditions.
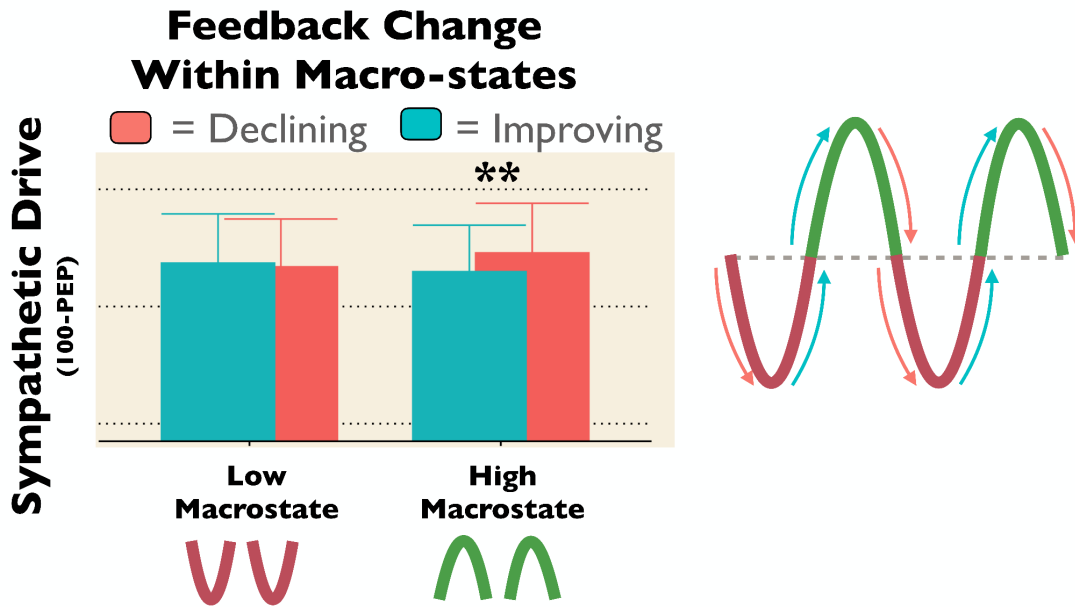
Figure 6.7 Feedback-change results from the sympathetic drive within the macro-states. Results represent the significance of increasing sympathetic activation with more increasingly negative feedback within the high macro-state.
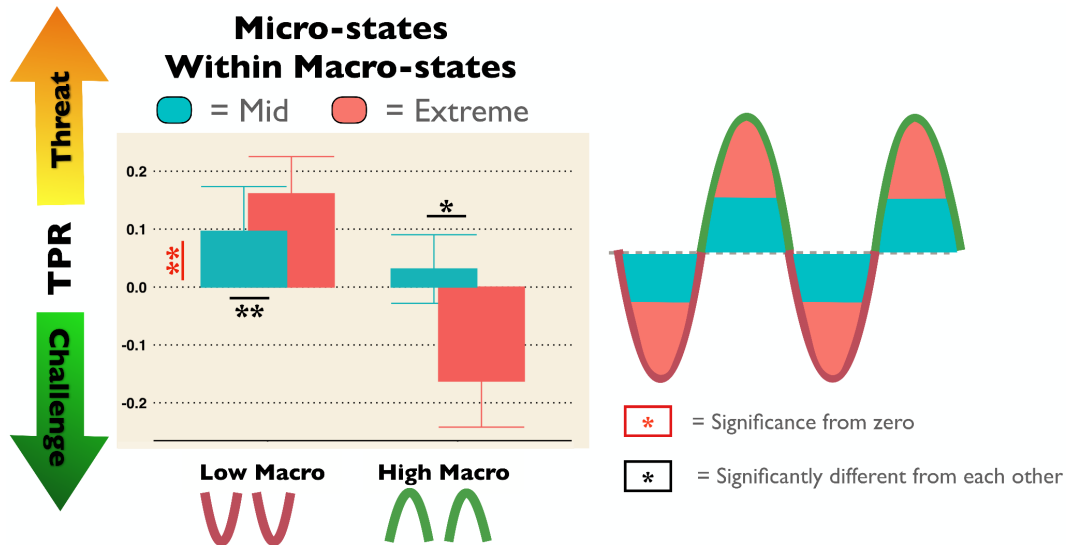
Figure 6.8 Total peripheral resistance (TPR) results showed significance from zero in the low macro-state, in which negative feedback was associated with an increase in TPR (threat response). Within the high macro-state, results showed significant differences between mid and extreme micro-states, such that very positive feedback (in the extreme micro-state) was associated with low TPR (a challenge response).
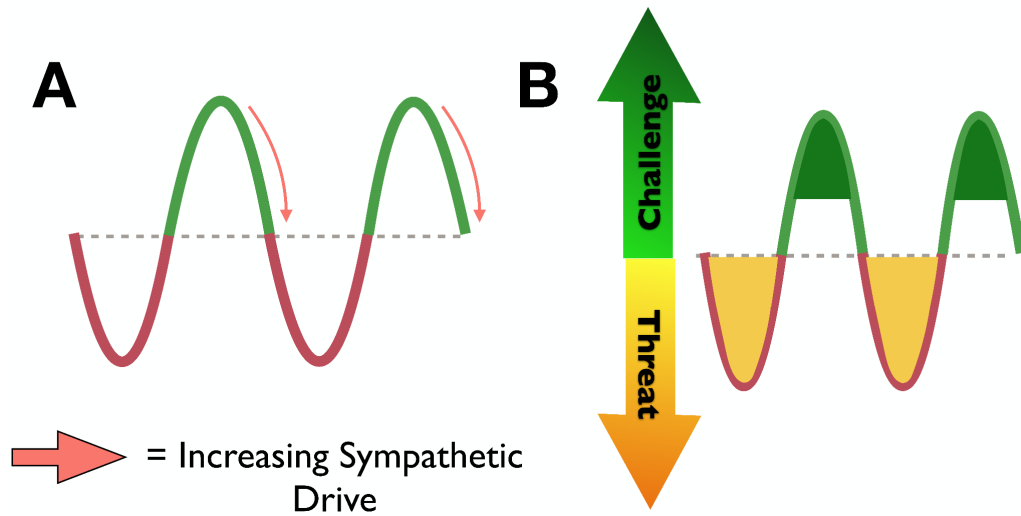
Figure 6.9   **(a)** Overall sympathetic drive results, showing an increase in sympathetic drive with increasingly negative performance feedback within the high macro-state **(b)** Overall total peripheral resistance (TPR) results showing an increased challenge response within the extreme high micro-state and an overall threat response in the low macro-state.

6.4   Discussion

The present study investigated whether predetermined fake performance feedback could dynamically activate an individual's sympathetic drive, or shift their stress response between states of challenge and threat, regardless of their true task performance. Our results suggest that an increase in sympathetic drive follows declining fortunes in an otherwise successful state, where a trend of continuously compounding feedback depicting poor performance following a trend of feedback depicting successful performance actuates sympathetic drive (Figure 6.9). On the other hand, TPR results support a state-tracking system rather than perturbation-tracking for states of challenge and threat, suggesting that it is relatively easy to push a person into a state of threat with "poor performance" feedback, whereas pushing them into a state of challenge requires extreme levels of "outstanding performance" feedback. With these results, the study demonstrated a trial-state rather than trial-wise dynamic. Previous research has observed individual differences in challenge and

threat states. However, with the present findings, we are detecting dynamic trial-by-trial changes within an individual, altering between states of challenge and threat. While these results may still suggest individual differences, they certainly show a state-based difference within an individual that can fluctuate rapidly.

Previous research has supported the ability of BPS states to modulate with the manipulation of situational demands. For instance, altering task instructions to influence resource appraisal has been shown to influence states of challenge and threat (Turner et al., 2014). The presentation of solely challenge-based instructions (such as focusing on approach goals and high perceptions of control) have shown to induce lower TPR and better performance in a group of individuals. Alternatively, solely receiving threat appraisals (such as focusing on avoidance goals and a low perception of control) were shown to significantly increase TPR. In some respects, the present study's conditions of high (positive) and low (negative) macro- and micro-states of feedback can be related to "challenge" or "threat" appraisal conditions. In this way, our findings are similar to those repeatedly witnessed in previous literature where the challenge condition (feedback depicting outstanding performance) was associated with decreased TPR, while the threat condition (feedback depicting poor performance) was associated with increased TPR. A growing area of literature supports the ability of an individual to change their appraisal between challenge and threat at larger time scales. However, the present research provides evidence that individuals can dynamically oscillate between states of challenge and threat in response to a given situation.

Furthermore, similar to literature that observed individuals exhibiting a challenge response to gain-framing conditions and a threat response to loss-framing conditions (Frings et al., 2014; Seery et al., 2009), our study has a manipulation of instructions that allows for an

alternation between avoiding losses and reaching for gains. For instance, when the feedback bar is set towards the border of the red region (the low micro-state), participants may be focusing on potential losses (avoiding the social embarrassment of being excluded from the study and wasting the experimenters' time, as well as avoiding the loss of all monetary bonus gain). Conversely, when they are in the high micro-state, they may be focusing on potential gains (social status and the ability to double their bonus reward). In this regard, our study would suggest that individuals may be inherently quicker to enter a state of threat when in loss-framing conditions, whereas the switch to a challenge state requires a condition where the gain is nearly-guaranteed.

Regarding the SNS, previous research supports sympathetic drive activation following the decline in profitability as a prosperous environment becomes scarce (Dundon et al., 2020). As this is essentially a response to losses, and these losses are most exaggerated when going from a state of doing well to accumulating losses, it is not surprising that our study observed sympathetic activation in response to a declining feedback state (performance accuracy continuously declining) following a strong and steady positive feedback trend towards a lucrative gain.

Another study used skin conductance level (SCL) to estimate sympathetic engagement in response to performance feedback (Venables & Fairclough, 2009). Similar to the present study, experimenters gave participants predetermined feedback regardless of their performance. However, they separated participants into either a "failure" or "success" group. The "failure" group received consecutive block-by-block feedback that their performance was decreasing in accuracy, while the "success" group received consecutive feedback that their accuracy performance was increasing. Both groups demonstrated decreasing SCL

(representing decreasing sympathetic drive) with each block, which is typical as participants adjust to the allostatic response to starting a new task. However, the "failure" group's SCL levels remained higher and more stable across the sessions, suggesting a sustained increase in sympathetic drive following negative feedback that is resilient to habituation. Our study did not observe such state-based effects of the sympathetic drive, although this may be due to the continuously changing states between "failure" and "success" inherent to our study design. Yet, this result may be reflective of the increased sympathetic engagement we observed in response to a trend of increasingly negative feedback. These observations may be suggestive of sympathetic reactivity towards an increasing "trend" of negative feedback.

Prior literature has connected increases in performance outcome with states of challenge (Hase et al., 2019; Turner et al., 2014). However, the present study did not observe any significant correlations in performance with either TPR (challenge and threat state) or PEP (sympathetic drive). This may suggest that performance outcome is resilient to dynamic fluctuations of stress states within an individual. Future directions will explore whether any data from our state questionnaires, math anxiety, stress scales, or challenge and threat personality assessments may provide further insight into our findings.

When external circumstances such as fake performance feedback that in actuality has nothing to do with our actual performance has the ability to quite easily push us into a state of threat and stress, it is abundantly clear that encountering stress is an inevitable part of life, and thus impossible to avoid. However, individual differences in stress reactivity and reappraisal methodology from prior literature suggests that one does not need to avoid stress to live a healthy lifestyle. Future expansion on the current experiment design could observe the interaction between reappraisal methodology and dynamic state-shifting. For instance, the

experiment design can include a "growth mindset" reappraisal condition (such as goal-directing and increasing the participant's perception of control) during feedback depicting negative performance. If this reappraisal can shift an individual away from a state of threat and towards a state of challenge, then there may be significant implications for stress management stemming from this area of research, such as providing an effective coping strategy for stress-inducing circumstances.

Chapter 7

Experiment 5: Behavioral, Allostatic, and Cerebral Changes Across the Human Menstrual Cycle

7.1   Introduction

Given the highly interconnected relationship between hypothalamic-pituitary-adrenal (HPA) stress hormones, hypothalamic-pituitary-gonadal (HPG) sex hormones, and fluctuations in neuronal structure, the present research examined whether there is a relationship between routine cyclic HPG hormone changes and cognition, allostasis, brain morphology, or functional connectivity (Jacobs et al., 2015; Mcewen et al., 2018). We examined concentration levels of estradiol, progesterone, luteinizing hormone (LH), and follicle stimulating hormone (FSH) in relation to dynamic allostatic reactivity and efficiency in response to motivating environmental triggers. Estimates of contractility, which are directly controlled by the sympathetic nervous system (SNS), were collected, such that greater contractility signifies greater sympathetic drive, and vice versa. Additionally, allostatic efficiency was measured by the rate at which contractility decreases following the presentation of task performance feedback (i.e. feedback recovery). For instance, once the feedback was presented, a slower rate of change from high to low contractility, represented by a smaller slope in the signal change, signified a low rating of allostatic efficiency. Whereas a high negative slope signified a faster rate of contractility decrease, hence a quicker feedback recovery, representative of high allostatic efficiency. Furthermore, given the density of HPG hormone receptors within major brain regions and recent studies discovering functional and structural effects related to hormone concentration, we examine brain functional connectivity, structural gray matter

volume within the medial temporal lobe (MTL), and whole-brain white matter integrity (WMI). A review on the relationship between HPG hormones and the ANS can be found in Chapter 1, Section 1.5.

7.1.1 Hypothalamic-pituitary-gonadal (HPG) Hormones and Brain Morphology and Function

Evidence in the animal and human model literature suggests that HPG hormones may influence the structure and volume of both gray and white matter in the brain via processes of synaptic plasticity (Barth et al., 2016; Brann et al., 2007; Curry & Heim, 1966). In rodents, estradiol has been shown to have a positive relationship with dendritic growth, synaptogenesis, and myelination in the brain (Haraguchi et al., 2011). In particular, the hippocampus, a brain region implicated in a number of important memory functions (Rubin et al., 2014), has well-characterized high densities of estrogen and progesterone receptors, and has been shown to be especially susceptible to structural changes in response to HPG hormones (Adams et al., 2001). Across the rodent's estrous cycle (i.e. their menstrual cycle), increased levels of estradiol were associated with increased dendritic branching within hippocampal subregions, while low estradiol levels were associated with decreased synaptic density (Woolley & McEwen, 1992). Estradiol's role in synaptic plasticity extends as far as containing the potential to restore synaptic profiles in aged rats or to attenuate depressive symptoms linked to postpartum depression (Adams et al., 2004; Galea et al., 2001). While both estradiol and progesterone have been implicated in promoting synaptic density in the hippocampal structures of rodents, the effects of progesterone may be shorter-acting and may have the ability to attenuate the effects of estradiol (Wooley & McEwen, 1993).

To understand the effect that HPG hormones have on human gray matter structures, researchers have begun to study changes occurring within human females. One such study on pregnant females observed a significant pattern of long-lasting gray matter volume reductions within regions of the cortical midline and the prefrontal, and temporal cortices, which were surprisingly correlated with metrics of infant-bonding (Hoekzema et al., 2017, 2022). These findings were likely linked to changes in HPG hormones that occur in pregnancy. Furthermore, many study results suggest that HPG hormones increase the gray matter volume of hippocampal subregions. For instance, right anterior hippocampal gray matter and parahippocampal density have been found to increase during the late-follicular phase, when estradiol levels are high and progesterone remains low (Lisofsky et al., 2015; Protopopescu et al., 2008). Conversely, estradiol concentrations during the luteal phase (when estradiol levels are high, but progesterone is dominant), have been shown to have a negative relationship with the volume of the anterior cingulate cortex (ACC), a brain region integral to cognitive and affective control (De Bondt et al., 2013). Furthermore, a recent study investigated changes within a single female's medial temporal lobe (MTL) gray matter and observed both positive and negative relationships between progesterone and various subregions of the hippocampus (Pritschet et al., 2020).

Based on findings from animal models, it is possible that white matter integrity (WMI) in humans may be susceptible to changes in HPG concentrations as a result of modulation of synaptic connectivity (e.g. by mechanisms of myelination, fiber density, and/or synaptic proliferation). Human WMI is commonly estimated by characterizing the diffusion of water molecules along white matter tracts, and the present literature largely employs the use of diffusion tensor imaging (DTI), estimating fractional anisotropy (FA). As of yet, few studies

have employed methods of examining WMI in response to HPG hormones in humans. Sexual dimorphism studies have indicated that HPG hormones directly impact white matter microstructural developments in both male and female brains (van Hemmen et al., 2017). For instance, female brains have been associated with higher levels of FA in the corpus callosum, while male brains have been associated with higher levels of FA in the superior longitudinal fasciculus (Kanaan et al., 2012). In studies on transgendered individuals, credible longitudinal changes have been observed in FA values across multiple brain regions following both female-to-male and male-to-female hormone transition treatments (Kranz et al., 2017; Rametti et al., 2012).

It is likely that these changes in WMI are due to differences in HPG hormone concentrations. Recent research is beginning to employ methods of examining fluctuations in white matter microstructure across the menstrual cycle and in response to changes in HPG hormone concentrations within females. One such study conducted a dense-sampling of a single subject across two menstrual cycles while estimating microstructural integrity within the hippocampus. Researchers observed a likely positive relationship between estradiol and bilateral hippocampus integrity, as FA values peaked around the time of ovulation (Barth et al., 2016). Another study employed voxel-based-morphometry techniques to estimate white matter density and discovered a positive correlation between estradiol concentrations and white matter density of the whole cortex, most prominently within the left parietal cortex (Meeker et al., 2020).

Modulation of neural activity within the hippocampus, hypothalamus, amygdala, and other regions via estrogen and progesterone receptor activation may impact communication between these regions as a functional connectivity network. Functional connectivity can be

assessed using fMRI to measure the degree to which brain regions interact and communicate with one another in a coherent, patterned manner (Van Den Heuvel & Pol, 2010). Recent research suggests that brain regions are not isolated units, but rather work together to process information and determine appropriate outputs. Particularly, the resting brain exhibits organized patterns of correlated activity in what is called resting-state functional connectivity (Greicius et al., 2003). For instance, the default mode network (DMN) displays higher levels of activity during rest and has been linked to executive function, becoming more or less attenuated during tasks dependent upon task demands (Fox et al., 2005, Raichle, 2015b, Raichle et al., 2001). Consequently, changes within the communication between the DMN and the executive control network (ECN) may have important consequences to an individual's attentional state and/or emotional affect. Abnormalities in the coherence of functional networks, including the DMN, are characteristic of attentional disorders such as attention-deficit/hyperactivity disorder (ADHD) (Konrad & Eickhoff, 2010; Uddin et al., 2008). Additionally, disruptions to the anterior cingulate cortex (ACC) within the ECN can result in difficulties in regulating one's attention and ability to shift between tasks (Petersen & Posner, 2012). Accordingly, increases in ACC connectivity with other brain regions have also been reported in ADHD patients (Tian et al., 2006) and in severely depressed patients (Horn et al., 2010).

Evidence suggests that the DMN, along with whole-brain resting state dynamics, is modulated by HPG hormones, with oscillations in connectivity found during pregnancy (Hoekzema et al., 2022) and across the menstrual cycle (De Filippi et al., 2021). However, a conclusive answer as to the directionality and specifics of this modulation with HPG hormones has yet to be established given the variability of results in the literature. While some studies

have failed to find any discernible menstrual cycle effects on resting-state functional network activity (De Bondt et al., 2015; Hjelmervik et al., 2014), other literature suggests a negative relationship between high levels of HPG hormones and connectivity. For instance, one such study found that high circulating levels of HPG hormones appear to correlate with reduced coherence and connectivity between brain regions within the DMN, and consequently the DMN appears more connected when hormone levels are low (Petersen et al., 2014). For instance, females in their early follicular phase presented greater connectivity between regions within the DMN and ECN as compared to the mid-luteal phase, or to those on oral contraceptives. Additionally, an increase in connectivity between the DMN and other brain regions has also been found in females during times of low estradiol (the early follicular) as compared to high estradiol (late follicular/ovulation) (Weis et al., 2019).

Alternatively, other evidence supports an increase in functional connectivity within DMN and control networks during the mid-luteal phase, when levels of progesterone and estradiol are high (Arelin et al., 2015; Pletzer et al., 2016). For instance, one study examining resting state connectivity across one participant's menstrual cycle found a positive relationship between progesterone and connectivity between the dorsolateral PFC, sensorimotor cortex, and hippocampi (Arelin et al., 2015). Conversely, one recent study investigated changes within a single individual's functional connectivity and endocrine levels across the menstrual cycle (Pritschet et al., 2020). The researchers observed a positive relationship between estradiol and resting-state functional connectivity coherence within networks, while progesterone was found to exhibit an inverse relationship with coherence (greater progesterone levels associated with reduced network coherence).

7.1.2 Study Overview

Naturally-cycling female participants underwent a repeated-measures study for a total of three sessions per participant, once per three distinct phases of their menstrual cycle (menstruation, ovulation, and the premenstrual mid-luteal phase). Starting phases were staggered across participants to account for session order effects (e.g., some participants came in for their first session during ovulation, while others came in during menstruation). Researchers tracked participants' menstrual cycles to gain an intimate understanding of each participant's cycle in order to schedule their sessions during these three distinct phases. The goal of the menstruation session was to bring participants in during a time of low hormone concentrations across estradiol, progesterone, LH and FSH (Figure 1), while the ovulation session was scheduled to bring participants in during a time of peak LH, estradiol, and FSH. Ovulation is triggered by an LH-surge, which begins the release of a mature egg from the ovary ~24 – 36 hrs following the surge (Zeeman et al., 2003). This LH-surge is marked by a peak-concentration of LH (and accompanying peak-levels of estradiol and FSH), and therefore was the goal timing for the present study's ovulation sessions. Lastly, the mid-luteal phase served to bring in participants during peak concentration of progesterone and high estradiol, and were scheduled half-way between ovulation and the upcoming predicted start of menstruation, following cycle predictions.

Per session, participants completed state questionnaires and underwent a task to induce mental stress (described in Section 7.2.6.a) simultaneously with psychophysiological recordings estimating SNS activity from a trans-radial bioimpedance velocimetry (TREV) device (Section 7.2.6.b). Afterwards, a blood sample was collected by a licensed phlebotomist (Section 7.2.6.c) and participants completed a magnetic resonance imaging (MRI) brain scan

protocol to estimate functional connectivity coherence, volumetric gray matter of their medial temporal lobe (MTL), and white matter integrity (WMI) (Section 7.2.6.d).

Numerous conflicting findings exist in the previous literature regarding the relationships between HPG hormones/the menstrual cycle and cognition, allostasis, and effects on brain structure/function. While the majority of previous research did not use dynamic allostatic metrics, but rather singular time scales, such as baseline, mid-task blocks, or post-task recovery, they did provide insight into potential mechanisms of HPG hormones on allostasis. This literature contributed to our expectations that progesterone would be associated with a positive relationship with contractility in response to MA trials and following performance feedback, meaning increasing concentrations of progesterone would be associated with a greater SNS response. Furthermore, we predicted that progesterone would have a negative relationship with allostatic efficiency. Hence, greater concentrations of progesterone would be associated with a lag in contractility recovery (i.e. decrease) following performance feedback. Contrarily, we believed it was possible that estradiol would present protective neurogenic properties and have the opposite effect: demonstrating a negative relationship with contractility following MA presentation and performance feedback, along with a positive relationship with allostatic efficiency. This would mean higher concentrations of estradiol would be associated with an attenuated allostatic response, and higher allostatic efficiency. Furthermore, we predicted to observe a positive relationship between progesterone concentrations and response time on the MA task such that greater concentrations of progesterone would be associated with slower response time, given its relationship to fatigue and drowsiness (Andersen et al., 2006). Consequently, this may be associated with a decrease in performance accuracy.

With regard to monetary reward, some evidence points toward a modulation of reward sensitivity with estradiol, given the influence that gonadotropin hormones have on dopaminergic reward systems (Creutz & Kritzer, 2004; Dreher et al., 2007; Jacobs & D'Esposito, 2011). Alternatively, other evidence points towards heightened responses to reward in females taking oral contraceptives (Bonenberger et al., 2013). Ultimately, we predicted a positive relationship between estradiol and contractility specific to high reward MA trials, such that higher concentrations of estradiol would be related to an exaggerated SNS drive and a quicker response time following the motivation for successfully completing high reward MA problems. Yet, we did not believe that this effect would be great enough to affect performance accuracy on these trials.

In line with the current trends in both animal and human models, we predicted to observe positive estradiol modulation of hippocampal subregion gray matter volume and WMI across the brain. In regards to resting-state functional connectivity, we predicted to observe HPG hormone concentration-modulated fluctuations of functional connectivity coherence, particularly within the DMN.

7.2   Methods

7.2.1   Participants

Following pre-screening procedures (described in Section 7.2.2), a total of 36 female participants (average age 21.3 years, +/- 2.8) were recruited via digital flyers emailed to students and faculty at the UC Santa Barbara campus and prescreened on health and birth control history. None of the participants were on any hormonal birth control during the three months preceding the study or throughout the entire study duration. Furthermore, 11 of the 36

participants reported having no history of hormonal birth control (e.g. pills, patches, or implants). Four participants dropped the study prior to completing all three sessions due to a loss of interest, and the remaining 32 completed all three sessions. Of these participants, one reported having a current physical ailment of an asymptomatic case of fibroids. Furthermore, three participants ingested an emergency contraceptive (morning-after pill), two participants contracted the SARS-CoV-2 virus, and 34 participants were vaccinated for the SARS-CoV-2 virus between study sessions. One complete menstrual cycle (menses-to-menses) was required to pass prior to returning for any sessions following SARS-CoV-2 vaccines, diagnoses, or ingestion of emergency contraceptives. Notably, two of the final participants did not take part in the behavioral or psychophysiological portion of the study due to familiarity with the behavioral task and study goals, and two other participants did not complete the MRI portion of the study due to MRI contraindications. Of the remaining participants with behavioral and contractility data, one participant's data were excluded from analyses due to an interruption during the study session that deemed the data-quality to be unusable. Given these exceptions, there were 30 total participants providing MRI data, and 29 total participants providing behavioral and contractility data.

All participants provided informed consent in accordance with the Institutional Review Board/Human Subjects Committee of UCSB, and were paid $50 upon completion of the pre-session cycle tracking, and $60 per in-lab session. Additionally, they were awarded a total bonus of up to $75 across all three sessions depending on task performance. All bonuses were calculated and awarded at the end of the third and final session for two reasons: 1) to prevent any session-to-session residual effect of bonus money received on task performance, and 2) to

serve as an incentive to complete all three sessions. Cumulatively, participants received a total of $180 – $255 for completing all three in-lab sessions.

7.2.2 Pre-screening

In order to be accepted into the study, candidates had to pass several phases of screening to ensure that they met all eligibility requirements and were aware of the study's extensive activities. As an initial measure of eligibility, 68 female candidates were interviewed on a video-call in which the study's purpose, eligibility prerequisites, and activities were discussed. Exclusionary criteria included current use of hormonal or implanted birth control, abnormal menstrual cycle, any history of cardiovascular, neurological or psychiatric abnormalities or disorders, or current usage of medication (i.e. antidepressants or anxiolytics; with the exception of over-the-counter pain relievers or allergy medications). The eligibility requirements included that they had to be female, between the ages of 18 – 30, have a regular menstrual cycle (between 21 – 40 days), and have no plans of beginning birth control or getting pregnant for a minimum of four months. Those interested and with no obvious conflicts with the eligibility requirements were sent consent forms and screening forms for cardiovascular abnormalities via Docusign. Fifty-eight individuals were deemed eligible after completing the screening form and were further asked to complete a health history questionnaire. The reproductive health questionnaire assessed their demographics and any history of medication usage, marijuana or nicotine usage, mental health conditions, menstrual cycle patterns, birth control usage, reproductive health surgeries, and related topics. If they were deemed ineligible for recruitment, participants received $10 compensation for completing the consent, screening form, and health questionnaire.

Following screening, 35 participants were recruited for the pre-study remote cycle tracking, after which 10 participants terminated their participation due to scheduling difficulties or a loss of interest. Therefore, a total of 25 participants completed ≥ three cycles of remote tracking and ovulation testing, after which a second video-call interview was conducted to gauge interest and continued eligibility for enrollment in the remainder of the study. Due to study-completion time constraints, an additional 11 participants were fast-tracked directly to the in-lab sessions of the study without a full 3-cycles of pre-study remote tracking, after completing all pre-screening requirements. Five of these participants had ≥ two cycles of pre-study tracking, and two had one cycle of pre-study tracking completed prior to their first session.

7.2.3 Experiment Protocol

Three total sessions were completed (with as many staggered starting sessions as scheduling constraints would allow) for each participant: during the menses, ovulation, and mid-luteal phases of their cycle. Each session lasted ~3 hours and was typically scheduled for any day of the week, between 11AM – 4PM, with a few exceptions made due to unavoidable scheduling conflicts. Researchers informed participants to make their best efforts towards sticking to their typical routine, whatever that may be, for each day of their sessions. For the menstruation session, participants informed researchers of the first day of their menses and were brought in typically within the first 1 – 4 days of active-menstrual bleeding. For ovulation sessions, participants took daily ovulation tests (as described in Section 7.2.5), and came in for their session on the same day as their positive test result. Lastly, participants were given a 3 – 5 day range within which they could schedule their mid-luteal session, following data collected from ovulation testing completed ~7 days prior. These mid-luteal sessions were scheduled to

occur in a predicted window half-way between ovulation and their upcoming first day of menses. If there were any scheduling conflicts that interfered with accurate cycle-phase scheduling for any of the sessions, then the scheduling of that cycle phase was postponed until the next cycle opportunity.

Upon arrival for each in-lab session, researchers verified participant's proof of SARS-CoV-2 virus clearance status, following the University of California, Santa Barbara guidelines. Afterwards, participants signed and dated their previously-completed consent and screening forms and noted any changes to the researchers. They then completed a state questionnaire to assess their mood and disposition for the day, evaluating factors such as caffeine intake, exercise, and consumption of OTC painkillers (collected for future analyses). Participants were then guided into a private changing room, where they were given scrubs to change into and a locker in which to leave their belongings. Once they were in their scrubs, researchers guided them to an experiment room in which the behavioral and psychophysiology task took place. Participants were fitted with psychophysiology sensors (described in Section 7.2.6.b) and took part in a 1-hour long modified version of a classic stressor task: Gauss's modular arithmetic (Section 7.2.6.a) (Beilock, 2008; Bogomolny, 1996). Following task completion, all psychophysiology sensors were removed, participants were allowed to use the restroom to wash off excess electrode residue from their arm, and a blood sample was collected by a licensed phlebotomist. Lastly, participants completed a 1-hour MRI brain scan protocol (Section 7.2.6.d). Following their final third session, participants continued to track their menses for one last cycle (without ovulation testing). For potential future analyses, as well as data collection towards describing any variations or irregularities detected in their data,

participants completed a final questionnaire reviewing their medical, physical, and psychological disposition throughout the time of the study.

7.2.4 Menstrual cycle tracking

Most participants took part in remote pre-study ovulation testing and menstrual cycle tracking for ≥ three cycles prior to their first session, and all participants completed cycle tracking throughout the study and into one cycle following their final third session. This tracking assisted researchers in predicting upcoming menstruation and ovulation dates based on cycle history, which was essential to scheduling the in-person sessions. Participants were instructed to inform the researchers of the start and end dates of their menses either via email, text, or the "Clue Connect" data sharing feature of the mobile application "Clue". Menstruation data was recorded into a spreadsheet, in which researchers manually calculated the average length of each participant's menses and menstrual cycles. Additionally, participants were asked to share any prior menstrual cycle history from before beginning the study that they may have from personal use. Using all tracking data, the researchers made predictions of future menstruation and ovulation dates (as described in Section 7.2.5).

Furthermore, over the course of the pre-study tracked cycles, participants completed a total of nine ovulation self-tests (three days/cycle for three cycles). For these, participants were informed of a 3-day peak within the "fertile window" and were asked to complete ovulation self-tests by 8PM for each of those three days, and around the same time for all nine tests. After concluding ~3 cycles of tracking and ovulation testing, participants completed a survey reviewing their medical, physical and psychological conditions throughout the time of tracking (such as the use of emergency oral contraceptives). Ovulation testing was repeated prior to

ovulation and luteal sessions, with a varying range of 3 – 15 daily tests per cycle, depending on their "fertile window" during which their ovulation was likely to occur.

7.2.5   Ovulation testing

Ovulation test kits were mailed or dropped off at the participant's residence, consisting of 12 – 15 ovulation testing strips (Easy@Home, Premom) and 13 – 16 40 mL disposable plastic urine cups. Detailed instructions of how to properly complete the ovulation tests were sent to participants following recommendation from Premom. Researchers informed participants of their dates of ovulation testing by phone or email. On each day of testing, participants took the test by dipping the strip into a urine sample to detect the presence of the "LH surge" that triggers ovulation. After completing the test, the participant sent a clear photo of the test strip results to the researcher and reported the time at which the test was taken. Ovulation data received was associated with the participant's subject ID number and stored for future analyses. For ovulation sessions, participants were asked to complete ovulation tests prior to 9 AM, and to complete their in-lab session on the same day as their positive test result. Specifically, when an ovulation result was positive, the researcher would immediately contact the participant and schedule a time for them to come into the lab for their session that same day. Furthermore, they completed one ovulation test the day after their ovulation session, to track whether the session occurred on their "peak" LH-surge (i.e. whether the post-session test was more or less positive than the test from the day of the session). When an ovulation session was impossible to schedule due to any conflicts, then the session would be postponed to their next viable cycle, and a new round of ovulation testing would be repeated.

To predict which day(s) participants were beginning ovulation (i.e. had their "LH surge"), researchers used all gathered menstrual cycle data, in conjunction with the most recent menses start date to estimate a 12-day "fertile window" during which ovulation was likely to occur. For the first cycle of tracking, if researchers did not have any previous tracking data, predictions were initially made based on a guiding trend that ovulation typically occurs anywhere from 12 – 14 days from the first day of the cycle (i.e. the first day of their menses). All ovulation predictions following the first cycle were adjusted to account for individual differences based on test results. A positive result was depicted by the "test" line being as-dark-as or darker than the "control" line. To assist in test result monitoring, researchers used the Premom mobile application to upload test result images and extract an LH-to-control line "ratio" that determined the presence or absence of an LH surge. A ratio ≥ 0.80 was considered positive, with the higher the ratio, the more positive the result. An example of an accurate prediction of LH surge occurring on day two of testing would be if day one of ovulation testing resulted in a ratio of 0.56, followed by a peak of 0.93 on day 2, and 0.52 on day 3. Alternatively, if the results were negative or not strong-positives (i.e. a ratio of 0.78, hence no LH surge detected), then future predictions were adjusted towards the closest direction of positivity. Researchers' prediction accuracy increased over time as more cycle and ovulation data was collected. For instance, while a participant's ovulation test ratio might never have reached $\geq$ 0.80, their highest peak ratio throughout a full cycle was considered a positive result for the next round of testing.

If researchers had data from at least three or more menstrual cycles, then the average menstrual cycle length of all tracked cycles was used to predict the ovulation dates. Alternatively, if less than three menstrual cycles had been tracked, then researchers would use

an average of participants' self-reported menstrual cycle length with any tracked menstrual cycle data. However, if no previous menstrual cycle data was collected yet, a combination of participants' self-reported average menstrual cycle length and any ovulation test results were used to inform predictions of future ovulation dates. Depending on the individual, our estimates led us to predict that the fertile window would most likely occur within days 10 – 16 of the cycle.

7.2.6 Assessments and Measures

7.2.6.a Behavioral Task

The behavioral task served the purpose of measuring the relationship between fluctuating levels of HPG sex hormones and allostatic responses of the SNS, cognitive performance in response to a motivated task, response to monetary reward sensitivity, and how the interaction between allostatic load and cognition might alter across hormone concentrations. This modular arithmetic (MA) task consisted of a 2x2 design in which problems varied in difficulty (easy or hard), and the amount of monetary reward (low or high) that was possible to gain from each problem (Figure 7.1; MA is described in Section 6.2.2.a). Throughout the task, participants had to respond accurately to MA problems before their trial time ran out, with challenging time limits personalized to the individual for each session. All responses were made using their right hand on a keyboard, selecting "n" with their index finger if they believed the MA problem was divisible, or "m" with their middle finger if they believed it was indivisible. Depending upon their task performance, participants were able to make a bonus of up to $75 across all three sessions.

Four separate MA conditions were formed: hard problems with high monetary reward, hard problems with low reward, easy problems with high reward, and easy problems with low reward. Additionally, a blank gray screen (a "rest screen") that lasted four seconds was included as a fifth condition. For the purpose of pseudo-randomizing the trial order, trials were m-sequenced with a base value of five (4 conditions + "rest") and a power of three (allowing no repeated sequences higher than 3) (Buracas, 2022). MA problems were split evenly between either hard or easy difficulty levels. Easy problems contained more single digits, and did not require numerical carry-over (e.g. $10 \equiv 2 \pmod 4$; $15 \equiv 4 \pmod 3$). Conversely, hard problems contained double digits and did require carry-over analysis (e.g. $54 \equiv 17 \pmod 9$; $82 \equiv 26 \pmod 8$). Regarding reward levels, high reward problems were set at $2.50, while low reward problems were set to $0.10, with high reward values occurring more infrequently (30% of MA problems) for the purpose of increasing the stakes of high reward opportunities. Across all five trial conditions, 20% of trials were "rest" screens, 30% were low reward x hard, 30% were low reward x easy, 10% were high reward x hard, and 10% were high reward x easy.

Each session's MA task began with instructions and a block of 30 practice trials. The last 10 practice trials were all hard problems, from which a median response time was recorded. To individualize the difficulty level per participant, as well as to account for possible learning effects across sessions, response time limits for the remainder of the task were adjusted per session to 75% of this median response time. Participants were kept unaware of how time-limits were set throughout their participation in the study, which was confirmed by self-report to the researchers after participants completed their third and final session.

The instructions familiarized participants with the format of MA and informed them that their goal was to complete these problems as quickly and as accurately as possible.

Furthermore, they were notified that trials were "worth" either $0.10 or $2.50, and that trials of $2.50 were rare. Additionally, the instructions stated that they are capable of making a bonus of up to $75 across all three of their sessions, and that how much money they received was dependent upon their performance: the better they performed, the more money they would get. Instructions further described that their performance was measured by correctly answering an MA problem quickly, before a set time limit. While they were made aware of this time-limit, they were not told how long the time limit would be or how it would be calculated.

They were also informed that when they conclude their third session's task, a number of random problems that they completed would be chosen from across their three sessions (worth up to $75). Of these chosen problems, they would receive the reward value attached to each problem that they answered accurately and before their time ran out. However, for the problems that they did not get correct or timed out for, they would receive $0.

The task order consisted of a four sec screen that informed participants of the trial's reward value presented in red large and bold font, after which the MA problem would appear, followed by a four sec feedback screen. The feedback screen would appear either immediately after the participant's response or once the MA problem timed-out prior to receiving a response. Feedback consisted of the following responses, accordingly: "CORRECT" (in green), "WRONG" (in red), or "TOO SLOW!" (in black). The "rest screen" consisted of a three sec blank gray screen that would appear between feedback and reward value screens. The overall task consisted of two blocks of 124 trials for a total of 248 trials. After the first block, a "break screen" would appear, informing participants that they can take a mental rest and to press the spacebar key when they were ready to continue the remainder of the task. Prior to the start of the task, they were informed that the break was purely meant to rest their mind, and

that they should continue to refrain from any movement throughout the break in order to avoid disruptions to the psychophysiology data. Once the second block was completed, a screen would appear instructing participants to ring a bell placed on the table to inform researchers that they had finished the task.
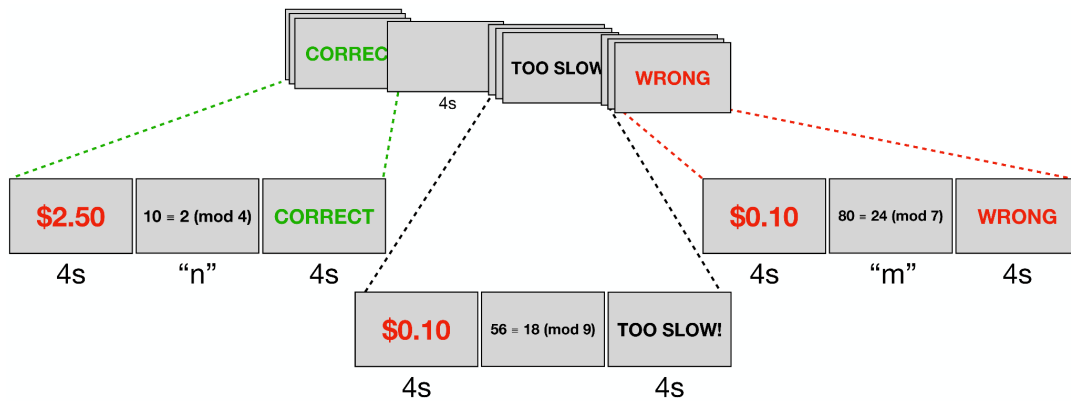
Figure 7.1   An example of four consecutive trials of the task. First, a reward value of the upcoming modular arithmetic (MA) problem is presented for four seconds. Then the MA problem is presented, to which the participant either responds "n" or "m", or the trial times out prior to receiving a response. This is followed by a four second feedback screen, which informs the participant if their response was correct, wrong, or too slow. From left to right, the three trial types shown here are: a high reward x easy trial, a "rest screen" trial (4 sec duration), a low reward x hard trial, and lastly another low reward x hard trial.

7.2.6.b Psychophysiology

The use of a trans-radial bioimpedance velocimetry device (TREV; described in Chapter 5) was combined with the MA task to estimate SNS responses to task conditions. For each in-lab session, TREV was placed on the participant's left forearm prior to the behavioral task, following the procedure listed in Section 5.2.5 (Figure 7.2). For the purposes of estimating respiration rate to regress respiration artifacts out of the TREV data during preprocessing, a respiration belt was secured around the waist with a hook and loop strap. All TREV and respiration materials and equipment were identical to those described in Section 5.2.4, without the inclusion of ECG. Experiment triggers were collected via Digital I/O using a LabJack U3-

LV (LabJack, Inc.) connected to a UIM100C amplifier (Biopac Systems Inc.). The participant's left arm (containing TREV electrodes), was set to rest on the experiment desk, such that their elbow and forearm were laid comfortably flat on the desk, requiring no muscle activity. During psychophysiology setup, the researcher reviewed the importance of minimizing all unnecessary movements, especially any muscle activity of their left arm, throughout the course of the study. Following the behavioral task instructions and practice trials, five minutes of baseline psychophysiology data was collected while the participant was at rest, during which researchers left them alone in the experiment room. After the five minutes concluded, researchers re-entered the room and stopped baseline data collection, ensured that the participant was ready to begin the study, re-started psychophysiology collection, and informed the participant that when they are ready to do so, they could click the spacebar key to begin the task. Researchers left the experiment room prior to the start of the task, and only returned once they heard the participant ring a bell, signifying that they completed the task. Following task completion, psychophysiology data collection was stopped and saved, the respiration belt and sensors were removed, and the participant was encouraged to use the restroom to wash off all excess residue remaining from the sensors in preparation for their proceeding blood draw and MRI scanning protocol.

Signal filtering was identical to that described in Section 5.2.6. Additionally, the subsequent preprocessing of the contractility timeseries closely resembled the procedure described in Section 5.2.6. The main difference being that we used contractility epochs instead of ECG R-peaks to estimate heartbeat time-indices and heart-rate. Specifically, MEAP automatically labeled each epoch peak of the continuous beatwise contractility waveform, which was used as a time indice for heartbeats in place of R-peaks. Additionally, MEAP

estimated heart rate from the distance between contractility peaks. The remainder of the preprocessing of the psychophysiology data matched those listed in Section 5.2.6, but time-matched to the present experiment protocol.
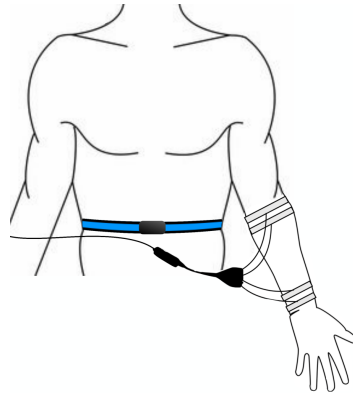
Figure 7.2   Psychophysiology setup, with the trans-radial electrical bioimpedance velocimetry device (TREV; represented by three strip electrodes) placed on the left forearm. Respiration belt (in blue) was secured around the waist with a hook and loop strap.

7.2.6.c Endocrine procedure

One blood sample (< 8.5 – 10 cc) was collected from each participant once per session (three total samples per participant), to assess serum levels of the gonadal hormones 17β-estradiol and progesterone, along with the pituitary gonadotropins luteinizing hormone (LH) and follicle stimulating hormone (FSH). For each blood draw, a licensed phlebotomist first inserted a vacutainer push button (BD Diagnostics) intravenous line into the hand or forearm of the participant. A 10mL vacutainer SST tube (BD Diagnostics) was attached to the intravenous line using an adapter. The sample was placed at room temperature for 30 minutes to clot, and then centrifuged at 2100 RPM for 10 minutes. Afterwards, the blood was aliquoted into three 2mL microtubes, each containing 1mL of serum. Serum samples were stored in a -80°C freezer until being shipped for analysis to the Endocrine Technologies Core (ETC) at the Oregon National Primate Research Center (ONPRC) (described in Section 7.2.7.a).

7.2.6.d MRI protocol

For each session, participants completed a one hour magnetic-resonance imaging (MRI) scanning sequence following the blood draw. Ninety six total scanning sessions were administered, with 30 of the 35 participants having completed all three of their MRI sessions, for a total of 90 full session-sets. MRI scans used a Siemens 3T Prisma MRI scanner with a 64-channel phased-array head/neck coil. First, high-resolution T1-weighted magnetization prepared rapid gradient echo (MPRAGE) anatomical scans were acquired and used for spatial normalization (TR = 2500 ms, TE = 2.22 ms, FOV = 241 mm, T_1 = 851 ms, flip angle = 7°, with 0.9 mm^3 voxel size). Followed by a gradient echo fieldmap (TR = 758 ms, TE_1 = 4.92 ms, TE_2 = 7.38 ms, FOV = 208 mm, flip angle = 60°, with 2.0 mm^3 voxel size). Next, the participant completed a 10 minute resting-state fMRI scan using a whole brain T_2*-weighted multiband echo-planar imaging (EPI) sequence sensitive to the blood oxygenation level-dependent (BOLD) contrast (72 oblique slices, TR = 720 ms, TE = 37 ms, FOV = 208 mm, voxel size = 2 mm^3, flip angle = 52°, multiband factor = 8). For this scan, participants were asked to focus their eyes on a plus sign in the middle of a projected screen, to blink regularly, to limit all movement, and to stay awake. Next, a high-resolution T2-weighted turbo spin echo (TSE) scan was acquired with an oblique coronal orientation positioned orthogonally to the main axis of the hippocampus (TR = 10,640 ms, TE = 50 ms, FOV = 175 mm, flip angle = 122°, 0.4 x 0.4 mm^2 in-plane resolution, 2 mm slice thickness, and 41 interleaved slices with no gap, with a total acquisition time of 5:42 min). Finally, a series of 4 spherical b-tensor (b = 0, 100 – 500, 1000, 1500 s/mm^2; 3 diffusion directions) and 4 linear b-tensor (b = 500, 1000, 1500, 2000 s/mm^2; 30 diffusion directions) q-space trajectory encoding (QTE) diffusion sequences were collected (TR = 6308 ms, TE = 80 ms, diffusion gradient amplitude = 80.0

mT/m, FOV = 230 mm, flip angle = 90°, 2.0 x 2.0 mm^2 in-plane resolution, 4.0 mm slice thickness, iPAT factor = 2).

7.2.7 Data Preprocessing & Analysis Methodology

7.2.7.a Analysis of HPG hormone concentrations

Serum estradiol (E2), progesterone (P4), luteinizing hormone (LH) and follicle-stimulating hormone (FSH) concentrations were measured by the Endocrine Technologies Core (ETC) at the Oregon National Primate Research Center (ONPRC, Beaverton, OR). Plots of these hormone concentrations across participant cycle phases and sessions are shown in Figures 7.3 and 7.4. Session-order differences are clear in mean concentration summaries in Figure 7.4, which was accounted for in all statistical models. E2 and P4 concentrations were measured using ultra-high performance liquid chromatography-heated electrospray ionization-tandem triple quadrupole mass spectrometry (LC-MS/MS) on a Shimadzu Nexera-LCMS-8060 instrument (Kyoto, Japan) as previously described (Bishop et al., 2019). Briefly, 150 µl of serum were mixed with 100 µl ultrapure water (Milli-Q, EMD Millipore, Billerica, MA) containing 2.5 ng/ml E2-d5 and 3.0 ng/ml P4-C3 isotopic standards (Cerilliant, Round Rock, TX) and added to a 400 µl SLE+ extraction plate (Biotage, Charlotte, NC). Steroids were eluted with 3 x 600 µl dichloromethane (Sigma, St. Louis, MO), dried with forced air and reconstituted in 50 µl of 25% (v:v) methanol:ultrapure water. For calibration curves, charcoal-stripped human serum (Golden West Biologicals) was spiked with unlabeled E2 and P4 standards (Cerilliant) in methanol and diluted serially to final concentrations between 0.002 and 20 ng/ml in a 15-point curve. The spiked standards were then subjected to the SLE+ extraction procedure. Using a Shimadzu SIL-30CAMP autosampler, 5 µl of each sample were

injected onto a Raptor 2.7 μm Biphenyl 100 mm X 2.1 mm column (Restek, Bellefonte, PA). Mobile phase consisted of 0.15 mM ammonium fluoride (Sigma) in water (A), and methanol (B) with a flow rate of 0.4 ml/min. Using a Shimadzu Nexera LC-30AD system (LC), gradient elution started at 97% B, increased to 100% B (4.00-5.10 min), held at 100% B (5.10-6.90 min), decreased to 65% B (7.00-10.4 min), and returned to 97% B for a total of 10.4 minutes/sample. E2 and P4 had retention times of 2.1 and 4.7 min, respectively. E2 was detected in negative ion mode and P4 was detected in positive ion mode, both with multiple reaction monitoring (MRM) using a Shimadzu LCMS-8060 tandem triple-quadrupole MS with heated electrospray ionization (ESI). The MRM transitions used were: E2, 271.05144.95 (quant), 271.05142.95 (qual), m/z; E2-d5, 276.20187.20 (quant), 276.20147.20 (qual), m/z; P4, 315.15109.25 (quant), 315.1597.05 (qual); P4-C3, 318.15112.15 (quant), 318.15100.15 (qual). The range for both standard curves was 0.002 to 20 ng/ml. Lower limit of quantification for E2 was 0.002 ng/ml and the lower limit of quantification for P4 was 0.010 ng/ml. Data processing and analysis was performed using LabSolutions Software, V5.72 (Shimadzu). Intra-assay variation was 2.1% for E2 and 12.3% for P4; accuracy was 100.9% for estradiol and 106.3% for P4. Because all samples were analyzed using one assay, no specific inter-assay variation was calculated for this experiment. The overall inter-assay variation for these assays in the ETC is less than 15%.

LH and FSH concentrations were measured using a Roche cobas e411 automated clinical immunoassay platform (Roche Diagnostics, Indianapolis, IN). The assay range for both LH and FSH assays was 0.1 – 200 mIU/ml. Intra- and inter-assay CVs for the LH assay were 2.3% and 2.4%, respectively (n = 2 assays). Intra- and inter-assay CVs for the FSH assay were 0.9% and 1.0%, respectively (n = 2 assays). The Endocrine Technologies Core (ETC) at
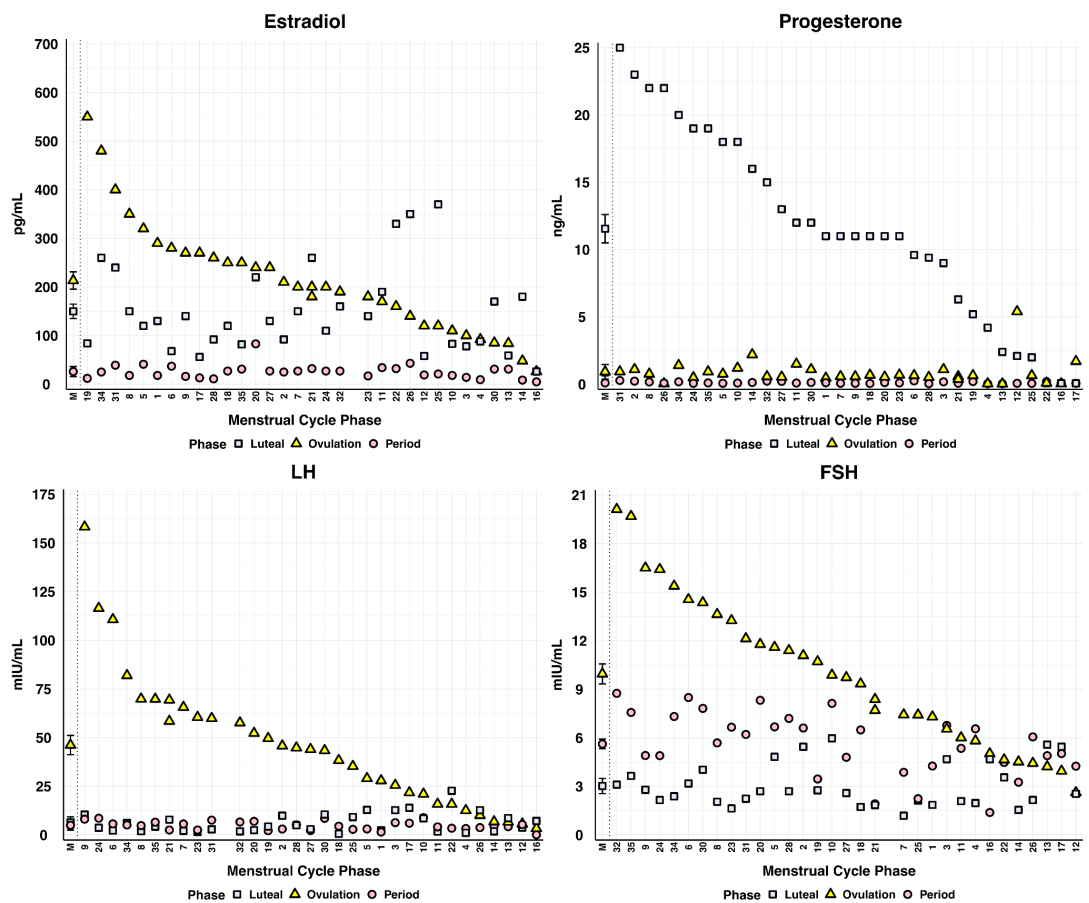
Figure 7.3 Concentrations of 17β-estradiol (E2), progesterone (P4), luteinizing hormone (LH) and follicle stimulating hormone (FSH), by cycle phase. The y-axis represents hormone concentration levels, and the x-axis contains each individual participant, with group-averages (M) on the farthest right. E2, LH, and FSH concentrations are rank-ordered by individuals' concentration from the ovulation session, while P4 concentrations are ordered by luteal sessions.

111
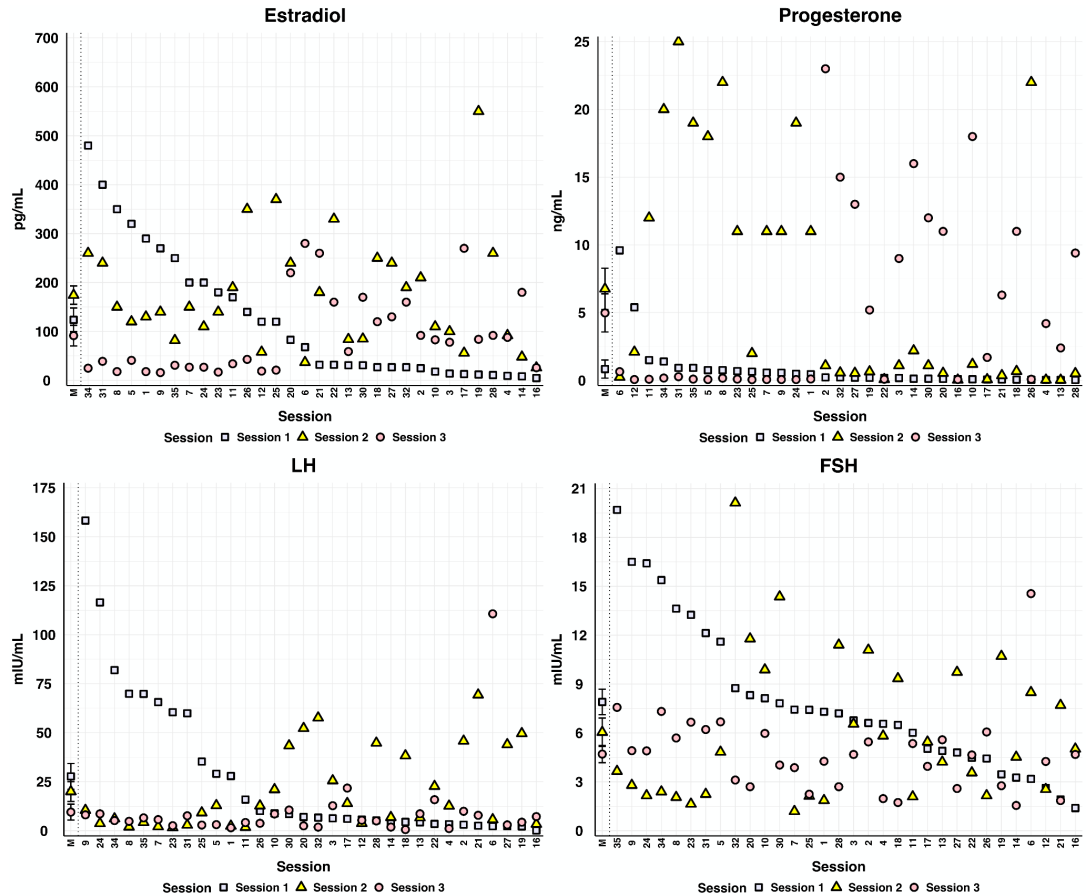
Figure 7.4   Concentrations of 17β-estradiol, progesterone, luteinizing hormone (LH) and follicle stimulating hormone (FSH), by session order. The y-axis represents hormone concentration levels, and the x-axis contains each individual participant, with group-averages (M) on the farthest right. All hormone concentrations are rank-ordered by individuals' concentrations in session 1.

7.2.7.b Statistical analysis of behavioral & contractility data

29 females came in for three sessions to complete a task with three conditions (trials with hard equations and easy equations, and trials with high reward and low reward). Thus, this task creates 12 different trial conditions, across three sessions, two difficulty levels, and two reward levels. For instance for session 1, the following four trial conditions emerge: session1_easy_lowReward, session1_easy_highReward, session1_hard_lowReward, and session1_hard_highReward. The structure of these three examples would then be repeated

across the remaining two sessions, to create a total of 12 trial conditions. Furthermore, for each session, a blood draw was taken and used to record participants' hormone levels across four HPG hormones (estradiol, progesterone, LH and FSH).

To first summarize each participant's behavior and contractility estimates across the 12 trial conditions, and thereafter relate these summaries to hormone concentrations (across subjects), we used a hierarchical Bayesian regression approach. This approach is capable of accounting for outliers by employing shrinkage on mean posteriors to avoid a Type I error, decreasing the chances that significant effects may be driven by a single outlier participant. Specifically, this Bayesian regression estimates the parameters (M and E) of a hierarchical Gaussian distribution from which each subject's condition specific mean (μ) is drawn for each of the 12 trial conditions, i.e., a M, E and μ for each, all fitted in a single model. Significance at the group level is determined by the posterior distribution of a hierarchical distribution's M parameter exceeding 0, using a 94% highest density interval (HDI). In other words, allowing for individual differences (the E parameter), the mean of the hierarchical distribution (M) characterizes μ across all subjects is confidently above or below 0 for a given condition. In addition, we included a region of practical equivalence (ROPE), as defined by Makowski et al. (2019), in which the HDI interval had to cross either 0.1 or -0.1 to be valued as credible (Kruschke, 2018).

In terms of behavior parameters, reaction time (RT) and accuracy of each response was recorded. For a mean average to be appropriate, RT was log transformed. Accuracy was estimated with a hierarchical binomial, which uses a theta parameter for each subject's accuracy (instead of a μ), and is pulled from a hierarchical beta distribution with parameters a and b (instead of M and E). In the first step of the modeling procedure, two hierarchical

Bayesian regression models with a similar model structure were created: one for mean logged RT, and one for accuracy. For each of these models, we estimated each participant's log RT and accuracy, and computed a separate mean log RT and accuracy for each of the 12 trial conditions. Therefore, for each trial condition, we extracted a mean log RT (or accuracy) per each individual and across the group level. Each group level estimate is created from the 29 individual estimates. This group level then acted as our Bayesian group level hierarchical prior for summarizing behavior effects across our conditions.

Then, separately for each of the 12 trial conditions, we ran deterministic regressions across participants using their individual estimates to examine if log RT and accuracy were predicted by session-specific hormone states. This allowed us to ask whether the session-specific hormone state predicted the condition-specific behavior, separately for all 12 trial-type groups. Due to the deterministic regression being performed for each moment of the task, the analysis is no longer subjected to learning or session order effects.

Finally, we created post-hoc main effects across these different group level trial conditions. For each of the deterministic regressions we ran, we extracted a regression coefficient. In order to look at main effects, we then averaged across the relevant combinations of these regression coefficients. For instance, to estimate the main effect of estradiol (E2) for RT during session 1 (session1_e2), we would average across the first four regression coefficients relating to that hormone: session1_easy_lowReward_e2, session1_easy_highReward_e2, session1_hard_lowReward_e2, and session1_hard_highReward_e2. Then, to further estimate the main effect of estradiol overall on RT, we would average across: session1_e2, session2_e2, and session3_e2.

For each participant, three different contractility measures were estimated in response to every trial: mean contractility during the two seconds following the equation being shown on the screen (further labeled as "contractility"), averaged contractility of the four seconds after the feedback screen appeared ("feedback contractility"), and the slope of the change in contractility in those four seconds following feedback presentation (i.e. "allostatic efficiency"). Then the same model structure as listed above for behavioral data was created for each of the contractility parameters: "contractility", "feedback contractility", and "allostatic efficiency". Interaction models of brain, behavior, and contractility were also created, in which the beta relates the parameters of contractility to those of behavior.

7.2.7.c Hippocampal segmentation

T1-weighted and high-resolution T2-weighted TSE images (n = 180 of 31 subjects) were submitted to the automatic segmentation of hippocampal subfields package (ASHS) (Yushkevich et al., 2015) for bilateral parcellation of seven MTL subregions: CA1, CA2/3, dentate gyrus (DG), subiculum (SUB), perirhinal cortex (PRC), entorhinal cortex (ERC), and parahippocampal cortex (PHC) (Figure 7.5). The ASHS segmentation pipeline automatically segmented the hippocampus in the T2-weighted MRI scans using a segmented population atlas, the Princeton Young Adult 3T ASHS Atlas template (n = 24, mean age 22.5 years; Aly & Turk-Browne, 2016). A rigid-body transformation aligned each T2 image to the respective T1 image for each participant and session. Using the Advanced Normalization Tools (ANTs) deformable registration, the T1 image was then registered to the population atlas. The resulting deformation fields were used to resample the data into the space of the left and right template MTL regions of interest (ROI).

Within each template ROI, each of the T2 scans of the atlas package were registered to that session's T2 scan. The manual atlas segmentations were then mapped into the space of the T2 scan, with segmentation of the T2 scan computed using joint label fusion. Finally, the corrective learning classifiers contained in the atlas package were applied to the consensus segmentation produced by joint label fusion. The output of this step is a corrected segmentation of the T2-weighted scan. Further description of the ASHS protocol can be found in (Yushkevich et al., 2015). For reasons yet to be determined, this automated process failed for seven of the T2-weighted scans. Right and left hemisphere values for homologous ROIs were averaged to obtain seven bilateral region values per participant session. For final analyses, only those participants who had completed all three sessions of MRI scans and for whom this preprocessing was successful for all three sessions were included (n = 21).
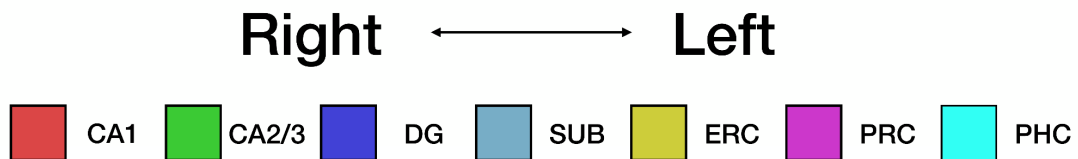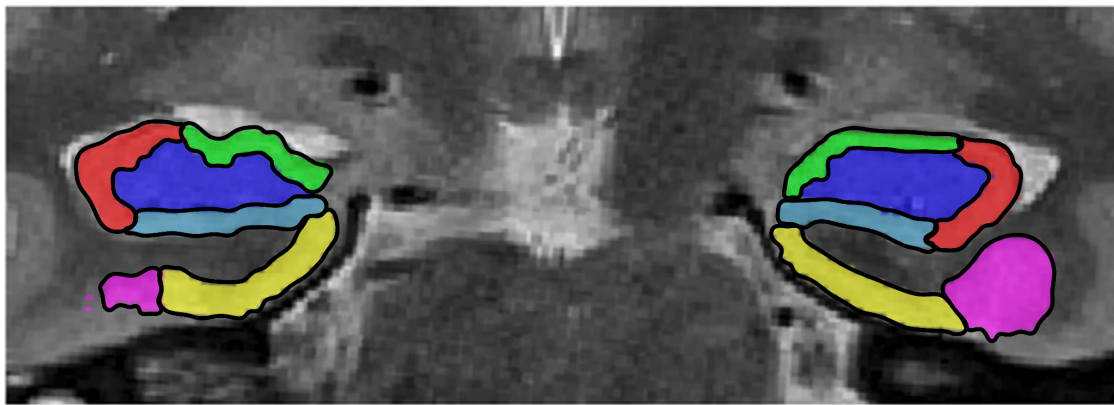
Figure 7.5   A sample slice of the hippocampus subfields and medial temporal lobe (MTL) cortex labels completed by the automatic hippocampal subfields package (ASHS).

7.2.7.d White matter integrity (WMI) estimation

MRI preprocessing was conducted with Advanced Normalization Tools (ANTs) (Avants et al., 2011). Specifically, T1-weighted anatomical data were skull stripped with antsBrainExtraction.sh and segmented using ANTsPy kmeans segmentation to obtain white matter (WM) probability maps, which were binarized to create individualized WM masks. QTE images were motion and eddy current corrected, and diffusion tensor distribution (DTD) parameters were estimated for each participant (Nilsson et al., 2018). HCP1065 Population-Averaged Tractography Atlas probabilistic region masks (thresholded at $\geq$ 50%) and participant DTD data were spatially normalized to their respective T1 anatomical space (Yeh, 2022). Gray matter and cerebrospinal fluid (CSF) were masked out using the anatomic segmentations, and white matter was segmented into 64 regions of interest (ROIs) using the atlas masks. Mean micro-fractional anisotropy (µFA), fractional anisotropy (FA), and orientation parameter (OP) values (Westin et al., 2016) were calculated for each ROI. Commonly used FA estimates of white matter integrity (WMI) are heavily dependent on the number of crossing, kissing, and fanning fibers in each voxel rendering them unreliable for group level analysis (Volz et al., 2018). In contrast, µFA values obtained from q-space trajectory encoding (QTE) diffusion sequences are not sensitive to crossing, kissing or fanning fibers, collectively estimated as an orientation parameter (OP). Right and left hemisphere values for homologous ROIs were averaged to obtain 34 bilateral region values per participant session. All further white matter integrity (WMI) analysis and results discussed are regarding the estimated mean µFA values per region.

7.2.7.e Statistical analysis of MTL gray matter volume and WMI

Female participants came in for three sessions to complete an MRI scan estimating values of medial temporal lobe (MTL) gray matter volume of seven MTL subregions (n = 21) and white matter integrity (WMI) within 34 regions (n = 30). Thus, this created 102 white matter ROI levels, and 21 MTL volume levels. For instance, for session 1, the following seven MTL levels emerge: session1_CA1, session1_CA2/3, session1_DG, session1_SUB, session1_PRC, session1_ERC, and session1_PHC). The structure of these seven examples would then be repeated across the remaining two sessions, to create a total of 21 levels. Further, for each session, a blood draw was taken and used to record participants' hormone levels across four HPG hormones (estradiol, progesterone, LH and FSH).

To test the relation between brain variables (MTL volumes and WMI) and hormone concentrations across the three testing sessions, we used a hierarchical Bayesian regression approach. This approach is capable of accounting for outliers by employing shrinkage on mean posteriors to avoid a Type I error, decreasing the chances that significant effects may be driven by a single outlier participant. In each model, this Bayesian regression estimates the distributions for coefficient $\beta_{n,r}$ that relate hormone level to brain variables for subject n and region r. $\beta_{n,r}$ parameters were assigned a Gaussian hierarchical prior with parameters μ_r and σ_r. We additionally constrained μ_r and σ_r with uninformative Gaussian ($\mu_{rr}\sim N(0,1)$) and half-Gaussian ($\mu_{rr}\sim halfN(1)$) priors. Given our prior that hormones selectively impact volumes of different regions of MTL, we separately fitted 28 models to cover the hormone (4) by region (7) space, and report significance at the group level from each model by the posterior distribution of its μ_r parameter, and whether it credibly exceeds 0, using a 94% highest density interval (HDI). In other words, allowing for individual differences (the σ_r parameter), the mean

of the hierarchical distribution (μ_r) characterizes whether β_r, across all subjects is confidently above or below 0 for a given region.

Given the exploratory nature of our investigation of hormones impacting WMI, we imposed an additional layer to the hierarchy. Here we fitted four models, one for each hormone. Each model fitted $\beta_{n,r}$ for each of the 34 brain regions, constraining region-specific distributions of participant coefficients with Gaussian priors ($\beta_{n,r} \sim N(\mu_r, \sigma_r)$). We additionally constrained μ_r and σ_r with brain-wide Gaussian priors, $\mu_r \sim N(M_\mu, E_\mu)$ and $\sigma_r \sim N(M_\sigma, E_\sigma)$. We report significance at the group level from each hormone model by converting the relevant brain-wide priors into an effect size, $d = M_\mu / M_\sigma$. This effect size (d) communicates the average group-level relation between a given hormone and all brain regions (M_μ) scaled by the average level of between-subject variation in this relation across regions (M_σ). We then imposed a region of practical equivalence (ROPE), as defined by Makowski et al. (2019), in which the effect size had to cross either 0.1 or -0.1 to be valued as credible. This whole brain prior constrains all individual region estimates, and thus the model may show more or less credible individual regions than the previous region-specific analysis, but only if the majority of other regions are showing a similar effect (i.e. the whole-brain effect being credible may pull the regions towards credibility).

7.2.7.f Network analysis of fMRI resting-state data

fMRI data was preprocessed using the Statistical Parametric Mapping 12 software (SPM12, Wellcome Trust Centre for Neuroimaging, London) and in-house Matlab code. All resting-state scans were first motion-corrected and unwarped using a voxel displacement map derived from the field map scan. The resulting mean EPI was bias-corrected and coregistered to the skull-stripped, bias-corrected anatomical scan via the Advanced Normalization Tools

(ANTs) symmetric normalization (SyN) algorithm (https://github.com/ANTsX/ANTs; Avants et al., 2008, 2011). All functional and anatomical data were then warped to the 2 mm³ MNI152 template in a single interpolation step. A 4 mm full-width at half-maximum (FWHM) isotropic Gaussian kernel was subsequently applied to smooth the functional data. Further preparation for functional connectivity analysis included global signal scaling (median = 1000), linear detrending, and nuisance regression of motion and physiological artifacts. The nuisance model included a 24-parameter Volterra expansion of translation/rotation estimates (accounting for both time-lagged and nonlinear effects of motion on the BOLD signal) and five principal components of physiological noise extracted from all cerebrospinal fluid (CSF) and white-matter voxels; each regressor was detrended to match the fMRI timeseries.

Functional network nodes were defined based on a 400-region cortical parcellation (Schaefer et al., 2018) and 32-region subcortical parcellation (Tian et al., 2020). For each region, a summary BOLD time course was obtained by taking the first eigenvariate over time and applying a maximal overlap discrete wavelet transform, retaining the low-frequency fluctuations in wavelet scales 3 – 6 (~0.01 Hz – 0.17 Hz). Next, the spectral association between all pairs of brain regions was estimated using magnitude-squared coherence, yielding a 432 x 432 functional connectivity matrix for each scan. Importantly, coherence offers several advantages over other functional connectivity metrics, including estimation of frequency-specific covariances and robustness to temporal variability in hemodynamics, which can otherwise introduce time-lag confounds to more traditional metrics such as the Pearson correlation.

Finally, a network-based statistics approach (Zalesky et al., 2010) was used to assess linear dependencies between whole-brain functional connectivity and levels of

ovarian/gonadotropin hormones. In this procedure, first, a series of general linear models were fitted in which Fisher Z-transformed coherence estimates at each edge were regressed against a hormonal predictor (e.g., estradiol) and two nuisance regressors (mean framewise displacement and its square). The resulting matrix of t-statistics, describing a given brain-hormone association, was thresholded at $|t| \geq 3.0$; the surviving edges were then topologically-clustered by identifying connected graph components (i.e., a subset of connections for which a path can be found between any two nodes). Subsequent inference and family-wise error correction was ultimately performed at the level of graph components rather than individual edges, allowing the capture of spatially-distributed effects across network subsystems. Empirical null distributions for maximal component extent (i.e., the number of participating nodes and overall intensity) were generated via 10000 iterations of nonparametric permutation testing, constraining exchangeability to respect the repeated-measures nature of the data, and additionally using the Freedman & Lane (1983) method to appropriately factor in the presence of nuisance effects. Thus, a component was deemed 'significant' at αFWE = .05 if its size/intensity exceeded the maximum component extent of each permutation more than 95% of the time.

7.3   Results

7.3.1   Accuracy and response time (RT) on MA task

The effects of four HPG hormone concentrations (estradiol, progesterone, LH, and FSH) were investigated on behavioral parameters of response time (RT) and accuracy for 29 participants. First, repeated measures ANOVAs were performed to compare the effect of difficulty and reward on normalized parameters of accuracy and RT across all sessions and

hormone levels. There was a statistically significant difference in both accuracy $(F(1, 28) = 790.6, p < 0.001)$ and RT $(F(1, 28) = 264.27, p < 0.001)$ on hard vs. easy trials, confirming that hard trials were more difficult. However, there was no statistical significance found between high vs. low reward levels for either accuracy $(F(1, 28) = 2.49, p = 0.126)$ or RT $(F(1, 28) = 0.19, p = 0.669)$ (Figures 7.6 and 7.7).
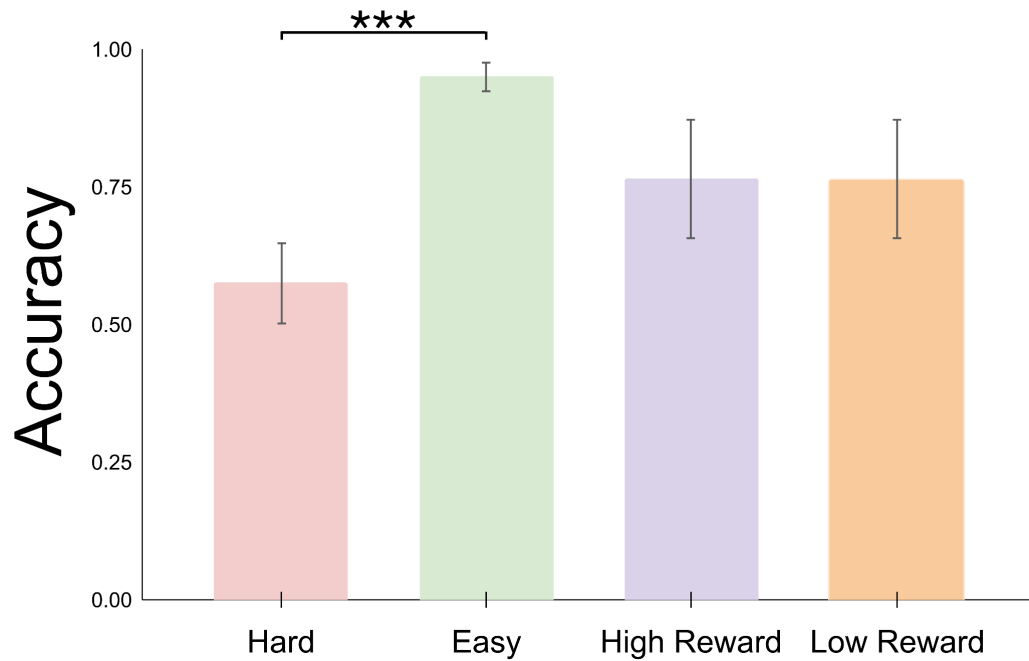
Figure 7.6 Group-averages of accuracy ratios (ranging from $0 - 1$) split by difficulty (easy vs. hard) and reward (high vs. low) across hormone concentrations. Error bars represent standard deviations. Overall, participants were significantly more accurate for easy trials compared to hard trials $(p < 0.001)$.
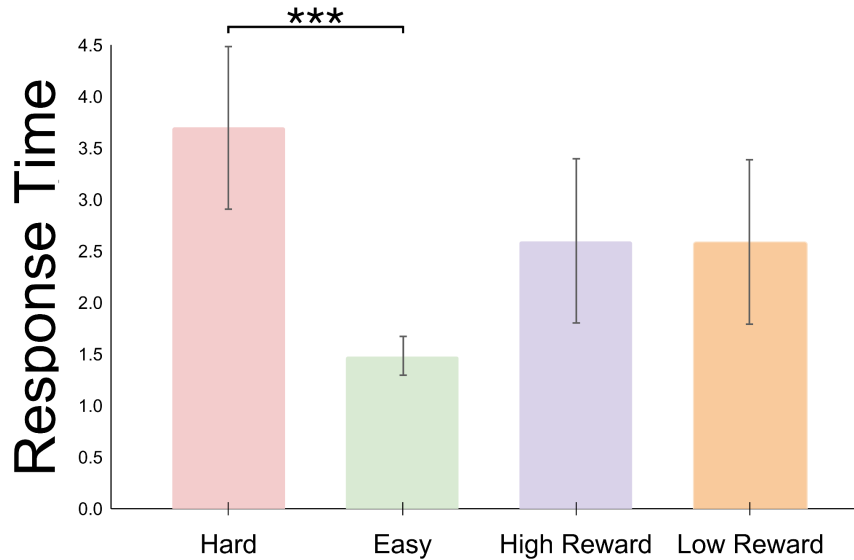
Figure 7.7   Group-averages of median response time (RT) values split by difficulty (easy vs. hard) and reward (high vs. low) across hormone concentrations. Error bars represent standard deviations. Overall, participants were significantly slower for hard trials compared to easy trials (p < 0.001).

Results of the Bayesian hierarchical regression between concentrations of HPG hormones and RT to MA problems confirmed a credible positive relationship between concentrations of both progesterone and FSH with RT, specifically to hard MA trials. The mean of the hierarchical posterior distribution of subjects' beta values for progesterone was 0.18 with a 94% HDI of [0.17, 0.20], and the mean for FSH was 0.14 with a 94% HDI of [0.12, 0.16] (Figure 7.8). These results suggest that greater concentrations of progesterone and FSH were related to greater RT on hard trials. This means that participants were slower to respond to cognitively demanding problems at times when they had higher levels of progesterone and FSH in their blood (Figure 7.9). However, there were no credible effects of any HPG hormones on task accuracy, suggesting that these hormones had no effect on which trials participants answered correctly or incorrectly. No other HPG hormones showed credible relations with either RT or accuracy. Any session effects are not reported due to session order being too convoluted with task learning effects and unequal distribution across menstrual phase (Figure

7.4). Complete tables of regression coefficients for all parameters of RT and accuracy (including possible session effects) are available in appendix A.

	Response Time Regression Coefficients				
	Relations	**Mean**	**Lower HDI**	**Upper HDI**	**Credible**
1	session1_easy_lo_E2	-0.08	-0.14	-0.03	
2	session1_easy_lo_P4	-0.14	-0.20	-0.09	
3	session1_easy_lo_LH	-0.01	-0.06	0.05	
4	session1_easy_lo_FSH	-0.11	-0.17	-0.05	
5	session1_easy_hi_E2	-0.10	-0.19	0.00	
6	session1_easy_hi_P4	-0.19	-0.27	-0.10	***
7	session1_easy_hi_LH	0.00	-0.09	0.09	
8	session1_easy_hi_FSH	-0.11	-0.20	-0.03	
...	...	...	...	...	
106	hard_lo_P4	0.18	0.16	0.19	***
107	hard_lo_LH	0.07	0.05	0.09	
108	hard_lo_FSH	0.15	0.13	0.17	***
109	hard_hi_E2	0.04	0.01	0.07	
110	hard_hi_P4	0.19	0.16	0.22	***
111	hard_hi_LH	0.07	0.04	0.10	
112	hard_hi_FSH	0.13	0.10	0.16	
113	easy_E2	-0.03	-0.07	0.00	
114	easy_P4	0.00	-0.03	0.03	
115	easy_LH	0.01	-0.03	0.04	
116	easy_FSH	-0.01	-0.04	0.02	
117	hard_E2	0.03	0.01	0.05	
118	hard_P4	0.18	0.17	0.20	***
119	hard_LH	0.07	0.05	0.09	
120	hard_FSH	0.14	0.12	0.16	***
...	...	...	...	...	
141	E2	0.00	-0.02	0.02	
142	P4	0.09	0.08	0.11	
143	LH	0.04	0.02	0.06	
144	FSH	0.06	0.05	0.08	

Figure 7.8　Regression coefficients of response time (RT) to modular arithmetic (MA) trials for 29 participants. Results show credible positive main effects of progesterone (P4) and follicle stimulating hormone (FSH), such that an increase in either P4 or FSH is associated with a slower response time to hard problems.
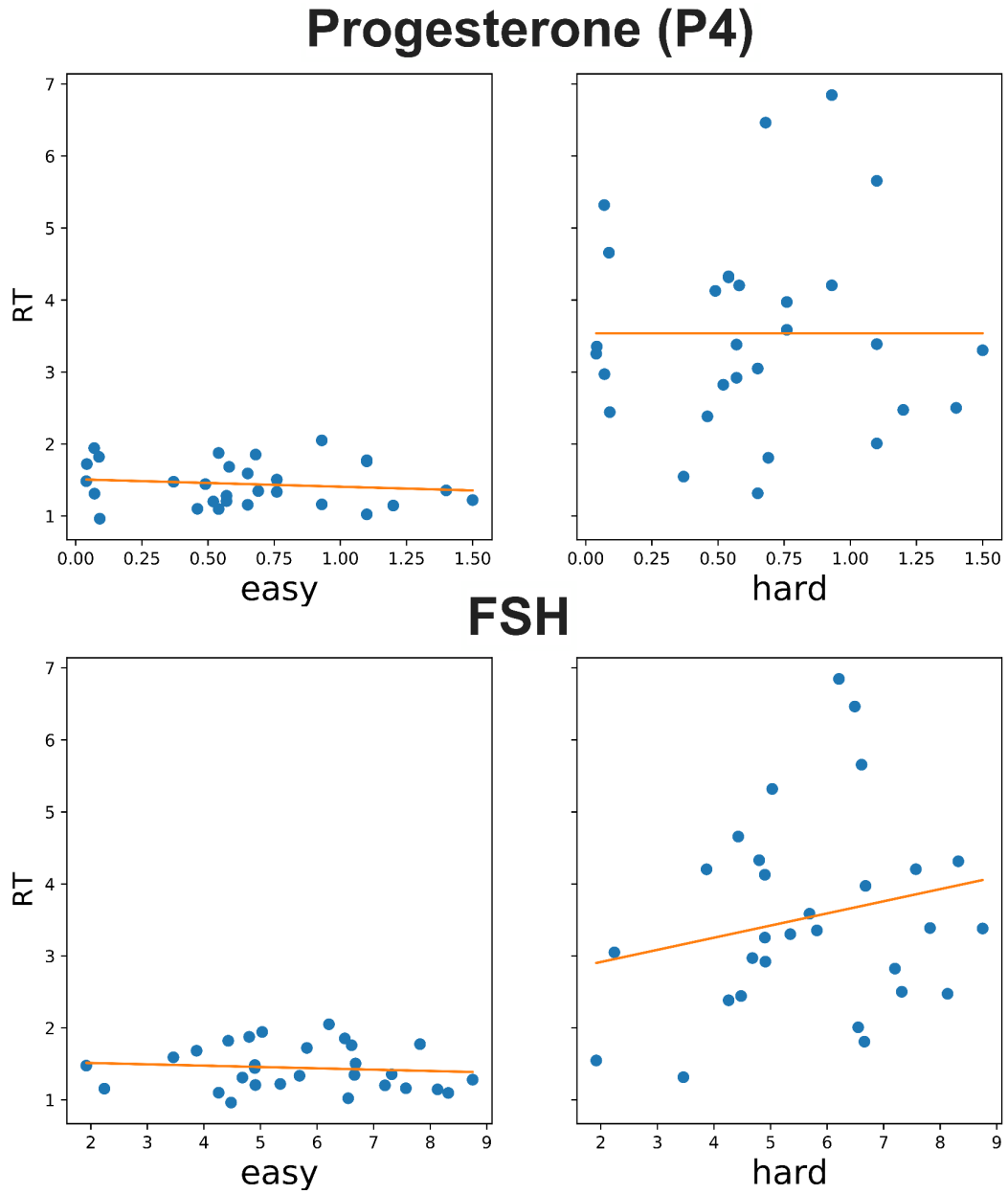
Figure 7.9 Raw values of median response time (RT) to easy and hard trials across concentrations of progesterone (P4) and follicle stimulating hormone (FSH), with trend lines in red. Trend lines suggest slower responses to hard trials with increasing concentrations of FSH. Due to these plots representing raw values, the trend in P4 with hard problems appears diminished; however, results from the hierarchical Bayesian regression confirm a similar trend for P4 and RT.

7.3.2 Contractility

Results of the Bayesian hierarchical regression for 29 participants between concentrations of HPG hormones and the two seconds of contractility following presentation of MA trials confirmed a credible positive main effect of estradiol, for which the mean of the hierarchical posterior distribution of subjects' beta values was 0.14 with a 94% HDI of [0.12, 0.16] (Figure 7.10). These results suggest that greater concentrations of estradiol are associated with increased SNS activity in response to the motivated MA task across all sessions, difficulty, and reward levels (Figure 7.11). While this effect holds through low and high reward levels, it is possible that it is driven more by easy problems (M = 0.14, 94% HDI [0.12, 0.17]) than by hard problems (M = 0.13, 94% HDI [0.10, 0.16]). No other HPG hormones showed credible relations with contractility.

	Modular Arithmetic Presentation Regression Coefficients				
	Relations	**Mean**	**Lower**	**Upper**	**Credible**
1	session1_easy_lo_E2	0.18	0.14	0.22	***
2	session1_easy_lo_P4	0.09	0.06	0.12	
3	session1_easy_lo_LH	-0.04	-0.07	-0.01	
4	session1_easy_lo_FSH	-0.03	-0.06	0.01	
5	session1_easy_hi_E2	0.16	0.09	0.22	
6	session1_easy_hi_P4	0.05	0.00	0.11	
7	session1_easy_hi_LH	-0.06	-0.11	-0.01	
...	...	...	...	...	
113	easy_E2	0.14	0.12	0.17	***
114	easy_P4	-0.01	-0.04	0.02	
115	easy_LH	0.04	0.02	0.07	
116	easy_FSH	-0.03	-0.06	-0.01	
117	hard_E2	0.13	0.10	0.16	
118	hard_P4	-0.06	-0.09	-0.03	
119	hard_LH	0.06	0.03	0.09	
120	hard_FSH	-0.01	-0.04	0.03	
121	lo_E2	0.13	0.11	0.15	***
122	lo_P4	-0.04	-0.06	-0.02	
123	lo_LH	0.05	0.03	0.08	
124	lo_FSH	-0.01	-0.04	0.01	
125	hi_E2	0.14	0.11	0.18	***
126	hi_P4	-0.03	-0.07	0.01	
127	hi_LH	0.05	0.02	0.08	
128	hi_FSH	-0.03	-0.06	0.01	
...	...	...	...	...	
141	E2	0.14	0.12	0.16	***
142	P4	-0.04	-0.06	-0.02	
143	LH	0.05	0.03	0.07	
144	FSH	-0.02	-0.04	0.00	

Figure 7.10   Regression coefficients for contractility across the two seconds following the modular arithmetic (MA) problem appearing on the screen. Results show a credible positive main effect of estradiol (E2) across all parameters.
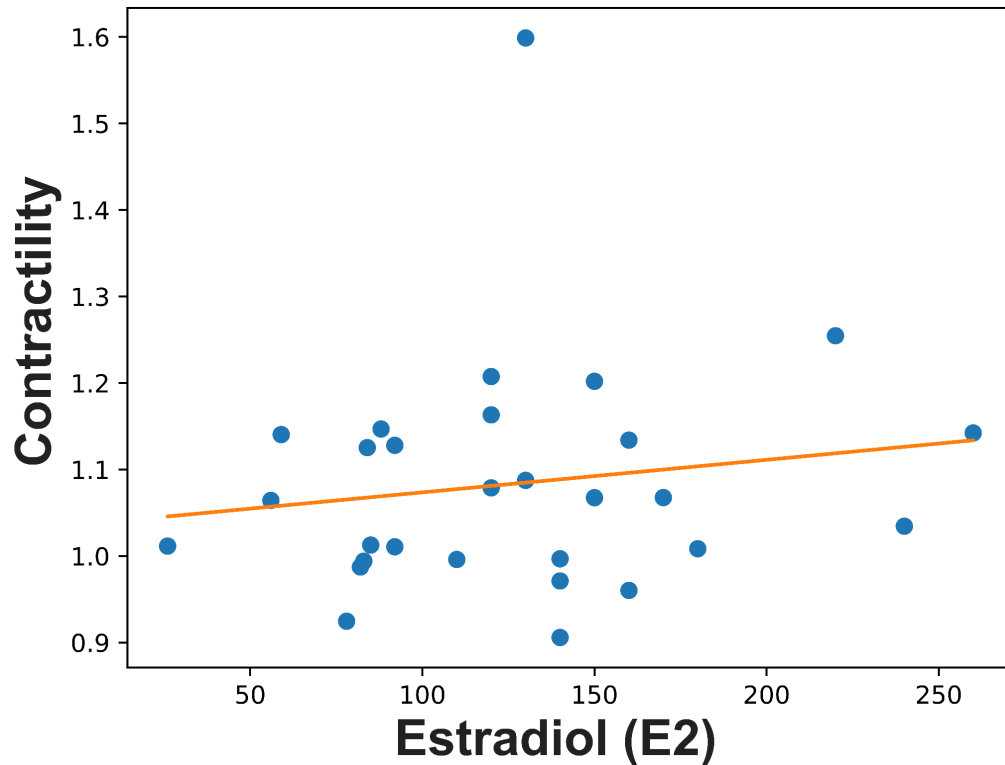
Figure 7.11 Raw values of mean contractility with estradiol (E2), with a positive trend line in red. The trend suggests increasing contractility with increasing concentrations of E2, which is confirmed in the Bayesian regression. Any influences of the outlier visible in this plot is accounted for in the statistical model.

Results of the Bayesian hierarchical regression between concentrations of HPG hormones and the four seconds of contractility following presentation of performance feedback confirmed a credible positive main effect of estradiol, for which the mean of the hierarchical posterior distribution of subjects' beta values was 0.16 with a 94% HDI of [0.13, 0.18] (Figure 7.12). These results suggest that greater concentrations of estradiol are associated with increased SNS activity following performance feedback, across sessions, difficulty, and reward levels (Figure 7.13). No other HPG hormones showed credible relations with feedback contractility.

	Feedback Presentation Regression Coefficients				
	Relations	**Mean**	**Lower**	**Upper**	**Credible**
1	session1_easy_lo_E2	0.13	0.08	0.19	
2	session1_easy_lo_P4	0.07	0.03	0.11	
3	session1_easy_lo_LH	-0.05	-0.10	-0.01	
4	session1_easy_lo_FSH	-0.06	-0.10	-0.01	
5	session1_easy_hi_E2	0.08	0.00	0.16	
6	session1_easy_hi_P4	0.02	-0.05	0.08	
7	session1_easy_hi_LH	-0.10	-0.17	-0.03	
...	...	...	...	...	
113	easy_E2	0.16	0.12	0.19	***
114	easy_P4	-0.01	-0.05	0.02	
115	easy_LH	0.06	0.03	0.10	
116	easy_FSH	-0.01	-0.05	0.02	
117	hard_E2	0.16	0.12	0.19	***
118	hard_P4	-0.01	-0.05	0.02	
119	hard_LH	0.05	0.01	0.08	
120	hard_FSH	-0.03	-0.07	0.01	
121	lo_E2	0.16	0.13	0.19	***
122	lo_P4	-0.01	-0.04	0.02	
123	lo_LH	0.06	0.03	0.09	
124	lo_FSH	-0.02	-0.05	0.01	
125	hi_E2	0.16	0.12	0.20	***
126	hi_P4	-0.02	-0.06	0.02	
127	hi_LH	0.05	0.01	0.09	
128	hi_FSH	-0.03	-0.07	0.01	
...	...	...	...		
141	E2	0.16	0.13	0.18	***
142	P4	-0.01	-0.04	0.01	
143	LH	0.06	0.03	0.08	
144	FSH	-0.02	-0.05	0.00	

Figure 7.12 Regression coefficients for contractility across the four seconds following feedback appearing on the screen. Results show a credible positive main effect of estradiol (E2) across all parameters.
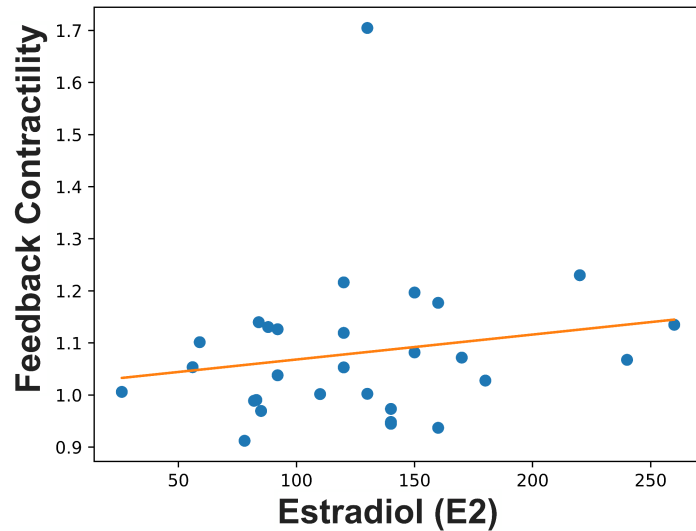
Figure 7.13   Raw values of mean contractility following performance feedback with concentrations of estradiol (E2), with a positive trend line in red. The trend suggests increasing contractility to feedback with increasing concentrations of E2, which is confirmed in the Bayesian regression. Any influences of the outlier visible in this plot is accounted for in the statistical model.

Results of the Bayesian hierarchical regression between concentrations of HPG hormones and allostatic efficiency (estimated by the slope change across four seconds of contractility following presentation of performance feedback) confirmed a credible negative main effect of progesterone on hard trials, for which the mean of the hierarchical posterior distribution of subjects' beta values was -0.18 with a 94% HDI of [-0.26, -0.11] (Figure 7.14). These results suggest that greater concentrations of progesterone are associated with a decrease in allostatic efficiency following performance feedback on cognitively demanding tasks (Figure 7.15). No other HPG hormones showed credible relations with allostatic efficiency, and there were no interaction effects between any contractility and behavior parameters. Any session effects are not reported due to session order being too convoluted with task learning effects and unequal distribution across menstrual phase (Figure 7.4). Complete tables of regression coefficients for all contractility parameters (including possible session effects) are available in appendix A.

	Allostatic Efficiency Regression Coefficients				
	Relations	**Mean**	**Lower**	**Upper**	**Credible**
1	session1_easy_lo_E2	-0.13	-0.46	0.20	
2	session1_easy_lo_P4	-0.13	-0.44	0.20	
3	session1_easy_lo_LH	-0.10	-0.40	0.23	
4	session1_easy_lo_FSH	-0.06	-0.39	0.27	
5	session1_easy_hi_E2	0.00	-0.32	0.33	
6	session1_easy_hi_P4	-0.02	-0.33	0.29	
7	session1_easy_hi_LH	0.07	-0.22	0.38	
...	...	...	...	...	
113	easy_E2	-0.10	-0.23	0.01	
114	easy_P4	0.00	-0.12	0.11	
115	easy_LH	-0.10	-0.21	0.02	
116	easy_FSH	-0.09	-0.20	0.03	
117	hard_E2	-0.15	-0.22	-0.07	
118	hard_P4	-0.18	-0.26	-0.11	***
119	hard_LH	0.00	-0.07	0.08	
120	hard_FSH	0.00	-0.08	0.08	
121	lo_E2	-0.14	-0.24	-0.04	
122	lo_P4	-0.12	-0.22	-0.03	
123	lo_LH	-0.07	-0.17	0.02	
124	lo_FSH	-0.07	-0.16	0.03	
125	hi_E2	-0.11	-0.22	0.00	
126	hi_P4	-0.06	-0.17	0.04	
127	hi_LH	-0.02	-0.12	0.08	
128	hi_FSH	-0.02	-0.12	0.08	
...	...	...	...	...	
141	E2	-0.13	-0.20	-0.06	
142	P4	-0.09	-0.16	-0.02	
143	LH	-0.05	-0.12	0.02	
144	FSH	-0.04	-0.12	0.03	

Figure 7.14   Regression coefficients for contractility recovery (a decrease in the slope of contractility) across the four seconds following performance feedback on the modular arithmetic (MA) task. Results show a credible negative main effect of progesterone (P4) with hard trials, suggesting that higher concentrations of P4 are associated with a slower sympathetic nervous system (SNS) recovery (hence decreased allostatic efficiency) following performance feedback on cognitively demanding tasks.
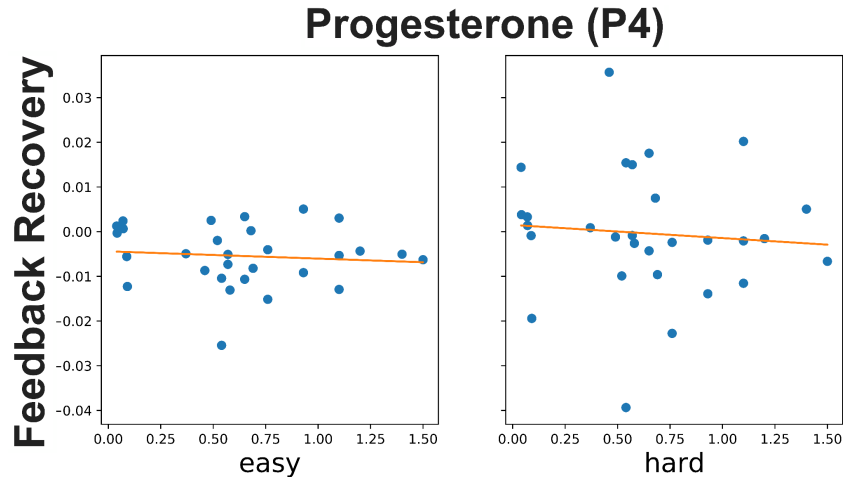
Figure 7.15   Raw values of contractility recovery (i.e. allostatic efficiency), following either easy or hard trial performance feedback with concentrations of progesterone (P4), with trend lines in red. The trend suggests that increasing concentrations of P4 are related to a decrease in allostatic efficiency following performance feedback on hard trials.

7.3.3   Gray matter volume of MTL hippocampal subregions

Results of the Bayesian hierarchical regression for 21 participants between concentrations of HPG hormones and gray matter volumes of MTL hippocampal subregions confirmed a credible positive main effect of estradiol with the subregion CA2/3, for which the mean of the hierarchical posterior distribution of subjects' beta values was 0.31 with a 94% HDI of [0.01, 0.61] (Figure 7.16). These results suggest that greater concentrations of estradiol are associated with an increase in CA2/3 gray matter volume. There were no other group-level HPG hormone effects for any other MTL region. However, notably, there were a number of marginally credible individual-level effects that were split between directions of credibility, potentially signifying individual variability in the type of relationship that these hormones have with MTL gray matter. Specifically, the effect of estradiol with the perirhinal cortex, progesterone with the CA1 subregion and the entorhinal cortex, LH with the subiculum subregion, and FSH with the CA1 subregion. Plots of these results can be found in appendix B.

Estradiol (E2) and CA2/3
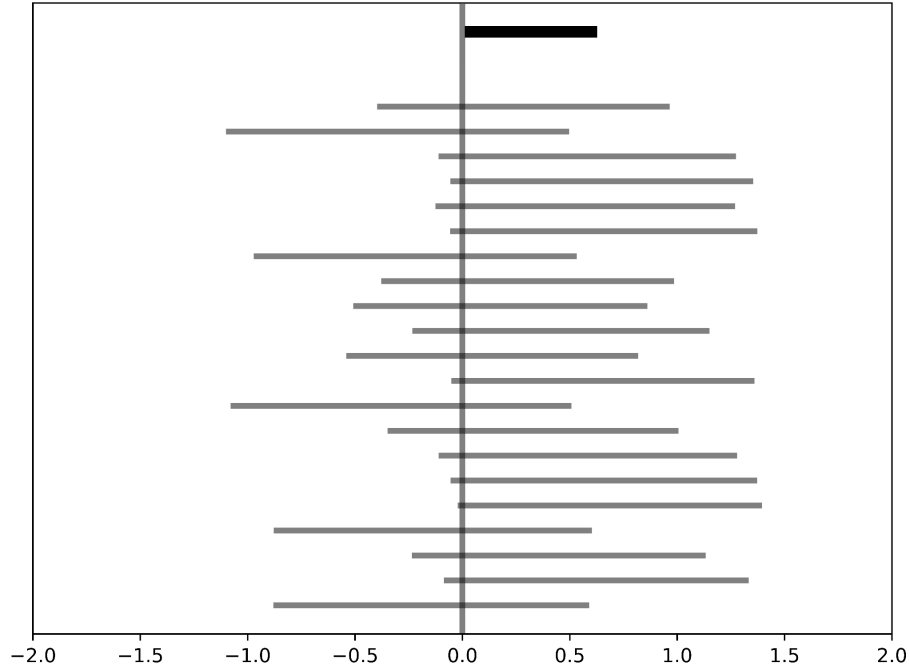
Figure 7.16   A plot of the Bayesian regression 94% HDI intervals for the relationship between concentration of estradiol (E2) and gray matter volume of the CA2/3 hippocampal subregion. The top line is the group result, with the 21 participants' highest density intervals (HDIs) below. Credible relationships are in black, while non-credible relationships are in gray. Results suggest a group-level credible positive relationship, where increasing concentrations of E2 are associated with increased gray matter volume in CA2/3.

7.3.4   White matter integrity (WMI)

Results of the Bayesian hierarchical regression for 30 participants between concentrations of HPG hormones and white matter integrity (WMI) as defined by μFA across the whole brain demonstrated a credible positive main effect of both estradiol and LH, for which the mean of the effect size for estradiol was 0.31 with a 94% HDI of [0.21, 0.40], and the mean effect size for LH was 0.26 with a 94% HDI of [0.16, 0.37] (Figures 7.17 and 7.18). These results suggest that greater concentrations of either estradiol or LH are associated with increased WMI across the whole brain. No other HPG hormones showed credible relations with whole-brain WMI.
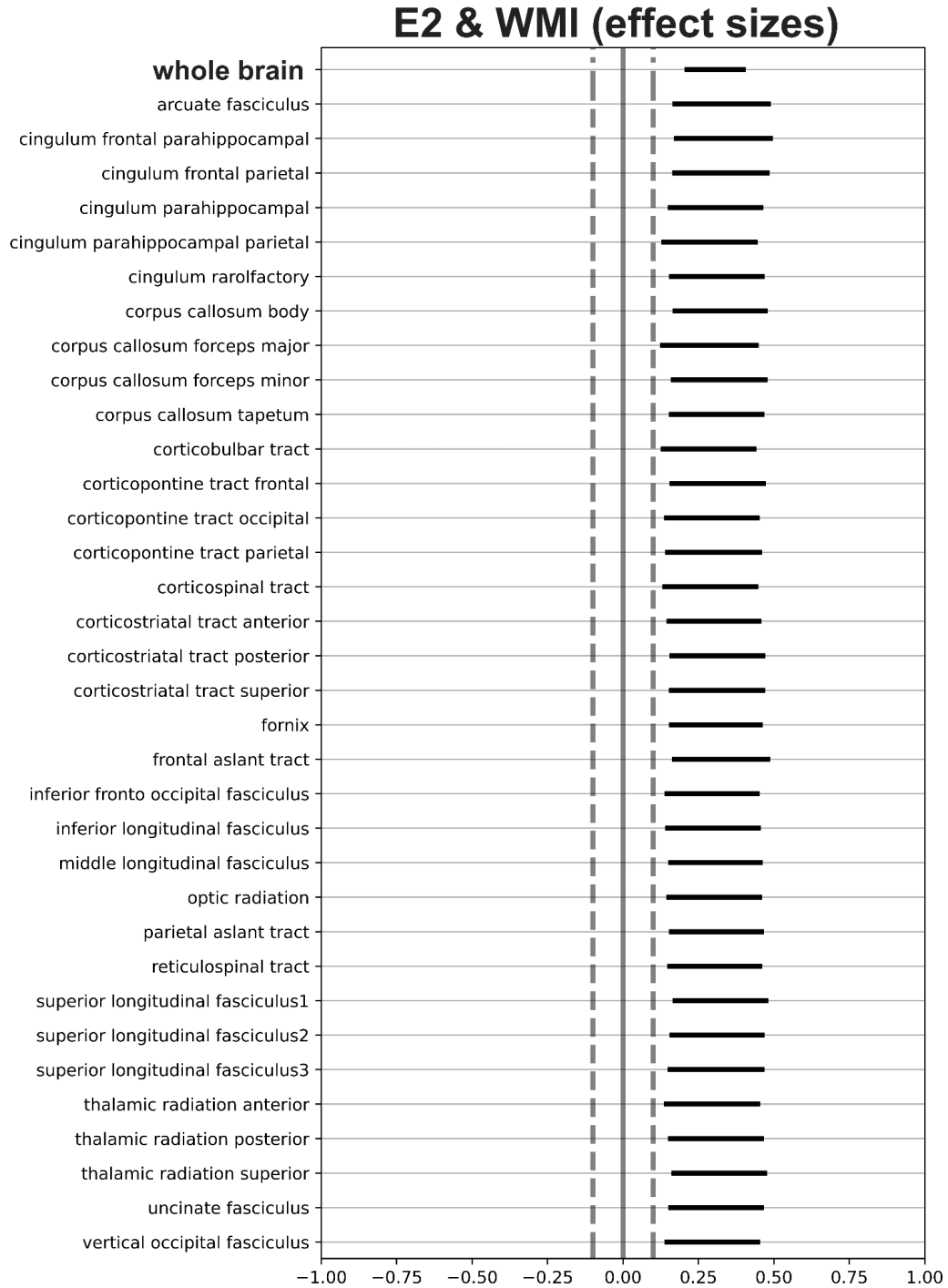
Figure 7.17   A plot of the effect sizes for the relationship between concentrations of estradiol (E2) and white matter integrity (WMI). The top line is the whole-brain result, with individual regions of interest (ROIs) below. The dotted lines represent our region of practical equivalence (ROPE), in which the effect size has to cross either 0.1 or -0.1 to be valued as credible. Credible relationships are in black, while non-credible relationships are in gray. Results suggest a whole-brain credible positive relationship, where increasing concentrations of E2 are associated with increases in WMI across the entire brain.
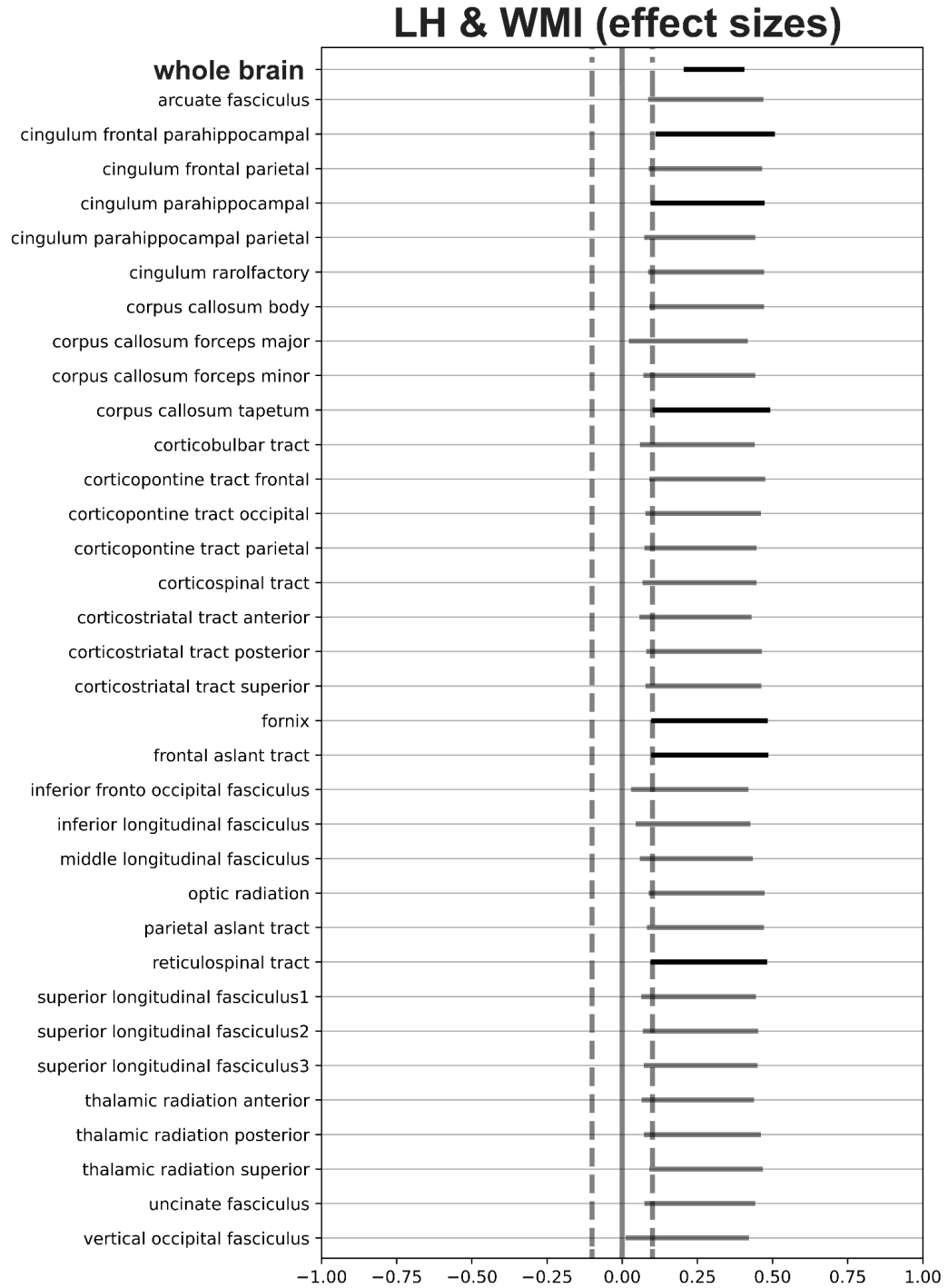
LH & WMI (effect sizes)

Figure 7.18   A plot of the effect sizes for the relationship between concentrations of luteinizing hormone (LH) and white matter integrity (WMI). The top line is the whole-brain result, with individual regions of interest (ROIs) below. The dotted lines represent our region of practical equivalence (ROPE), in which the effect size has to cross either 0.1 or -0.1 to be valued as credible. Credible relationships are in black, while non-credible relationships are in gray. Results suggest a whole-brain credible positive relationship, where increasing concentrations of LH are associated with increases in WMI across the entire brain.

135

7.3.5 Resting-state functional network connectivity

We found that whole-brain functional connectivity at rest across 30 participants was associated with concentrations of estradiol (Figure 7.19a). This subgraph included 174 regions, spanning nearly all canonical networks of the cortex, as well as a number of subcortical regions. Notably, the preponderance of effects was in the negative direction, such that higher levels of estradiol predicted lower levels of functional connectivity (Figure 7.19c). All other HPG hormones did not demonstrate significant associations with whole-brain functional connectivity.
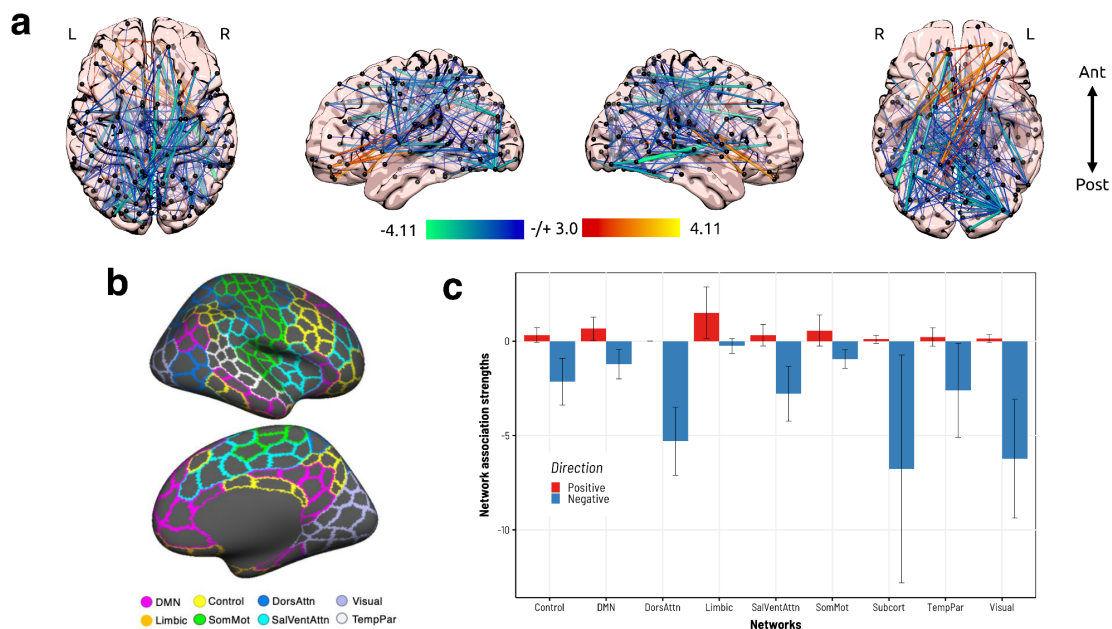
Figure 7.19 Whole-brain functional connectivity at rest is associated with levels of estradiol (E2). **(a)** Spatial map of a 174-region functional network component demonstrating sensitivity to E2. 'Hotter' colors indicate increased coherence with higher levels of E2; 'cooler' colors indicate the reverse. **(b)** Canonical grouping of 400 cortical brain regions into functional networks, per the Schaefer atlas. An additional 32 regions from the Tian subcortical atlas were also included (but not visualized here). **(c)** Summary of brain-hormone relationships across each network in (b). 'Positive' refers to the average magnitude of positive associations (more network regions showing stronger coherence with higher E2); 'Negative' refers to the average magnitude of inverse associations (more regions showing decreased coherence with higher E2). Error bars give 95% confidence intervals.

136

7.4   Discussion

The present study investigated the effect that biologic endogenous factors have on dynamic allostatic processes, cognitive behavior, and cerebral structure and function. Specifically, we examined the relationship between these factors and naturally-occurring cyclic fluctuations of hypothalamic-pituitary-gonadal (HPG) hormones that occur within individual females across their menstrual cycles. We found that peripheral concentrations of progesterone and follicle-stimulating hormone (FSH) were negatively related to response time (RT) on hard modular arithmetic (MA) problems, such that higher levels of progesterone and FSH were related to slower RT. Notably, we did not find any credible relationships between HPG hormones and performance accuracy, therefore the FSH and progesterone effect on RT was irrespective of task accuracy. Additionally, no credible relationships were found between HPG hormones and behavioral or SNS effects and the magnitude of monetary reward.

Furthermore, we investigated the relationship between HPG hormones and allostasis (i.e. contractility) by estimating the activity of the sympathetic nervous system (SNS) in response to MA trials. We found that progesterone had a negative relationship with allostatic efficiency, such that increased concentrations of progesterone were linked to slower SNS recovery following performance feedback given for difficult MA trials.

Estradiol was in turn linked to a number of both sympathetic and central nervous system processes. It presented a positive relationship with SNS activity across the task and in response to performance feedback, such that greater levels of estradiol were linked to enhanced levels of SNS drive in response to every variation of MA trial conditions and to every feedback condition. Furthermore, estradiol was positively associated with the volume of the CA2/3

hippocampal subregion, and white matter integrity (WMI), such that increased concentrations of estradiol were linked to larger CA2/3 subregion volume and enhanced WMI across the whole brain. On the contrary, estradiol was found to have a predominantly negative relationship with functional coherence across the resting brain, such that a higher concentration of estradiol within an individual was related to a decoupling effect within resting-state functional networks. Furthermore, LH was found to accompany estradiol in its relationship with WMI, such that greater levels of LH were associated with increased WMI across the brain.

In our findings, the only HPG hormones that were credibly related to behavioral outcomes on a stress-inducing MA task were progesterone and FSH. Specifically, we found a positive relationship for both progesterone and FSH concentration levels with response time on hard MA trials, such that when participants had higher levels of progesterone or FSH, they responded to cognitively demanding tasks more slowly. While a number of studies have sought to unravel progesterone's effect on cognitive functions and behavior, research examining the relationship between FSH and cognition has been profoundly limited. Notably, peripheral concentrations of FSH levels show a 3-fold increase in postmenopausal females (Chakravarti et al., 1976), and some research has linked FSH to dementia and Alzheimer's disease (Bowen et al., 2000; Hogervorst et al., 2004; Short et al., 2001). One study found evidence that a ratio of FSH/estradiol possessed the potential to be used as a screening measure for cognitive impairment (Hestiantoro et al., 2017). Furthermore, another study found a negative correlation between FSH levels and verbal fluency in females around the menopausal stage. Conversely, a handful of other studies did not find any credible relations between FSH and cognitive performance in this population (Luetters et al., 2007; Weber et al., 2013). While the majority of previous literature investigating FSH and cognition has been centered around aging, one

recent study found a significant relationship between the fluctuations of day-to-day luteinizing hormone (LH) and FSH concentrations across the menstrual cycle with the frequency of high-amplitude network states in the brain (Greenwell et al., 2021). While our study design is not suited to make causal claims, our findings suggest that FSH may play a significant role in cognition on demanding tasks across the menstrual cycle within single individuals, outside of the aging process.

In regards to progesterone, it is evident from the literature that the effect that progesterone has on task performance may be dependent upon the specifics of the task. For instance, while progesterone has been linked to decreased accuracy on recognition tasks (Van Wingen et al., 2007) and slower RT to reaction tasks (Little et al., 1974), it has also been associated with performance improvement on attentional and sensory tasks (Brotzner et al., 2015; Veena et al., 2017). Additionally, females in their luteal phase have demonstrated slower RT to a spatial rotation task and decreased performance on stress-inducing mental arithmetic tasks when compared to the follicular phase (Chung et al., 2016; Noreika et al., 2014; Pletzer et al., 2011). Furthermore, females have demonstrated enhanced numerical abilities during their early follicular phase, when HPG hormones are low. While we cannot definitively link progesterone and FSH levels to decreased cognitive abilities, our results provide further evidence that these hormones may have a negative effect on the processing of cognitively challenging tasks. However, it is important to note that this effect did not extend into accuracy, suggesting the presence of a speed/accuracy tradeoff that preserved accuracy; one that is resilient to the endogenous cyclic fluctuations of FSH and progesterone within the menstrual cycle of healthy and relatively young individuals.

Our findings also linked progesterone levels with a decrease in allostatic efficiency following hard MA trials, and estradiol with increased SNS activity in response to the entire MA task. Interestingly, a longitudinal double-blind study found that males who were administered progesterone demonstrated an increase in resting-levels of skin conductance (SC; a measure of SNS activity and "sluggish" responses of spontaneous and evoked SC, which persisted for a week after drug administration (Little et al., 1974). Meanwhile, in females, one study found an increase in skin conductance during the ovulatory phase of the cycle, accompanied by a decrease in SC during the luteal phase (Little & Zahn, 1974). These results suggest that high levels of estradiol may be responsible for an exacerbated autonomic drive, while progesterone may attenuate autonomic responses to tasks. Additionally, progesterone, along with some of its metabolites, have been shown to have a depressant effect on the central nervous system, increasing fatigue and drowsiness (Andersen et al., 2006; Van Broekhoven et al., 2006). Progesterone's effect on sedation and its link to the attenuation of allostatic responses may provide an explanation of our findings that relate it to decreased allostatic efficiency and slower RT. Specifically, it is possible that progesterone levels may be related to a "sluggish" sympathetic engagement in response to cognitively demanding tasks, leading to slower RT and slower allostatic recovery.

Conversely, a potential connection can be drawn between estradiol and a heightened dynamic SNS response with evidence of its relationship to enhanced energy, alertness, and even certain senses. While some studies have found no differences in baseline levels of stress hormones (i.e. norepinephrine and cortisol) in response to stressors across the menstrual cycle (Abplanalp et al., 1977; Mills et al., 1996), another study found heightened concentrations of salivary cortisol upon awakening during the ovulatory phase (Wolfram et al., 2011).

Furthermore, estradiol may modulate mitochondrial function resulting in greater energy-producing capacity (Stirone et al., 2005). Females in their ovulation phase have demonstrated a heightened sensitivity to fear processing and the recognition of negative emotions in others (Guapo et al., 2009; Pearson & Lewis, 2005). Additionally, during ovulation, females have shown increased activation within their prefrontal cortex (PFC) and attentional networks, potentially linked to increased vigilance and evaluation (Banbers et al., 2012; Meeker et al., 2020). Ovulation is a time of high-pregnancy susceptibility; hence, there may be benefits for a more activated attentional network in helping females evaluate threats and avoid risk, as well as to aid in the detection of males with greater reproductive fitness. Remarkably, even heightened abilities of the olfactory system have been linked to estradiol. For instance, the ovulation phase has been associated with a preference towards the smell of shirts worn by males with higher levels of testosterone (Thornhill et al., 2013). While our findings are not a direct measure of vigilance, the literature suggests that it is possible that estradiol may be associated with greater vigilance, resulting in a higher SNS drive in response to the MA task.

Overall, there are still a number of conflicting results in the literature regarding the effect that HPG hormones may have on allostatic dynamics. This may be in part due to the lack of previous research using robust measures of dynamic sympathetic drive, given that the majority have examined allostatic processes along extended time frames, such as at baseline, blocked times across a task, or pre- vs. post- task. Furthermore, extraneous life factors that are found to change across the menstrual cycle, such as diet, sleep, and exercise, may have influences on autonomic functions, affecting the results of such study designs (Tada et al., 2017). Ultimately, our study provides new insights into the relationship between HPG hormones and dynamic fluctuations of the sympathetic drive across the menstrual cycle.

Additionally, our findings suggest that HPG hormones have robust relationships with the central nervous system, particularly with regard to brain morphology and function. In the observation of gray matter volume within medial temporal lobe (MTL) subregions, we found a positive relationship between concentrations of estradiol and the volume of the CA2/3 hippocampal subregion. Estradiol has been commonly linked with the increase in hippocampal volume and synaptic plasticity in mammals (Cooke & Woolley, 2005; Micevych & Christensen, 2012). In humans, prior research has supported sexually dimorphic differences in hippocampal volume, for instance, male puberty has been linked with smaller hippocampal volume, while female puberty has been associated with greater hippocampal volume (Hu et al., 2013). Furthermore, sexually dimorphic differences in volume size have been found particularly within the CA2/3 subregion (Krogsrud et al., 2014).

Notably, our results diverge from those found in a recent study that tracked gray matter volume within a single female's MTL subregions and endocrine levels across the menstrual cycle for 30 consecutive days (Pritschet et al., 2020). The researchers had observed a combination of positive and negative relationships between progesterone and various hippocampal subregions, including CA2/3, parahippocampal, perirhinal, and entorhinal cortex (ERC). Specifically, the volume of CA2/3 was positively correlated with progesterone. Interestingly, when the study was repeated with the same female on a hormonal oral contraceptive which suppressed circulating progesterone, ERC and CA2/3 were the only significantly modulated subregions identified, and they were modulated by estradiol. In particular, CA2/3 was found to be negatively correlated with estradiol. There may be a number of reasons as to why our findings resulted in differing relationships between HPG hormones and CA2/3 volume, including individual differences in cyclicity, hormone sensitivity, or

estrogen receptor genotype and sensitivity (Ryan et al., 2014). However, our findings both implicate the CA2/3 subregion's morphological volume in its particular sensitivity to HPG hormone modulation across the menstrual cycle.

From prior work, it is possible to infer that the hippocampus, and CA2/3 subregion, may be susceptible to volumetric changes following trauma or disease. Interestingly, one of the largest neuroimaging studies conducted on individuals diagnosed with PTSD found a negative relationship between hippocampal volume and PTSD severity (Logue et al., 2018). Furthermore, people with PTSD have been shown to possess smaller volumes of their CA3 region (Wang et al., 2010). This association has also been found in adolescents, linking smaller CA2/3 volume with adolescent PTSD, and further linking smaller CA2/3 volume to an increase in the severity of intrusive thoughts (Mutluer et al., 2018; Postel et al., 2019). Additionally, prior research has found decreased CA2/3 volume within individuals who are dependent upon cannabis, and in those diagnosed with major depressive disorder (MDD) and insomnia (Chye et al., 2017; Cole et al., 2010; Neylan et al., 2010). The volume of the CA2/3 subregion has been positively associated with cognitive ability, and signs of atrophy within the CA2/3 subregion in amnestic elderly patients with mild cognitive impairment has been linked to future diagnosis of Alzheimer's disease (Apostolova et al., 2010; Tamnes et al., 2018). With regard to the specialized function of the CA2/3, evidence has supported its critical role in the encoding of episodic memory and in social behavior (Oliva, 2022). One study found increased functional activity within the CA2/3 subregion during memory encoding (Suthana et al., 2011), while another study found greater CA2/3 volume within individuals possessing greater episodic memory ability (Palombo et al., 2018). This observation may provide further evidence linking the effects of structural changes on functional behavior.

One possible reason for greater susceptibility of the CA2/3 subregion to volumetric changes as opposed to other regions may be due to molecular differences, such as sensitivity to the stress-induced decrease in the concentration of brain derived neurotrophic factor (BDNF; a neurotrophin essential for neuronal growth and synaptic plasticity), commonly associated with psychological trauma (Aas et al., 2014). Additionally, data gathered from mice showed that the CA2 subregion contains 3-fold the quantity of genes associated with axonal guidance and neuropeptide signaling as compared to hippocampal CA1 and CA3 subregions (Cembrowski et al., 2016). Alternatively, some evidence suggests that a heritably smaller hippocampus may be a risk factor causing individuals to be more susceptible to stress-induced psychiatric disorders (Gilbertson et al., 2002). In this study, researchers studied pairs of monozygotic twins in which one twin was exposed to military combat and the other was not. Of the twin pairs where the combat-exposed twin had developed PTSD, both twins possessed reduced hippocampal volumes. Whatever the cause, our findings support evidence that fluctuations in estradiol may be linked to volumetric changes that occur in the hippocampal gray matter within single individuals.

With the present study, we introduce an advanced and robust method of relating HPG hormone concentrations to WMI by estimating µFA values obtained from q-space trajectory encoding (QTE) diffusion sequences, which are resilient to the crossing, kissing or fanning fibers that can devalue FA measures (Nilsson et al., 2018; Westin et al., 2016). Across the whole brain, we found that concentrations of both estradiol and luteinizing hormone (LH) presented credible positive relationships with white matter integrity (WMI), such that increasing levels of estradiol and LH were associated with an increase in µFA across the whole brain white matter. Critically, our results with a state of the art method can be contrasted with

a number of studies that have used conventional diffusion imaging and measures of fractional anisotropy (FA). For instance, one study in adolescents found a negative relationship between estradiol and white matter FA (Herting et al., 2012). In contrast, another study found that WMI based on FA in young adult brains was modulated by when they first started their menses, in which females who had early timing of menses onset presented greater frontal tract WMI (Chahal et al., 2018). With regard to adults, our findings detailing estradiol's relationship with WMI reflect findings from prior literature that examined both WMI (using fractional anisotropy) and white matter density (Barth et al., 2016; Meeker et al., 2020). However, the conventional methods that are commonly used to estimate white matter microstructural details using FA are susceptible to error, commonly due to the complex nature of crossing fibers within white matter voxels (Anderson et al., 2020; Volz et al., 2018). Thus, we believe our findings provide a more reliable and consistent description of microscopically small-scale cyclical changes within white matter associated with estrogen. These changes could be driven by interstitial or extracellular free water or membrane properties.

Furthermore, our results indicate a positive relationship between LH and WMI across the brain. Recently, there has been a rise in the investigation of the effects of LH on the brain, following evidence that the brain contains LH receptors, and that LH concentrations are linked to cognition, dementia, Alzheimer's disease, and Schizophrenia in both females and males (Bowen et al., 2000; Ferrier et al., 1983; Lei et al., 1993). Furthermore, peripheral LH concentrations show a 3-fold increase in postmenopausal females (Chakravarti et al., 1976). Some evidence has been shown that decreasing peripheral LH has the potential to reduce cognitive deficits and effects of Alzheimer's disease (Blair et al., 2015; Casadesus et al., 2016). Furthermore, LH production is a major contributor to puberty onset in both males and females

(De Waal et al., 1991). For example, one study of 9-year-olds found a positive relationship between urinary LH concentrations, global white matter proportion (in comparison to gray matter), and regional white matter density in the brain regions most known to develop rapidly between the ages of 9 – 13 (Peper et al., 2008). Additionally, they found that a common genetic factor under-lied the association between LH levels and white matter density. It seems apparent that the link between HPG hormones and brain structural reorganization can have profound effects, not only across the menstrual cycle, but throughout the lifecycle as well.

Our functional resting-state results suggest that the concentration of estradiol has a negative relationship with coherence within networks across the brain (Figure 7.19c). Specifically, we provide evidence that estradiol may be associated with decoupling across multiple brain regions within their respective functional networks. These findings are reflective of prior literature, which has discovered negative relationships between HPG hormones and coherence metrics. Specifically, two studies have found decreased functional connectivity during cycle phases of high HPG hormone concentrations (luteal), and increased connectivity at low concentrations (early follicular) (Petersen et al., 2014; Weis et al., 2019). Given that both estradiol and progesterone concentrations are high in the luteal phase, it is difficult to give value to one over the other for this effect; however, our results would suggest that estradiol may be driving this negative association.

Notably, the preponderance of our effects was in the negative direction, such that higher levels of estradiol predicted lower levels of functional connectivity, contradicting a recent dense-sampling study in which estradiol was almost-exclusively associated with increases in coherence, while progesterone was associated with decreases in coherence (Pritschet et al., 2020). In the study by Pristchet and colleagues, a single individual's resting-state functional

connectivity and endocrine levels were collected across their menstrual cycle. Possible reasons for the difference in our findings may be due to fundamental contrasts in our study designs, as theirs was a dense-sampling study across 30 consecutive days, whereas our sample was across three unique time points within and across 30 females. Alternatively, these deviations may be due to individual differences in hormone sensitivities and ratios (Ryan et al., 2014).

It is possible that HPG hormones produce different effects within individuals based on the unique combination of hormone concentrations occurring at each phase of the cycle. For instance, one study found that progesterone was negatively correlated with connectivity within the DMN during the mid-follicular phase (when all HPG concentrations were low) and positively correlated with DMN within the late luteal phase (when both progesterone and estradiol are high) (Pletzer et al., 2016). Additionally, another study found that estradiol levels were negatively correlated with resting-state connectivity during the mid-follicular phase and positively correlated in the late luteal phase, with differing brain networks in each phase (Syan et al., 2017). Notably, even estradiol levels from the two days prior to scanning have been shown to influence resting-state functional connectivity and efficiency metrics (Pritschet et al., 2020). Furthermore, other factors may be contributing to the variability in results found across the literature. For instance, given our findings of estradiol's influence on the hippocampal subregion CA2/3 volume, it is important to note that these changes may be integrated in the unique role that the hippocampus has within the DMN and other networks, and hence may modulate the potential influence it may impose on network function. Ultimately, both the similarities and the differences between our findings and that of prior literature may provide further evidence that brain function is susceptible to constant modulations by fluctuating HPG hormone concentrations.

One potential consequence of our finding linking estradiol to brain-wide reductions in functional connectivity within networks is reduced efficiency within these networks; however, it is also plausible that multiple networks may be becoming more or less segregated (i.e., more reductions or enhancements in between-network connectivity relative to within-network connectivity). Future investigation of the present research should include the added factor of cycle phase into analyses, in order to investigate potential hormone-phase interactions. Furthermore, additional graph theoretical methods (similar to those utilized by Pritschet et al., 2020), should be integrated into the analyses to better examine specific intra-/inter-network features and investigate potential correlations between hormones and network efficiency. While it is possible that there is a uniquely "global" phenomenon across brain networks with estradiol, furthering our analysis in this way may help disentangle what may be happening with respect to individual networks and their relationship with one another.

One limitation to our study is that we found a number of irregularities in a handful of our participants' menstrual cycles, despite them having claimed to experience regular cycles in self-report measures and passing all eligibility requirements prior to enrollment. This may be in-part due to potential side effects following the SARS-CoV-2 virus vaccine or diagnoses, which have both been shown to disrupt the menstrual cycle (Khan et al., 2022; Lee et al., 2022; Li et al., 2021). All but one participant received at least one dose of the vaccine, a number of participants received second doses half-way through the study, and two participants contracted the SARS-CoV-2 virus in-between sessions. In an attempt to avoid potential effects of the vaccine or virus contraction in our data, all participants completed virus-clearance requirements prior to each session, and we required one full cycle to pass (menses-to-menses) following either the vaccine or any diagnoses before completion of the next session.

There are a number of discrepant findings in the literature regarding HPG hormones, which may be reflective of study design differences, or effects modulated by individual differences (Ryan et al., 2014). Moreover, it is possible that HPG hormones may be linked to separate effects across or even within individuals, based on the unique dose or combination of hormone concentration occurring at each phase of the cycle. For instance, prior research has found that the administration of low-dose or short-term estradiol can inhibit activity of the HPA axis (Dayas et al., 2000; Young et al., 2001), while HPA activity can be enhanced at higher-doses or long-term administration (Redei et al., 1994; Schmidt & Rubinow, 2009). Future research should replicate and extend the results from this study before confirmatory statements can be made regarding causality and directionality. The present study is unable to form conclusive statements regarding the causality and direct neural mechanisms of HPG hormones, but rather supports the importance of understanding the role that HPG hormones have on cognition and behavior by providing evidence that endogenous cyclic fluctuations of HPG hormones within menstruating people show credible relations with both functions of the central and autonomic nervous system and brain structure and function.

Chapter 8

General Discussion

The present research sought to improve our understanding of the influence that both exogenous and endogenous factors have on stress, cognition, and the human brain. To this end, we define stress in terms of "allostasis", defined as the actions exerted by the body to adjust to exogenous or endogenous challenges and then return to homeostasis. First, we aimed to unravel the complexity of the dynamic allostatic response and the methods used to quantify it on a moment-to-moment basis. In scientific research, such acute time-scales of the human stress-response are often quantified by measuring the activity of the sympathetic nervous system (SNS), one of the two branches within the autonomic nervous system (ANS). Thus, we began by exploring the current leading non-invasive psychophysiological methods of estimating functions of the SNS, by way of impedance cardiography (ICG) and electrocardiogram (ECG). Furthermore, in Experiments 1 – 3, we collaborated with a leading psychophysiology company, Biopac Systems, Inc., as we investigated ways in which to improve upon these current methods. Next, we applied these techniques to two experiments (Experiments 4 and 5), in which we explored how exogenous factors (i.e. environmental stimuli that are separate from our immediate biological functions, such as social pressure) and endogenous factors (i.e. internal and biological mechanisms, such as natural hormone fluctuations) can influence dynamic allostatic responses. We further extended this question to investigate the relationship that endogenous cyclic fluctuations of hypothalamic-pituitary-gonadal (HPG) sex hormones have with brain morphology and function.

Summary of Key Findings

In Experiments 1 and 2, we discovered that a wearable electro-resonator (Experiment 1) and a single accelerometer (Experiment 2) were each able to detect cardiac contractility in response to reliable physiological perturbations. Additionally, we provided accompanying software for preprocessing the data collected by utilizing each method. These devices provided an alternative approach for estimating responses of the SNS that allowed for simpler and faster application methods as compared to ICG and ECG. However, they introduced some new challenges as well, such as a sensitivity to movement, and some difficulty in preprocessing. Finally, in Experiment 3, we presented the trans-radial electrical bioimpedance velocimetry (TREV) device, and provided evidence of its ability to quantify dynamic SNS responses during a physical maximum-grip task. TREV is a recently-developed state-of-the-art technique for estimating contractility that simply requires that four strip electrodes be placed on the arm, as compared to the 10 required electrodes placed throughout the neck and torso for ICG and ECG. We believe that TREV has the ability to replace the need for ICG and ECG in quantifying the activity of the SNS due to its simpler and quicker application process and generation of easily analyzable data output.

In Experiment 4, we demonstrated the ability to dynamically modulate fine-tuned ANS responses with appraised performance. In particular, we investigated the degree to which exogenous factors can modulate psychophysiological stress (measured using the classic methodology of ICG and ECG). We defined "exogenous" as elements in our environment that are separate from our immediate biological functions, and employed the use of predetermined and false performance feedback on a stress-inducing task. We further quantified "stress" as the activity of the SNS and categorized the physiological stress response into either one resembling

a state of "threat" or "challenge". Our results suggest that exogenous factors of social pressure and judgment are capable of manipulating trial-by-trial SNS activity, as well as states of challenge and threat, regardless of an individual's true performance. Specifically, we found that, following a trend of preconceived success, continuously compounding feedback depicting poor performance actuates sympathetic drive. Additionally, our findings suggest that it is relatively easy to push an individual into a physiological state of "threat" with negative performance feedback, whereas it requires excessively "outstanding performance" feedback to push them into a state of "challenge". We reflect upon these findings and prior literature exploring individual differences in stress appraisals and discuss their implications towards stress management techniques.

In Experiment 5, we demonstrated that cyclic endogenous fluctuations of HPG sex hormones across the female menstrual cycle have significant relationships with the response and efficiency of the SNS, cognitive performance, and brain structure and function. We used the TREV device to estimate SNS responses to a stress-inducing task and then extended our investigations into the brain by relating HPG levels to changes in medial temporal lobe (MTL) hippocampal subregion volume, cerebral white matter integrity (WMI), and resting-state functional connectivity within brain networks. We found that progesterone was associated with slower response time (RT) to hard modular arithmetic (MA) trials, suggesting that higher levels of progesterone are linked to slower RT on cognitively demanding tasks. However, this was irrespective of performance accuracy, which remained unaffected. Additionally, both progesterone and follicle stimulating hormone (FSH) were negatively associated with SNS efficiency following performance feedback on hard MA trials, suggesting that high levels of progesterone and FSH are related to slower stress recovery following feedback on difficult

152

tasks. Furthermore, estradiol was positively associated with SNS activity in response to all variations of MA trials, and this effect persisted after receiving feedback. In the brain, higher estradiol levels were associated with an increase in the volume of the CA2/3 hippocampal subregion and a decrease in functional coherence across the resting brain. Moreover, both estradiol and luteinizing hormone (LH) were positively associated with WMI across the whole brain. Our findings suggest that HPG hormones affect behavior, along with stress reactivity and recovery. Additionally, HPG hormones not only affect the structure of one of the most fundamental regions of our brain (the hippocampus), but also affect the way in which brain regions communicate with one another across at both structural (cortex white matter connectivity) and functional (brain network activity at rest) levels.

Theoretical Implications

The overarching goal of the present research has been to enhance the ability to assess stress by quantifying it with a definitive measure of sympathetic drive and zoning in on dynamic fluctuations of allostatic processes and recovery in relation to performance appraisal and quantitative concentrations of HPG hormones within menstruating females. With the present research, we introduce the development of state-of-the-art techniques in measuring dynamic allostatic responses, and provide further evidence that both exogenous and endogenous factors are important to consider in their effects on autonomic and cognitive processes. Specifically, allostatic dynamics are tightly interlinked with exogenous performance appraisal, such that appraisal can modulate fine-tuned allostatic responses moment-to-moment, even in situations when the appraisal is unrelated to the performance itself. Further intertwined in these allostatic processes are the cyclic endogenous fluctuations of HPG hormones that occur naturally across the menstrual cycle; which are linked to both the

degree of SNS activation, and to its recovery. Moreover, the modulating effects of these HPG hormones extend past allostatic processes and into behavior, brain structure, and brain function.

Our findings may hold adaptive implications for the role of HPG hormones in cognition, allostatic mechanisms, and brain morphology. For instance, progesterone peaks during the luteal phase, which is when the body typically prepares itself for the possibility of a newly-fertilized egg following ovulation, with processes such as a thickening of the uterine lining, whether or not that egg exists (Haselton & Buss, 2000; Reed and Carr, 2015). This preparation for pregnancy may extend into cognitive processes as well, by way of increasing vigilance and social threat-detection. Prior research has supported a link between progesterone and an increase in sensitivity towards social information (Maner & Miller, 2017). Furthermore, our findings that increased progesterone concentrations are associated with slower RT to hard MA problems may imply a heightened level of attentiveness, thoughtfulness, and caution. Importantly, this link between progesterone and RT was not credible in response to easy problems, suggesting that it does not have an all-inclusive effect, but rather one that is specifically attuned to tasks that require higher-cognitive load. Another important note is that this effect is not associated with a decrease in performance accuracy, suggesting that there is no hindrance to cognitive ability, but rather an effect specifically on information processing-time. In addition, our finding that progesterone is negatively associated with allostatic recovery following feedback on these hard MA problems may provide further support for this theory. Specifically, if progesterone is related to a heightened degree of caution and careful behavior, then it may be adaptive for the SNS response to remain heightened and vigilant following an environmental stressor, particularly if that stressor may bear social repercussions. In fact, there

has been evidence linking the luteal phase to an increased sensitivity to social feedback, providing further support for this theory (Wang et al., 2021).

Conversely, estradiol and LH levels peak during the ovulation phase, which has been associated with females being more socially active, outgoing, engaging in a greater degree of mate-seeking behavior, and being more sexually active (Durante et al., 2008; Guéguen, 2009; Haselton & Gangestad, 2006; Haselton et al., 2007; Morris & Udry, 1982; Wilcox et al., 1995). Furthermore, there's been evidence that females are more physically and energetically active around ovulation (Anantharaman-Barr & Decombaz, 1989; Morris & Udry, 1970). Simultaneously, this increased social engagement and activity may require a heightened sense of social intelligence and awareness, given that there is a heightened risk of pregnancy. These findings may be representative of our results linking estradiol to an increased SNS response to all MA problems and in response to performance feedback. Specifically, it may be adaptive for estradiol to heighten SNS responsiveness to all incoming stimuli, and to upregulate an individual's sense of awareness as they increase their social engagement and become more active during a vulnerable time. Notably, this increase in sympathetic engagement is not related to allostatic efficiency, hence participants may be more reactive to stimuli, but this reactivity is not hindering their allostatic recovery. Furthermore, this adaptation theory may extend into our findings relating estradiol to morphological changes in the brain. For instance, the associated increase in the volume of the CA2/3 hippocampal subregion with estradiol, and increased WMI across the brain with both estradiol and LH, may have implications towards heightened social cognitive capabilities. Prior research has supported the CA2/3 subregion's critical role in the encoding of social episodic memory, and in social behavior (Oliva, 2022). In addition, a reduction in WMI has been associated with a number of social disorders,

including autism, antisocial personality, borderline personality, and intermittent explosive disorder (Cai et al., 2020; Jiang et al., 2017; Lee et al., 2016; Whalley et al., 2015). Conversely, increases in WMI have been linked to an increase in social cognition in children with autism, further supporting its potential importance to social awareness.

Overall, it is clear that human development is influenced and guided by the actions of HPG sex hormones throughout the lifespan. Markedly, two major shifts in HPG hormone production, puberty and menopause, drastically alter the physical appearance, reproductive capabilities, and physiological functioning of an individual (Burger et al., 2002; Grumbach, 2002; Sisk and Foster, 2004). With the present literature, we provide further evidence that these HPG hormones also play an important role in our daily lives. We believe that allostatic mechanisms and the role of HPG hormones are not only at the core for understanding stress and health, but also are at the core of what makes us….us. HPG hormones work at the most basic levels that make up the human body, affecting our mitochondria (often referred to as the "powerhouse" of the cell), our DNA, our nervous system, our brain structure, our brain function, and ultimately, our behavior (Mahmoodzadeh & Dworatzek, 2019; McEwen, 2006, 2018). Furthermore, our research has shown that they influence the dynamic ways in which we process and respond to the world around us and to the social cues that we interact with daily on a moment-to-moment, beat-to-beat basis. Yet, this is not a clear-cut and simple story. Instead, it is one that has filled the scientific literature with discrepancies. One thing that is apparent is that hormones can affect individuals in significant ways, but the details of those ways are yet to be solidified. Moreover, they may be dependent upon factors such as the individual's genetic composition, biological microstructures and functions, social surroundings, and physical environments.

It has been extensively proven that dimorphic differences between male and female bodies are extensive and important, ranging from functions in brain processes to endocrine reactions to medication, and beyond (Cahill et al., 2006). Nonetheless, to this day, the study of females remains largely underrepresented amongst the scientific and clinical community (De Lange et al., 2021; Taylor et al., 2021). Most of what we know about the human body is from studies carried out primarily on males, in both human and animal research. Importantly, clinical research is largely centered around the male body, notwithstanding significant differences in pharmacological and neuroendocrine responses between the sexes (Ferretti & Galea, 2018). Females make up 50% of the world's population, yet the majority of the present-day's scientific knowledge and clinical practices have been attempting to mold female biology into a male framework. The consequences to females have been extensive, including a higher likelihood to to be misdiagnosed (Colsch & Lindseth, 2018; Newman-Toker et al., 2014; Seetahal et al., 2011), to be given an inappropriate dosage of medication (Parekh et al., 2014), and to experience adverse effects from medications (Zucker & Prendergast, 2020). Furthermore, more than 250 million females worldwide use hormonal forms of contraception (i.e. oral contraceptives, implants, injections, and IUDs), of which the majority involve the manipulation of HPG hormones (United Nations Population Division, 2019). However, the scientific community is just beginning to investigate how these contraceptives may modulate the brain and body (Taylor et al., 2021).

Ultimately, it is apparent from our work that HPG hormones can affect females in significant ways, including via moment-to-moment processes and cyclic cognitive and mental modifications across the menstrual cycle. We hope that the combination of research that we have presented will provide better methods for tracking various health factors. Furthermore,

more research needs to be conducted to understand the complex and dynamic ways in which both exogenous and endogenous factors are constantly affecting individuals. The clinical community can harness this knowledge in making more thoughtful decisions for their patients by considering their patients as a whole: understanding their internal hormonal compositions, as well as their external symptoms and environmental conditions, in order to make more informed decisions in their diagnoses, prescriptions, and preventative care. Our hope for the future of the scientific literature is that it guides individuals to not see their endogenous biology as something that mysteriously happens *to* them, but instead, as something that they can understand, and in turn, harness that knowledge to have their biology work *for* them; thus, enabling them to lead more informed lives conducive to their wellbeing.

References

1. Aas, M., Haukvik, U. K., Djurovic, S., Tesli, M., Athanasiu, L., Bjella, T., Hansson, L., Cattaneo, A., Agartz, I., Andreassen, O. A., & Melle, I. (2014). Interplay between childhood trauma and BDNF val66met variants on blood BDNF mRNA levels and on hippocampus subfields volumes in schizophrenia spectrum and bipolar disorders. *Journal of psychiatric research*, *59*, 14-21. https://doi.org/10.1016/j.jpsychires.2014.08.011

2. Abplanalp, J. M., Livingston, L., Rose, R. M., & Sandwisch, D. (1977). Cortisol and growth hormone responses to psychological stress during the menstrual cycle. *Psychosomatic Medicine*, *39*(3), 158-177.. https://doi.org/10.1097/00006842-197705000-00002

3. Adams, M. M., Fink, S. E., Janssen, W. G., Shah, R. A., & Morrison, J. H. (2004). Estrogen modulates synaptic N-methyl-D-aspartate receptor subunit distribution in the aged hippocampus. *Journal of Comparative Neurology*, *474*(3), 419-426. https://doi.org/10.1002/cne.20148

4. Adams, M. M., Shah, R. A., Janssen, W. G., & Morrison, J. H. (2001). Different modes of hippocampal plasticity in response to estrogen in young and aged female rats. *Proceedings of the National Academy of Sciences*, *98*(14), 8071-8076. https://doi.org/10.1073/pnas.141215898

5. Albert, K., Pruessner, J., & Newhouse, P. (2015). Estradiol levels modulate brain activity and negative responses to psychosocial stress across the menstrual cycle. *Psychoneuroendocrinology*, *59*, 14-24. https://doi.org/10.1016/j.psyneuen.2015.04.022

6. Aly, M., & Turk-Browne, N. B. (2016). Attention stabilizes representations in the human hippocampus. *Cerebral Cortex*, *26*(2), 783-796. https://doi.org/10.1093/cercor/bhv041

7. Amin, H. Z., Amin, L. Z., & Pradipta, A. (2020). Takotsubo cardiomyopathy: a brief review. *Journal of medicine and life*, *13*(1), 3. https://doi.org/10.25122/jml-2018-0067

8. Anantharaman-Barr, H. G., & Decombaz, J. (1989). The effect of wheel running and the estrous cycle on energy expenditure in female rats. *Physiology & behavior*, *46*(2), 259-263. https://doi.org/10.1016/0031-9384(89)90265-5

9. Andersen, M. L., Bittencourt, L. R.A., Antunes, I. B., & Tufik, S. (2006). Effects of progesterone on sleep: a possible pharmacological treatment for sleep-breathing disorders? *Current medicinal chemistry*, *13*(29), 3575-3582. https://doi.org/10.2174/092986706779026200

10. Andersen, K. W., Lasič, S., Lundell, H., Nilsson, M., Topgaard, D., Sellebjerg, F., Szczepankiewicz, F., Siebner, H. R., Blinkenberg, M., & Dyrby, T. B. (2020). Disentangling white-matter damage from physiological fibre orientation dispersion in multiple sclerosis. *Brain communications*, *2*(2), fcaa077. https://doi.org/10.1093/braincomms/fcaa077

11. Apostolova, L. G., Mosconi, L., Thompson, P. M., Green, A. E., Hwang, K. S., Ramirez, A., Mistur, R., Tsui, W. H., & de Leon, M. J. (2010). Subregional hippocampal atrophy predicts Alzheimer's dementia in the cognitively normal. *Neurobiology of aging*, *31*(7), 1077-1088. https://doi.org/10.1016/j.neurobiolaging.2008.08.008

12. Arélin, K., Mueller, K., Barth, C., Rekkas, P. V., Kratzsch, J., Burmann, I., Villringer, A., & Sacher, J. (2015). Progesterone mediates brain functional connectivity changes during the menstrual cycle—a pilot resting state MRI study. *Frontiers in neuroscience*, *9*, 44. https://doi.org/10.3389/fnins.2015.00044

13. Asso, D., & Braier, J. R. (1982). Changes with the menstrual cycle in psychophysiological and self-report measures of activation. *Biological Psychology*, *15*(1-2), 95-107. https://doi.org/10.1016/0301-0511(82)90034-5

14. Avants, B. B., Epstein, C. L., Grossman, M., & Gee, J. C. (2008). Symmetric diffeomorphic image registration with cross-correlation: evaluating automated labeling of elderly and neurodegenerative brain. *Medical image analysis*, *12*(1), 26-41. https://doi.org/10.1016/j.media.2007.06.004

15. Avants, B. B., Tustison, N. J., Song, G., Cook, P. A., Klein, A., & Gee, J. C. (2011). A reproducible evaluation of ANTs similarity metric performance in brain image registration. *Neuroimage*, *54*(3), 2033-2044. https://doi.org/10.1016/j.neuroimage.2010.09.025

16. Baird, D. T. (1987). A model for follicular selection and ovulation: lessons from superovulation. *Journal of steroid biochemistry*, *27*(1-3), 15-23. https://doi.org/10.1016/0022-4731(87)90289-5

17. Bannbers, E., Gingnell, M., Engman, J., Morell, A., Comasco, E., Kask, K., Garavan, H., Wikström, J., & Poromaa, I. S. (2012). The effect of premenstrual dysphoric disorder and menstrual cycle phase on brain activity during response inhibition. *Journal of affective disorders*, *142*(1-3), 347-350. https://doi.org/10.1016/j.jad.2012.04.006

18. Barth, C., Steele, C. J., Mueller, K., Rekkas, V. P., Arélin, K., Pampel, A., Burmann, I., Kratzsch, J., Villringer, A., & Sacher, J. (2016). In-vivo dynamics of the human hippocampus across the menstrual cycle. *Scientific reports*, *6*(1), 1-9. https://doi.org/10.1038/srep32833

19. Bates, D., Mächler, M., Bolker, B., & Walker, S. (2014). Fitting linear mixed-effects models using lme4. *arXiv preprint arXiv:1406.5823.* https://doi.org/10.48550/arXiv.1406.5823

20. Beilock, S. L. (2008). Math performance in stressful situations. *Current Directions in Psychological Science, 17*(5), 339-343. https://doi.org/10.1111/j.1467-8721.2008.00602.x

21. Beilock, S. L., & Carr, T. H. (2005). When High-Powered People Fail: Working Memory and "Choking Under Pressure" in Math. *Psychological Science*, *16*(2), 101–105. https://doi.org/10.1111/j.0956-7976.2005.00789.x

22. Beltz, A. M., & Moser, J. S. (2020). Ovarian hormones: a long overlooked but critical contributor to cognitive brain structures and function. *Annals of the New York Academy of Sciences*, *1464*(1), 156-180. https://doi.org/10.1111/nyas.14255

23. Bernstein, D. P. (1986). Continuous noninvasive real-time monitoring of stroke volume and cardiac output by thoracic electrical bioimpedance. *Critical care medicine, 14*(10), 898-901. https://doi.org/10.1097/00003246-198610000-00015

24. Bernstein, D. P., Henry, I. C., Lemmens, H. J., Chaltas, J. L., DeMaria, A. N., Moon, J. B., & Kahn, A. M. (2015). Validation of stroke volume and cardiac output by electrical interrogation of the brachial artery in normals: assessment of strengths, limitations, and sources of error. *Journal of clinical monitoring and computing*, *29*(6), 789-800. https://doi.org/10.1007/s10877-015-9668-9

25. Berntson, G. G., Bigger, J. T., Eckberg, D. L., Grossman, P., Kaufmann, P. G., Malik, M., Nagaraja, H. N., Porges, S. W., Saul, J. S., Stone, P. H., & Van Der Molen, M. W. (1997). Heart rate variability: origins, methods, and interpretive caveats. *Psychophysiology*, *34*(6), 623-648. https://doi.org/10.1111/j.1469-8986.1997.tb02140.x

26. Besser, A., Flett, G. L., & Hewitt, P. L. (2004). Perfectionism, cognition, and affect in response to performance failure vs. success. *Journal of Rational-Emotive and Cognitive-Behavior Therapy*, *22*(4), 297-324. https://doi.org/10.1023/B:JORE.0000047313.35872.5c

27. Bishop, C. V., Reiter, T. E., Erikson, D. W., Hanna, C. B., Daughtry, B. L., Chavez, S. L., Hennebold, J. D., & Stouffer, R. L. (2019). Chronically elevated androgen and/or consumption of a Western-style diet impairs oocyte quality and granulosa cell function in the nonhuman primate periovulatory follicle. *Journal of assisted reproduction and genetics*, *36*(7), 1497-1511. https://doi.org/10.1007/s10815-019-01497-8

28. Blackburn, J. P., Conway, C. M., Davies, R. M., Enderby, G. E. H., Edridge, A. W., Leigh, J. M., Lindop, M. J., Phillips, G. D., Strickland, D. A. P., Tennant, R., & Knight, H. (1973). Valsalva responses and systolic time intervals during anaesthesia and induced hypotension. *British Journal of Anaesthesia*, *45*(7), 704-710. https://doi.org/10.1093/bja/45.7.704

29. Blackburn, E., & Epel, E. (2017). *The telomere effect: A revolutionary approach to living younger, healthier, longer*. Hachette UK.

30. Blair, J. A., Bhatta, S., McGee, H., & Casadesus, G. (2015). Luteinizing hormone: evidence for direct action in the CNS. *Hormones and behavior*, *76*, 57-62. https://doi.org/10.1016/j.yhbeh.2015.06.020

31. Blascovich, J. (2008a). Challenge and threat. In A.J. Elliot (Ed.), *Handbook of Approach and Avoidance Motivation* (pp. 431–445). New York, NY: Psychology Press.

32. Blascovich, J. (2008b). Challenge, threat, and health. In J. Y. Shah and W. L. Gardner (Eds.), *Handbook of Motivation Science* (pp. 481–493). New York, NY: Guildford Press.

33.   Blascovich, J., & Mendes, W. B. (2010). Social psychophysiology and embodiment. In S. T. Fiske, D. T. Gilbert, and G. Lindzey (Eds.), *Handbook of social psychology.* (5th ed., pp. 194–227). New York, NY: Wiley. https://doi.org/10.1002/9780470561119.socpsy001006

34.   Blascovich, J., Mendes, W. B., Hunter, S. B., & Salomon, K. (1999). Social" facilitation" as challenge and threat. *Journal of personality and social psychology*, *77*(1), 68. https://doi.org/10.1037/0022-3514.77.1.68

35.   Bogomolny, A. (1996). *Modular arithmetic*. Retrieved March, 1(2000), 584-600.

36.   Bonenberger, M., Groschwitz, R. C., Kumpfmueller, D., Groen, G., Plener, P. L., & Abler, B. (2013). It's all about money: oral contraception alters neural reward processing. *Neuroreport, 24*(17), 951-955. https://doi.org/10.1097/WNR.0000000000000024

37.   Bowen, R. L., Isley, J. P., & Atkinson, R. L. (2000). An association of elevated serum gonadotropin concentrations and Alzheimer disease? *Journal of neuroendocrinology*, *12*(4), 351-354. https://doi.org/10.1046/j.1365-2826.2000.00461.x

38.   Braden, B. B., Dassel, K. B., Bimonte-Nelson, H. A., O'Rourke, H. P., Connor, D. J., Moorhous, S., Sabbagh, M. N., Caselli, R. J., & Baxter, L. C. (2017). Sex and post-menopause hormone therapy effects on hippocampal volume and verbal memory. *Aging, Neuropsychology, and Cognition*, *24*(3), 227-246. https://doi.org/10.1080/13825585.2016.1182962

39.   Brann, D. W., Dhandapani, K., Wakade, C., Mahesh, V. B., & Khan, M. M. (2007). Neurotrophic and neuroprotective actions of estrogen: basic mechanisms and clinical implications. *Steroids*, *72*(5), 381-405. https://doi.org/10.1016/j.steroids.2007.02.003

40.   Brooks, A. W. (2014). Get excited: Reappraising pre-performance anxiety as excitement. *Journal of Experimental Psychology: General*, *143*(3), 1144–1158. https://doi.org/10.1037/a0035325

41.   Brötzner, C. P., Klimesch, W., & Kerschbaum, H. H. (2015). Progesterone-associated increase in ERP amplitude correlates with an improvement in performance in a spatial attention paradigm. *Brain Research*, *1595*, 74-83. https://doi.org/10.1016/j.brainres.2014.11.004

42.   Bull, J. R., Rowland, S. P., Scherwitzl, E. B., Scherwitzl, R., Danielsson, K. G., & Harper, J. (2019). Real-world menstrual cycle characteristics of more than 600,000 menstrual cycles. *NPJ digital medicine*, *2*(1), 1-8. https://doi.org/10.1038/s41746-019-0152-7

43.   Bullock, T., MacLean, M. H., Santander, T., Boone, A. P., Babenko, V., Dundon, N. M., Stuber, A., Jimmons, L., Raymer, J., Okafor, G. N., Miller M. B., Giesbrecht, B., & Grafton, S. T. (2023). Habituation of the stress response multiplex to repeated cold pressor exposure. *Frontiers in Physiology*, 2542. https://doi.org/10.3389/fphys.2022.752900

44. Buracas, G. (2022). *M-sequence Generation Program.* MATLAB Central File Exchange. Retrieved October 30, 2021. https://www.mathworks.com/matlabcentral/fileexchange/990-m-sequence-generation-program

45. Burger, H. G., Dudley, E. C., Robertson, D. M., & Dennerstein, L. (2002). Hormonal changes in the menopause transition. *Recent progress in hormone research*, *57*, 257-276.

46. Cacioppo, J. T., & Tassinary, L. G. (1990). Inferring psychological significance from physiological signals. *American psychologist, 45*(1), 16. https://doi.org/10.1037/0003-066X.45.1.16

47. Cahill, L. (2006). Why sex matters for neuroscience. *Nature reviews neuroscience*, *7*(6), 477-484. https://doi.org/10.1038/nrn1909

48. Cai, K., Yu, Q., Herold, F., Liu, Z., Wang, J., Zhu, L., Xiong, X., Chen, A., Müller, P., Kramer, A. F., Müller, N. G., & Zou, L. (2020). Mini-basketball training program improves social communication and white matter integrity in children with autism. *Brain sciences*, *10*(11), 803. https://doi.org/10.3390/brainsci10110803

49. Calado, R. T., & Young, N. S. (2009). Telomere diseases. *New England Journal of Medicine*, *361*(24), 2353-2365. https://doi.org/10.1056/NEJMra0903373

50. Cappuccio, M. L., Gray, R., Hill, D. M., Mesagno, C., & Carr, T. H. (2019). The many threats of self-consciousness: Embodied approaches to choking under pressure in sensorimotor skills. In M. L. Cappuccio (Ed.), *Handbook of embodied cognition and sport psychology* (pp. 101–155). The MIT Press.

51. Carter, J. R., & Lawrence, J. E. (2007). Effects of the menstrual cycle on sympathetic neural responses to mental stress in humans. *The Journal of physiology, 585*(2), 635-641. https://doi.org/10.1113/jphysiol.2007.141051

52. Casadesus, G., Webber, K. M., Atwood, C. S., Pappolla, M. A., Perry, G., Bowen, R. L., & Smith, M. A. (2006). Luteinizing hormone modulates cognition and amyloid-β deposition in Alzheimer APP transgenic mice. *Biochimica et Biophysica Acta (BBA)-Molecular Basis of Disease*, *1762*(4), 447-452. https://doi.org/10.1016/j.bbadis.2006.01.008

53. Cembrowski, M. S., Wang, L., Sugino, K., Shields, B. C., & Spruston, N. (2016). Hipposeq: a comprehensive RNA-seq database of gene expression in hippocampal principal neurons. *elife*, 5. https://doi.org/10.7554/eLife.14997

54. Chakravarti, S., Collins, W. P., Forecast, J. D., Newton, J. R., Oram, D. H., & Studd, J. W. (1976). Hormonal profiles after the menopause. *Br Med J*, *2*(6039), 784-787. https://doi.org/10.1136/bmj.2.6039.784

55. Childs, E., Van Dam, N. T., & Wit, H. D. (2010). Effects of acute progesterone administration upon responses to acute psychosocial stress in men. *Experimental and clinical psychopharmacology, 18*(1), 78. https://doi.org/10.1037/a0018060

56. Chrousos, G. P. (2009). Stress and disorders of the stress system. *Nature reviews endocrinology, 5*(7), 374. https://doi.org/10.1038/nrendo.2009.106

57. Chung, K. C., Peisen, F., Kogler, L., Radke, S., Turetsky, B., Freiherr, J., & Derntl, B. (2016). The influence of menstrual cycle and androstadienone on female stress reactions: an fMRI study. *Frontiers in human neuroscience*, *10*, 44. https://doi.org/10.3389/fnhum.2016.00044

58. Chye, Y., Suo, C., Yücel, M., Den Ouden, L., Solowij, N., & Lorenzetti, V. (2017). Cannabis-related hippocampal volumetric abnormalities specific to subregions in dependent users. *Psychopharmacology*, *234*(14), 2149-2157. https://doi.org/10.1007/s00213-017-4620-y

59. Cicchetti, D. V. (1994). Guidelines, criteria, and rules of thumb for evaluating normed and standardized assessment instruments in psychology. *Psychological assessment*, *6*(4), 284. https://doi.org/10.1037/1040-3590.6.4.284

60. Cieslak, M., Ryan, W. S., Babenko, V., Erro, H., Rathbun, Z. M., Meiring, W., Kelsey, R. M., Blascovich, J., & Grafton, S. T. (2018). Quantifying rapid changes in cardiovascular state with a moving ensemble average. *Psychophysiology, 55*(4), e13018. https://doi.org/10.1111/psyp.13018

61. Cieslak, M., Ryan, W. S., Macy, A., Kelsey, R. M., Cornick, J. E., Verket, M., Blascovich, J., & Grafton, S. (2015). Simultaneous acquisition of functional magnetic resonance images and impedance cardiography. *Psychophysiology, 52*(4), 481-488. https://doi.org/10.1111/psyp.12385

62. Cohn, L. N., Pechlivanoglou, P., Lee, Y., Mahant, S., Orkin, J., Marson, A., & Cohen, E. (2020). Health outcomes of parents of children with chronic illness: a systematic review and meta-analysis. *The Journal of pediatrics*, *218*, 166-177. https://doi.org/10.1016/j.jpeds.2019.10.068

63. Cole, J., Toga, A. W., Hojatkashani, C., Thompson, P., Costafreda, S. G., Cleare, A. J., Williams, S. C. R., Bullmore, E. T., Scott, J. L., Mitterschiffthaler, M. T., Walshe, N. D., Donaldson, C., Mirza, M., Marquand, A., Nosarti, C., McGuffin, P., & Fu, C. H. (2010). Subregional hippocampal deformations in major depressive disorder. *Journal of affective disorders*, *126*(1-2), 272-277. https://doi.org/10.1016/j.jad.2010.03.004

64. Collins, A., Eneroth, P., & Landgren, B. M. (1985). Psychoneuroendocrine stress responses and mood as related to the menstrual cycle. *Psychosomatic medicine*, *47*(6), 512-527.

65. Colsch, R., & Lindseth, G. (2018). Unique stroke symptoms in women: a review. *Journal of Neuroscience Nursing*, *50*(6), 336-342. https://doi.org/10.1097/JNN.0000000000000402

66. Cooke, B. M., & Woolley, C. S. (2005). Gonadal hormone modulation of dendrites in the mammalian CNS. *Journal of neurobiology*, *64*(1), 34-46. https://doi.org/10.1002/neu.20143

67. Critchley, H. D. (2005). Neural mechanisms of autonomic, affective, and cognitive integration. *Journal of comparative neurology*, *493*(1), 154-166. https://doi.org/10.1002/cne.20749

68. Curry, J. J., & Heim, L. M. (1966). Brain myelination after neonatal administration of oestradiol. *Nature*, *209*(5026), 915-916. https://doi.org/10.1038/209915a0

69. Cybulski, G., Strasz, A., Niewiadomski, W., & Gąsiorowska, A. (2012). Impedance cardiography: recent advancements. *Cardiology journal*, *19*(5), 550-556. https://doi.org/10.5603/CJ.2012.0104

70. Dayas, C. V., Xu, Y., Buller, K. M., & Day, T. A. (2000). Effects of chronic oestrogen replacement on stress-induced activation of hypothalamic-pituitary-adrenal axis control pathways. *Journal of neuroendocrinology*, *12*(8), 784-794. https://doi.org/10.1046/j.1365-2826.2000.00527.x

71. De Bondt, T., Smeets, D., Pullens, P., Van Hecke, W., Jacquemyn, Y., & Parizel, P. M. (2015). Stability of resting state networks in the female brain during hormonal changes and their relation to premenstrual symptoms. *Brain Research*, *1624*, 275-285. https://doi.org/10.1016/j.brainres.2015.07.045

72. De Bondt, T., Van Hecke, W., Veraart, J., Leemans, A., Sijbers, J., Sunaert, S., Jacquemyn, Y., & Parizel, P. M. (2013). Does the use of hormonal contraceptives cause microstructural changes in cerebral white matter? Preliminary results of a DTI and tractography study. *European radiology*, *23*(1), 57-64. https://doi.org/10.1007/s00330-012-2572-5

73. De Filippi, E., Uribe, C., Avila-Varela, D. S., Martínez-Molina, N., Gashaj, V., Pritschet, L., Santander, T., Jacobs, E. G., Kringelbach, M. L., Sanz Perl, Y., Deco, G., & Escrichs, A. (2021). The Menstrual Cycle Modulates Whole-Brain Turbulent Dynamics. *Frontiers in neuroscience*, *15*, 753820. https://doi.org/10.3389/fnins.2021.753820

74. De Lange, A. M. G., Jacobs, E. G., & Galea, L. A. (2021). The scientific body of knowledge: Whose body does it serve? a spotlight on women's brain health. *Frontiers in Neuroendocrinology*, *60*, 100898. https://doi.org/10.1016/j.yfrne.2020.100898

75. Dw Waal, L, H. D. V., Wennink, J. M. B., & Odink, R. J. H. (1991). Gonadotrophin and growth hormone secretion throughout puberty. *Acta Pædiatrica*, *80*, 26-31. https://doi.org/10.1111/j.1651-2227.1991.tb17964.x

76. Dedovic, K., Renwick, R., Mahani, N. K., Engert, V., Lupien, S. J., & Pruessner, J. C. (2005). The Montreal Imaging Stress Task: using functional imaging to investigate the effects of perceiving and processing psychosocial stress in the human brain. *Journal of Psychiatry and Neuroscience, 30*(5), 319.

77. Del Rio, G., Velardo, A., Menozzi, R., Zizzo, G., Tavernari, V., Venneri, M. G., Marrama, P., & Petraglia, F. (1998). Acute estradiol and progesterone administration reduced cardiovascular and catecholamine responses to mental stress in menopausal women. *Neuroendocrinology, 67*(4), 269-274. https://doi.org/10.1159/000054322

78. Dickerson, S. S., & Kemeny, M. E. (2004). Acute stressors and cortisol responses: a theoretical integration and synthesis of laboratory research. *Psychological bulletin, 130*(3), 355. https://doi.org/10.1037/0033-2909.130.3.355

79. Donahue, J. E., Stopa, E. G., Chorsky, R. L., King, J. C., Schipper, H. M., Tobet, S. A., Blaustein, J. D., & Reichlin, S. (2000). Cells containing immunoreactive estrogen receptor-α in the human basal forebrain. *Brain research*, *856*(1-2), 142-151. https://doi.org/10.1016/S0006-8993(99)02413-0

80. Dreher, J. C., Schmidt, P. J., Kohn, P., Furman, D., Rubinow, D., & Berman, K. F. (2007). Menstrual cycle phase modulates reward-related neural function in women. *Proceedings of the National Academy of Sciences, 104*(7), 2465-2470. https://doi.org/10.1073/pnas.0605569104

81. Dundon, N. M., Garrett, N., Babenko, V., Cieslak, M., Daw, N. D., & Grafton, S. T. (2020). Sympathetic involvement in time-constrained sequential foraging. *Cognitive, Affective, & Behavioral Neuroscience*, *20*(4), 730-745. https://doi.org/10.3758/s13415-020-00799-0

82. Dundon, N. M., Shapiro, A. D., Babenko, V., Okafor, G. N., & Grafton, S. T. (2021). Ventromedial prefrontal cortex activity and sympathetic allostasis during value-based ambivalence. *Frontiers in Behavioral Neuroscience*, *15*, 24. https://doi.org/10.3389/fnbeh.2021.615796

83. Durand, L. G., & Pibarot, P. (1995). Digital signal processing of the phonocardiogram: review of the most recent advancements. *Critical Reviews™ in biomedical engineering*, *23*(3-4). https://doi.org/10.1615/CritRevBiomedEng.v23.i3-4.10

84. Durante, K. M., Li, N. P., & Haselton, M. G. (2008). Changes in women's choice of dress across the ovulatory cycle: Naturalistic and laboratory task-based evidence. *Personality and Social Psychology Bulletin*, *34*(11), 1451-1460. https://doi.org/10.1177/0146167208323103

85. Epel, E. S., Blackburn, E. H., Lin, J., Dhabhar, F. S., Adler, N. E., Morrow, J. D., & Cawthon, R. M. (2004). Accelerated telomere shortening in response to life stress. *Proceedings of the National Academy of Sciences*, *101*(49), 17312-17315. https://doi.org/10.1073/pnas.0407162101

86. Ermishkin, V. V., Lukoshkova, E. V., Bersenev, E. Y., Saidova, M. A., Shitov, V. N., Vinogradova, O. L., & Khayutin, V. M. (2007). Beat-by-beat changes in pre-ejection period during functional tests evaluated by impedance aortography: a step to a left ventricular contractility monitoring. *13th International Conference on Electrical Bioimpedance and the 8th Conference on Electrical Impedance Tomography* (pp. 655-658). Springer, Berlin, Heidelberg. https://doi.org/10.1007/978-3-540-73841-1_169

87. Eskandari, F., & Sternberg, E. M. (2002). Neural-immune interactions in health and disease. *Annals of the New York Academy of Sciences*, *966*(1), 20-27. https://doi.org/10.1111/j.1749-6632.2002.tb04198.x

88. Ferretti, M. T., & Galea, L. A. (2018). Improving pharmacological treatment in brain and mental health disorders: The need for gender and sex analyses. *Frontiers in neuroendocrinology*, *50*, 1-2. https://doi.org/10.1016/j.yfrne.2018.06.007

89. Ferrier, I. N., Johnstone, E. C., Crow, T. J., & Rincon-Rodriguez, I. (1983). Anterior pituitary hormone secretion in chronic schizophrenics: responses to administration of hypothalamic releasing hormones. *Archives of General Psychiatry*, *40*(7), 755-761. https://doi.org/10.1001/archpsyc.1983.01790060053007

90. Fox, M. D., Snyder, A. Z., Vincent, J. L., Corbetta, M., Van Essen, D. C., & Raichle, M. E. (2005). The human brain is intrinsically organized into dynamic, anticorrelated functional networks. *Proceedings of the National Academy of Sciences*, *102*(27), 9673-9678. https://doi.org/10.1073/pnas.0504136102

91. Freedman, D., & Lane, D. (1983). A nonstochastic interpretation of reported significance levels. *Journal of Business & Economic Statistics*, *1*(4), 292-298. https://doi.org/10.2307/1391660

92. Frings, D., Rycroft, N., Allen, M. S., & Fenn, R. (2014). Watching for gains and losses: The effects of motivational challenge and threat on attention allocation during a visual search task. *Motivation and Emotion*, *38*(4), 513-522. https://doi.org/10.1007/s11031-014-9399-0

93. Frye, C. A., Sumida, K., Dudek, B. C., Harney, J. P., Lydon, J. P., O'Malley, B. W., Pfaff, D. W., & Rhodes, M. E. (2006). Progesterone's effects to reduce anxiety behavior of aged mice do not require actions via intracellular progestin receptors. *Psychopharmacology, 186*(3), 312. https://doi.org/10.1007/s00213-006-0309-3

94. Gaab, J., Rohleder, N., Nater, U. M., & Ehlert, U. (2005). Psychological determinants of the cortisol stress response: the role of anticipatory cognitive appraisal. *Psychoneuroendocrinology*, *30*(6), 599-610. https://doi.org/10.1016/j.psyneuen.2005.02.001

95. Galea, L. A., Wide, J. K., & Barr, A. M. (2001). Estradiol alleviates depressive-like symptoms in a novel animal model of post-partum depression. *Behavioural brain research*, *122*(1), 1-9. https://doi.org/10.1016/S0166-4328(01)00170-X

96. Goldstein, J. M., Jerram, M., Poldrack, R., Ahern, T., Kennedy, D. N., Seidman, L. J., & Makris, N. (2005). Hormonal cycle modulates arousal circuitry in women using functional magnetic resonance imaging. *Journal of Neuroscience*, *25*(40), 9309-9316. https://doi.org/10.1523/JNEUROSCI.2239-05.2005

97. Goldstein, J. M., Seidman, L. J., Horton, N. J., Makris, N., Kennedy, D. N., Caviness Jr, V. S., Faraone, S. V., & Tsuang, M. T. (2001). Normal sexual dimorphism of the adult human brain assessed by in vivo magnetic resonance imaging. *Cerebral cortex, 11*(6), 490-497. https://doi.org/10.1093/cercor/11.6.490

98. Golkar, A., Johansson, E., Kasahara, M., Osika, W., Perski, A., & Savic, I. (2014). The influence of work-related chronic stress on the regulation of emotion and on functional connectivity in the brain. *PloS one*, *9*(9), e104550. https://doi.org/10.1371/journal.pone.0104550

99. Gorlin, R., Knowles, J. H., & Storey, C. F. (1957). The Valsalva maneuver as a test of cardiac function: pathologic physiology and clinical significance. *The American journal of medicine*, *22*(2), 197-212. https://doi.org/10.1016/0002-9343(57)90004-9

100. Greenwell, S., Faskowitz, J., Pritschet, L., Santander, T., Jacobs, E. G., & Betzel, R. F. (2021). High-amplitude network co-fluctuations linked to variation in hormone concentrations over menstrual cycle. *bioRxiv*. https://doi.org/10.1101/2021.07.29.453892

101. Grumbach, M. M. (2002). The neuroendocrinology of human puberty revisited. Hormone *Research in Paediatrics*, *57*(Suppl. 2), 2-14. https://doi.org/10.1159/000058094

102. Grundy, D., Al–Chaer, E. D., Aziz, Q., Collins, S. M., Ke, M., Taché, Y., & Wood, J. D. (2006). Fundamentals of neurogastroenterology: basic science. *Gastroenterology*, *130*(5), 1391-1411. https://doi.org/10.1053/j.gastro.2005.11.060

103. Guapo, V. G., Graeff, F. G., Zani, A. C. T., Labate, C. M., dos Reis, R. M., & Del-Ben, C. M. (2009). Effects of sex hormonal levels and phases of the menstrual cycle in the processing of emotional faces. *Psychoneuroendocrinology*, *34*(7), 1087-1094. https://doi.org/10.1016/j.psyneuen.2009.02.007

104. Guasti, L., Grimoldi, P., Mainardi, L. T., Petrozzino, M. R., Piantanida, E., Garganico, D., Diolisi, A., Zanotta, D., Bertolini, A., Ageno, W., Grandi, A.M., & Grandi, A. M. (1999). Autonomic function and baroreflex sensitivity during a normal ovulatory cycle in humans. *Acta cardiologica*, *54*(4), 209-213.

105. Guéguen, N. (2009). Menstrual cycle phases and female receptivity to a courtship solicitation: An evaluation in a nightclub. *Evolution and Human Behavior*, *30*(5), 351-355. https://doi.org/10.1016/j.evolhumbehav.2009.03.004

106. Handa, R. J., Burgess, L. H., Kerr, J. E., & O'Keefe, J. A. (1994). Gonadal steroid hormone receptors and sex differences in the hypothalamo-pituitary-adrenal axis. *Hormones and behavior*, *28*(4), 464-476. https://doi.org/10.1006/hbeh.1994.1044

107. Hanifin, C. (2010). Cardiac auscultation 101: a basic science approach to heart murmurs. *Jaapa*, *23*(4), 44-48.

108. Haraguchi, S., Sasahara, K., Shikimi, H., Honda, S. I., Harada, N., & Tsutsui, K. (2012). Estradiol promotes purkinje dendritic growth, spinogenesis, and synaptogenesis during neonatal life by inducing the expression of BDNF. *The Cerebellum*, *11*(2), 416-417. https://doi.org/10.1007/s12311-011-0342-6

109. Hase, A., O'Brien, J., Moore, L. J., & Freeman, P. (2019). The relationship between challenge and threat states and performance: A systematic review. *Sport, Exercise, and Performance Psychology*, *8*(2), 123. http://dx.doi.org/10.1037/spy0000132

110. Haselton, M. G., & Buss, D. M. (2000). Error management theory: a new perspective on biases in cross-sex mind reading. *Journal of personality and social psychology*, *78*(1), 81. https://doi.org/10.1037/0022-3514.78.1.81

111. Haselton, M. G., & Gangestad, S. W. (2006). Conditional expression of women's desires and men's mate guarding across the ovulatory cycle. *Hormones and behavior*, *49*(4), 509-518. https://doi.org/10.1016/j.yhbeh.2005.10.006

112. Haselton, M. G., Mortezaie, M., Pillsworth, E. G., Bleske-Rechek, A., & Frederick, D. A. (2007). Ovulatory shifts in human female ornamentation: Near ovulation, women dress to impress. *Hormones and behavior,* *51*(1), 40-45. https://doi.org/10.1016/j.yhbeh.2006.07.007

113. Hassan, S., & Turner, P. (1983). Systolic time intervals: a review of the method in the non-invasive investigation of cardiac function in health, disease and clinical pharmacology. *Postgraduate Medical Journal*, *59*(693), 423-434. http://dx.doi.org/10.1136/pgmj.59.693.423

114. Herting, M. M., Maxwell, E. C., Irvine, C., & Nagel, B. J. (2012). The impact of sex, puberty, and hormones on white matter microstructure in adolescents. *Cerebral cortex*, *22*(9), 1979-1992. https://doi.org/10.1093/cercor/bhr246

115. Hestiantoro, A., Wiwie, M., Shadrina, A., Ibrahim, N., & Purba, J. S. (2017). FSH to estradiol ratio can be used as screening method for mild cognitive impairment in postmenopausal women. *Climacteric*, *20*(6), 577-582. https://doi.org/10.1080/13697137.2017.1377696

116. Hjelmervik, H., Hausmann, M., Osnes, B., Westerhausen, R., & Specht, K. (2014). Resting states are resting traits–an FMRI study of sex differences and menstrual cycle effects in resting state cognitive control networks. *PloS one*, *9*(7), e103492. https://doi.org/10.1371/journal.pone.0103492

117. Hochman, G., & Yechiam, E. (2011). Loss aversion in the eye and in the heart: The autonomic nervous system's responses to losses. *Journal of behavioral decision making*, *24*(2), 140-156. https://doi.org/10.1002/bdm.692

118. Hoekzema, E., Barba-Müller, E., Pozzobon, C., Picado, M., Lucco, F., García-García, D., Soliva, J. C., Tobeña, A, Desco, M., Crone, E. A., Ballesteros, A, Carmona, S., & Vilarroya, O. (2017). Pregnancy leads to long-lasting changes in human brain structure. *Nature neuroscience*, *20*(2), 287-296. https://doi.org/10.1038/nn.4458

119. Hoekzema, E., van Steenbergen, H., Straathof, M., Beekmans, A., Freund, I. M., Pouwels, P. J., & Crone, E. A. (2022). Mapping the effects of pregnancy on resting state brain activity, white matter microstructure, neural metabolite concentrations and grey matter architecture. *Nature Communications*, *13*(1), 1-17. https://doi.org/10.1038/s41467-022-33884-8

120. Hogervorst, E., Bandelow, S., Combrinck, M., & Smith, A. D. (2004). Low free testosterone is an independent risk factor for Alzheimer's disease. *Experimental gerontology*, *39*(11-12), 1633-1639. https://doi.org/10.1016/j.exger.2004.06.019

121. Horn, D. I., Yu, C., Steiner, J., Buchmann, J., Kaufmann, J., Osoba, A., Eckert, U., Zierhut, K. C., Schiltz, K., He, H., Biswal, B., Bogerts, B., & Walter, M. (2010). Glutamatergic and resting-state functional connectivity correlates of severity in major depression–the role of pregenual anterior cingulate cortex and anterior insula. *Frontiers in systems neuroscience*, *4*, 33. https://doi.org/10.3389/fnsys.2010.00033

122. Hu, S., Pruessner, J. C., Coupé, P., & Collins, D. L. (2013). Volumetric analysis of medial temporal lobe structures in brain development from childhood to adolescence. *Neuroimage*, *74*, 276-287. https://doi.org/10.1016/j.neuroimage.2013.02.032

123. Indorato, F., Akashi, Y. J., Rossitto, C., Raffino, C., & Bartoloni, G. (2015). Takotsubo cardiomyopathy associated with rupture of the left ventricular apex: assessment of histopathological features of a fatal case and literature review. *Forensic science, medicine, and pathology*, *11*(4), 577-583. https://doi.org/10.1007/s12024-015-9711-7

124. Jacobs, E., & D'Esposito, M. (2011). Estrogen shapes dopamine-dependent cognitive processes: implications for women's health. *Journal of Neuroscience*, *31*(14), 5286-5293. https://doi.org/10.1523/JNEUROSCI.6394-10.2011

125. Jacobs, E. G., Holsen, L. M., Lancaster, K., Makris, N., Whitfield-Gabrieli, S., Remington, A., Weiss, B., Buka, S., Klibanski, A., & Goldstein, J. M. (2015). 17β-estradiol differentially regulates stress circuitry activity in healthy and depressed women. *Neuropsychopharmacology, 40*(3), 566-576. https://doi.org/10.1038/npp.2014.203

126. Jamieson, J. P., Nock, M. K., & Mendes, W. B. (2012). Mind over matter: Reappraising arousal improves cardiovascular and cognitive responses to stress. *Journal of Experimental Psychology: Genera*l, *141*(3), 417–422. https://doi.org/10.1037/a0025719

127. Jiang, W., Shi, F., Liu, H., Li, G., Ding, Z., Shen, H., Lee, S., Hu, D., Wang, W., & Shen, D. (2017). Reduced white matter integrity in antisocial personality disorder: a diffusion tensor imaging study. *Scientific reports*, *7*(1), 1-11. https://doi.org/10.1038/srep43002

128. Kanaan RA, Allin M, Picchioni M, Barker GJ, Daly E, et al. (2012) Gender Differences in White Matter Microstructure. *PLOS ONE* *7*(6): e38272. https://doi.org/10.1371/journal.pone.0038272

129. Kasagi, F., Akahoshi, M., & Shimaoka, K. (1995). Relation between cold pressor test and development of hypertension based on 28-year follow-up. *Hypertension, 25*(1), 71–76. https://doi.org/10.1161/01.HYP.25.1.71

130. Kassam, K. S., Koslov, K., & Mendes, W. B. (2009). Decisions under distress: Stress profiles influence anchoring and adjustment. *Psychological science*, *20*(11), 1394-1399. https://doi.org/10.1111/j.1467-9280.2009.02455.x

131. Kawata, M. (1995). Roles of steroid hormones and their receptors in structural organization in the nervous system. *Neuroscience research*, *24*(1), 1-46. https://doi.org/10.1016/0168-0102(96)81278-8

132. Kelsey, R. M. (1991). Electrodermal lability and myocardial reactivity to stress. *Psychophysiology, 28*(6), 619-631. https://doi.org/10.1111/j.1469-8986.1991.tb01005.x

133. Kelsey, R. M. (2004). Heart disease and reactivity. In N. B. Anderson (Ed.), *Encyclopedia of Health and Behavior* (pp. 510–517). Thousand Oaks, CA: Sage Publications.

134. Kelsey, R. M., Alpert, B. S., Patterson, S. M., & Barnard, M. (2000). Racial differences in hemodynamic responses to environmental thermal stress among adolescents. *Circulation, 101*(19), 2284-2289. https://doi.org/10.1161/01.CIR.101.19.2284

135. Kelsey, R. M., Ornduff, S. R., & Alpert, B. S. (2007). Reliability of cardiovascular reactivity to stress: Internal consistency. *Psychophysiology, 44*(2), 216–225. https://doi.org/10.1111/j.1469-8986.2007.00499.x

136. Kelsey, R. M., Ornduff, S. R., McCann, C. M., & Reiff, S. (2001). Psychophysiological characteristics of narcissism during active and passive coping. *Psychophysiology, 38*(2), 292-303. https://doi.org/10.1111/1469-8986.3820292

137. Kelsey, R. M., Soderlund, K., & Arthur, C. M. (2004). Cardiovascular reactivity and adaptation to recurrent psychological stress: Replication and extension. *Psychophysiology, 41*(6), 924-934. https://doi.org/10.1111/j.1469-8986.2004.00245.x

138. Kemeny, M. E. (2003). The Psychobiology of Stress. *Current Directions in Psychological Science*, *12*(4), 124–129. https://doi.org/10.1111/1467-8721.01246

139. Kessler, R. C., McGonagle, K. A., Swartz, M., Blazer, D. G., & Nelson, C. B. (1993). Sex and depression in the National Comorbidity Survey I: Lifetime prevalence, chronicity and recurrence. *Journal of affective disorders, 29*(2-3), 85-96. https://doi.org/10.1016/0165-0327(93)90026-G

140. Kessler, R. C., Sonnega, A., Bromet, E., Hughes, M., & Nelson, C. B. (1995). Posttraumatic stress disorder in the National Comorbidity Survey. *Archives of general psychiatry, 52*(12), 1048-1060. https://doi.org/10.1001/archpsyc.1995.03950240066012

141. Khan, S. M., Shilen, A., Heslin, K. M., Ishimwe, P., Allen, A. M., Jacobs, E. T., & Farland, L. V. (2022). SARS-CoV-2 infection and subsequent changes in the menstrual cycle among participants in the Arizona CoVHORT study. *American Journal of Obstetrics & Gynecology*, *226*(2), 270-273. https://doi.org/10.1016/j.ajog.2021.09.016

142. Kirschbaum, C., Pirke, K. M., & Hellhammer, D. H. (1993). The 'Trier Social Stress Test'– a tool for investigating psychobiological stress responses in a laboratory setting. *Neuropsychobiology, 28*(1-2), 76-81. https://doi.org/10.1159/000119004

143. Konrad, K., & Eickhoff, S. B. (2010). Is the ADHD brain wired differently? A review on structural and functional connectivity in attention deficit hyperactivity disorder. *Human brain mapping*, *31*(6), 904-916. https://doi.org/10.1002/hbm.21058

144. Kornstein, S. G., Schatzberg, A. F., Thase, M. E., Yonkers, K. A., McCullough, J. P., Keitner, G. I., Gelenberg, A. J., Davis, S. M., Harrison, W. M., & Keller, M. B. (2000). Gender differences in treatment response to sertraline versus imipramine in chronic depression. *American Journal of Psychiatry, 157*(9), 1445-1452. https://doi.org/10.1176/appi.ajp.157.9.1445

145. Kranz, G. S., Seiger, R., Kaufmann, U., Hummer, A., Hahn, A., Ganger, S., Tik, M., Windischberger, C., Kasper, S., & Lanzenberger, R. (2017). Effects of sex hormone treatment on white matter microstructure in individuals with gender dysphoria. *Neuroimage*, *150*, 60-67. https://doi.org/10.1016/j.neuroimage.2017.02.027

146. Kreibig, S. D. (2010). Autonomic nervous system activity in emotion: A review. *Biological psychology*, *84*(3), 394-421. https://doi.org/10.1016/j.biopsycho.2010.03.010

147. Kreibig, S. D., Samson, A. C., & Gross, J. J. (2013). The psychophysiology of mixed emotional states. *Psychophysiology, 50*(8), 799-811. https://doi.org/10.1111/psyp.12064

148. Krogsrud, S. K., Tamnes, C. K., Fjell, A. M., Amlien, I., Grydeland, H., Sulutvedt, U., Due-Tønnessen, P., Bjørnerud, A., Sølsnes, A. E., Håberg, A. K., Skrane, J., & Walhovd, K. B. (2014). Development of hippocampal subfield volumes from 4 to 22 years. *Human brain mapping*, *35*(11), 5646-5657. https://doi.org/10.1002/hbm.22576

149. Kruschke, J. K. (2018). Rejecting or accepting parameter values in Bayesian estimation. *Advances in methods and practices in psychological science*, *1*(2), 270-280. https://doi.org/10.1177/2515245918771304

150. Kuipers, M., Richter, M., Scheepers, D., Immink, M. A., Sjak-Shie, E., & van Steenbergen, H. (2017). How effortful is cognitive control? Insights from a novel method measuring single-trial evoked beta-adrenergic cardiac reactivity. *International Journal of Psychophysiology*, *119*, 87-92. https://doi.org/10.1016/j.ijpsycho.2016.10.007

151. Kuznetsova, A., Brockhoff, P. B., & Christensen, R. H. (2017). lmerTest package: tests in linear mixed effects models. *Journal of statistical software*, *82*(13), 1-26. https://doi.org/10.18637/jss.v082.i13

152. Landgren, S., Aasly, J., Bäckström, T., Dubrovsky, B., & Danielsson, E. (1987). The effect of progesterone and its metabolites on the interictal epileptiform discharge in the cat's cerebral cortex. *Acta physiologica scandinavica, 131*(1), 33-42. https://doi.org/10.1111/j.1748-1716.1987.tb08202.x

153. Lee, R., Arfanakis, K., Evia, A. M., Fanning, J., Keedy, S., & Coccaro, E. F. (2016). White matter integrity reductions in intermittent explosive disorder. *Neuropsychopharmacology*, *41*(11), 2697-2703. https://doi.org/10.1038/npp.2016.74

154. Lee, K. M., Junkins, E. J., Luo, C., Fatima, U. A., Cox, M. L., & Clancy, K. B. (2022). Investigating trends in those who experience menstrual bleeding changes after SARS-CoV-2 vaccination. *Science advances*, *8*(28). https://doi.org/10.1126/sciadv.abm7201

155. Lei, Z., Rao, C. V., Kornyei, J. L., Licht, P., & Hiatt, E. S. (1993). Novel expression of human chorionic gonadotropin/luteinizing hormone receptor gene in brain. *Endocrinology*, *132*(5), 2262-2270. https://doi.org/10.1210/endo.132.5.8477671

156. Levin, A. B. (1966). A simple test of cardiac function based upon the heart rate changes induced by the Valsalva maneuver. *American Journal of Cardiology, 18*(1), 90–99. https://doi.org/10.1016/0002-9149(66)90200-1

157. Li, K., Chen, G., Hou, H., Liao, Q., Chen, J., Bai, H., Lee, S., Wang, C., Li, H., Cheng, L. & Ai, J. (2021). Analysis of sex hormones and menstruation in COVID-19 women of child-bearing age. *Reproductive biomedicine online*, *42*(1), 260-267. https://doi.org/10.1016/j.rbmo.2020.09.020

158. Lindheim, S. R., Legro, R. S., Morris, R. S., Wong, I. L., Tran, D. Q., Vijod, M. A., Stanczyk, F. Z., & Lobo, R. A. (1994). The effect of progestins on behavioral stress responses in postmenopausal women. *The Journal of the Society for Gynecologic Investigation: JSGI*, *1*(1), 79-83. https://doi.org/10.1177/107155769400100116

159. Lisofsky, N., Mårtensson, J., Eckert, A., Lindenberger, U., Gallinat, J., & Kühn, S. (2015). Hippocampal volume and functional connectivity changes during the female menstrual cycle. *Neuroimage*, *118*, 154-162. https://doi.org/10.1016/j.neuroimage.2015.06.012

160. Little, B. C., Matta, R. J., & Zahn, T. P. (1974). Physiological and psychological effects of progesterone in man. *The Journal of nervous and mental disease*, *159*(4), 256-262.

161. Little, B. C., & Zahn, T. P. (1974). Changes in mood and autonomic functioning during the menstrual cycle. *Psychophysiology, 11*(5), 579-590. https://doi.org/10.1111/j.1469-8986.1974.tb01118.x

162. Logue, M. W., van Rooij, S. J. H., Dennis, E. L., Davis, S. L., Hayes, J. P., Stevens, J. S., Densmore, M., Haswell, C. C., Ipser, J., Koch, S.B.J., Korgaonkar, M., Lebois, L.A.M., Peverill, M., Baker, J. T., Boedhoe, P.S.W., Frijling, J. L., Gruber, S. A., Harpaz-Rotem, I., Jahanshad, N., … Morey, R. A. (2018). Smaller hippocampal volume in posttraumatic stress disorder: A multisite ENIGMA-PGC study: Subcortical Volumetry results from posttraumatic stress disorder consortia. *Biological Psychiatry*, *83*, 244–253. https://doi.org/10.1016/j.biopsych.2017.09.006

163. Lovell, B., & Wetherell, M. A. (2011). The cost of caregiving: endocrine and immune implications in elderly and non elderly caregivers. *Neuroscience & Biobehavioral Reviews*, *35*(6), 1342-1352. https://doi.org/10.1016/j.neubiorev.2011.02.007

164. Luetters, C., Huang, M. H., Seeman, T., Buckwalter, G., Meyer, P. M., Avis, N. E., Sternfeld, B., Johnston, J. M., & Greendale, G. A. (2007). Menopause transition stage and endogenous estradiol and follicle-stimulating hormone levels are not related to cognitive performance: cross-sectional results from the study of women's health across the nation (SWAN). *Journal of women's health*, *16*(3), 331-344. https://doi.org/10.1089/jwh.2006.0057

165. Macy, A., & Bernstein, D. (2020). Trans-radial electrical bioimpedance velocimetry (TREV). BIOPAC.

166. Mahmoodzadeh, S., & Dworatzek, E. (2019). The role of 17β-estradiol and estrogen receptors in regulation of Ca2+ channels and mitochondrial function in cardiomyocytes. *Frontiers in Endocrinology*, *10*, 310. https://doi.org/10.3389/fendo.2019.00310

167. Makowski, D., Ben-Shachar, M. S., & Lüdecke, D. (2019). bayestestR: Describing Effects and their Uncertainty, Existence and Significance within the Bayesian Framework. *Journal of Open Source Software*, *4*(40), 1541. https://doi.org/10.21105/joss.01541

168. Maloney, E. A., & Beilock, S. L. (2012). Math anxiety: Who has it, why it develops, and how to guard against it. *Trends in cognitive sciences*, *16*(8), 404-406. https://doi.org/10.1016/j.tics.2012.06.008

169. Maner, J. K., & Miller, S. L. (2014). Hormones and social monitoring: Menstrual cycle shifts in progesterone underlie women's sensitivity to social information. *Evolution and Human Behavior*, *35*(1), 9-16. https://doi.org/10.1016/j.evolhumbehav.2013.09.001

170. Mattarella-Micke, A., Mateo, J., Kozak, M. N., Foster, K., & Beilock, S. L. (2011). Choke or thrive? The relation between salivary cortisol and math performance depends on individual differences in working memory and math-anxiety. *Emotion*, *11*(4), 1000. https://doi.org/10.1037/a0023224

171. Matthews, G., Campbell, S. E., Falconer, S., Joyner, L. A., Huggins, J., Gilliland, K., Grier, R., & Warm, J. S. (2002). Fundamental dimensions of subjective state in performance settings: task engagement, distress, and worry. *Emotion*, *2*(4), 315. https://doi.org/10.1037//1528-3542.2.4.315

172. Matthews, K. A., Salomon, K., Brady, S. S., & Allen, M. T. (2003). Cardiovascular reactivity to stress predicts future blood pressure in adolescence. *Psychosomatic medicine,* *65*(3), 410-415. https://doi.org/10.1097/01.PSY.0000057612.94797.5F

173. Matthews, G., Warm, J.S., Reinerman, L.E., Langheim, L.K., Saxby, D.J. (2010). Task Engagement, Attention, and Executive Control. In A. Gruszka, G. Matthews, and B. Szymura (Eds.), *Handbook of Individual Differences in Cognition. The Springer Series on Human Exceptionality* (pp. 205-230). Springer, New York, NY. https://doi.org/10.1007/978-1-4419-1210-7_13

174. McCorry, L. K. (2007). Physiology of the autonomic nervous system. *American journal of pharmaceutical education*, *71*(4). https://doi.org/10.5688/aj710478

175. Meeker, T. J., Veldhuijzen, D. S., Keaser, M. L., Gullapalli, R. P., & Greenspan, J. D. (2020). Menstrual Cycle Variations in Gray Matter Volume, White Matter Volume and Functional Connectivity: Critical Impact on Parietal Lobe. *Frontiers in neuroscience*, *14*, 1336. https://doi.org/10.3389/fnins.2020.594588

176. McEwen, B. S. (2006). Protective and damaging effects of stress mediators: central role of the brain, *Dialogues in Clinical Neuroscience*, *8*(4), 367-381. https://doi.org/10.31887/DCNS.2006.8.4/bmcewen

177. McEwen, B. S. (2018). Redefining neuroendocrinology: epigenetics of brain-body communication over the life course. *Frontiers in neuroendocrinology, 49*, 8-30. https://doi.org/10.1016/j.yfrne.2017.11.001

178. McEwen, B. S., & Sapolsky, R. M. (1995). Stress and cognitive function. *Current opinion in neurobiology*, *5*(2), 205-216. https://doi.org/10.1016/0959-4388(95)80028-X

179. Micevych, P., & Christensen, A. (2012). Membrane-initiated estradiol actions mediate structural plasticity and reproduction. *Frontiers in neuroendocrinology*, *33*(4), 331-341. https://doi.org/10.1016/j.yfrne.2012.07.003

180. Minson, C. T., Halliwill, J. R., Young, T. M., & Joyner, M. J. (2000). Influence of the menstrual cycle on sympathetic activity, baroreflex sensitivity, and vascular transduction in young women. *Circulation, 101*(8), 862-868. https://doi.org/10.1161/01.CIR.101.8.862

181. Mills, P. J., Nelesen, R. A., Ziegler, M. G., Parry, B. L., Berry, C. C., Dillon, E., & Dimsdale, J. E. (1996). Menstrual cycle effects on catecholamine and cardiovascular responses to acute stress in black but not white normotensive women. *Hypertension, 27*(4), 962-967. https://doi.org/10.1161/01.HYP.27.4.962

182. Moore, L. J., Freeman, P., Hase, A., Solomon-Moore, E., & Arnold, R. (2019). How consistent are challenge and threat evaluations? A generalizability analysis. *Frontiers in psychology*, *10*, 1778. https://doi.org/10.3389/fpsyg.2019.01778

183. Moore, L. J., Wilson, M. R., Vine, S. J., Coussens, A. H., & Freeman, P. (2013). Champ or chump? Challenge and threat states during pressurized competition. *Journal of Sport and Exercise Psychology*, *35*(6), pp. 551 - 562. https://doi.org/10.1123/jsep.35.6.551

184. Morris, N. M., & Udry, J. R. (1982). Epidemiological patterns of sexual behavior in the menstrual cycle. *Behavior and the menstrual cycle*, 129-153.

185. Morris, N. M., & Udry, J. R. (1970). Variations in pedometer activity during the menstrual cycle. *Obstetrics & Gynecology*, *35*(2), 199-201.

186. Mulkey, S. B., & du Plessis, A. J. (2019). Autonomic nervous system development and its impact on neuropsychiatric outcome. *Pediatric Research*, *85*(2), 120-126. https://doi.org/10.1038/s41390-018-0155-0

187. Mutluer, T., Şar, V., Kose-Demiray, Ç., Arslan, H., Tamer, S., Inal, S., & Kaçar, A. Ş. (2018). Lateralization of neurobiological response in adolescents with post-traumatic stress disorder related to severe childhood sexual abuse: The tri-modal reaction (T-MR) model of protection. *Journal of Trauma & Dissociation*, *19*(1), 108-125. https://doi.org/10.1080/15299732.2017.1304489

188. Newman-Toker, D. E., Moy, E., Valente, E., Coffey, R., & Hines, A. L. (2014). Missed diagnosis of stroke in the emergency department: a cross-sectional analysis of a large population-based sample. *Diagnosis*, *1*(2), 155-166. https://doi.org/10.1515/dx-2013-0038

189. Neylan, T. C., Mueller, S. G., Wang, Z., Metzler, T. J., Lenoci, M., Truran, D., Marmar, C. R., Weiner, M. W., & Schuff, N. (2010). Insomnia severity is associated with a decreased volume of the CA3/dentate gyrus hippocampal subfield. *Biological psychiatry*, *68*(5), 494-496. https://doi.org/10.1016/j.biopsych.2010.04.035

190. Nilsson, M., Szczepankiewicz, F., Lampinen, B., Ahlgren, A., de Almeida Martins, J. P., Lasic, S., Westin, C.F., & Topgaard, D. (2018, June). An open-source framework for analysis of multidimensional diffusion MRI data implemented in MATLAB. *Proc Intl Soc Mag Reson Med*, *26*, 5355.

191. Noreika, D., Griškova-Bulanova, I., Alaburda, A., Baranauskas, M., & Grikšienė, R. (2014). Progesterone and mental rotation task: is there any effect? *BioMed research international*. https://doi.org/10.1155/2014/741758

192. Novak, P. (2011). Assessment of sympathetic index from the Valsalva maneuver. *Neurology*, *76*(23), 2010-2016. https://doi.org/10.1212/WNL.0b013e31821e5563

193. O'Donovan, A., Tomiyama, A. J., Lin, J., Puterman, E., Adler, N. E., Kemeny, M., Wolkowitz, O. M., Blackburn, E. H., & Epel, E. S. (2012). Stress appraisals and cellular aging: A key role for anticipatory threat in the relationship between psychological stress and telomere length. *Brain, behavior, and immunity*, *26*(4), 573-579. https://doi.org/10.1016/j.bbi.2012.01.007

194. Oliva, A. (2022). CA2 physiology underlying social memory. *Current Opinion in Neurobiology*, *77*, 102642. https://doi.org/10.1016/j.conb.2022.102642

195. Österlund, M. K., & Hurd, Y. L. (2001). Estrogen receptors in the human forebrain and the relation to neuropsychiatric disorders. *Progress in neurobiology*, *64*(3), 251-267. https://doi.org/10.1016/S0301-0082(00)00059-9

196. Palombo, D. J., Bacopulos, A., Amaral, R. S., Olsen, R. K., Todd, R. M., Anderson, A. K., & Levine, B. (2018). Episodic autobiographical memory is associated with variation in the size of hippocampal subregions. *Hippocampus*, *28*(2), 69-75. https://doi.org/10.1002/hipo.22818

197. Parekh, A., Fadiran, E. O., Uhl, K., & Throckmorton, D. C. (2011). Adverse effects in women: implications for drug development and regulatory policies. *Expert review of clinical pharmacology*, *4*(4), 453-466. https://doi.org/10.1586/ecp.11.29

198. Pearson, R., & Lewis, M. B. (2005). Fear recognition across the menstrual cycle. *Hormones and Behavio*r, *47*(3), 267-271. https://doi.org/10.1016/j.yhbeh.2004.11.003

199. Peper, J. S., Brouwer, R. M., Schnack, H. G., van Baal, G. C. M., van Leeuwen, M., van den Berg, S. M., de Waal, H. A. D., Janke, A. L., Collins, D. L., Evans, A. C., Boomsma, D. I., Kahn, R. S., & Pol, H. E. H. (2008). Cerebral white matter in early puberty is associated with luteinizing hormone concentrations. *Psychoneuroendocrinology*, *33*(7), 909-915. https://doi.org/10.1016/j.psyneuen.2008.03.017

200. Peters, B. J., & Jamieson, J. P. (2016). The consequences of suppressing affective displays in romantic relationships: A challenge and threat perspective. *Emotion*, *16*(7), 1050–1066. https://doi.org/10.1037/emo0000202

201. Petersen, N., Kilpatrick, L. A., Goharzad, A., & Cahill, L. (2014). Oral contraceptive pill use and menstrual cycle phase are associated with altered resting state functional connectivity. *NeuroImage*, *90*, 24–32. https://doi.org/10.1016/j.neuroimage.2013.12.016

202. Petersen, S. E., & Posner, M. I. (2012). The attention system of the human brain: 20 years after. *Annual review of neuroscience*, *35*, 73. https://doi.org/10.1146/annurev-neuro-062111-150525

203. Phan, J. M., Schneider, E., Peres, J., Miocevic, O., Meyer, V., & Shirtcliff, E. A. (2017). Social evaluative threat with verbal performance feedback alters neuroendocrine response to stress. *Hormones and behavior*, *96*, 104-115. https://doi.org/10.1016/j.yhbeh.2017.09.007

204. Pletzer, B., Crone, J. S., Kronbichler, M., & Kerschbaum, H. (2016). Menstrual cycle and hormonal contraceptive-dependent changes in intrinsic connectivity of resting-state brain networks correspond to behavioral changes due to hormonal status. *Brain Connectivity*, *6*(7), 572-585. https://doi.org/10.1089/brain.2015.0407

205. Pletzer, B., Kronbichler, M., Ladurner, G., Nuerk, H. C., & Kerschbaum, H. (2011). Menstrual cycle variations in the BOLD-response to a number bisection task: implications for research on sex differences. *Brain research*, *1420*, 37-47. https://doi.org/10.1016/j.brainres.2011.08.058

206. Postel, C., Viard, A., André, C., Guénolé, F., de Flores, R., Baleyte, J. M., Gerardin, P., Eustache, F., Dayan, J., & Guillery-Girard, B. (2019). Hippocampal subfields alterations in adolescents with post-traumatic stress disorder. *Human Brain Mapping*, *40*(4), 1244-1252. https://doi.org/10.1002/hbm.24443

207. Pritschet, L., Santander, T., Taylor, C. M., Layher, E., Yu, S., Miller, M. B., Grafton, S. T., & Jacobs, E. G. (2020). Functional reorganization of brain networks across the human menstrual cycle. *Neuroimage*, *220*, 117091. https://doi.org/10.1016/j.neuroimage.2020.117091

208. Protopopescu, X., Butler, T., Pan, H., Root, J., Altemus, M., Polanecsky, M., McEwen, B., Silbersweig, D., & Stern, E. (2008). Hippocampal structural changes across the menstrual cycle. *Hippocampus*, *18*(10), 985-988. https://doi.org/10.1002/hipo.20468

209. Pruessner, J. C., Hellhammer, D. H., & Kirschbaum, C. (1999). Low self-esteem, induced failure and the adrenocortical stress response. *Personality and individual differences, 27*(3), 477-489. https://doi.org/10.1016/S0191-8869(98)00256-6

210. Rametti, G., Carrillo, B., Gómez-Gil, E., Junque, C., Zubiaurre-Elorza, L., Segovia, S., Gomez, A., Karadi, K., & Guillamon, A. (2012). Effects of androgenization on the white matter microstructure of female-to-male transsexuals. A diffusion tensor imaging study. *Psychoneuroendocrinology*, *37*(8), 1261-1269. https://doi.org/10.1016/j.psyneuen.2011.12.019

211. Raichle, M. E. (2015). The brain's default mode network. *Annual review of neuroscience*, *38*, 433-447. https://doi.org/10.1146/annurev-neuro-071013-014030

212. Rapaport, M. H., Thompson, P. M., Kelsoe, J. R., Golshan, S., Judd, L. L., & Gillin, J. C. (1995). Gender differences in outpatient research subjects with affective disorders: a comparison of descriptive variables. *The journal of clinical psychiatry*, *56*(2), 67–72.

213. Redei, E., Li, L., Halasz, I., McGivern, R. F., & Aird, F. (1994). Fast glucocorticoid feedback inhibition of ACTH secretion in the ovariectomized rat: effect of chronic estrogen and progesterone. *Neuroendocrinology*, *60*(2), 113-123. https://doi.org/10.1159/000126741

214. Reed, B. G., & Carr, B. R. (2015). The normal menstrual cycle and the control of ovulation. [Updated 2018 Aug 5]. In: Feingold KR, Anawalt B, Boyce A, et al., (Eds.), *Endotext* [Internet]. South Dartmouth (MA): MDText.com, Inc. https://www.ncbi.nlm.nih.gov/books/NBK279054/

215. Revelle, W. (2018). psych: Procedures for psychological, psychometric, and personality research. *R package version*, *1*(10).

216. Reyes del Paso, G. A., Langewitz, W., Mulder, L. J., Van Roon, A., & Duschek, S. (2013). The utility of low frequency heart rate variability as an index of sympathetic cardiac tone: a review with emphasis on a reanalysis of previous studies. *Psychophysiology*, *50*(5), 477-487. https://doi.org/10.1111/psyp.12027

217. Richter, M. (2015). Goal pursuit and energy conservation: Energy investment increases with task demand but does not equal it. *Motivation and Emotion*, *39*(1), 25-33. https://doi.org/10.1007/s11031-014-9429-y

218. Richter, M., Friedrich, A., & Gendolla, G. H. (2008). Task difficulty effects on cardiac activity. *Psychophysiology*, *45*(5), 869-875. https://doi.org/10.1111/j.1469-8986.2008.00688.x

219. Richter, M., & Gendolla, G. H. (2007). Incentive value, unclear task difficulty, and cardiovascular reactivity in active coping. *International journal of psychophysiology*, *63*(3), 294-301. https://doi.org/10.1016/j.ijpsycho.2006.12.002

220. Richter, M., & Gendolla, G. H. (2009). The heart contracts to reward: Monetary incentives and preejection period. *Psychophysiology*, *46*(3), 451-457. https://doi.org/10.1111/j.1469-8986.2009.00795.x

221. Richter, M., Gendolla, G., & Wright R. (2016). Chapter Five - Three Decades of Research on Motivational Intensity Theory: What We Have Learned About Effort and What We Still Don't Know. *Elselvier*, *3*, 149–186. https://doi.org/10.1016/bs.adms.2016.02.001

222. Roby, K. F. (2019). 17 Beta Estradiol. In: *Reference Module in Biomedical Sciences*. Elsevier. https://doi.org/10.1016/B978-0-12-801238-3.98019-X

223. Rubin, R. D., Watson, P. D., Duff, M. C., & Cohen, N. J. (2014). The role of the hippocampus in flexible cognition and social behavior. Frontiers in human neuroscience, *8*, *742*. https://doi.org/10.3389/fnhum.2014.00742

224. Ryan, J., Artero, S., Carrière, I., Scali, J., Maller, J. J., Meslin, C., Ritchie, K., Scarabin, P., & Ancelin, M. L. (2014). Brain volumes in late life: gender, hormone treatment, and estrogen receptor variants. *Neurobiology of aging*, *35*(3), 645-654. https://doi.org/10.1016/j.neurobiolaging.2013.09.026

225. Salem, J. E., Alexandre, J., Bachelot, A., & Funck-Brentano, C. (2016). Influence of steroid hormones on ventricular repolarization. *Pharmacology & Therapeutics*, *167*, 38-47. https://doi.org/10.1016/j.pharmthera.2016.07.005

226. Salvatier, J., Wiecki, T. V., & Fonnesbeck, C. (2016). Probabilistic programming in Python using PyMC3. *PeerJ Computer Science, 2*, e55. https://doi.org/10.7717/peerj-cs.55

227. Sapolsky, R. M., Krey, L. C., & McEwen, B. S. (1986). The neuroendocrinology of stress and aging: the glucocorticoid cascade hypothesis. *Endocrine reviews, 7*(3), 284-301. https://doi.org/10.1126/sageke.2002.38.cp21

228. Sato, N., & Miyake, S. (2004). Cardiovascular reactivity to mental stress: relationship with menstrual cycle and gender. *Journal of Physiological Anthropology and Applied Human Science, 23*(6), 215-223. https://doi.org/10.2114/jpa.23.215

229. Schaefer, A., Kong, R., Gordon, E. M., Laumann, T. O., Zuo, X. N., Holmes, A. J., Eickhoff, S. B., & Yeo, B. T. (2018). Local-global parcellation of the human cerebral cortex from intrinsic functional connectivity MRI. *Cerebral cortex*, *28*(9), 3095-3114. https://doi.org/10.1093/cercor/bhx179

230. Schlotz, W., Hammerfald, K., Ehlert, U., & Gaab, J. (2011). Individual differences in the cortisol response to stress in young healthy men: Testing the roles of perceived stress reactivity and threat appraisal using multiphase latent growth curve modeling. *Biological psychology*, *87*(2), 257-264. https://doi.org/10.1016/j.biopsycho.2011.03.005

231. Schmidt, P. J., & Rubinow, D. R. (2009). Sex hormones and mood in the perimenopause. *Annals of the New York Academy of Sciences*, *1179*(1), 70-85. https://doi.org/10.1111/j.1749-6632.2009.04982.x

232. Sisk, C. L., & Foster, D. L. (2004). The neural basis of puberty and adolescence. *Nature neuroscience*, *7*(10), 1040-1047. https://doi.org/10.1038/nn1326

233. Seetahal, S. A., Bolorunduro, O. B., Sookdeo, T. C., Oyetunji, T. A., Greene, W. R., Frederick, W., Cornwell, E. E., Chang, D. C., & Siram, S. M. (2011). Negative appendectomy: a 10-year review of a nationally representative sample. *The American Journal of Surgery*, *201*(4), 433-437. https://doi.org/10.1016/j.amjsurg.2010.10.009

234. Seery, M. D. (2011). Challenge or threat? Cardiovascular indexes of resilience and vulnerability to potential stress in humans. *Neuroscience & Biobehavioral Reviews*, *35*(7), 1603-1610. https://doi.org/10.1016/j.neubiorev.2011.03.003

235. Seery, M. D. (2013). The biopsychosocial model of challenge and threat: Using the heart to measure the mind. *Social and Personality Psychology Compass, 7*(9), 637-653. https://doi.org/10.1111/spc3.12052

236. Seery, M. D., Blascovich, J., Weisbuch, M., & Vick, S. B. (2004). The relationship between self-esteem level, self-esteem stability, and cardiovascular reactions to performance feedback. *Journal of personality and social psychology*, *87*(1), 133. https://doi.org/10.1037/0022-3514.87.1.133

237. Seery, M. D., Weisbuch, M., & Blascovich, J. (2009). Something to gain, something to lose: The cardiovascular consequences of outcome framing. *International Journal of Psychophysiology*, *73*(3), 308-312. https://doi.org/10.1016/j.ijpsycho.2009.05.006

238. Shansky, R. M., Glavis-Bloom, C., Lerman, D., McRae, P., Benson, C., Miller, K., Cosand, L., Horvath, T. L., & Arnsten, A. F. T. (2004). Estrogen mediates sex differences in stress-induced prefrontal cortex dysfunction. *Molecular psychiatry, 9*(5), 531. https://doi.org/10.1038/sj.mp.4001435

239. Shansky, R. M., & Lipps, J. (2013). Stress-induced cognitive dysfunction: hormone-neurotransmitter interactions in the prefrontal cortex. *Frontiers in human neuroscience, 7*, 123. https://doi.org/10.3389/fnhum.2013.00123

240. Shoemaker, J. K., Wong, S. W., & Cechetto, D. F. (2012). Cortical circuitry associated with reflex cardiovascular control in humans: does the cortical autonomic network "speak" or "listen" during cardiovascular arousal. *The Anatomical Record*, *295*(9), 1375-1384. https://doi.org/10.1002/ar.22528

241. Short, R. A., O'Brien, P. C., Graff-Radford, N. R., & Bowen, R. L. (2001, September). Elevated gonadotropin levels in patients with Alzheimer disease. In *Mayo Clinic Proceedings* (Vol. 76, No. 9, pp. 906-909). Elsevier. https://doi.org/10.4065/76.9.906

242. Shupnik, M. A. (2003). Luteinizing hormone (LH), In H. L. Henry & A. W. Norman (Eds.), *Encyclopedia of Hormones* (pp. 602-612), Academic Press. https://doi.org/10.1016/B0-12-341103-3/00191-1

243. Simon, N. M., Zalta, A. K., Worthington Iii, J. J., Hoge, E. A., Christian, K. M., Stevens, J. C., & Pollack, M. H. (2006). Preliminary support for gender differences in response to fluoxetine for generalized anxiety disorder. *Depression and anxiety, 23*(6), 373-376. https://doi.org/10.1002/da.20184

244. Stanek, J., & Richter, M. (2016). Evidence against the primacy of energy conservation: Exerted force in possible and impossible handgrip tasks. *Motivation Science*, *2*(1), 49. https://doi.org/10.1037/mot0000028

245. Stanek, J. C., & Richter, M. (2021). Energy investment and motivation: The additive impact of task demand and reward value on exerted force in hand grip tasks. *Motivation and Emotion*, *45*(2), 131-145. https://doi.org/10.1007/s11031-020-09862-2

246. Steptoe, A., & Kivimäki, M. (2012). Stress and cardiovascular disease. *Nature Reviews Cardiology*, *9*(6), 360-370. https://doi.org/10.1038/nrcardio.2012.45

247. Stirone, C., Duckles, S. P., Krause, D. N., & Procaccio, V. (2005). Estrogen increases mitochondrial efficiency and reduces oxidative stress in cerebral blood vessels. *Molecular pharmacology*, *68*(4), 959-965. https://doi.org/10.1124/mol.105.014662

248. Suthana, N., Ekstrom, A., Moshirvaziri, S., Knowlton, B., & Bookheimer, S. (2011). Dissociations within human hippocampal subregions during encoding and retrieval of spatial information. *Hippocampus*, *21*(7), 694-701. https://doi.org/10.1002/hipo.20833

249. Spiers, C. (2011). Cardiac auscultation. *British Journal of Cardiac Nursing*, *6*(10), 482-486. https://doi.org/10.12968/bjca.2011.6.10.482

250. Spodick, D. H. (1979). Frank-Starling effect. *Circulation*, *60*(3), 718-719.

251. Syan, S. K., Minuzzi, L., Costescu, D., Smith, M., Allega, O. R., Coote, M., Hall, G. B. C., & Frey, B. N. (2017). Influence of endogenous estradiol, progesterone, allopregnanolone, and dehydroepiandrosterone sulfate on brain resting state functional connectivity across the menstrual cycle. *Fertility and sterility*, *107*(5), 1246-1255. https://doi.org/10.1016/j.fertnstert.2017.03.021

252. Tada, Y., Yoshizaki, T., Tomata, Y., Yokoyama, Y., Sunami, A., Hida, A., & Kawano, Y. (2017). The impact of menstrual cycle phases on cardiac autonomic nervous system activity: an observational study considering lifestyle (diet, physical activity, and sleep) among female college students. *Journal of nutritional science and vitaminology*, *63*(4), 249-255. https://doi.org/10.3177/jnsv.63.249

253. Tamnes, C. K., Bos, M. G., van de Kamp, F. C., Peters, S., & Crone, E. A. (2018). Longitudinal development of hippocampal subregions from childhood to adulthood. *Developmental cognitive neuroscience*, *30*, 212-222. https://doi.org/10.1016/j.dcn.2018.03.009

254. Taylor, S. E., Klein, L. C., Lewis, B. P., Gruenewald, T. L., Gurung, R. A., & Updegraff, J. A. (2000). Biobehavioral responses to stress in females: tend-and-befriend, not fight-or-flight. *Psychological review*, *107*(3), 411. https://doi.org/10.1037/0033-295X.107.3.411

255. Taylor, C. M., Pritschet, L., & Jacobs, E. G. (2021). The scientific body of knowledge–Whose body does it serve? A spotlight on oral contraceptives and women's health factors in neuroimaging. *Frontiers in neuroendocrinology*, *60*, 100874. https://doi.org/10.1016/j.yfrne.2020.100874

256. Taylor, C. M., Pritschet, L., Olsen, R. K., Layher, E., Santander, T., Grafton, S. T., & Jacobs, E. G. (2020). Progesterone shapes medial temporal lobe volume across the human menstrual cycle. *NeuroImage*, *220*, 117125. https://doi.org/10.1016/j.neuroimage.2020.117125

257. Thayer, J. F., & Brosschot, J. F. (2005). Psychosomatics and psychopathology: looking up and down from the brain. *Psychoneuroendocrinology*, *30*(10), 1050-1058. https://doi.org/10.1016/j.psyneuen.2005.04.014

258. Thayer, J. F., Hansen, A. L., & Johnsen, B. H. (2010). The non-invasive assessment of autonomic influences on the heart using impedance cardiography and heart rate variability. *In Handbook of behavioral medicine* (pp. 723-740). Springer, New York, NY. https://doi.org/10.1007/978-0-387-09488-5_47

259. Thornhill, R., Chapman, J. F., & Gangestad, S. W. (2013). Women's preferences for men's scents associated with testosterone and cortisol levels: Patterns across the ovulatory cycle. *Evolution and Human Behavior*, *34*(3), 216-221. https://doi.org/10.1016/j.evolhumbehav.2013.01.003

260. Tian, L., Jiang, T., Wang, Y., Zang, Y., He, Y., Liang, M., Sui, M., Cao, Q., Hu, S., Peng, M., & Zhuo, Y. (2006). Altered resting-state functional connectivity patterns of anterior cingulate cortex in adolescents with attention deficit hyperactivity disorder. *Neuroscience letters*, *400*(1-2), 39-43. https://doi.org/10.1016/j.neulet.2006.02.022

261. Tian, Y., Margulies, D. S., Breakspear, M., & Zalesky, A. (2020). Topographic organization of the human subcortex unveiled with functional connectivity gradients. *Nature neuroscience*, *23*(11), 1421-1432. https://doi.org/10.1038/s41593-020-00711-6

262. Toffoletto, S., Lanzenberger, R., Gingnell, M., Sundström-Poromaa, I., & Comasco, E. (2014). Emotional and cognitive functional imaging of estrogen and progesterone effects in the female human brain: a systematic review. *Psychoneuroendocrinology*, *50*, 28-52. https://doi.org/10.1016/j.psyneuen.2014.07.025

263. Tomaka, J., Blascovich, J., Kibler, J., & Ernst, J. M. (1997). Cognitive and physiological antecedents of threat and challenge appraisal. *Journal of personality and social psychology, 73*(1), 63. https://doi.org/10.1037/0022-3514.73.1.63

264. Turner, M. J., Jones, M. V., Sheffield, D., Barker, J. B., & Coffee, P. (2014). Manipulating cardiovascular indices of challenge and threat using resource appraisals. *International Journal of Psychophysiology*, *94*(1), 9-18. https://doi.org/10.1016/j.ijpsycho.2014.07.004

265. Uddin, L. Q., Kelly, A. C., Biswal, B. B., Margulies, D. S., Shehzad, Z., Shaw, D., Ghaffari, M., Rotrosen, J., Adler, L. A., Castellanos, F. X., & Milham, M. P. (2008). Network homogeneity reveals decreased integrity of default-mode network in ADHD. *Journal of neuroscience methods*, *169*(1), 249-254. https://doi.org/10.1016/j.jneumeth.2007.11.031

266. Uijtdehaage, S. H., & Thayer, J. F. (2000). Accentuated antagonism in the control of human heart rate. *Clinical Autonomic Research*, *10*(3), 107-110. https://doi.org/10.1007/BF02278013

267. United Nations Population Division. (2019). *Contraceptive use by method 2019 : data booklet.* https://www.un.org/development/desa/pd/sites/www.un.org.development.desa.pd/files/files/documents/2020/Jan/un_2019_contraceptiveusebymethod_databooklet.pdf

268. Valenza, G., Citi, L., Saul, J. P., & Barbieri, R. (2018). Measures of sympathetic and parasympathetic autonomic outflow from heartbeat dynamics. *Journal of applied physiology*, *125*(1), 19-39. https://doi.org/10.1152/japplphysiol.00842.2017

269. Van Broekhoven, F., Bäckström, T., & Verkes, R. J. (2006). Oral progesterone decreases saccadic eye velocity and increases sedation in women. *Psychoneuroendocrinology*, *31*(10), 1190-1199. https://doi.org/10.1016/j.psyneuen.2006.08.007

270. Van Den Heuvel, M. P., & Pol, H. E. H. (2010). Exploring the brain network: a review on resting-state fMRI functional connectivity. *European neuropsychopharmacology*, *20*(8), 519-534. https://doi.org/10.1016/j.euroneuro.2010.03.008

271. Van Wingen, G., Van Broekhoven, F., Verkes, R. J., Petersson, K. M., Bäckström, T., Buitelaar, J., & Fernández, G. (2007). How progesterone impairs memory for biologically salient stimuli in healthy young women. *Journal of Neuroscience*, *27*(42), 11416-11423. https://doi.org/10.1523/JNEUROSCI.1715-07.2007

272. Veena, C. N., Vastrad, B. C., & Nandan, T. M. (2017). Study of auditory and visual reaction time across various phases of menstrual cycle. *National Journal of Physiology, Pharmacy and Pharmacology*, *7*(4), 339. https://doi.org/10.5455/njppp.2017.7.0928205102016

273. Veer, I. M., Oei, N. Y., Spinhoven, P., van Buchem, M. A., Elzinga, B. M., & Rombouts, S. A. (2011). Beyond acute social stress: increased functional connectivity between amygdala and cortical midline structures. *NeuroImage*, *57*(4), 1534-1541. https://doi.org/10.1016/j.neuroimage.2011.05.074

274. Venables, L., & Fairclough, S. H. (2009). The influence of performance feedback on goal-setting and mental effort regulation. *Motivation and Emotion*, *33*(1), 63-74. https://doi.org/10.1007/s11031-008-9116-y

275. Volz, L. J., Cieslak, M., & Grafton, S. T. (2018). A probabilistic atlas of fiber crossings for variability reduction of anisotropy measures. *Brain Structure and Function*, *223*(2), 635-651. https://doi.org/10.1007/s00429-017-1508-x

276. Wang, Z., Neylan, T. C., Mueller, S. G., Lenoci, M., Truran, D., Marmar, C. R., Weiner, M. W., & Schuff, N. (2010). Magnetic resonance imaging of hippocampal subfields in posttraumatic stress disorder. *Archives of general psychiatry*, *67*(3), 296-303. https://doi.org/10.1001/archgenpsychiatry.2009.205

277. Wang, J. X., Zhuang, J. Y., Fu, L., & Lei, Q. (2021). Social orientation in the luteal phase: increased social feedback sensitivity, inhibitory response, interpersonal anxiety and cooperation preference. *Evolutionary Psychology*, *19*(1). https://doi.org/10.1177/1474704920986866

278. Weber, M. T., Rubin, L. H., & Maki, P. M. (2013). Cognition in perimenopause: the effect of transition stage. *Menopause*, *20*(5). https://doi.org/10.1097/GME.0b013e31827655e5

279. Wei, J., Yuen, E. Y., Liu, W., Li, X., Zhong, P., Karatsoreos, I. N., McEwen, B. S., & Yan, Z. (2014). Estrogen protects against the detrimental effects of repeated stress on glutamatergic transmission and cognition. *Molecular psychiatry, 19*(5), 588. https://doi.org/10.1038/mp.2013.83

280. Weis, S., Hodgetts, S., & Hausmann, M. (2019). Sex differences and menstrual cycle effects in cognitive and sensory resting state networks. *Brain and cognition*, *131*, 66-73. https://doi.org/10.1016/j.bandc.2017.09.003

281. Westin, C. F., Knutsson, H., Pasternak, O., Szczepankiewicz, F., Özarslan, E., van Westen, D., Mattisson, C., Bogren, M., O'Donnell, L. J., Kubicki, M., Topgaard, D., & Nilsson, M. (2016). Q-space trajectory imaging for multidimensional diffusion MRI of the human brain. *Neuroimage*, *135*, 345-362. https://doi.org/10.1016/j.neuroimage.2016.02.039

282. Whalley, H. C., Nickson, T., Pope, M., Nicol, K., Romaniuk, L., Bastin, M. E., Semple, S. I., McIntosh, A. M., & Hall, J. (2015). White matter integrity and its association with affective and interpersonal symptoms in borderline personality disorder. *NeuroImage: Clinical, 7*, 476-481. https://doi.org/10.1016/j.nicl.2015.01.016

283. Whirledge, S., & Cidlowski, J. A. (2010). Glucocorticoids, stress, and fertility. *Minerva endocrinologica*, *35*(2), 109.

284. Wilcox, A. J., Weinberg, C. R., & Baird, D. D. (1995). Timing of sexual intercourse in relation to ovulation—effects on the probability of conception, survival of the pregnancy, and sex of the baby. *New England Journal of Medicine*, *333*(23), 1517-1521. https://doi.org/10.1093/humrep/deh305

285. Wolfram, M., Bellingrath, S., & Kudielka, B. M. (2011). The cortisol awakening response (CAR) across the female menstrual cycle. *Psychoneuroendocrinology*, *36*(6), 905-912. https://doi.org/10.1016/j.psyneuen.2010.12.006

286. Woolley, C. S., & McEwen, B. S. (1992). Estradiol mediates fluctuation in hippocampal synapse density during the estrous cycle in the adult rat [published erratum appears in J Neurosci 1992 Oct; 12 (10): following table of contents]. *Journal of Neuroscience*, *12*(7), 2549-2554. https://doi.org/10.1523/JNEUROSCI.12-07-02549.1992

287. Woolley, C. S., & McEwen, B. S. (1993). Roles of estradiol and progesterone in regulation of hippocampal dendritic spine density during the estrous cycle in the rat. *Journal of Comparative Neurology*, *336*(2), 293-306. https://doi.org/10.1002/cne.903360210

288. Wormwood, J. B., Khan, Z., Siegel, E., Lynn, S. K., Dy, J., Barrett, L. F., & Quigley, K. S. (2019). Physiological indices of challenge and threat: A data-driven investigation of autonomic nervous system reactivity during an active coping stressor task. *Psychophysiology*, *56*(12), e13454. https://doi.org/10.1111/psyp.13454

289. Wright, R. A., Contrada, R. J., & Patane, M. J. (1986). Task difficulty, cardiovascular response, and the magnitude of goal valence. *Journal of Personality and Social Psychology, 51*(4), 837. https://doi.org/10.1037/0022-3514.51.4.837

290. Wright, R. A., & Kirby, L. D. (2001). Effort determination of cardiovascular response: An integrative analysis with applications in social psychology. *Advances in experimental social psychology, 33*, 255-307. https://doi.org/10.1016/S0065-2601(01)80007-1

291. Yeh, F. C. (2022). Population-based tract-to-region connectome of the human brain and its hierarchical topology. *Nature communications*, *13*(1), 1-13. https://doi.org/10.1038/s41467-022-32595-4

292. Young, E. A., Altemus, M., Parkison, V., & Shastry, S. (2001). Effects of estrogen antagonists and agonists on the ACTH response to restraint stress in female rats. *Neuropsychopharmacology*, *25*(6), 881-891. https://doi.org/10.1016/S0893-133X(01)00301-3

293. Yu, R. (2015). Choking under pressure: the neuropsychological mechanisms of incentive-induced performance decrements. *Frontiers in behavioral neuroscience*, *9*, 19. https://doi.org/10.3389/fnbeh.2015.00019

294. Yushkevich, P. A., Pluta, J. B., Wang, H., Xie, L., Ding, S. L., Gertje, E. C., Mancuso, L., Kliot, D., Das, S. R., & Wolk, D. A. (2015). Automated volumetry and regional thickness analysis of hippocampal subfields and medial temporal cortical structures in mild cognitive impairment. *Human brain mapping*, *36*(1), 258-287. https://doi.org/10.1002/hbm.22627

295. Zalesky, A., Fornito, A., & Bullmore, E. T. (2010). Network-based statistic: identifying differences in brain networks. *Neuroimage*, *53*(4), 1197-1207. https://doi.org/10.1016/j.neuroimage.2010.06.041

296. Zeeman, M. L., Weckesser, W., & Gokhman, D. (2003). Resonance in the menstrual cycle: a new model of the LH surge. *Reproductive BioMedicine Online*, *7*(3), 295-300. https://doi.org/10.1016/S1472-6483(10)61867-6

297. Zhang, J., Rane, G., Dai, X., Shanmugam, M. K., Arfuso, F., Samy, R. P., Lai, M. K. P., Kappei, D., Kumar, A. P., & Sethi, G. (2016). Ageing and the telomere connection: An intimate relationship with inflammation. *Ageing research reviews*, *25*, 55-69. https://doi.org/10.1016/j.arr.2015.11.006

298. Zhu, D., Birzniece, V., Bäckström, T., & Wahlström, G. (2004). Dynamic aspects of acute tolerance to allopregnanolone evaluated using anaesthesia threshold in male rats. *British journal of anaesthesia, 93*(4), 560-567. https://doi.org/10.1093/bja/aeh233

299. Zucker, I., & Prendergast, B. J. (2020). Sex differences in pharmacokinetics predict adverse drug reactions in women. *Biology of sex differences*, *11*(1), 1-14. https://doi.org/10.1186/s13293-020-00308-5

Appendix A

A.1   Response Time (RT) Regression Coefficients

Complete list of regression coefficients across all tested trial conditions and parameters for response time (RT) to modular arithmetic (MA) problems.

	Relations	Mean	Lower HDI	Upper HDI	Credible
	Response Time Regression Coefficients				
1	session1_easy_lo_E2	-0.08	-0.14	-0.03	
2	session1_easy_lo_P4	-0.14	-0.20	-0.09	
3	session1_easy_lo_LH	-0.01	-0.06	0.05	
4	session1_easy_lo_FSH	-0.11	-0.17	-0.05	
5	session1_easy_hi_E2	-0.10	-0.19	0.00	
6	session1_easy_hi_P4	-0.19	-0.27	-0.10	***
7	session1_easy_hi_LH	0.00	-0.09	0.09	
8	session1_easy_hi_FSH	-0.11	-0.20	-0.03	
9	session1_hard_lo_E2	0.24	0.21	0.28	***
10	session1_hard_lo_P4	0.19	0.15	0.22	***
11	session1_hard_lo_LH	0.18	0.14	0.22	***
12	session1_hard_lo_FSH	0.28	0.24	0.32	***
13	session1_hard_hi_E2	0.27	0.22	0.33	***
14	session1_hard_hi_P4	0.17	0.11	0.23	***
15	session1_hard_hi_LH	0.19	0.13	0.25	***
16	session1_hard_hi_FSH	0.29	0.23	0.36	***
17	session2_easy_lo_E2	-0.06	-0.14	0.02	
18	session2_easy_lo_P4	0.10	0.05	0.16	
19	session2_easy_lo_LH	0.10	0.05	0.16	
20	session2_easy_lo_FSH	0.11	0.06	0.17	
21	session2_easy_hi_E2	-0.11	-0.23	0.01	
22	session2_easy_hi_P4	0.10	0.01	0.18	
23	session2_easy_hi_LH	0.07	-0.02	0.17	
24	session2_easy_hi_FSH	0.08	0.00	0.17	
25	session2_hard_lo_E2	-0.19	-0.22	-0.15	***
26	session2_hard_lo_P4	0.21	0.19	0.23	***
27	session2_hard_lo_LH	-0.06	-0.09	-0.04	
28	session2_hard_lo_FSH	0.06	0.03	0.08	

	Relations	Mean	Lower HDI	Upper HDI	Credible
29	session2_hard_hi_E2	-0.21	-0.26	-0.16	***
30	session2_hard_hi_P4	0.20	0.17	0.23	***
31	session2_hard_hi_LH	-0.06	-0.10	-0.02	
32	session2_hard_hi_FSH	0.06	0.02	0.10	
33	session3_easy_lo_E2	0.11	0.05	0.17	
34	session3_easy_lo_P4	0.10	0.04	0.17	
35	session3_easy_lo_LH	-0.02	-0.09	0.05	
36	session3_easy_lo_FSH	-0.05	-0.11	0.01	
37	session3_easy_hi_E2	0.03	-0.07	0.13	
38	session3_easy_hi_P4	0.04	-0.05	0.12	
39	session3_easy_hi_LH	-0.11	-0.21	0.00	
40	session3_easy_hi_FSH	0.02	-0.07	0.12	
41	session3_hard_lo_E2	0.02	-0.02	0.05	
42	session3_hard_lo_P4	0.13	0.10	0.16	
43	session3_hard_lo_LH	0.09	0.05	0.12	
44	session3_hard_lo_FSH	0.10	0.07	0.13	
45	session3_hard_hi_E2	0.06	0.01	0.11	
46	session3_hard_hi_P4	0.20	0.15	0.25	***
47	session3_hard_hi_LH	0.09	0.04	0.13	
48	session3_hard_hi_FSH	0.04	-0.01	0.09	
49	session1_easy_E2	-0.09	-0.14	-0.03	
50	session1_easy_P4	-0.17	-0.22	-0.11	***
51	session1_easy_LH	0.00	-0.06	0.05	
52	session1_easy_FSH	-0.11	-0.16	-0.06	
53	session1_hard_E2	0.26	0.23	0.29	***
54	session1_hard_P4	0.18	0.14	0.21	***
55	session1_hard_LH	0.19	0.15	0.22	***
56	session1_hard_FSH	0.29	0.25	0.33	***
57	session2_easy_E2	-0.08	-0.16	-0.01	
58	session2_easy_P4	0.10	0.05	0.15	
59	session2_easy_LH	0.09	0.03	0.14	
60	session2_easy_FSH	0.10	0.04	0.15	
61	session2_hard_E2	-0.20	-0.23	-0.17	***
62	session2_hard_P4	0.21	0.19	0.23	***
63	session2_hard_LH	-0.06	-0.08	-0.04	
64	session2_hard_FSH	0.06	0.04	0.08	
65	session3_easy_E2	0.07	0.01	0.13	
66	session3_easy_P4	0.07	0.02	0.13	

	Relations	Mean	Lower HDI	Upper HDI	Credible
67	session3_easy_LH	-0.06	-0.13	0.00	
68	session3_easy_FSH	-0.01	-0.07	0.04	
69	session3_hard_E2	0.04	0.01	0.07	
70	session3_hard_P4	0.16	0.14	0.19	***
71	session3_hard_LH	0.09	0.06	0.12	
72	session3_hard_FSH	0.07	0.04	0.10	
73	session1_lo_E2	0.08	0.04	0.11	
74	session1_lo_P4	0.02	-0.01	0.05	
75	session1_lo_LH	0.09	0.05	0.12	
76	session1_lo_FSH	0.09	0.05	0.12	
77	session1_hi_E2	0.09	0.03	0.14	
78	session1_hi_P4	-0.01	-0.06	0.04	
79	session1_hi_LH	0.09	0.04	0.15	
80	session1_hi_FSH	0.09	0.04	0.14	
81	session2_lo_E2	-0.12	-0.16	-0.08	
82	session2_lo_P4	0.16	0.13	0.19	***
83	session2_lo_LH	0.02	-0.01	0.05	
84	session2_lo_FSH	0.08	0.06	0.11	
85	session2_hi_E2	-0.16	-0.22	-0.10	
86	session2_hi_P4	0.15	0.10	0.19	***
87	session2_hi_LH	0.01	-0.05	0.06	
88	session2_hi_FSH	0.07	0.02	0.11	
89	session3_lo_E2	0.06	0.03	0.10	
90	session3_lo_P4	0.12	0.08	0.15	
91	session3_lo_LH	0.03	-0.01	0.07	
92	session3_lo_FSH	0.02	-0.01	0.06	
93	session3_hi_E2	0.04	-0.01	0.10	
94	session3_hi_P4	0.12	0.07	0.17	
95	session3_hi_LH	-0.01	-0.06	0.05	
96	session3_hi_FSH	0.03	-0.02	0.08	
97	easy_lo_E2	-0.01	-0.05	0.03	
98	easy_lo_P4	0.02	-0.01	0.06	
99	easy_lo_LH	0.02	-0.01	0.06	
100	easy_lo_FSH	-0.02	-0.05	0.02	
101	easy_hi_E2	-0.06	-0.12	0.00	
102	easy_hi_P4	-0.02	-0.07	0.03	
103	easy_hi_LH	-0.01	-0.07	0.04	
104	easy_hi_FSH	0.00	-0.06	0.05	
105	hard_lo_E2	0.02	0.00	0.04	

	Relations	Mean	Lower HDI	Upper HDI	Credible
106	hard_lo_P4	0.18	0.16	0.19	***
107	hard_lo_LH	0.07	0.05	0.09	
108	hard_lo_FSH	0.15	0.13	0.17	***
109	hard_hi_E2	0.04	0.01	0.07	
110	hard_hi_P4	0.19	0.16	0.22	***
111	hard_hi_LH	0.07	0.04	0.10	
112	hard_hi_FSH	0.13	0.10	0.16	
113	easy_E2	-0.03	-0.07	0.00	
114	easy_P4	0.00	-0.03	0.03	
115	easy_LH	0.01	-0.03	0.04	
116	easy_FSH	-0.01	-0.04	0.02	
117	hard_E2	0.03	0.01	0.05	
118	hard_P4	0.18	0.17	0.20	***
119	hard_LH	0.07	0.05	0.09	
120	hard_FSH	0.14	0.12	0.16	***
121	lo_E2	0.01	-0.01	0.03	
122	lo_P4	0.10	0.08	0.12	
123	lo_LH	0.05	0.03	0.07	
124	lo_FSH	0.07	0.05	0.08	
125	hi_E2	-0.01	-0.04	0.02	
126	hi_P4	0.09	0.06	0.11	
127	hi_LH	0.03	0.00	0.06	
128	hi_FSH	0.06	0.03	0.09	
129	session1_E2	0.08	0.05	0.12	
130	session1_P4	0.01	-0.03	0.04	
131	session1_LH	0.09	0.06	0.12	
132	session1_FSH	0.09	0.06	0.12	
133	session2_E2	-0.14	-0.18	-0.10	***
134	session2_P4	0.15	0.13	0.18	***
135	session2_LH	0.01	-0.02	0.04	
136	session2_FSH	0.08	0.05	0.10	
137	session3_E2	0.05	0.02	0.09	
138	session3_P4	0.12	0.09	0.15	
139	session3_LH	0.01	-0.02	0.05	
140	session3_FSH	0.03	0.00	0.06	
141	E2	0.00	-0.02	0.02	
142	P4	0.09	0.08	0.11	
143	LH	0.04	0.02	0.06	
144	FSH	0.06	0.05	0.08	

A.2 Contractility to Modular Arithmetic Presentation Regression Coefficients

Complete list of regression coefficients across all tested trial conditions and parameters for contractility following presentation of the modular arithmetic (MA) problems.

	Modular Arithmetic Presentation Regression Coefficients				
	Relations	**Mean**	**Lower HDI**	**Upper HDI**	**Credible**
1	session1_easy_lo_E2	0.18	0.14	0.22	***
2	session1_easy_lo_P4	0.09	0.06	0.12	
3	session1_easy_lo_LH	-0.04	-0.07	-0.01	
4	session1_easy_lo_FSH	-0.03	-0.06	0.01	
5	session1_easy_hi_E2	0.16	0.09	0.22	
6	session1_easy_hi_P4	0.05	0.00	0.11	
7	session1_easy_hi_LH	-0.06	-0.11	-0.01	
8	session1_easy_hi_FSH	-0.05	-0.11	0.00	
9	session1_hard_lo_E2	0.14	0.10	0.18	
10	session1_hard_lo_P4	0.05	0.01	0.08	
11	session1_hard_lo_LH	-0.03	-0.07	0.00	
12	session1_hard_lo_FSH	-0.03	-0.07	0.00	
13	session1_hard_hi_E2	0.18	0.12	0.24	***
14	session1_hard_hi_P4	0.08	0.03	0.13	
15	session1_hard_hi_LH	-0.03	-0.08	0.03	
16	session1_hard_hi_FSH	0.00	-0.05	0.06	
17	session2_easy_lo_E2	0.23	0.17	0.28	***
18	session2_easy_lo_P4	-0.22	-0.28	-0.17	***
19	session2_easy_lo_LH	0.24	0.18	0.30	***
20	session2_easy_lo_FSH	0.15	0.10	0.20	***
21	session2_easy_hi_E2	0.17	0.09	0.24	
22	session2_easy_hi_P4	-0.15	-0.22	-0.07	
23	session2_easy_hi_LH	0.16	0.08	0.24	
24	session2_easy_hi_FSH	0.12	0.05	0.20	
25	session2_hard_lo_E2	0.13	0.08	0.19	
26	session2_hard_lo_P4	-0.20	-0.26	-0.14	***
27	session2_hard_lo_LH	0.20	0.14	0.26	***
28	session2_hard_lo_FSH	0.15	0.09	0.21	
29	session2_hard_hi_E2	0.27	0.15	0.37	***
30	session2_hard_hi_P4	-0.24	-0.33	-0.15	***
31	session2_hard_hi_LH	0.24	0.15	0.34	***

	Relations	Mean	Lower HDI	Upper HDI	Credible
32	session2_hard_hi_FSH	0.18	0.09	0.26	
33	session3_easy_lo_E2	0.06	-0.01	0.13	
34	session3_easy_lo_P4	0.07	0.01	0.14	
35	session3_easy_lo_LH	-0.04	-0.10	0.03	
36	session3_easy_lo_FSH	-0.18	-0.26	-0.10	***
37	session3_easy_hi_E2	0.08	-0.02	0.16	
38	session3_easy_hi_P4	0.07	-0.05	0.18	
39	session3_easy_hi_LH	0.00	-0.10	0.10	
40	session3_easy_hi_FSH	-0.22	-0.32	-0.12	***
41	session3_hard_lo_E2	0.05	-0.03	0.13	
42	session3_hard_lo_P4	-0.04	-0.12	0.04	
43	session3_hard_lo_LH	-0.01	-0.08	0.06	
44	session3_hard_lo_FSH	-0.15	-0.24	-0.05	
45	session3_hard_hi_E2	0.01	-0.09	0.10	
46	session3_hard_hi_P4	0.00	-0.12	0.11	
47	session3_hard_hi_LH	-0.02	-0.12	0.08	
48	session3_hard_hi_FSH	-0.18	-0.30	-0.07	
49	session1_easy_E2	0.17	0.13	0.21	***
50	session1_easy_P4	0.07	0.04	0.10	
51	session1_easy_LH	-0.05	-0.08	-0.02	
52	session1_easy_FSH	-0.04	-0.07	-0.01	
53	session1_hard_E2	0.16	0.13	0.20	***
54	session1_hard_P4	0.06	0.03	0.09	
55	session1_hard_LH	-0.03	-0.06	0.00	
56	session1_hard_FSH	-0.01	-0.05	0.02	
57	session2_easy_E2	0.20	0.15	0.24	***
58	session2_easy_P4	-0.18	-0.23	-0.14	***
59	session2_easy_LH	0.20	0.15	0.25	***
60	session2_easy_FSH	0.14	0.09	0.18	
61	session2_hard_E2	0.20	0.14	0.26	***
62	session2_hard_P4	-0.22	-0.27	-0.17	***
63	session2_hard_LH	0.22	0.17	0.28	***
64	session2_hard_FSH	0.16	0.11	0.21	***
65	session3_easy_E2	0.07	0.01	0.12	
66	session3_easy_P4	0.07	0.01	0.14	
67	session3_easy_LH	-0.02	-0.08	0.04	
68	session3_easy_FSH	-0.20	-0.26	-0.14	***
69	session3_hard_E2	0.03	-0.03	0.09	

	Relations	Mean	Lower HDI	Upper HDI	Credible
70	session3_hard_P4	-0.02	-0.09	0.05	
71	session3_hard_LH	-0.02	-0.08	0.04	
72	session3_hard_FSH	-0.16	-0.24	-0.09	
73	session1_lo_E2	0.16	0.13	0.19	***
74	session1_lo_P4	0.07	0.04	0.09	
75	session1_lo_LH	-0.04	-0.06	-0.01	
76	session1_lo_FSH	-0.03	-0.05	-0.01	
77	session1_hi_E2	0.17	0.13	0.21	***
78	session1_hi_P4	0.07	0.03	0.10	
79	session1_hi_LH	-0.04	-0.08	-0.01	
80	session1_hi_FSH	-0.03	-0.06	0.01	
81	session2_lo_E2	0.18	0.14	0.22	***
82	session2_lo_P4	-0.21	-0.25	-0.17	***
83	session2_lo_LH	0.22	0.18	0.26	***
84	session2_lo_FSH	0.15	0.11	0.19	***
85	session2_hi_E2	0.22	0.15	0.28	***
86	session2_hi_P4	-0.19	-0.25	-0.13	***
87	session2_hi_LH	0.20	0.14	0.26	***
88	session2_hi_FSH	0.15	0.09	0.21	
89	session3_lo_E2	0.05	0.00	0.10	
90	session3_lo_P4	0.02	-0.03	0.07	
91	session3_lo_LH	-0.02	-0.07	0.02	
92	session3_lo_FSH	-0.16	-0.22	-0.10	***
93	session3_hi_E2	0.04	-0.02	0.11	
94	session3_hi_P4	0.04	-0.04	0.12	
95	session3_hi_LH	-0.01	-0.08	0.06	
96	session3_hi_FSH	-0.20	-0.28	-0.13	***
97	easy_lo_E2	0.15	0.12	0.19	***
98	easy_lo_P4	-0.02	-0.05	0.01	
99	easy_lo_LH	0.05	0.02	0.08	
100	easy_lo_FSH	-0.02	-0.05	0.02	
101	easy_hi_E2	0.13	0.09	0.18	
102	easy_hi_P4	-0.01	-0.06	0.04	
103	easy_hi_LH	0.03	-0.01	0.08	
104	easy_hi_FSH	-0.05	-0.09	0.00	
105	hard_lo_E2	0.11	0.07	0.14	
106	hard_lo_P4	-0.06	-0.10	-0.03	

	Relations	Mean	Lower HDI	Upper HDI	Credible
107	hard_lo_LH	0.05	0.02	0.09	
108	hard_lo_FSH	-0.01	-0.05	0.03	
109	hard_hi_E2	0.15	0.10	0.20	
110	hard_hi_P4	-0.05	-0.10	0.00	
111	hard_hi_LH	0.06	0.01	0.11	
112	hard_hi_FSH	0.00	-0.05	0.05	
113	easy_E2	0.14	0.12	0.17	***
114	easy_P4	-0.01	-0.04	0.02	
115	easy_LH	0.04	0.02	0.07	
116	easy_FSH	-0.03	-0.06	-0.01	
117	hard_E2	0.13	0.10	0.16	
118	hard_P4	-0.06	-0.09	-0.03	
119	hard_LH	0.06	0.03	0.09	
120	hard_FSH	-0.01	-0.04	0.03	
121	lo_E2	0.13	0.11	0.15	***
122	lo_P4	-0.04	-0.06	-0.02	
123	lo_LH	0.05	0.03	0.08	
124	lo_FSH	-0.01	-0.04	0.01	
125	hi_E2	0.14	0.11	0.18	***
126	hi_P4	-0.03	-0.07	0.01	
127	hi_LH	0.05	0.02	0.08	
128	hi_FSH	-0.03	-0.06	0.01	
129	session1_E2	0.16	0.14	0.19	***
130	session1_P4	0.07	0.05	0.09	
131	session1_LH	-0.04	-0.06	-0.02	
132	session1_FSH	-0.03	-0.05	-0.01	
133	session2_E2	0.20	0.16	0.24	***
134	session2_P4	-0.20	-0.24	-0.17	***
135	session2_LH	0.21	0.17	0.25	***
136	session2_FSH	0.15	0.12	0.18	***
137	session3_E2	0.05	0.00	0.09	
138	session3_P4	0.03	-0.02	0.08	
139	session3_LH	-0.02	-0.06	0.02	
140	session3_FSH	-0.18	-0.23	-0.13	***
141	E2	0.14	0.12	0.16	***
142	P4	-0.04	-0.06	-0.02	
143	LH	0.05	0.03	0.07	
144	FSH	-0.02	-0.04	0.00	

A.3 Feedback Presentation Regression Coefficients

Complete list of regression coefficients across all tested trial conditions and parameters for contractility following feedback presentation to modular arithmetic (MA) problems.

	Relations	Mean	Lower HDI	Upper HDI	Credible
	Feedback Presentation Regression Coefficients				
1	session1_easy_lo_E2	0.13	0.08	0.19	
2	session1_easy_lo_P4	0.07	0.03	0.11	
3	session1_easy_lo_LH	-0.05	-0.10	-0.01	
4	session1_easy_lo_FSH	-0.06	-0.10	-0.01	
5	session1_easy_hi_E2	0.08	0.00	0.16	
6	session1_easy_hi_P4	0.02	-0.05	0.08	
7	session1_easy_hi_LH	-0.10	-0.17	-0.03	
8	session1_easy_hi_FSH	-0.10	-0.17	-0.03	
9	session1_hard_lo_E2	0.12	0.07	0.17	
10	session1_hard_lo_P4	0.09	0.05	0.13	
11	session1_hard_lo_LH	-0.04	-0.08	0.01	
12	session1_hard_lo_FSH	0.00	-0.04	0.05	
13	session1_hard_hi_E2	0.11	0.04	0.18	
14	session1_hard_hi_P4	0.06	0.00	0.12	
15	session1_hard_hi_LH	-0.06	-0.12	0.00	
16	session1_hard_hi_FSH	-0.03	-0.10	0.03	
17	session2_easy_lo_E2	0.29	0.23	0.36	***
18	session2_easy_lo_P4	-0.21	-0.27	-0.14	***
19	session2_easy_lo_LH	0.27	0.20	0.34	***
20	session2_easy_lo_FSH	0.16	0.10	0.22	***
21	session2_easy_hi_E2	0.24	0.16	0.33	***
22	session2_easy_hi_P4	-0.11	-0.20	-0.02	
23	session2_easy_hi_LH	0.22	0.12	0.31	***
24	session2_easy_hi_FSH	0.15	0.06	0.24	
25	session2_hard_lo_E2	0.18	0.12	0.25	***
26	session2_hard_lo_P4	-0.11	-0.18	-0.04	
27	session2_hard_lo_LH	0.13	0.06	0.20	
28	session2_hard_lo_FSH	0.05	-0.02	0.11	
29	session2_hard_hi_E2	0.36	0.24	0.49	***
30	session2_hard_hi_P4	-0.16	-0.27	-0.05	
31	session2_hard_hi_LH	0.20	0.09	0.30	

	Relations	Mean	Lower HDI	Upper HDI	Credible
32	session2_hard_hi_FSH	0.05	-0.06	0.15	
33	session3_easy_lo_E2	0.06	-0.02	0.14	
34	session3_easy_lo_P4	0.07	-0.01	0.15	
35	session3_easy_lo_LH	-0.01	-0.08	0.07	
36	session3_easy_lo_FSH	-0.10	-0.19	-0.01	
37	session3_easy_hi_E2	0.12	0.01	0.22	
38	session3_easy_hi_P4	0.08	-0.05	0.20	
39	session3_easy_hi_LH	0.05	-0.06	0.15	
40	session3_easy_hi_FSH	-0.14	-0.27	-0.02	
41	session3_hard_lo_E2	0.14	0.04	0.25	
42	session3_hard_lo_P4	0.04	-0.08	0.15	
43	session3_hard_lo_LH	0.06	-0.04	0.16	
44	session3_hard_lo_FSH	-0.15	-0.27	-0.03	
45	session3_hard_hi_E2	0.02	-0.10	0.13	
46	session3_hard_hi_P4	0.02	-0.09	0.14	
47	session3_hard_hi_LH	0.00	-0.12	0.11	
48	session3_hard_hi_FSH	-0.09	-0.24	0.05	
49	session1_easy_E2	0.11	0.06	0.16	
50	session1_easy_P4	0.04	0.00	0.08	
51	session1_easy_LH	-0.08	-0.11	-0.03	
52	session1_easy_FSH	-0.08	-0.12	-0.03	
53	session1_hard_E2	0.12	0.07	0.16	
54	session1_hard_P4	0.07	0.04	0.11	
55	session1_hard_LH	-0.05	-0.09	-0.01	
56	session1_hard_FSH	-0.02	-0.06	0.02	
57	session2_easy_E2	0.27	0.22	0.33	***
58	session2_easy_P4	-0.16	-0.21	-0.10	
59	session2_easy_LH	0.25	0.19	0.30	***
60	session2_easy_FSH	0.16	0.10	0.21	***
61	session2_hard_E2	0.27	0.20	0.34	***
62	session2_hard_P4	-0.14	-0.20	-0.07	
63	session2_hard_LH	0.17	0.10	0.23	***
64	session2_hard_FSH	0.05	-0.02	0.11	
65	session3_easy_E2	0.09	0.03	0.16	
66	session3_easy_P4	0.07	0.00	0.15	
67	session3_easy_LH	0.02	-0.04	0.09	
68	session3_easy_FSH	-0.12	-0.20	-0.04	
69	session3_hard_E2	0.08	0.00	0.16	

	Relations	Mean	Lower HDI	Upper HDI	Credible
70	session3_hard_P4	0.03	-0.05	0.11	
71	session3_hard_LH	0.03	-0.05	0.10	
72	session3_hard_FSH	-0.12	-0.22	-0.03	
73	session1_lo_E2	0.13	0.09	0.16	
74	session1_lo_P4	0.08	0.05	0.11	
75	session1_lo_LH	-0.04	-0.08	-0.01	
76	session1_lo_FSH	-0.03	-0.06	0.00	
77	session1_hi_E2	0.10	0.04	0.15	
78	session1_hi_P4	0.04	-0.01	0.09	
79	session1_hi_LH	-0.08	-0.12	-0.03	
80	session1_hi_FSH	-0.07	-0.11	-0.02	
81	session2_lo_E2	0.24	0.19	0.28	***
82	session2_lo_P4	-0.16	-0.21	-0.11	***
83	session2_lo_LH	0.20	0.15	0.25	***
84	session2_lo_FSH	0.10	0.06	0.15	
85	session2_hi_E2	0.30	0.23	0.38	***
86	session2_hi_P4	-0.14	-0.21	-0.06	
87	session2_hi_LH	0.21	0.13	0.28	***
88	session2_hi_FSH	0.10	0.03	0.16	
89	session3_lo_E2	0.10	0.03	0.17	
90	session3_lo_P4	0.05	-0.02	0.12	
91	session3_lo_LH	0.02	-0.04	0.09	
92	session3_lo_FSH	-0.13	-0.21	-0.05	
93	session3_hi_E2	0.07	-0.01	0.14	
94	session3_hi_P4	0.05	-0.03	0.14	
95	session3_hi_LH	0.02	-0.06	0.10	
96	session3_hi_FSH	-0.12	-0.21	-0.02	
97	easy_lo_E2	0.16	0.12	0.20	***
98	easy_lo_P4	-0.02	-0.06	0.02	
99	easy_lo_LH	0.07	0.03	0.11	
100	easy_lo_FSH	0.00	-0.04	0.04	
101	easy_hi_E2	0.15	0.10	0.20	
102	easy_hi_P4	-0.01	-0.06	0.05	
103	easy_hi_LH	0.06	0.00	0.11	
104	easy_hi_FSH	-0.03	-0.09	0.03	
105	hard_lo_E2	0.15	0.10	0.19	***
106	hard_lo_P4	0.00	-0.04	0.05	

	Relations	Mean	Lower HDI	Upper HDI	Credible
107	hard_lo_LH	0.05	0.01	0.10	
108	hard_lo_FSH	-0.04	-0.08	0.01	
109	hard_hi_E2	0.17	0.11	0.23	***
110	hard_hi_P4	-0.03	-0.08	0.03	
111	hard_hi_LH	0.05	-0.01	0.10	
112	hard_hi_FSH	-0.03	-0.09	0.04	
113	easy_E2	0.16	0.12	0.19	***
114	easy_P4	-0.01	-0.05	0.02	
115	easy_LH	0.06	0.03	0.10	
116	easy_FSH	-0.01	-0.05	0.02	
117	hard_E2	0.16	0.12	0.19	***
118	hard_P4	-0.01	-0.05	0.02	
119	hard_LH	0.05	0.01	0.08	
120	hard_FSH	-0.03	-0.07	0.01	
121	lo_E2	0.16	0.13	0.19	***
122	lo_P4	-0.01	-0.04	0.02	
123	lo_LH	0.06	0.03	0.09	
124	lo_FSH	-0.02	-0.05	0.01	
125	hi_E2	0.16	0.12	0.20	***
126	hi_P4	-0.02	-0.06	0.02	
127	hi_LH	0.05	0.01	0.09	
128	hi_FSH	-0.03	-0.07	0.01	
129	session1_E2	0.11	0.08	0.15	
130	session1_P4	0.06	0.03	0.09	
131	session1_LH	-0.06	-0.09	-0.04	
132	session1_FSH	-0.05	-0.07	-0.02	
133	session2_E2	0.27	0.23	0.32	***
134	session2_P4	-0.15	-0.19	-0.11	***
135	session2_LH	0.21	0.16	0.25	***
136	session2_FSH	0.10	0.06	0.14	
137	session3_E2	0.09	0.03	0.14	
138	session3_P4	0.05	0.00	0.11	
139	session3_LH	0.02	-0.03	0.07	
140	session3_FSH	-0.12	-0.18	-0.06	
141	E2	0.16	0.13	0.18	***
142	P4	-0.01	-0.04	0.01	
143	LH	0.06	0.03	0.08	
144	FSH	-0.02	-0.05	0.00	

A.4 Allostatic Efficiency Regression Coefficients

Complete list of regression coefficients across all tested trial conditions and parameters for allostatic efficiency following feedback presentation to modular arithmetic (MA) problems.

	Relations	Mean	Lower HDI	Upper HDI	Credible
	Allostatic Efficiency Regression Coefficients				
1	session1_easy_lo_E2	-0.13	-0.46	0.20	
2	session1_easy_lo_P4	-0.13	-0.44	0.20	
3	session1_easy_lo_LH	-0.10	-0.40	0.23	
4	session1_easy_lo_FSH	-0.06	-0.39	0.27	
5	session1_easy_hi_E2	0.00	-0.32	0.33	
6	session1_easy_hi_P4	-0.02	-0.33	0.29	
7	session1_easy_hi_LH	0.07	-0.22	0.38	
8	session1_easy_hi_FSH	0.06	-0.25	0.38	
9	session1_hard_lo_E2	-0.02	-0.18	0.14	
10	session1_hard_lo_P4	-0.23	-0.38	-0.10	
11	session1_hard_lo_LH	-0.02	-0.16	0.12	
12	session1_hard_lo_FSH	-0.18	-0.32	-0.02	
13	session1_hard_hi_E2	0.04	-0.18	0.25	
14	session1_hard_hi_P4	-0.08	-0.28	0.11	
15	session1_hard_hi_LH	0.17	0.00	0.35	
16	session1_hard_hi_FSH	-0.04	-0.23	0.16	
17	session2_easy_lo_E2	-0.31	-0.53	-0.08	
18	session2_easy_lo_P4	0.06	-0.17	0.27	
19	session2_easy_lo_LH	-0.29	-0.51	-0.07	
20	session2_easy_lo_FSH	-0.22	-0.42	-0.01	
21	session2_easy_hi_E2	-0.15	-0.38	0.09	
22	session2_easy_hi_P4	0.03	-0.22	0.26	
23	session2_easy_hi_LH	-0.23	-0.46	0.00	
24	session2_easy_hi_FSH	-0.22	-0.43	-0.01	
25	session2_hard_lo_E2	-0.18	-0.32	-0.04	
26	session2_hard_lo_P4	-0.23	-0.37	-0.09	
27	session2_hard_lo_LH	0.12	-0.02	0.27	
28	session2_hard_lo_FSH	0.17	0.03	0.30	
29	session2_hard_hi_E2	-0.30	-0.48	-0.12	***
30	session2_hard_hi_P4	-0.01	-0.18	0.16	
31	session2_hard_hi_LH	0.00	-0.18	0.18	

	Relations	Mean	Lower HDI	Upper HDI	Credible
32	session2_hard_hi_FSH	0.11	-0.05	0.29	
33	session3_easy_lo_E2	0.03	-0.28	0.33	
34	session3_easy_lo_P4	0.04	-0.27	0.34	
35	session3_easy_lo_LH	0.01	-0.30	0.32	
36	session3_easy_lo_FSH	-0.09	-0.40	0.23	
37	session3_easy_hi_E2	-0.07	-0.40	0.28	
38	session3_easy_hi_P4	0.00	-0.34	0.33	
39	session3_easy_hi_LH	-0.04	-0.37	0.30	
40	session3_easy_hi_FSH	0.01	-0.33	0.35	
41	session3_hard_lo_E2	-0.25	-0.46	-0.03	
42	session3_hard_lo_P4	-0.23	-0.45	0.01	
43	session3_hard_lo_LH	-0.16	-0.36	0.07	
44	session3_hard_lo_FSH	-0.01	-0.25	0.23	
45	session3_hard_hi_E2	-0.18	-0.39	0.02	
46	session3_hard_hi_P4	-0.31	-0.51	-0.10	***
47	session3_hard_hi_LH	-0.10	-0.31	0.11	
48	session3_hard_hi_FSH	-0.05	-0.27	0.17	
49	session1_easy_E2	-0.06	-0.30	0.16	
50	session1_easy_P4	-0.07	-0.29	0.15	
51	session1_easy_LH	-0.01	-0.22	0.21	
52	session1_easy_FSH	0.00	-0.23	0.22	
53	session1_hard_E2	0.01	-0.12	0.14	
54	session1_hard_P4	-0.16	-0.28	-0.04	
55	session1_hard_LH	0.08	-0.04	0.19	
56	session1_hard_FSH	-0.11	-0.23	0.02	
57	session2_easy_E2	-0.23	-0.39	-0.07	
58	session2_easy_P4	0.05	-0.11	0.21	
59	session2_easy_LH	-0.26	-0.41	-0.10	
60	session2_easy_FSH	-0.22	-0.36	-0.07	
61	session2_hard_E2	-0.24	-0.36	-0.13	***
62	session2_hard_P4	-0.12	-0.23	-0.01	
63	session2_hard_LH	0.06	-0.06	0.18	
64	session2_hard_FSH	0.14	0.03	0.25	
65	session3_easy_E2	-0.02	-0.24	0.21	
66	session3_easy_P4	0.02	-0.21	0.24	
67	session3_easy_LH	-0.01	-0.24	0.21	
68	session3_easy_FSH	-0.04	-0.26	0.20	
69	session3_hard_E2	-0.21	-0.36	-0.06	

	Relations	Mean	Lower HDI	Upper HDI	Credible
70	session3_hard_P4	-0.27	-0.42	-0.11	***
71	session3_hard_LH	-0.13	-0.28	0.02	
72	session3_hard_FSH	-0.03	-0.20	0.13	
73	session1_lo_E2	-0.07	-0.25	0.11	
74	session1_lo_P4	-0.18	-0.35	0.00	
75	session1_lo_LH	-0.06	-0.23	0.11	
76	session1_lo_FSH	-0.12	-0.30	0.06	
77	session1_hi_E2	0.02	-0.18	0.21	
78	session1_hi_P4	-0.05	-0.23	0.13	
79	session1_hi_LH	0.12	-0.06	0.30	
80	session1_hi_FSH	0.01	-0.18	0.19	
81	session2_lo_E2	-0.25	-0.38	-0.11	***
82	session2_lo_P4	-0.09	-0.22	0.04	
83	session2_lo_LH	-0.08	-0.21	0.05	
84	session2_lo_FSH	-0.03	-0.15	0.10	
85	session2_hi_E2	-0.23	-0.38	-0.08	
86	session2_hi_P4	0.01	-0.13	0.16	
87	session2_hi_LH	-0.12	-0.26	0.03	
88	session2_hi_FSH	-0.05	-0.19	0.08	
89	session3_lo_E2	-0.11	-0.30	0.08	
90	session3_lo_P4	-0.10	-0.29	0.10	
91	session3_lo_LH	-0.07	-0.27	0.11	
92	session3_lo_FSH	-0.05	-0.25	0.14	
93	session3_hi_E2	-0.12	-0.32	0.08	
94	session3_hi_P4	-0.15	-0.35	0.04	
95	session3_hi_LH	-0.07	-0.27	0.13	
96	session3_hi_FSH	-0.02	-0.22	0.19	
97	easy_lo_E2	-0.14	-0.30	0.03	
98	easy_lo_P4	-0.01	-0.18	0.16	
99	easy_lo_LH	-0.13	-0.29	0.04	
100	easy_lo_FSH	-0.12	-0.29	0.04	
101	easy_hi_E2	-0.07	-0.25	0.10	
102	easy_hi_P4	0.01	-0.17	0.18	
103	easy_hi_LH	-0.07	-0.24	0.10	
104	easy_hi_FSH	-0.05	-0.22	0.12	
105	hard_lo_E2	-0.15	-0.25	-0.05	
106	hard_lo_P4	-0.23	-0.33	-0.13	***

	Relations	Mean	Lower HDI	Upper HDI	Credible
107	hard_lo_LH	-0.02	-0.12	0.08	
108	hard_lo_FSH	-0.01	-0.11	0.09	
109	hard_hi_E2	-0.15	-0.26	-0.03	
110	hard_hi_P4	-0.13	-0.24	-0.02	
111	hard_hi_LH	0.02	-0.09	0.13	
112	hard_hi_FSH	0.01	-0.11	0.12	
113	easy_E2	-0.10	-0.23	0.01	
114	easy_P4	0.00	-0.12	0.11	
115	easy_LH	-0.10	-0.21	0.02	
116	easy_FSH	-0.09	-0.20	0.03	
117	hard_E2	-0.15	-0.22	-0.07	
118	hard_P4	-0.18	-0.26	-0.11	***
119	hard_LH	0.00	-0.07	0.08	
120	hard_FSH	0.00	-0.08	0.08	
121	lo_E2	-0.14	-0.24	-0.04	
122	lo_P4	-0.12	-0.22	-0.03	
123	lo_LH	-0.07	-0.17	0.02	
124	lo_FSH	-0.07	-0.16	0.03	
125	hi_E2	-0.11	-0.22	0.00	
126	hi_P4	-0.06	-0.17	0.04	
127	hi_LH	-0.02	-0.12	0.08	
128	hi_FSH	-0.02	-0.12	0.08	
129	session1_E2	-0.03	-0.16	0.10	
130	session1_P4	-0.12	-0.24	0.01	
131	session1_LH	0.03	-0.09	0.16	
132	session1_FSH	-0.06	-0.18	0.08	
133	session2_E2	-0.24	-0.34	-0.14	***
134	session2_P4	-0.04	-0.14	0.06	
135	session2_LH	-0.10	-0.20	0.00	
136	session2_FSH	-0.04	-0.13	0.05	
137	session3_E2	-0.12	-0.26	0.02	
138	session3_P4	-0.13	-0.26	0.01	
139	session3_LH	-0.07	-0.21	0.06	
140	session3_FSH	-0.03	-0.18	0.10	
141	E2	-0.13	-0.20	-0.06	
142	P4	-0.09	-0.16	-0.02	
143	LH	-0.05	-0.12	0.02	
144	FSH	-0.04	-0.12	0.03	

Appendix B
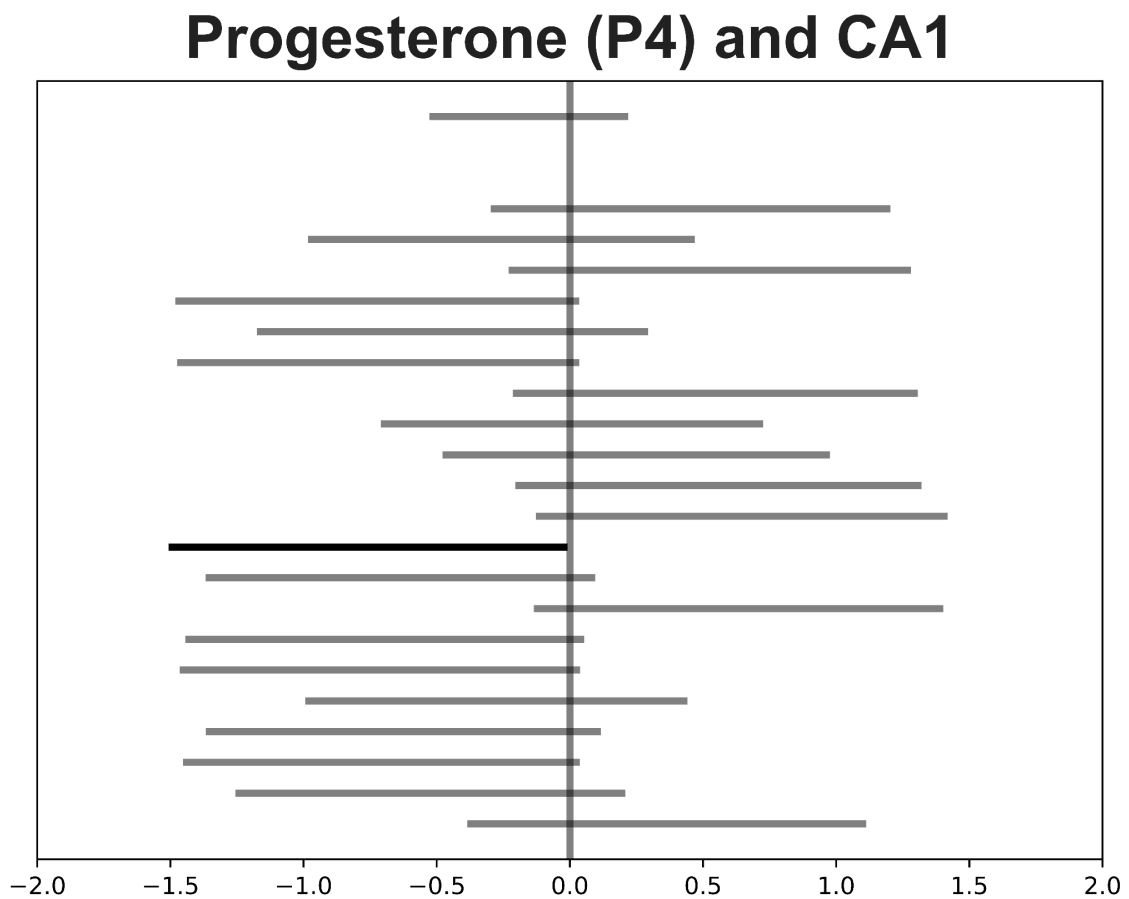
B.1   Estradiol and Perirhinal Cortex

A plot of the Bayesian regression 94% HDI intervals for the relationship between concentration of estradiol (E2) and gray matter volume of the perirhinal cortex. The top line is the group result, with the 21 participants' highest density intervals (HDIs) below. Notably, there were a number of marginally credible individual-level effects that were split between directions of credibility.

Estradiol (E2) and Perirhinal Cortex
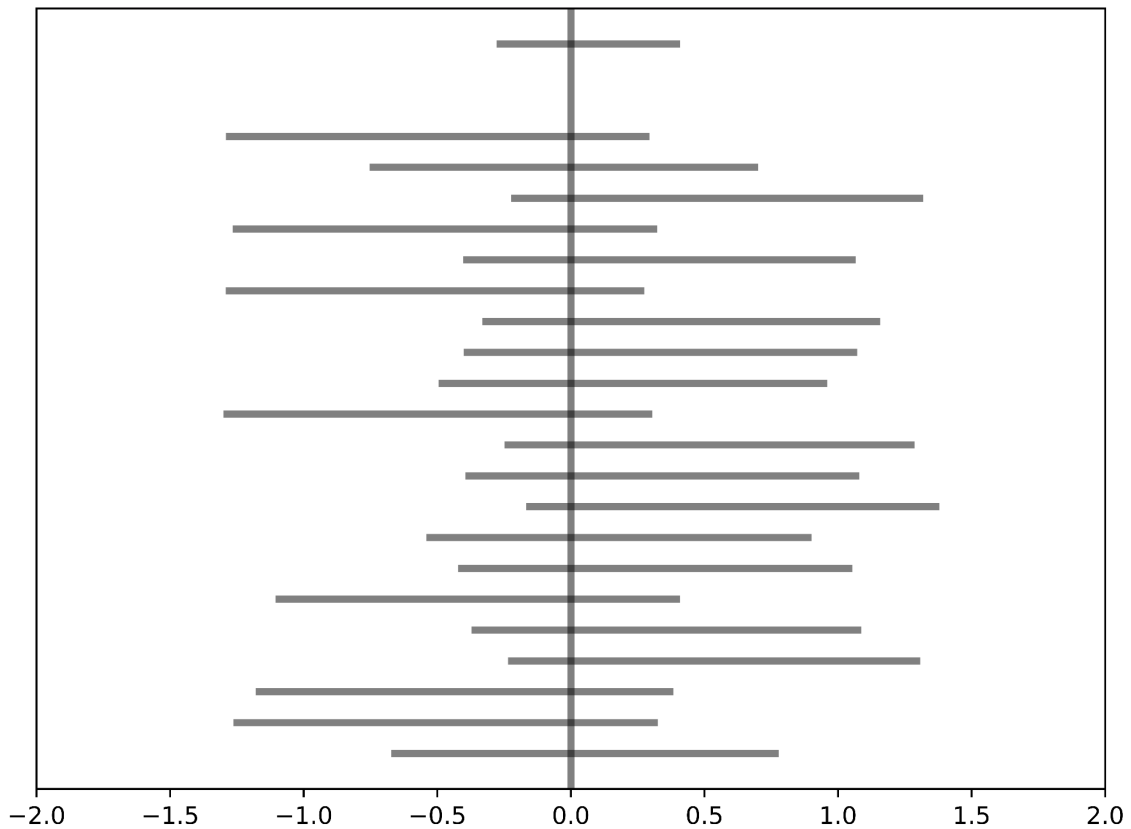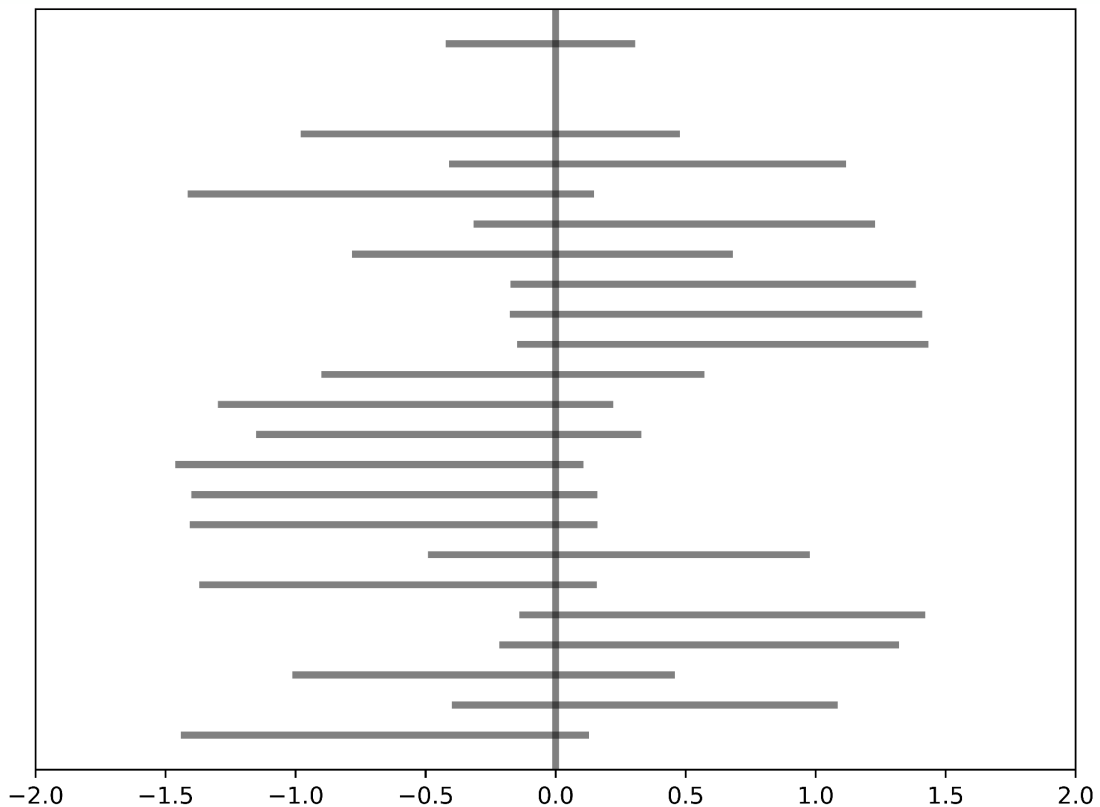
B.2 Progesterone and CA1 Subregion

A plot of the Bayesian regression 94% HDI intervals for the relationship between concentration of progesterone (P4) and gray matter volume of the CA1 subregion. The top line is the group result, with the 21 participants' highest density intervals (HDIs) below. Notably, there were a number of marginally credible individual-level effects that were split between directions of credibility.

Progesterone (P4) and CA1

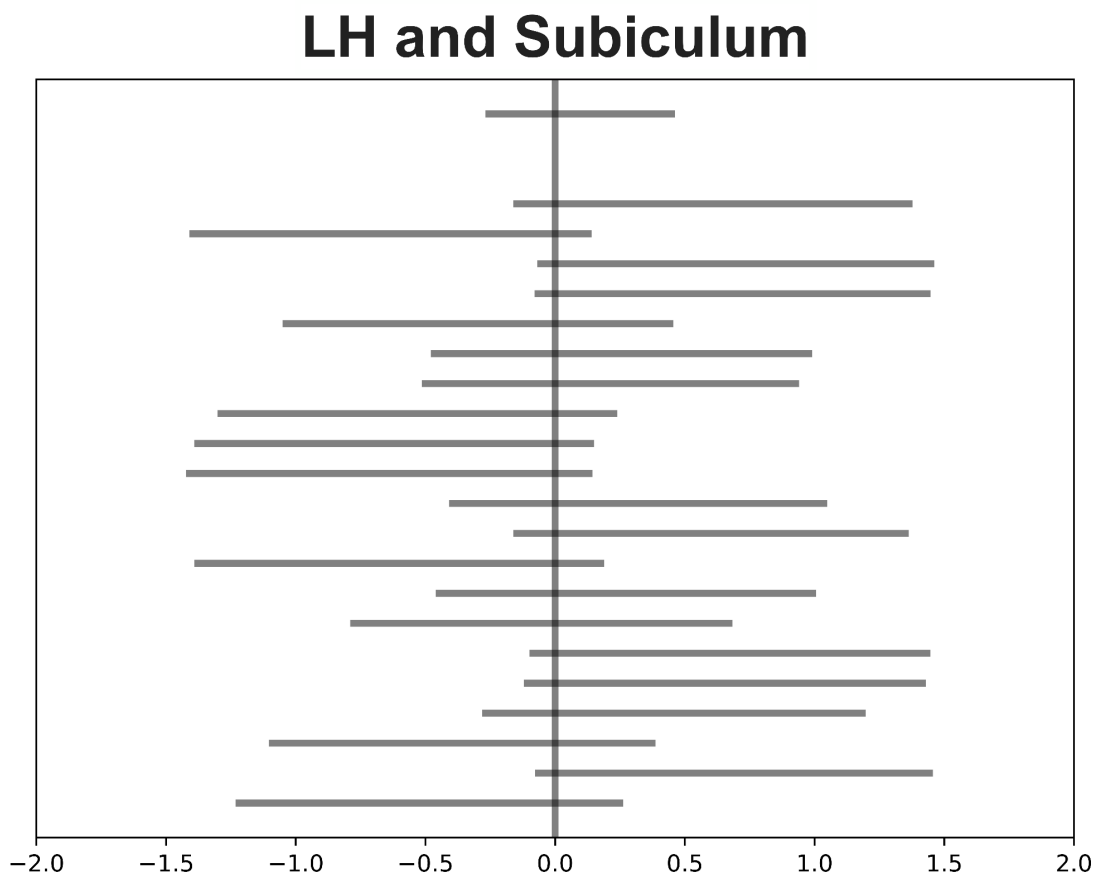### B.3 Progesterone and Entorhinal Cortex

A plot of the Bayesian regression 94% HDI intervals for the relationship between concentration of progesterone (P4) and gray matter volume of the entorhinal cortex. The top line is the group result, with the 21 participants' highest density intervals (HDIs) below. Notably, there were a number of marginally credible individual-level effects that were split between directions of credibility.

Progesterone (P4) and Entorhinal Cortex

B.4 Luteinizing Hormone (LH) and the Subiculum Subregion

A plot of the Bayesian regression 94% HDI intervals for the relationship between concentration of luteinizing hormone (LH) and gray matter volume of the subiculum subregion. The top line is the group result, with the 21 participants' highest density intervals (HDIs) below. Notably, there were a number of marginally credible individual-level effects that were split between directions of credibility.

LH and Subiculum

B.5 Follicle Stimulating Hormone (FSH) and CA1 Subregion

A plot of the Bayesian regression 94% HDI intervals for the relationship between concentration of follicle stimulating hormone (FSH) and gray matter volume of the CA1 subregion. The top line is the group result, with the 21 participants' highest density intervals (HDIs) below. Notably, there were a number of marginally credible individual-level effects that were split between directions of credibility.

FSH and CA1